CRACK DETECTION IN SLENDER CANTILEVER PLATES USING MODAL ANALYSIS

DEREK REX PERCHARD

CRACK DETECTION IN SLENDER CANTILEVER PLATES USING MODAL ANALYSIS

By

Derek Rex Perchard, B.Eng.

A thesis submitted to the School of Graduate
Studies in partial fulfilment of the
requirements for the degree of
Master of Engineering

Faculty of Engineering and Applied Science
Memorial University of Newfoundland
April 1993

St. John's Newfoundland Canada

ISBN 0-315-86673-X

Canada

Abstract

Research over the past decade or so, has found a new application for modal analysis theory and experimentation. It involves non-destructive evaluation, with the primary intent of detecting and locating structural faults (cracks, voids, etc.) in structures such as off-shore oil platforms which are vulnerable to fatigue and other forms of inconspicuous damage.

This current research program was conducted in an attempt to add to the existing body of knowledge on this subject. It illustrates through analytical and experimental modelling, the effect that a simulated crack has on the modal characteristics of a simple structure, ie., a cantilever plate, with 5 levels of damage.

The assessment involved creating a finite element model of the structure using an integrated software package, SDRC - I-DEAS, to estimate the changes in various modal parameters, caused by a notch type crack. Additionally, a series of tests were carried out using response measurement equipment to experimentally determine the effect of the imposed defect. This was accomplished via measurement of dynamic response, using both accelerometers and strain gauges, and subsequent test data analysis using I-DEAS.

Results obtained from both phases of analysis showed that the crack could be detected, primarily through observation of reduction in natural frequency for a number of modes. The analytical model, in particular, provided a useful technique of crack location via observed inconsistencies in the plots derived from differences in both displacement and rotation mode shapes for cracked plates, with respect to a reference plate. The experimentation performed verified the analytical results, and provided additional insight into changes in damping, residue, and amplitude of dynamic response for frequency values at, and offset from those associated with the natural modes. This latter phenomena proved to be very sensitive and correlated well with observed changes in frequency. The measurement of strain response also proved to be a good indicator of crack existence with major increases in response magnitude, far exceeding the corresponding acceleration response.

Acknowledgements

This thesis was compiled from research conducted at Memorial University of Newfoundland, with primary funding provided by a grant from the National Science and Engineering Research Council. This funding, in conjunction with departmental support was essential in the successful completion of this course of study, and is gratefully acknowledged.

I would like to sincerely thank my supervisor, Dr. A.S.J. Swamidas, Professor of Civil Engineering, whose support, encouragement, and guidance, were always present during the period I spent as a graduate student at MUN. Thanks are also extended to both Assistant Deans which served during this period, Dr. T.R. Chari, and Dr. J.J Sharp, for continued support of this program of research. I would also like to acknowledge the technical assistance and advise of the many individuals working in the laboratories of this faculty.

Finally, I would like to express my gratitude to members of my family, and especially my wife Jackie, for support, encouragement, and affection provided during this trying period.

Contents

Contents (cont'd)

List of Tables

List of Figures

List of Figures (cont'd)

List of Figures (cont'd)

List of Figures (cont'd)

Chapter 1

Introduction

The ever increasing demand for petroleum products has made it necessary for the world's population to begin searching under the earth's ocean floors for what remains of the earth's untapped oil reserves. Accomplishment of this task has been a true feat of modern engineering. This is due mainly to the fulfilment of the design requirements for large structures, with long term durability, which have been designed, built, and installed in the harsh ocean environment.

This ocean environment is one of the most severe and challenging loading regimes that an engineer could ever expect to face. This is so, largely because of the cyclic action that is inherent in wave, current and wind loading, an action that imposes on structures, a continuous series of load reversals. This results in a phenomena known as fatigue, a condition caused by cyclic loading of significant magnitude that over time weakens the material of the structure, reducing its ability to withstand load. If the action continues over an extended period of time, a point is reached where the material actually ruptures, thus initiating a crack. This crack will grow over time, as the load reversals continue, and may reach a point where it poses a threat to the integrity of the structure. To design a structure that can operate in the ocean regime is a challenge at best. To make the structure immune to fatigue would seem an impossibility or at the very least would make it extremely expensive and impractical. As a compromise the designer has to make the structure safe

for all known loading conditions of short term duration and attempt to make the structure serviceable through maintenance and inspection, for its intended life span. Without explicit design consideration, fatigue cracking is still likely to occur at some point in the life of a structure.

This fact has been well documented over the years by inspection and monitoring teams as well as by the many researchers who have studied this phenomena. As a result, all such structures must be carefully maintained and monitored so that in the event of the development of a fatigue crack or any other defect, it can be located and repaired before it can impair the safety of the structure.

While fatigue is by far the type of damage most difficult to control, there are other forms of defects or faults that can be very dangerous. A concise summary of what constitutes a fault is given in Richardson and Mannan (1991) as any of the following occurrences:

- **Failure of the Structural Material due to Fatigue.** For example, cracking, breaking, or delamination.
- **Loosening of Assembled Parts.** For Example loose bolts, rivets, glued joints or wear out of parts.
- **Manufacturing Defects.** For example, flaws, voids, or thin spots due to casting, moulding or forming operations. Improper assembly of parts.

Structural integrity is of utmost importance in these types of structures which history has shown to be far from invulnerable. One major component of safety assurance in this regard is, as alluded to above, a monitoring system to detect damage wherever it is and despite

its cause. The evolution of such systems has led to the development of a relatively new field of research called Non-Destructive Evaluation, whose primary objective is to detect structural defects, on-site, with facilities that can be located on the structure itself.

This research has resulted in the development of several useful techniques that perform the desired task of defect detection. Some of the more notable of these techniques include: Alternating Current Potential Drop (ACPD), Radiography (X-Ray), Magnetic Particle Inspection, Eddy Current and Ultrasound. While each of these techniques has certain desirable features they are often difficult to use under the operating conditions of the structures they are intended to monitor. In addition they usually require the use of divers, specially trained to carry out inspections. This is obviously a danger to personnel and a very undesirable aspect of a monitoring system.

An ideal system should be centrally located on the structure and should not be dependant on the services of divers. It should be operable from a computer control centre and should be able to function automatically with only a periodic inspection of results by trained personnel. In an effort to attain this type of system, a new approach has been the focus of numerous research programs over the past number of years. This approach is the study of dynamic properties of a system through a technique known as modal analysis. Research to date, has shown that in its initial state, a structure has several characteristic properties or modal parameters. These include natural frequencies, damping, dynamic amplitude of displacement, residue and mode shapes. By observing these parameters and noting changes it is hoped that a technique can be developed that can correlate specific shifts in one or more of these parameters with the occurrence of structural defects. It is hoped that such

a system would not only be able to identify the existence of a defect, but also indicate its location and extent, through the measurement of global and local response parameters using permanently attached transducers interacting with a central interpretation centre.

1.1 Scope of Thesis

The main purpose of this course of study is to conduct a series of experiments on a number of slender cantilever plates with artificial cracks of varying degree. All specimens are considered identical, except for the extent to which they are cracked. It is hoped that changes in the measured modal parameters can be correlated to crack depth and in some way provide an indication of crack location. Besides actually determining the crack induced changes the experimentation will compare results using two different types of response transducers. The main experiment will be carried out using traditional means of response measurement using accelerometers. A subsequent experiment will attempt to use strain gauges as response transducers. Results from both types of measurement will be analyzed independently and compared.

Secondary to the experimental objective is the development of an analytical model using finite element analysis. This analytical model will provide a basis for comparison with the experiment results, and thereby provide reinforcement of its findings. It is also to be used as an indicator of the appropriateness of the experimental set-up, highlighting experimental errors and providing insight into the validity of assumptions used in the development of such models.

1.2 Objectives

The specific intents of this research can be outlined by the following objectives:

- To develop appropriate procedures for experimental modal analysis as it applies to response measurement using cracked and uncracked slender cantilever plates.
- To identify from test results and by analytical modelling, changes in modal parameters that can be directly attributable to the existence of a crack.
- To correlate the trend of observed changes with the extent of the crack.
- To determine if any aspect of the behaviour of the specimens or their dynamic response can be indicative of crack location.
- To determine if ordinary strain gauges are appropriate response transducers in a dynamic test environment and if so, whether the measurement of strain would be a useful tool in crack identification.

1.3 Outline of Thesis

The remaining portion of this thesis is divided into five chapters. Chapter 2 reviews some of the literature published on this topic and attempts to illustrate what is the current state of the art in this realm of research. Chapter 3 contains a review of relevant theory concerning the topics of structural dynamics, modal analysis, and selected procedures used in analysis of experimental results. Chapter 4 discusses the results of the analytical study conducted as part of this research. Chapter 5 discusses the experimental results and what was learned from them. Chapter 6 concludes this thesis with a review of its findings and comments on some recommendations for future work.

Chapter 2

Literature Review

It has become increasingly important to understand the phenomena associated with vibration early in the design phase of any structure. When the attempt is made to account for dynamic response and resonance during the design it often eliminates costly experimentation and evaluation of problems that may arise after the commissioning of a project. Modal analysis is particularly important in this phase of a project. It is also a useful tool in the implementation of structural modification that attempts to modify a structure's dynamic behaviour to reduce excessive or otherwise unwanted vibrational characteristics.

In its simplest form the definition of modal analysis is simply:

> *The process of determining the dynamic properties of a structure either by experimentation, mathematical modelling, or through a combination of both, and subsequently characterizing these properties in terms of the structure's modes of vibration.*

Modal analysis, an inseparable combination of analytical and experimental evaluation, is a specific category within the broad realm of structural dynamics. While this is a somewhat new category, the principles on which it is based have been firmly established for many years. Early development work on this subject can be attributed in part to pioneers like

Kennedy and Pancu (1947) whose research on aircraft structures led to the development of accurate techniques for estimation of natural frequencies and damping. Their work paved the way for the development of the modern techniques used in modal analysis.

In the 50 years that have transpired since then, the processes of modal analysis have been refined by the combined effort of the many individuals who have worked in this field. One such individual, noted for his work on this subject, is D. J. Ewins, a professor of Vibration Engineering at Imperial College of Science and Technology, in London, England. His 1984 book, *Modal Testing: Theory and Practice*, is probably the most complete single reference available on this subject. In this book and among his papers [ie., Ewins (1987)] can be found invaluable information concerning the proper use of the methods of modal testing and its associated theory.

Numerous specific applications have been found for the results obtained through the use of modal analysis. These include the development of modal models of substructure components that are to be integrated into a structural assembly. This allows prediction of the effects of the addition, on the overall structural properties. Another application is in the area of force determination. It is not always possible to measure the applied dynamic force directly but through evaluation of the system's response characteristics an inverse type of analysis can be performed to deduce the force characteristics from the system's physical properties and its response characteristics. Yet another, is predicting the effect of structural modifications such as the addition of stiffeners on the dynamic behaviour of a system.

Modification of the theory used for this latter application led to the development of an entirely new application, damage detection, the focal point of this thesis. Here the

structural modification is a passive one and the modal analysis of the structure attempts to verify the existence of the defect and determine its location.

The remaining portion of this chapter is divided into three sections, the first discusses literature pertaining to various theoretical methods developed for defect detection in structures. The second discusses the results that have been obtained by various authors who have studied this topic using experimental modal analysis. The third, relates to the secondary objective of this research, applications of strain measurement in modal analysis.

2.1 Theoretical Approaches to Defect Detection

Many individuals have attempted to develop a methodology that would analyze the vibration of structures with embedded defects. In Petyt (1968) the vibration characteristics of a simplified model of an aircraft fuselage panel containing a fatigue crack were obtained using the finite element displacement method. This was an attempt to derive a theoretical method for determining the vibrational characteristics of a simplified physical model that had been evaluated experimentally by Clarkson (1965). The model was derived by substituting a rectangular plate under tensile load to simulate the hoop stress of the fuselage. A crack was centrally located and perpendicular to the direction of the applied load. It was found that by using finite elements the effect of the crack could be accurately predicted. The results showed that as the length of the crack grew, the frequency of the fundamental mode of vibration decreased until a point was reached when the free edge of the crack buckled outward permanently, at which point the frequency increased.

In a later investigation, Roman Solecki of the University of Connecticut, published several papers that attempted to derive theoretical relationships between the natural frequencies of a rectangular plate with crack type defects. In one of his earlier papers, Solecki (1980) supplemented a previously derived invariant expression for the amplitude of the displacement of homogenous, isotropic, harmonically vibrating plates with internal rigid supports or cracks.

A few years later, Solecki (1983) considered the natural flexural vibration of a simply supported rectangular plate with a symmetrically located crack parallel to one edge, as shown in Figure 2.1. He analyzed the problem using finite Fourier transformation of discontinuous functions, the unknowns of which were the discontinuities of the displacement and the slope across the crack. Conditional equations were obtained by satisfying the boundary conditions at the cracks's edge by differentiating a Fourier series representing a discontinuous function. He then obtained the characteristic equation in the form of an infinite determinant and used it in comparison with earlier published results.

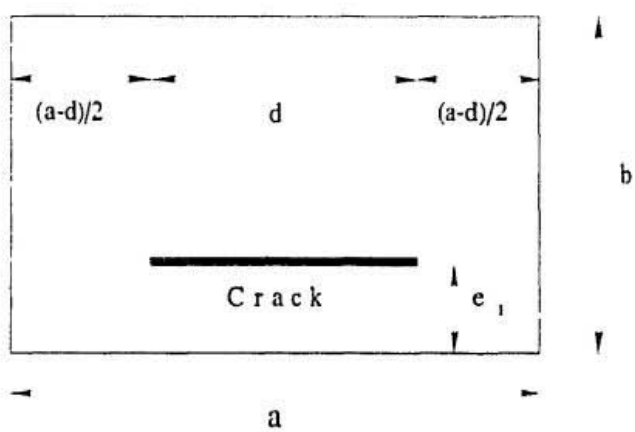

FIGURE 2.1 - SOLECKI'S PLATE

The results obtained showed that the first two frequencies were greatly influenced by the length of the crack and its location on the plate. For d/a = 0.5 the frequency factor for mode 1 dropped by almost 10% as the ratio e_1/a was varied from 0.01 to 0.50. Using the same range of values the frequency factor for mode 2 fell by 9% for e_1/a = 0.20 and rebounded to a 6% drop for e_1/a = 0.50. With e_1/a held constant the ratio d/a was varied from 0.1 to 1, the mode 1 frequency factor dropped by 18% over this range while the mode 2 value fell by 44%.

Continuing to explore these phenomena, Solecki (1985) expanded his technique to solve for an arbitrarily located crack, the first to attempt this complicated problem. Using an expanded form of the methodology derived for the parallel crack he tested his approach on a square plate with a diagonal crack of varying length (d/a ranged from 0 to 1.4). His results for the first three natural frequencies showed significant drops in frequency for each mode, especially mode two, which fell by 72%.

One of the first efforts to use a theoretical approach to determine the location of defects is presented by Stubbs (1990). The author applied a first difference to the homogeneous equations of motion of an undamaged structure to yield expressions for changes in modal stiffness in terms of modal masses, along with changes in modal damping, natural frequencies and mode shapes. In addition, expressions relating variations in stiffness of structural elements to the variations in modal stiffness were generated using matrix structural analysis. The formulation was tested using an Euler-Bernoulli beam and showed that for the beam, the method accurately indicated the crack location.

A more recent study is discussed in Pandey *et al.* (1991) that considered the effect of damage on two beam structures, the first, a simply supported beam, and the second, a cantilever. Here the authors attempted to devise a technique for locating the point of damage by close inspection of the changes in the curvature mode shapes. It was found that the absolute changes in the curvature mode shapes are localized in the region of damage and therefore provided a useful tool for location estimates. The study was carried out using finite element analysis of bear.. element models. The damage was simulated by reducing the modulus of elasticity for one of the beam elements. Each element was first considered in turn so as to move the location of the damage and subsequently a single element was chosen and a variety of levels of damage was evaluated. The results showed that when plotting the absolute difference in curvature mode shape between the cracked and uncracked specimens, a notable peak occurred in the vicinity of the crack.

In a more classical approach Richardson and Mannan (1991) derived expressions for sensitivity functions for mass, stiffness and damping in an attempt to show that it is possible to detect, locate and quantify structural faults by monitoring only frequency and damping. The technique used the orthogonality conditions, for classically damped structures, to derive from established structural dynamics theory, the following stiffness sensitivity equation:

$$\{\phi_k + d\phi_k\}^T [dK] \{\phi_k + d\phi_k\} + 2\{d\phi_k\}^T [K] \{\phi_k\} + \{d\phi_k\}^T [K] \{d\phi_k\} = \omega_{1_k}^2 - \omega_{0_k}^2 \tag{2.1}$$

Similarly, the damping sensitivity equation:

$$\{\phi_k + d\phi_k\}^T [dC] \{\phi_k + d\phi_k\} + 2\{d\phi_k\}^T [C] \{\phi_k\} + \{d\phi_k\}^T [C] \{d\phi_k\} = 2\left(\zeta_{1_k} - \zeta_{0_k}\right) \tag{2.2}$$

And finally the mass sensitivity equation:

$$\{\phi_k + d\phi_k\}^T [dM] \{\phi_k + d\phi_k\} + 2\{d\phi_k\}^T [M] \{\phi_k\} + \{d\phi_k\}^T [M] \{d\phi_k\} = \frac{\omega_{1_k}^2 - \omega_{0_k}^2}{\omega_{1_k}^2} \tag{2.3}$$

where k = 1 ... number of modes

For small changes in ϕ_k, the mode shape does not change significantly,

(ie., $\{d\phi_k\} = \{0\}$) and these equations simplify to

$$\{\phi_k\}^T [dK] \{\phi_k\} = \omega_{1_k}^2 - \omega_{0_k}^2 \tag{2.4}$$

$$\{\phi_k\}^T [dC] \{\phi_k\} = 2(\zeta_{1_k} - \zeta_{0_k}) \tag{2.5}$$

$$\{\phi_k\}^T [dM] \{\phi_k\} = \frac{\omega_{1_k}^2 - \omega_{0_k}^2}{\omega_{1_k}^2} \tag{2.6}$$

In an example using a 3-DOF structure the author made fourteen changes to various stiffness parameters to simulate different fault conditions. The method worked well in verifying the locations of the various changes.

2.1 Experimental Approaches to Defect Detection

Modal analysis is often an inevitable combination of experiment and theory. The preceding discussion showed that even authors approaching defect detection from a purely analytical viewpoint often rely on the experiments of others to verify their results. The discussion that follows, illustrates literature that is far more indicative of the type found in this subject

area. These are papers that discuss either results obtained from a purely experimental approach or the results of a combination of analytical and experimental analysis.

There are two main categories within the realm of experimental analysis that are dependant on the type of structure evaluated. The first category, generally uses simple structures such as plates or beams. This type of experiment generally strives to develop fundamental relationships between modal parameters and structural defects or to test theories pertaining to these relationships. The primary advantage of this type of experiment is the flexibility permitted in evaluating modal parameters over a wide range of frequency and for a number of controlled operating conditions. They are conducted in a lab environment with little possibility of outside interference from external sources.

The second type of experiment uses either real structures or large scale models of real structures. The objective here is generally to discern whether or not derived relationships and theories are applicable to real structures. While the ability to strictly control all aspects of the operating environment is greatly diminished for real structures, this type of experimentation remains invaluable, since only a real structure will behave like a real structure and if this course of research ever hopes to develop a functional NDT method it must be used on a real structure.

2.1.1 Experimentation Using Simple Models

One of the earliest successful attempts to develop a relationship between frequency shift and cracking in cantilever beams is described in Chondros and Dimarogonas (1980). Here the authors performed a number of experiments using both fixed-free (cantilever) beams as well as fixed-fixed beams with welded end connections. Cracks were developed by fatiguing and the progress of the reduction in natural frequency as the crack propagated was monitored. The results were used to develop nomographs that could be used to determine the crack depth from the measured frequency drop. The authors went on to propose a method for implementation of their procedure on real structures suggesting the use of local rather than global modes in inspection techniques. Given the state of portable computer technology of the day this work was very advanced in scope.

A unique attempt to model the effect of cracking on beams is given by Ju and Mimovich (1986) that expands on earlier work by Ju (1982). These authors illustrate how a crack can be represented as a fracture hinge as shown in Figure 2.2. It is shown that the spring constant is dependant only on the damage geometry and not on the crack location. In addition it is illustrated that the changes in frequency can be used to locate the defect on the beam by determining the inflection points of modes that had little notable frequency shift. The results showed that the fracture hinge provided better results than simpler analytic assumptions due to the action of the crack under cyclic loading. The authors highlighted the errors attributable to the difficulty in modelling a true fixed support in addition to the differences between milled "test" cracks and true zero width fatigue cracks.

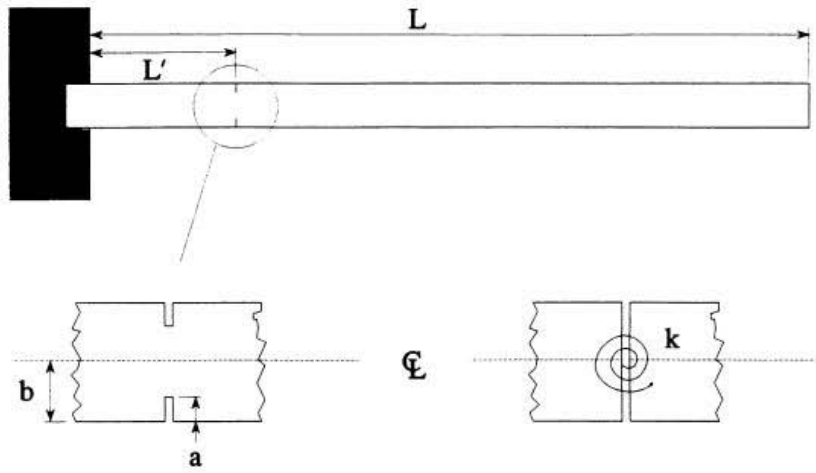

FIGURE 2.2 - JU AND MIMOVICH IDEALIZATION

In Mannan and Richardson (1990) additional work was carried out in an attempt to develop a method for detecting and locating cracks from measured modal parameters as derived from Frequency Response Functions. These authors believed that FRF measurement, along with subsequent processing, was the superior method of modal parameter estimation. In support of this argument, they listed the following advantages:

- A variety of multi-input/multi-output FFT analyzers are commercially available for making FRF measurements.
- A variety of broad band excitation methods can be used, employing low level random, sine, or transient signals.
- Measurement noise can be removed by using frequency domain averaging methods.
- Non-linear motion (distortion) of the structure can be removed by using random excitation and averaging.

- Acceleration responses, which are typically measured, are easily converted to displacement responses without approximations.
- A variety of single and multiple reference estimation techniques are available for obtaining modal parameters from FRF's.

The computational method employed, involved using the mass, damping, and stiffness matrices as defined for a lightly damped structure. These matrices are square and of a dimension equal to the number of DOF's in the system. As such they can be computed from measured data containing all DOF's and are not dependant on measurement of any predefined number of modes although a minimum is required to ensure accuracy. Computation of these matrices from experimental data allowed comparison of a test specimen before and after the introduction of a defect. It was found that the largest differences in the matrices were localized in the area of the defects. Another notable result was the determination that higher modes were found to be better predictors of crack existence and location, and governed the structural stiffness.

Another notable research team, A.J.M. Araújo Gomes, and J.M. Montalvão e Silva of Portugal have produced numerous papers that report the findings of their research into defect detection using modal analysis. In Araújo Gomes and Montalvão e Silva (1990), results are presented that concern the dynamic behaviour of a cracked, free-free straight beam, with rectangular cross-section. The beams were analyzed theoretically using Ju's fracture hinge method, and tested experimentally using specimens with both thin (0.2 mm.) simulated cracks, cut with a milling machine, as well as with real fatigue cracks. Measurements were carried out for both in-plane, and out-of plane bending. The primary

purpose of this experimentation was simply to show that the effects of cracking could be accurately and precisely determined from experimental data. This extensive evaluation looked at four crack depths ranging from 1/8 the beam depth to 1/2 the beam depth in increments of 1/8, in each of four different locations (from Fig. 2.2, L'/L = 1/8, 1/4, 3/8 & 1/2). In addition a series of beams were fatigued sufficiently to develop real cracks and these were tested as well. The results clearly showed that the change in natural frequency was highly dependant on both the location of the crack and the particular mode being considered. It also showed that the effect of a milled crack was indeed representative of the effect of a real crack.

These authors continued to expand on their work and in Araújo Gomes and Montalvão e Silva (1991) presented the findings of an extensive experimental and analytical evaluation that observed the effects of real fatigue cracks on 0.8 m long free-free beams with three different square cross-sections. In total 60 beams were tested in both planes of bending to determine the effect of cracking in each of 5 different crack locations (L'/L = 1/10, 1/5, 3/10, 2/5 & 1/2) with four levels of crack depth ratios (1/6, 1/3, 1/2, 2/3). Additionally these authors presented a detailed derivation of the torsional spring model showing how it could be used to determine from theory the natural frequencies of a cracked beam. The spring constant k, alluded to previously, was shown to be

$$k = \frac{2EI^2}{\pi h d^2(1 - \nu^2) \int_o^p p \left[f\left(\frac{p}{d}\right)\right]^2 dp} \qquad (2.7)$$

where

E = Young's Modulus

I = Moment of Inertia of Cracked Section

h = width of beam

d = depth of beam

p = depth of crack

ν = Poisson's Ratio

and

$$f\left[\frac{p}{d}\right] = 1.222 - 1.40\left[\frac{p}{d}\right] + 7.33\left[\frac{p}{d}\right]^2 - 13.08\left[\frac{p}{d}\right]^3 + 14.00\left[\frac{p}{d}\right]^4 \quad (2.8)$$

The authors used this expression along with their formulation to derive theoretical values for each of the tested beams. The results showed reasonable correlation between experimental measurements and theoretical predictions. In addition it was shown that the natural frequencies of larger beams were affected more by cracking than were smaller beams. For all beams, both theory and experiment showed that the sensitivity of the change in frequency to crack depth increased for the larger cracks and additionally that as the crack depth increased, some modes became more sensitive than others.

The most current work by these authors is presented in Araújo Gomes and Montalvão e Silva (1992) and Montalvão e Silva and Araújo Gomes (1992). Here the authors shift their attention to the analysis of cantilever, rather than free-free, beams. These papers present the results of their attempt to modify their previously developed theoretical procedures for use on a cantilever with a lumped end mass and an axial load. Additionally they present for

comparison, their findings of experimentation on this type of specimen, which they tested both in air and immersed in water. This latter experiment was performed to determine the extent of change that could be expected from water immersion alone and additionally to determine how the effect of cracking in beams is moderated by immersion. The results of this program showed that the existence of a crack in a cantilever caused its frequencies to change in a way that could be easily measured even when the crack was close to the free end. The addition of the end mass, however, tended to decrease the sensitivity to cracking especially for cracks near the free end. Additionally, it was determined from these results that while immersion in water does tend to decrease the natural frequencies, the effect is small and tends to disappear when the end mass is large. The authors attributed this small effect to the stiffness of their beams.

2.1.2 Experimentation Using Real Structures

Analysis of real structures is often very different from that of simple structures. Simply determining the modes of real structure can be a forbidding task due to the vast number of modes that exist. A typical structure is in reality made up from simple structures (ie. beams, plates, etc.) and as such all the modes of these simple structures also become local modes of the real structure. There are, in addition to these local modes, global modes where the motion involves the entire structure. It is these global modes that are generally considered to be of primary importance to this type of experimentation but the task of distinguishing them from the numerous local modes can often be a challenge, one that must be carefully performed to ensure the applicability of results. The following discussion

highlights a representative selection of literature that has been produced as a result of experimentation on real structures[1].

Illustration of the usefulness of testing a scaled model of a real structure was presented in Shahrivar and Bouwkamp (1986). The model used for this research was a 1/50th scale plastic model that represented the structural system of a typical full scale tower in 66m of water. This experimentation sought to determine the effects of severance of diagonal bracing members on selected vibration frequencies and mode shape parameters. To illustrate the distinctiveness of the parameter shifts resulting from damage, additional tests were carried out to determine and compare the parameter changes resulting from the addition in deck mass, jacket mass, and deck mass eccentricity. The procedure used finite element analysis in combination with test results and found the two to correlate quite well. Significant useful observations were made from the results of the program; in abbreviated format, these are as follows:

- Damage in the structure is detectable from surface measurements only, ie., no underwater instrumentation was necessary.
- The most significant indicator of damage was deck displacement (ie. mode shape) which proved much more sensitive to damage than did the observed frequency shifts.
- The characteristics of the damage induced changes were insensitive to deck loading and loading eccentricity.

---

[1] Included in the definition of real structures are large scale models of real structures since they generally represent as much complexity as their prototypes.

- The changes observed as a result of damage were easily distinguishable from those resulting from changes in loading conditions. Observations showed that while displacement differences could be similar, corresponding frequency shifts were not. Additionally, normalized displacement at the deck extremes showed distinct differences.

Successful results using model structures were also obtained by Debao *et al.* (1992). They presented a method that not only detected, but also located, a defect using only one row and one column of the FRF matrix. The procedure used a successively deduced least squares method to determine stiffness changes using data at the half-power points of FRF's for a given mode. In testing the theory on test results from a 1/30 scale jacket type structure, it was shown that performing the iterative method on various structural elements quickly deduced the defective member.

It is of obvious importance in this domain of research to be able to perform these experiments on actual structures. One of the most difficult aspects of performing modal analysis on a real structure is the ability to provide controlled excitation of sufficient magnitude to excite a response in the structure. Notwithstanding the difficulty involved, various programs of research have successfully accomplished this feat. In Chiarito and Mlakar (1984), for instance, a concrete gravity dam was exited by inertial force provided by a 17000 lb mass attached to a hydraulic actuator. In Haynes (1986) a step unloading excitation was used to test a concrete light-pier by plucking the structure with a winched cable attached to the structure through a v-notched bolt of known strength. Loading the structure until the bolt failed in tension provided the impetus for dynamic motion. Using

this technique provided static loads of up to 450 kN at the break point of the bolt. Another example is given in Ohlsson (1986) when a suspension bridge with a 366 m span was tested. Here the exciter was a motor/gear driven eccentric wheel that moved a 3 ton mass up and down as it rotated.

Other authors have approached this matter differently in that they did not use any form of physical excitation. In White and Pardoen (1987) for instance one of the towers of the Golden Gate Bridge was analyzed using traditional FRF analysis. The input selected for analysis was actually the output of one of the deck mounted accelerometers. The method, while not perfect, did produce usable results.

Another example of non-forced experimentation is given in Kopff (1987). Here an attempt was made to test a 130m tall, 30000 ton, cooling tower. The method used here was the Random Decrement Signature Analysis [this theory is presented in Cole (1973) and further elaborated upon in Li-Chung (1985)] that allows the determination of direct or cross frequency response functions. This author illustrated the use of this method and highlighted it potential for defect detection through the accurate determination of modal parameters for this huge structure.

As the methodology of modal analysis for crack detection in real structures is refined, there is a growing realization that the use of this method relies on an accurate theoretical prediction for comparison purposes. In this regard, no other analytical tool has proved as powerful as the finite element method in predicting structural behaviour. Numerous authors have focused their research solely on improving correlation between test and finite element

results. In Stimpson and Griffith (1982) as well as in Blakely (1982) the result of experimentation was used to improve an analytical model by refining boundary conditions. Ramsey and Firmin (1982) compared results from experiment and finite element analysis and showed that it could be accomplished using a desktop computer. In Dobson (1984) and in Sidhu and Ewins (1984) validation studies were carried out to improved correlation by using modal parameters to modify finite element matrices.

While this type of work was considered useful in the earlier days of this investigation (during the mid to late 1980's), newer work began to look specifically at this partnership in light of damage detection. Springer *et al.* (1990) conducted an extensive set of experiments with analytical comparison using a boxbeam structure. Here the structural response was measured at 40 different locations to define the effects of multiple damage levels at six locations. The work showed that the finite element method was a valid predictor of experimental results.

Extensive work was also carried out by Lopes and Raposo (1991) who used data from an operating offshore structure to improve their model's prediction of modal changes resulting from fatigue damage. The method used a computer algorithm based on Bayesian Parameter Identification to obtain better numerical representation. The authors were able to obtain some promising results in the detection of fatigue damage, but admitted that additional work was still necessary.

Experimental and analytical prediction of damage detection using classical modal analysis is now a very large part of modal analysis research. Literature on this subject is increasing

at an exponential rate, primarily as a result of the International Modal Analysis Conferences that are held on a yearly basis. Continued exploration of this literature could fill many volumes equal in size to this thesis. In the effort of space conservation, the literature presented thus far will suffice as a representation of the current state of work in this field. The remaining section of this chapter is devoted to reviewing a limited selection of papers dealing with the measurement of strain as a response parameter in modal analysis.

2.3 Modal Testing Utilizing Strain Measurements

In recent studies a number of researchers have attempted to use dynamic measurement of strain in the determination of modal parameters. Obviously, the parameters of frequency and damping are not affected, but the amplitude of the measured signal, however, used in determining the mode shapes, is a completely independent variable that behaves very differently from displacement or acceleration.

An early exploration of the uses of strain measurement in modal analysis is described by Zhang *et al.* (1986). These authors used cantilever beams with notches cut near the fixed end, to compare results obtained through the classical method of acceleration measurement and those obtained through strain measurement. The results of the experimentation clearly showed that good results could be obtained using strain gauges. The discussion of changes in the measured parameters as a result of cracking was limited to frequency drop and changes in mode shape. The results from both sets of measurements showed significant changes in mode shape, both from displacement and strain measurements.

A very useful application of modal analysis with both strain and acceleration measurements for solving a repetitive defect problem is reported by Powel and Goldberger (1990). These authors reported on a continuing problem with a finned-tube heat exchanger that developed cracks around weld points. Here the analysis was not used to find the defect, but rather to determine why it was occurring and to recommend remedial measures. The results from both sets of transducers confirmed that excitation caused by vortex shedding of fluid, in the exchanger, excited the primary mode of the structure resulting in extremely high dynamic stress levels. While the problem was subsequently solved as a result of the test, it also confirmed the applicability of strain measurement in modal analysis.

A modelling approach based on experimental strain measurements is presented in Tsang (1990). This author approached the development of an analytical procedure entirely from the strain measurement aspect. The theory focused on deriving a set of governing system matrices from experimental measurements. The author first derived proposed methodology through finite element modelling followed by a computer simulation experiment and a practical test using real data. The method proved quite reliable in a number of cases although the author admits a more rigorous proof, combined with additional experimental research, is necessary.

Recent research in damage detection was reported in Swamidas and Chen (1992). These authors conducted modal testing on a 9m tall, 1/50th scale model of a tripod tower platform (TTP). The measured parameters included acceleration, displacement (using LVDT's), along with strain, at numerous sites on the structure. The primary focus of this test was to determine the effect of simulated damage on the modal parameters of the structure and to

compare the various modes of response measurement. Typical results were obtained in terms of frequency changes, and additionally it was concluded that the measurement of strain was an appropriate measurement parameter and particularly useful when the measurement site was close to the site of damage.

The work by these and other authors in strain based modal analysis has increased interest in this form of response measurement. It is likely that the volume of literature on this subject will increase over the next few years as larger numbers of current researchers look into this relatively new field of testing.

2.4 Summary

This concludes the literature review portion of this thesis. This presentation, while only a sample of the existing body of literature, is thought to contain an adequate overview of aspects of current and past research into modal analysis and its applications in defect detection in structures. Chapter 3, which follows, precedes the discussion of results obtained by this author, with an overview of applicable theory concerning modal analysis and selected topics from structural dynamics.

Chapter 3

Review of Theory

The theoretical approach to vibrational analysis is conducted in three stages. These must be evaluated in order to characterize completely the properties of a vibrational system.

First, the system must be described in terms of its physical characteristics. The three primary characteristics, important to all vibrational analysis, are: *mass*, *stiffness*, and *damping*. Each of these must be defined according to the physical geometry of the system in order to determine its vibrational characteristics. This level of characterization leads to the definition of the *spatial model* for the system.

The second stage involves performing a numerical analysis to determine the fundamental vibrational characteristics of the system. This leads to a description in terms of its natural frequencies of vibration, corresponding mode shapes and damping factors. The system as described in this manner is called a *modal model*, and is used to illustrate the various normal modes, which characterize the structure during free vibration, ie., vibration without the application of external force.

The third stage is the determination of the response characteristics of the system to an applied force. Here the system in analyzed to determine the various displacement amplitudes and deformation characteristics that will occur as a result of the application

of a time varying force, defined in terms of its magnitude and frequency. The system is thereby described in terms of a *response model*. There are of coarse an infinite number of response models due to the infinite number of variations that can be made to the forcing function. The function chosen must illustrate the particular type of analysis that is to be undertaken. A broad multi-frequency force might be useful to find the frequency response functions (FRFs) over a range covering several natural modes, or a more refined function may be used to simulate the vibrational characteristics due to the service loads that the physical system may be exposed to.

The theoretical analysis of the current research was carried out using the finite element module of the integrated analysis program, I-DEAS™, produced and marketed by Structural Dynamics Research Corporation (SDRC), of Milford, Ohio. Likewise, the experimental data manipulation and analysis was carried out by the test data analysis module of the same program. The data acquisition, performed during the experimental phase of this research, was accomplished using a locally written program which interacted with the acquisition hardware. A second locally written program manipulated the data into a format compatible with the I-DEAS software. Using these tools, this research investigated a number of phenomena relating to the use of modal analysis in crack detection. In an attempt to provide an insight into the subsequent presentation of these analytical and experimental results, several topics concerning vibr ional theory, relevant to issues at hand, are discussed in the following sections of this chapter. These sections emphasize topics specifically related to modal analysis both from analytical and experimental viewpoints.

3.1 General Analysis of Spring-Mass-Damper Systems

In a typical system consisting of multiple degrees of freedom, there is one equation of motion for each degree of freedom, of which there are an equal number of normal modes. These equations are expressed in a matrix format that separates the various components of mass, stiffness, and damping. Using this format the basic equation of motion is

$$[M]\{\ddot{x}\} + [C]\{\dot{x}\} + [K]\{x\} = \{f\} \tag{3.1}$$

Here $[M]$, $[C]$, and $[K]$ refer to the mass, damping and stiffness matrices respectively, and $\{\ddot{x}\}$, $\{\dot{x}\}$, and $\{x\}$ refer to the column vectors for acceleration, velocity, and displacement, respectively. The term $\{f\}$ is the column vector of forces acting on the system. While this expression describes the general behaviour of a complete system, the first step in MDOF analysis is to find the natural frequencies and mode shapes of the system. This is accomplished by finding the eigenvalues and eigenvectors of an undamped, free vibration system expressed in matrix format. To do this, it is necessary to derive the general solution to the MDOF system as given by Equation (3.1). The equation for undamped, unforced, motion is

$$[M]\{\ddot{x}\} + [K]\{x\} = 0 \tag{3.2}$$

The most general solution of the equation is to assume that the displacement of any given mass is comprised of a time varying unit function (which is common to all coordinates) multiplied by an amplitude scale factor (which varies from location to location). This is written as

$$x_i(t) = \phi_i q(t), \quad i = 1,2,\ldots n \tag{3.3}$$

where

ϕ_i = a constant applicable to coordinate i.

$q(t)$ = a time function common to all coordinates

If the ratio of two displacement coordinates x_i and x_j is determined, the result shows that the deflection shape is independent of time. In other words all coordinates have synchronous motion and during single mode oscillation, while the amplitude of displacement varies with time, the pattern or shape of deformation does not. This effectively defines the mode shape of a system as being comprised of a vector of time invariant amplitudes, written as

$$\{\phi\} = \begin{Bmatrix} \phi_1 \\ \phi_2 \\ \cdot \\ \cdot \\ \cdot \\ \phi_n \end{Bmatrix} \tag{3.4}$$

Substituting Equation (3.3) into Equation (3.2) yields

$$[M]\{\phi\}\ddot{q}(t) + [K]\{\phi\}q(t) = 0 \tag{3.5}$$

Which can be written in scalar form as n separate equations:

$$\left[\sum_{j=1}^{n} m_{ij}\phi_j\right]\ddot{q}(t) + \left[\sum_{j=1}^{n} k_{ij}\phi_j\right]q(t) = 0, \quad i = 1,2,\ldots,n \tag{3.6}$$

From which we obtain

$$-\frac{\ddot{q}(t)}{q(t)} = \frac{\sum_{j=1}^{n} k_{ij}\phi_j}{\sum_{j=1}^{n} m_{ij}\phi_j}, \quad i = 1,2,\ldots,n \tag{3.7}$$

Considering this result, it is obvious that the left hand side is independent of the coordinate i (a length parameter), while the right hand side is independent of time. Both sides, therefore, must be equal to a constant that is taken as ω^2. Equation (3.7) can then be rewritten as

$$\ddot{q}(t) + \omega^2 q(t) = 0 \tag{3.8}$$

for the left hand side, and for the right hand side as

$$\sum_{j=1}^{n} \left(k_{ij} - \omega^2 m_{ij}\right)\phi_j = 0, \quad i = 1,2,\ldots,n \tag{3.9}$$

or using matrix notation as

$$([K] - \omega^2[M])\{\phi\} = \{0\} \tag{3.10}$$

In order for this equation to hold true either $([K] - \omega^2[M])$ or $\{\phi\}$ must be zero. The solution that has all the ϕ values set to zero will satisfy the equation but it will yield no usable results. Therefore, for non-trivial solution the following expression, must hold true,

$$\left|[K] - \omega^2[M]\right| = 0 \tag{3.11}$$

Which states that the determinant of the matrix resulting from the difference must equal zero. The solution of this expression will yield the eigenvalues (ie., the natural frequencies, ω_i) of the system. The $\{\phi\}$ vector (ie., the mode shapes or eigenvectors) cannot be solved

for uniquely due to the singularity of the ($[K]$ - $\omega^2[M]$) matrix. As a result, the eigenvectors are derived by setting one of the mode shape constants (usually $\{\phi_1\}_i$) equal to 1 and solving for the others in terms of it.

For the general case where $\omega_i \neq \omega_j$, it can be shown that the modal vectors $\{\phi\}_i$ and $\{\phi\}_j$ are orthogonal with respect to both mass and stiffness, ie.,

$$\{\phi\}_j^T [M] \{\phi\}_i = \{0\} \quad , \quad i \neq j \tag{3.12}$$

$$\{\phi\}_j^T [K] \{\phi\}_i = \{0\} \quad , \quad i \neq j \tag{3.13}$$

In the case where $\omega_i = \omega_j$, substitution into Equations (3.12) and (3.13) results in the formulation of the generalized mass and stiffness coefficients of the i^{th} mode

$$\overline{M_{ii}} = \{\phi\}_i^T [M] \{\phi\}_i \quad , \quad i = 1,2, \ldots ,n \tag{3.14}$$

$$\overline{K_{ii}} = \{\phi\}_i^T [K] \{\phi\}_i \quad , \quad i = 1,2, \ldots ,n \tag{3.15}$$

The modal matrix, $[\phi]$ is often mass normalized such that

$$[\phi]^T [M] [\phi] = [I] \tag{3.16}$$

where $[I]$ is the identity matrix. In this case, the mass normalized stiffness matrix becomes

$$[K] = [\omega^2] = \begin{bmatrix} \omega_1^2 & & & \\ & \omega_2^2 & & \\ & & \ddots & \\ & & & \omega_n^2 \end{bmatrix} \tag{3.17}$$

In future reference to distinguish this special case, $[\phi]$ will refer to an un-normalized modal matrix and $[\Psi]$ will refer to a mass normalized modal matrix.

For most general cases the mass and stiffness matrix are non-diagonal and have non-zero terms in locations other than along their diagonals. This indicates that the system's modes are coupled and cannot be treated independently. It is said to have *inertial coupling* if the mass matrix is non-diagonal and *dynamic coupling* if the stiffness matrix is non-diagonal. Previous discussion showed how orthogonality is used to diagonalize both the system matrices for an unforced system but did not treat the more general case of forced systems.

Consider first that the mode shape vectors (eigenvectors) of a system are linearly independent due to the orthogonality condition. In other words, no eigenvector of the system can be obtained by a linear combination of the others. Hence, they form a *basis* in *n-dimensional* space. This means that any other vector in the n-dimensional space can be made up of a linear combination of n linearly independent vectors. Consider an arbitrary vector $\{x\}$ in n-dimensional space, expressed as

$$\{x\} = \sum_{i=1}^{n} c_i \{\phi\}_i \tag{3.18}$$

where c_i are constant scale factors, whose values can be determined by pre-multiplying this equation by the transpose of the modal vectors;

$$c_i = \frac{\{\phi\}_i^T [M]\{x\}}{\{\phi\}_i^T [M]\{\phi\}_i} = \frac{\{\phi\}_i^T [M]\{x\}}{\overline{M_{ii}}} \qquad i = 1,2,\ldots,n \tag{3.19}$$

where $\bar{M}_{ii}$ is the generalized mass of the i^{th} normal mode. In the case where the modal vectors are mass normalized the previous equation can be written as

$$c_i = \{\psi\}_i^T [M] \{x\} \frac{1}{\sqrt{\bar{M}_{ii}}} \tag{3.20}$$

This represents what is known as the *expansion theorem*, a useful device in determining system response to arbitrary forcing conditions.

Consider then the case of an undamped system which has external forces acting on it. The equations of motion can be written as

$$[M]\{\ddot{x}\} + [K]\{x\} = \{f\} \tag{3.21}$$

where $\{f\}$ is a vector of arbitrary external forces.

Solving the eigenvalue problem will result in the determination of n natural frequencies, $(\omega_1, \omega_2, \ldots, \omega_n)$ and a series of n modal vectors $\{\phi\}_i$ which are subsequently compiled into a modal matrix (of size n × n). Using the expansion theorem, the solution of the system can be written as a linear combination of the normal mode vectors:

$$\{x(t)\} = [\phi]\{q(t)\} \qquad \textit{where} \qquad \{q(t)\} = \begin{Bmatrix} q_1(t) \\ q_2(t) \\ . \\ . \\ q_n(t) \end{Bmatrix} \tag{3.22}$$

where $q_1(t) \ldots q_n(t)$ are time dependant generalized coordinates, called *modal participation factors*.

Since we know that the modal matrix is independent of time, the second time derivative of displacement must equal the second derivative of the time dependant participation factors multiplied by the modal matrix. The equations of motion can then be written as

$$[M][\phi]\{\ddot{q}\} + [K][\phi]\{q\} = \{f\} \tag{3.23}$$

Pre-multiplying by the transpose of the modal matrix $[\phi]^T$, and assuming the modal matrix to be mass normalized yields the general equation of motion in the form

$$\{\ddot{q}(t)\} + [\omega^2]\{q(t)\} = \{Q(t)\} \tag{3.24}$$

where $\{Q(t)\}$ is the vector of generalized forces $[\psi]^T\{F\}$.

The equations of motion have now been uncoupled, resulting in a set of n independent SDOF equations:

$$\ddot{q}_i(t) + \omega_i^2 q_i(t) = Q_i(t) \qquad i = 1, 2, \ldots, n \tag{3.25}$$

3.2 The Effect of Damping on Structural Response

The analysis as presented thus far is applicable only to systems which are undamped. This type of analysis is used quite often since in many cases damping values are small enough that their inclusion can be considered negligible. In other cases, however, if the system response is required for long periods of time with respect to the natural periods of the system, the effect of damping must be included. In addition the effect of damping becomes vitally important when considering system response to dynamic forces with a frequency close to one of the natural frequencies of the system.

There are in general two types of damping, the first of which is called *viscous* damping, and the second, *hysteretic* or *structural* damping. The first of these is the standard type of damping usually considered in dynamic problems; it is defined as being linearly proportional to velocity and is typical of the type of damping that would be provided by a dashpot. The second type of damping, hysteretic, is somewhat different and is more dependant upon the material properties of the structural members. It is defined as the dissipation of energy due to cyclic stress that through a given cycle traces a hysteresis loop. While both are slightly different the analysis which includes damping is derived in a similar manner; hence, for illustration purposes, only viscous damping will be dealt with here.

The general expression for a viscously damped system with external excitation was given in Equation (3.1). To introduce this topic we will first of all assume that the damping matrix $[C]$ specifies a special type of damping known as *proportional damping*, a situation where the damping matrix is linearly proportional to the mass and or stiffness matrix.

This is generally written as

$$[C] = \alpha[M] + \beta[K] \tag{3.26}$$

Where the terms α and β are constants.

The equations of motion can then be rewritten as

$$[M]\{\ddot{x}\} + [\alpha[M] + \beta[K]]\{\dot{x}\} + [K]\{x\} = \{f\} \tag{3.27}$$

If as before, we express the solution vector $\{x(t)\}$ as a linear combination of the modal vectors of the system, Equation (3.27) can be written as

$$[M][\phi]\{\ddot{q}(t)\} + [\alpha[M] + \beta[K]][\phi]\{\dot{q}(t)\} + [K][\phi]\{q(t)\} = \{f(t)\} \tag{3.28}$$

Pre-multiplication of this result by the mass normalized modal matrix will then yield

$$[I]\{\ddot{q}(t)\} + [\alpha[I] + \beta[\omega^2]]\{\dot{q}(t)\} + [\omega^2]\{q(t)\} = \{Q(t)\} \tag{3.29}$$

which can be written as a system of independent equations as

$$\ddot{q}_i(t) + (\alpha + \omega_i^2\beta)\dot{q}_i(t) + \omega_i^2 q_i(t) = Q_i(t) \qquad i = 1,2,\ldots,n \tag{3.30}$$

If the following substitution is made:

$$\alpha + \omega^2\beta = 2\zeta_i\omega_i \tag{3.31}$$

Equation (3.30) can be rewritten as

$$\ddot{q}_i(t) + 2\zeta_i\omega_i\dot{q}_i(t) + \omega_i^2 q_i(t) = Q_i(t) \qquad i = 1,2,\ldots,n \tag{3.32}$$

It is therefore seen that for this special case of damping, the uncoupling of the matrices is possible. Here, as before, the n equations can be treated independently and solved as damped SDOF systems.

As is often the case for real systems, the damping matrix is not proportional and cannot be diagonalized as shown in the above derivation. The occurrence of non-proportional damping generally results in eigenvalues which are either negative real, or complex with negative real parts. In the latter case both the eigenvectors and the eigenvalues exist as conjugate pairs. In handling cases like this a common procedure is to transform n coupled second order differential equations into $2n$ uncoupled first order equations.

3.3 Frequency Response Function Analysis

The theories presented thus far are typically concerned with finding the modal parameters of an analytical system. In modal analysis a common objective is to verify analytical models using results from experimentation. A common link between the theoretical solution to a system and results obtained through experimentation is called the *Transfer Function*, otherwise known as the *Frequency Response Function (FRF)*. The fundamental description of the FRF is the complex frequency domain ratio of response output to force input. To help bridge the gap between theory and experimentation it is appropriate to discuss this topic and to develop a general expression for the FRF of a MDOF system.

Consider the expression for an undamped system:

$$[M]\{\ddot{x}\} + [K]\{x\} = \{F\} \tag{3.33}$$

The transformation of this equation into the Laplace domain yields

$$\left[s^2[M] + [K]\right]\{X(s)\} = \{F(s)\} \tag{3.34}$$

where s is the Laplace variable which can be shown to be equal to $i\omega$.

If we let $[B(s)] = [s^2[M] + [K]]$ then the equation becomes

$$[B(s)]\{X(s)\} = \{F(s)\} \tag{3.35}$$

where $[B(s)]$ is sometimes referred to as the system impedance matrix. If we now pre-multiply the latter equation by $[B(s)]^{-1}$ we obtain

$$[B(s)]^{-1}\{F(s)\} = \{X(s)\} \tag{3.36}$$

and by letting $[H(s)] = [B(s)]^{-1}$

$$[H(s)]\{F(s)\} = \{X(s)\} \tag{3.37}$$

where $[H(s)]$ is referred to as the *Transfer Function Matrix*.

To further illustrate the components of this matrix consider the expression for a two degree of freedom system:

$$\begin{bmatrix} M_{11} & M_{12} \\ M_{21} & M_{22} \end{bmatrix} \begin{Bmatrix} \ddot{x}_1 \\ \ddot{x}_2 \end{Bmatrix} + \begin{bmatrix} K_{11} & K_{12} \\ K_{21} & K_{22} \end{bmatrix} \begin{Bmatrix} x_1 \\ x_2 \end{Bmatrix} = \begin{Bmatrix} F_1 \\ F_2 \end{Bmatrix} \tag{3.38}$$

In the Laplace domain this becomes

$$\left[\begin{bmatrix} M_{11} & M_{12} \\ M_{21} & M_{22} \end{bmatrix} s^2 + \begin{bmatrix} K_{11} & K_{12} \\ K_{21} & K_{22} \end{bmatrix} \right] \begin{Bmatrix} X_1(s) \\ X_2(s) \end{Bmatrix} = \begin{Bmatrix} F_1(s) \\ F_2(s) \end{Bmatrix} \tag{3.39}$$

thus the matrix $[B]$ is defined as

$$[B] = \begin{bmatrix} M_{11}s^2+K_{11} & M_{12}s^2+K_{12} \\ M_{21}s^2+K_{21} & M_{22}s^2+K_{22} \end{bmatrix} \tag{3.40}$$

and the Transfer Matrix $[H]$ as

$$[H(s)] = \frac{\begin{bmatrix} M_{22}s^2+K_{22} & -(M_{21}s^2+K_{21}) \\ -(M_{12}s^2+K_{12}) & M_{11}s^2+K_{11} \end{bmatrix}}{(M_{11}s^2+K_{11})(M_{22}s^2+K_{22}) - (M_{21}s^2+K_{21})(M_{12}s^2+K_{12})} \tag{3.41}$$

The numerator of this equation is the adjoint of the $[B]$ matrix, while the denominator is the determinant of the $[B]$ matrix, from which the system's characteristic equation is derived. Therefore Equation (3.41) can be written as

$$[H(s)] = \frac{Adj[B(s)]}{|B(s)|} \tag{3.42}$$

This highlights the fact that the modal frequencies (usually complex, designated as λ) are global properties of the system since s, appears in every term of $[H(s)]$. This characteristic equation can alternately be expressed as a product of its roots:

$$|B(s)| = E(s-\lambda_1)(s-\lambda_2)(s-\lambda_3)(s-\lambda_4) \tag{3.43}$$

where $|B(s)|$ is the determinant of the $[B]$ matrix expressed by constant E and the four roots λ_1 through λ_4.

In general the roots form complex conjugate pairs such that $\lambda_2 = \lambda_1^*$, and $\lambda_4 = \lambda_3^*$. The equations of motion can then be written as

$$\begin{Bmatrix} X_1(s) \\ X_2(s) \end{Bmatrix} = \left[\frac{\begin{bmatrix} M_{22}s^2+K_{22} & -(M_{21}s^2+K_{21}) \\ -(M_{12}s^2+K_{12}) & M_{11}s^2+K_{11} \end{bmatrix}}{E(s-\lambda_1)(s-\lambda_1^*)(s-\lambda_3)(s-\lambda_3^*)} \right] \begin{Bmatrix} F_1(s) \\ F_2(s) \end{Bmatrix} \tag{3.44}$$

Hence the transfer matrix for this 2 DOF system can be expressed as

$$[H(s)] = \begin{bmatrix} H_{11}(s) & H_{12}(s) \\ H_{21}(s) & H_{22}(s) \end{bmatrix} \tag{3.45}$$

If this expression for the transfer function is then substituted back into the equation of motion the result is two equations, one for X_1 and the other for X_2.

Written as:

$$H_{11}(s)F_1(s) + H_{12}(s)F_2(s) = X_1(s) \tag{3.46a}$$

$$H_{21}(s)F_1(s) + H_{22}(s)F_2(s) = X_2(s) \tag{3.46b}$$

If $F_2(s)$ is set to zero we can write

$$H_{11}(s)F_1(s) = X_1(s) \tag{3.47a}$$

$$H_{21}(s)F_1(s) = X_2(s) \tag{3.47b}$$

or

$$H_{11}(s) = \frac{X_1(s)}{F_1(s)} \tag{3.48a}$$

$$H_{21}(s) = \frac{X_2(s)}{F_1(s)} \tag{3.48b}$$

which can be expressed in general format as

$$H_{ij}(s) = \frac{X_i(s)}{F_j(s)} \tag{3.49}$$

where i is the coordinate at which the response is determined and j is the coordinate at which the force is applied.

This generalized expression shows that to measure a column of the transfer matrix the location of the force input does not need to vary, only the location at which response is measured needs to vary. Alternately, to measure a row of the matrix, the response location is fixed while the force input location is varied.

To derive the general expression for the transfer function between two points consider an element of the transfer matrix. Recalling that in general, the roots of the characteristic equation appear as complex conjugates, the expression for H_{11} can be written as

$$H_{11} = \frac{M_{22}s^2 + K_{22}}{E(s-\lambda_1)(s-\lambda_1^*)(s-\lambda_2)(s-\lambda_2^*)} \tag{3.50}$$

This expression can be expanded by partial fractions and written as

$$H_{11} = \frac{X_1(s)}{F_1(s)} = \left[\frac{c_1}{(s-\lambda_1)} + \frac{c_2}{(s-\lambda_1^*)} + \frac{c_3}{(s-\lambda_2)} + \frac{c_4}{(s-\lambda_2^*)} \right] \tag{3.51}$$

Values of the constants c_i can be evaluated by equating the previous two equations, multiplying by $(s - \lambda_i)$ and evaluating the result at $s = \lambda_i$. For c_1 this manipulation yields

$$c_1 = \frac{M_{22}\lambda_1^2 + K_{22}}{E(\lambda_1-\lambda_1^*)(\lambda_1-\lambda_2)(\lambda_1-\lambda_2^*)} = A_{11}^1 \tag{3.52}$$

and similarly for c_2

$$c_2 = \frac{M_{22}\lambda_1^{2*} + K_{22}}{E(\lambda_1^*-\lambda_1)(\lambda_1^*-\lambda_2)(\lambda_1^*-\lambda_2^*)} = c_1^* = A_{11}^{1*} \tag{3.53}$$

The term A is used here to denote what is called the *modal residue*, or as some call it the *modal constant*, associated with the pole λ_r. The preceding result can also be applied to c_3 and c_4, yielding A_{11}^2 and A_{11}^{2*}.

Equation (3.51) can then be expressed as

$$H_{11} = \frac{X_1(s)}{F_1(s)} = \frac{A_{11}^1}{(s-\lambda_1)} + \frac{A_{11}^{1*}}{(s-\lambda_1^*)} + \frac{A_{11}^2}{(s-\lambda_2)} + \frac{A_{11}^{2*}}{(s-\lambda_2^*)} \tag{3.54}$$

Expanding this derivation to an n degree of freedom system it can be shown that the most general expression for the transfer function is written as

$$H_{ij} = \sum_{r=1}^{n} \frac{A_{ij}^r}{s-\lambda_r} + \frac{A_{ij}^{r*}}{s-\lambda_r^*} \tag{3.55}$$

where the s and λ_r can be equated as

$$s = i\omega \tag{3.56}$$

and

$$\lambda_r = -\zeta_r\omega_r \pm i\omega_r\sqrt{1-\zeta_r^2} \tag{3.57}$$

3.4 Experimental Curve-Fitting Procedures

The discussion thus far has dealt with modal analysis theory, purely from an analytical approach. While understanding this theory is important it must be realized that many of the variables used in the formulations are only obtainable from experimental results, through parameter estimation. The determination of these parameters is, therefore, of vital importance if the dynamic behaviour of a structure is to be correctly modelled.

The ultimate objective of any modal test is to derive the modal parameters of the system being tested. It is in this phase of the analysis that the objective is achieved. The term *Curve Fitting* is, as implied a process by which a theoretical function is derived that fits the measured data. With this derivation the modal parameters are obtained by subsequent evaluation of the fitted curve. The FRF, thus derived, is used to obtain the fundamental modal parameters in a three stage process. First, the natural frequencies of the system are determined by locating the frequency values at which peaks in the FRF occur. Secondly, damping parameters are determined from the shape of the resonant peaks. Thirdly, mode shapes are determined from the amplitude of the peaks occurring in the various FRFs, derived from numerous locations on the structure. As with the other phases of modal testing, there are a number of methods available to perform this task. In a general sense, the various methods use three fundamental procedures to derive the fitted curve. In order of increasing complexity these three fundamental procedures can be described as: i) curve fitting a part of a single FRF (SDOF techniques); ii) curve fitting a complete FRF (MDOF techniques); and iii) curve fitting a number of FRF curves derived from the same structure (Multi-Curve Technique). The method chosen for a given test is dependant on the specific objectives of the experiment and the final application to which the results will be applied.

3.4.1 SDOF Curve Fitting Techniques

The discussion of curve fitting techniques should logically commence with the simplest methods, the SDOF methods. These methods fall into the first category of curve fitting methods. That is, they attempt to fit a curve through only a part of the derived FRF. The

term SDOF is applicable to these methods since they share the common assumption that in the vicinity of a resonant peak the system response is dominated by the contribution of a single mode whose natural frequency is the frequency at the peak. The variations between the SDOF methods, occur in the extent to which they make this underlying assumption. While some methods assume all of the response is due to that one mode, others assume that other modes are present and are accounted for by simple approximations.

Two common SDOF methods that will be discussed in this section are:

- The Peak Amplitude Method
- The Circle Fit Method

3.4.1.1 The Peak Amplitude Method

Probably the simplest parameter extraction technique is the peak amplitude method. This method is not actually a curve fit technique since it only relies on a small number of points surrounding each resonant peak. It is most applicable to FRFs which have well separated peaks indicating that the modes of the structure are only lightly coupled. In addition the method does not work well with structures that are very lightly or very heavily damped. This effectively limits the usefulness of the method but due to its ease of use and simplicity it is still appropriate for initial estimates before proceeding with the more detailed methods.

The procedural steps of this method, in association with Figure 3.1, are given as follows:

- Locate the individual peaks on the FRF plot and note the frequency at which the maximum amplitude is found (ω_r). These values are then indicative of the systems natural frequencies.
- Concentrating on one peak at a time, note the maximum amplitude $|\alpha|$ and determine the frequency bandwidth at that peak by locating on both sides of the peak points which have an amplitude value of $2^{-1/2}$ times that of the peak amplitude. The bandwidth is designated as $\Delta\omega$ and is bounded by ω_a on the lower side and ω_b on the upper side (ie.. $\Delta\omega = \omega_b - \omega_a$).
- The damping for the particular mode in question is determined from

$$\zeta = \frac{\omega_b - \omega_a}{2\omega_r} \simeq \frac{\Delta\omega}{2\omega_r} \tag{3.58}$$

- An estimate for the residue of the particular mode is obtained from

$$A_r = 2|\alpha|\omega_r^2\zeta \tag{3.59}$$

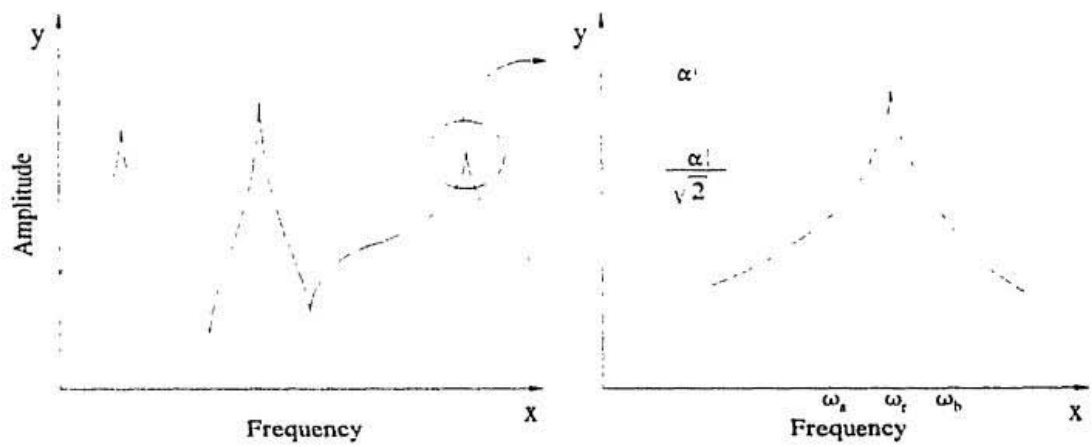

FIGURE 3.1 - THE PEAK AMPLITUDE METHOD

This method is generally easy to apply and gives quick results, but it must be noted that there are several limitations to the method which makes it less than ideal for accurate

measurements. First, the accuracy of results obtained is highly dependant upon the accuracy of the measured peak amplitude. Since it is very difficult to obtain accurate amplitude values the accuracy of the method must also be questioned. The second problem arises as a result of the single mode assumption which is not strictly applicable. Even with well separated modes, contributions from other modes is significant and cannot generally be neglected. It was to overcome this problem that the circle fit method was developed. This method is discussed as follows, in Section 3.4.1.2.

In general the Peak Amplitude Method is not reliable and should only be used for preliminary checks or very approximate evaluation of the modal parameters.

3.4.1.2 The Circle Fit Method

The Circle Fit Method is a popular curve fit method that generally results in a better approximation of the modal parameters than the methods previously discussed. The method utilizes a plot format commonly referred to as the Nyquist or Argand plot. Essentially this format is arrived at by plotting FRF data on a coordinate grid that has real components as the ordinate axis and imaginary components as the abscissa axis. In order to fully illustrate this technique it is necessary to backtrack and review an alternate solution of the basic SDOF equation of motion given as Equation 3.1. If we consider a solution for x of the form $Xe^{i\omega t}$ and a forcing function of the form $Fe^{i\omega t}$, the basic equation of motion can be written as

$$(-\omega^2 m + i\omega c + k) X e^{i\omega t} = F e^{i\omega t} \tag{3.60}$$

If the ratio of X to F is taken as a form of frequency response function, then this ratio, designated as $H(\omega)$, the can be written as

$$H(\omega) = \frac{1}{(k - \omega^2 m) + i(\omega c)} \tag{3.61}$$

Using this formulation, and the relationship between velocity and displacement (ie., $v = \dot{x} = i\omega X e^{i\omega t}$) the following velocity form of the FRF (designated as $Y(\omega)$) can be written as

$$Y(\omega) = i\omega H(\omega) = \frac{i\omega}{(k - \omega^2 m) + i(\omega c)} = \frac{\omega^2 c + i\omega(k - \omega^2 m)}{(k - \omega^2 m)^2 + (\omega c)^2} \tag{3.62}$$

The real and imaginary parts can now easily be separated as

$$Re\ Y(\omega) = \frac{\omega^2 c}{(k - \omega^2 m)^2 + (\omega c)^2} \tag{3.63}$$

$$Im\ Y(\omega) = \frac{\omega(k - \omega^2 m)}{(k - \omega^2 m)^2 + (\omega c)^2} \tag{3.64}$$

Letting $U = (Re\ Y - \frac{1}{2c})$ and $V = (Im\ Y)$, yields

$$U^2 + V^2 = \frac{\left[(k - \omega^2 m)^2 + (\omega c)^2\right]^2}{4c^2\left[(k - \omega^2 m)^2 + (\omega c)^2\right]^2} = \left(\frac{1}{2c}\right)^2 \tag{3.65}$$

which describes the a circle with radius $\frac{1}{2c}$, centred at Re = $\frac{1}{2c}$, Im = 0.

An advantage of this method is that it can be extended to the multi-degree of freedom case to account for the effect of adjacent modes. Consider a general solution for the FRF

designated as H_{ij} (which indicates that the FRF is derived for location i with respect to j, or vice verse due to reciprocity) given as follows:

$$H_{ij} = \sum_{k=1}^{2n} \frac{A_{ij}^{k}}{i\omega + \zeta_k\omega_k - i\omega_k\sqrt{1-\zeta_k^2}} \tag{3.66}$$

where A^{k}_{ij} = the modal constant (or residue) for mode k linking locations i and j

= $[\phi_i\ \phi_j]^k$

ζ = the viscous damping factor

If for a particular peak at mode r we assume that the majority of the response is due the effects of this mode the contribution of modes other than the r^{th} mode can be accounted for by writing Equation (3.66) as

$$H_{ij} = \frac{A_{ij}^{r}}{i\omega + \zeta_r\omega_r - i\omega_r\sqrt{1-\zeta_r^2}} + k \neq r\sum_{k=1}^{2n} \frac{A_{ij}^{k}}{i\omega + \zeta_k\omega_k - i\omega_k\sqrt{1-\zeta_k^2}} \tag{3.67}$$

which is equivalent to

$$H_{ij} = \frac{A_{ij}^{r}}{i\omega + \zeta_r\omega_r - i\omega_r\sqrt{1-\zeta_r^2}} + B_{ij}^{r} \tag{3.68}$$

where the first part of the equation is representative of the contribution of the r^{th} mode while the second term is representative of the contribution from all other modes. Thus, when plotted the circle can be considered to have all of the basic properties of the SDOF

circle for the particular mode but displaced from the origin by an amount determined from the contribution of the other modes.

Properties of the Circle

Considering the circle shown in Figure 3.2 the various modal properties can be determined as follows:

Natural Frequency:

The natural frequency is found by locating the point of maximum sweep rate on the circle. This is performed by numerically constructing radial lines between successive points and determining the subtended angle. The frequency at which a maximum is reached is indicative of the natural frequency. During the computations an estimate of damping can be obtained from the measured angles. Alternate methods of determining natural frequency include: i) the point of maximum amplitude (ie., the circle location furthest from the origin), ii) the point at which the circle meets the imaginary axis (furthest from the origin), iii) the point on the circle furthest from the real axis. While results vary from method to method all are generally close to the true value of natural frequency.

Damping:

Using any two points on the circle θ_a and θ_b the value of the viscous damping factor can be determined from the following;

$$\zeta_r = \frac{\left(\omega_b^2 - \omega_a^2\right)}{2\omega_r\left\{\omega_a \tan\left(\frac{\theta_a}{2}\right) + \omega_b \tan\left(\frac{\theta_b}{2}\right)\right\}} \tag{3.69}$$

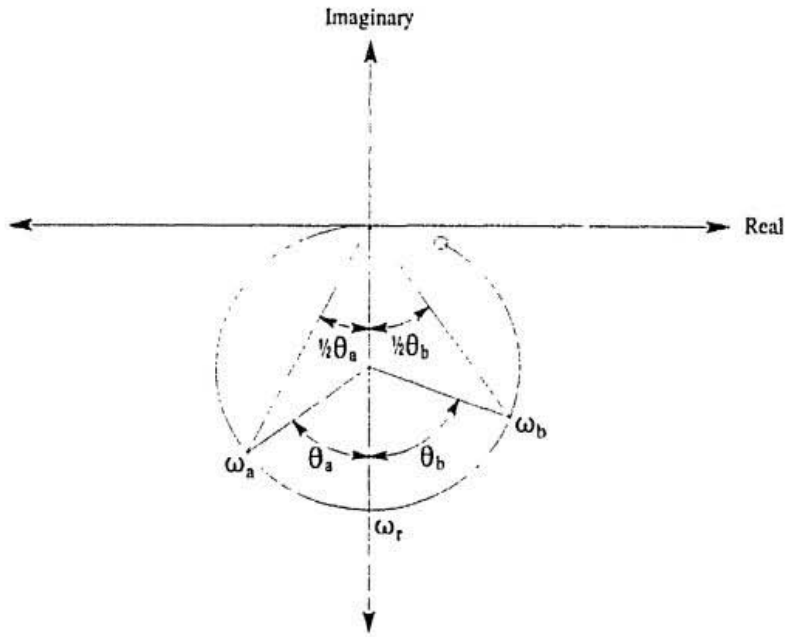

FIGURE 3.2 - PROPERTIES OF THE MODAL CIRCLE

Note that if both θ_a and θ_b are taken as 90° (ie., the half-power points) the above reduces to the expression

$$\zeta = \frac{\omega_b - \omega_a}{2\omega_r} \tag{3.70}$$

Modal Constant (or residue): Derived from the circle diameter using

$$A_{ij}^r = 2D\omega_r^2\zeta_r \tag{3.71}$$

where D is the circle diameter.

3.4.2 MDOF Curve Fitting Techniques

As implied from the discussion of the SDOF methods all have the restriction of being applicable to well separated modes that are not strongly coupled. In real situations, however, modal coupling occurs quite frequently and neglecting its effect or simply approximating it will result in poor quality curve fits and subsequent parameter estimation. It was for this reason that MDOF methods were developed. These methods, while each having particular strengths, generally result in better curve fits and more accurate estimation of modal parameters than the simpler SDOF methods. The following list contains the names of methods, available in I-DEAS, which fall into the category of MDOF curve fitting:

- The Complex Exponential Method
- The Direct Parameter Method
- The Polyreference Method
- The Orthogonal Polyreference Method

In the interest of space conservation only the method which was actually used in the subsequent experimental analysis is reviewed in the following section. The first of the preceding list, the Complex Exponential Technique, is therefore chosen for illustration of the MDOF methodology[2].

---

[2] The names given for these methods, while shared by many authors may be found under different names in various references.

3.4.2.1 The Complex Exponential Technique

This technique varies from most others in that it is performed in the time domain rather than in the frequency domain. It was chosen for this research due to its desirable combination of flexibility and efficiency in deriving modal parameters. There are variations of this method which differ in computational efficiency; the discussion which follows, however, outlines the fundamental principles common to all.

As a result of the use of time domain data, the method is only applicable to systems which are viscously damped (as opposed to hysteretically damped). Therefore, to begin discussion consider once again, the general expression for the FRF (compliance) of a viscously damped MDOF system, previously given in Equation (3.55).

If the complex conjugate term is considered independent the FRF (dropping the subscripts) can be rewritten as

$$H(\omega) = \sum_{r=1}^{2N} \frac{A_r}{s - \lambda_r} \tag{3.72}$$

Note that $A_{r+1} = A_r^*$, and $\lambda_{r+1} = \lambda_r^*$, where r = 1,3,5,7...

The time domain representation of this function (called the Impulse Response Function) is found by taking the inverse Fourier transform of $H(\omega)$, and is written as

$$x(t) = \sum_{r=1}^{2N} A_r e^{\lambda_r t} \tag{3.73}$$

If the original FRF was derived from digitized measurements then it is subsequently defined in terms of $2N$ evenly spaced frequency increments. Likewise $x(t)$ is defined by the same number of points spaced at time intervals of Δt ($= 1/\Delta f$). The function value of $x(t)$ at the k^{th} subinterval can then be written as

$$x(t_k) = \sum_{r=1}^{2N} A_r e^{\lambda_r k \Delta t} = \sum_{r=1}^{2N} A_r U_r^k \tag{3.74}$$

where k is valid anywhere in the range 0 to $2N$ (the number of degrees of freedom, and hence modes, in the system model) and Δt is as described above.

It then follows logically that;

$$\begin{aligned}
x(t_0) &= A_1 + A_2 + A_3 + \ldots\ldots\ldots\ldots + A_{2N} \\
x(t_1) &= A_1U_1 + A_2U_2 + A_3U_3 + \ldots\ldots\ldots + A_{2N}U_{2N} \\
x(t_2) &= A_1U_1^2 + A_2U_2^2 + A_3U_3^2 + \ldots\ldots\ldots + A_{2N}U_{2N}^2 \\
&\vdots \\
x(t_{2n}) &= A_1U_1^{2n} + A_2U_2^{2n} + A_3U_3^{2n} + \ldots\ldots + A_{2N}U_{2N}^{2n}
\end{aligned} \tag{3.75}$$

for the full set of $2n$ samples.

If $N=n$ then there are $2n$ $+1$ rows in the previous expression. There must then, exist a polynomial of order $2n$ that satisfies the expression

$$U^{2n} + a_1U^{2n-1} + a_2U^{2n-2} + \ldots\ldots\ldots a_{2n-1}U + a_{2n} = 0 \tag{3.76}$$

the roots of which can be designated as U_1, U_2, U_3 etc. If the rows of Equation (3.75) are then multiplied by the coefficients in descending order from $2n$ to 0 (ie., $a_{2n} \times$ row 1, $a_{2n-1} \times$ row 2, ... $a_0 \times$ row 2n), the result is:

$$\begin{aligned}
a_{2n}x(t_0) &= a_{2n}(A_1 + A_2 + A_3 + \ldots\ldots\ldots + A_{2n}) \\
a_{2n-1}x(t_1) &= a_{2n-1}(A_1U_1 + A_2U_2 + A_3U_3 + \ldots + A_{2n}U_{2n}) \\
a_{2n-2}x(t_2) &= a_{2n-2}(A_1U_1^2 + A_2U_2^2 + A_3U_3^2 + \ldots + A_{2n}U_{2n}^2) \\
&\vdots \\
a_0x(t_{2n}) &= a_0(A_1U_1^{2n} + A_2U_2^{2n} + A_3U_3^{2n} + \ldots + A_{2n}U_{2n}^{2n})
\end{aligned} \tag{3.77}$$

Adding the equations yields

$$\sum_{k=0}^{2n} a_{2n-k}x(t_k) = \sum_{k=0}^{2n} a_{2n-k}\left[\sum_{r=1}^{n} A_rU_r^k\right] = \sum_{r=1}^{n} A_r\left[\sum_{k=0}^{2n} a_{2n-k}U_r^k\right] \tag{3.78}$$

Recalling that U_1, U_2, ... U_{2n} are roots (which will yield the natural frequencies of the system) of the polynomial given previously as Equation (3.76), it follows that

$$\sum_{k=0}^{2n} a_{2n-k}U_r^k = 0 \tag{3.79}$$

and subsequently

$$\sum_{k=0}^{2n} a_{2n-k}x(t_k) = 0 \tag{3.80}$$

where the value of a_0 is set equal to 1;

If the series is now incremented by a value of Δt and the procedure repeated, then a second set of $2n$ equations can be generated starting with the second equation of the previous set. The number of repetitions that must be performed is $2n$-1 resulting in a complete series of equations that can be written as

$$\begin{aligned}
&x(t_{2n}) + A_1 x(t_{2n-1}) + A_2 x(t_{2n-2}) + \ldots\ldots\ldots\ldots + A_{2n} x(t_0) = 0 \\
&x(t_{2n+1}) + A_1 x(t_{2n}) + A_2 x(t_{2n-1}) + \ldots\ldots\ldots\ldots + A_{2n} x(t_1) = 0 \\
&x(t_{2n+2}) + A_1 x(t_{2n+1}) + A_2 x(t_{2n}) + \ldots\ldots\ldots\ldots + A_{2n} x(t_2) = 0 \\
&\quad\vdots \\
&x(t_{4n-1}) + A_1 x(t_{4n-2}) + A_2 x(t_{4n-3}) + \ldots\ldots\ldots + A_{2n} x(t_{2n-1}) = 0
\end{aligned} \tag{3.81}$$

or in matrix form as

$$\begin{bmatrix} x(t_{2n-1}) & x(t_{2n-2}) & \ldots\ldots & x(t_0) \\ x(t_{2n}) & x(t_{2n-1}) & \ldots\ldots & x(t_1) \\ \cdot & \cdot & \cdot & \cdot \\ \cdot & \cdot & \cdot & \cdot \\ x(t_{4n-2}) & x(t_{4n-3}) & \ldots\ldots & x(t_{2n-1}) \end{bmatrix} \begin{Bmatrix} A_1 \\ A_2 \\ \cdot \\ \cdot \\ A_{2n} \end{Bmatrix} = - \begin{Bmatrix} x(t_{2n}) \\ x(t_{2n+1}) \\ \cdot \\ \cdot \\ x(t_{4n-1}) \end{Bmatrix} \tag{3.82}$$

which is given the representation $[x]\{a\} = -[x']$. The unknown coefficient matrix can the be solved for simply as $[a] = -[x]^{-1}[x']$.

At this point the coefficients are known and the system parameters can be determined from Equation (3.76) by solving for U_1, U_2, ... U_{2n} and using the relationship

$$U_r = e^{\lambda_r \Delta t} = e^{\Delta t(-\zeta_r \omega_r \pm i\omega_r\sqrt{1-\zeta_r^2})} \tag{3.83}$$

Finally the modal constants (or residues) are determined from

$$\begin{bmatrix} 1 & 1 & \cdots\cdots & 1 \\ U_1 & U_2 & \cdots\cdots & U_{2n} \\ U_1^2 & U_2^2 & \cdots\cdots & U_{2n}^2 \\ \cdot & \cdot & \cdot & \cdot \\ U_1^{2n-1} & U_2^{2n-1} & \cdots\cdots & U_{2n}^{2n-1} \end{bmatrix} \begin{Bmatrix} A_1 \\ A_2 \\ A_3 \\ \cdot \\ A_{2n} \end{Bmatrix} = \begin{Bmatrix} x(t_0) \\ x(t_1) \\ x(t_2) \\ \cdot \\ x(t_{2n-1}) \end{Bmatrix} \tag{3.84}$$

To employ this method one might follow the steps outlined below:

- Make an initial estimate of the number of degrees of freedom and carry out an initial analysis using the above procedure.
- When complete the modal properties are used in Equation (3.55) to compute the first fitted approximation to the measured FRF. The generated curve is compared with the measurement derived curve to determine the deviation or error between the two.
- Choose an improved estimate for the number of degrees of freedom and repeat the whole procedure. The error between the two curves will reduce as the approximation gets better. If the estimate is higher than the true number then there will result fictitious modes in the generated FRF. These are generally easy to identify as those which have unusually high damping factors or very low modal constants.

3.5 Summary

This concludes the review of the relevant portion of the theory associated with analytical and experimental modal analysis. There are, obviously, many topics associated with modal analysis and structural dynamics which could not be presented here in greater detail. The interested reader might look to any of a number of references available for additional information on this subject; several are listed in the final section of this document.

Chapter 4, which follows, discusses the results of the finite element analysis, prepared as part of this research. This analysis models several cantilever plates to determine the effect of notched cracks on the various modal properties of the plates.

Chapter 4

Analytical Results

The concept of using modal analysis as a tool in monitoring structural integrity, is at best in its early stages of development, due primarily to the relatively small amount of research that has been performed in this area. Because of this, it was decided that the main focus of this course of study would be to show through experimentation the effect of crack type defects on the modal properties of a typical structure. Before commencing with experimentation, however, it was necessary to develop a method of prediction to be used as a comparison for results obtained from the experiment, and to provide verification of the adequacy and applicability of the experimental set-up. This was accomplished by developing a finite element model of each of the plates and performing an eigenvector/eigenvalue solution to obtain an analytical estimate of their natural frequencies and mode shapes. These results were additionally used to illustrate a crack locating technique that compared the mode shapes of cracked plates to those of the reference plate. As with the test result evaluation, the software used for this analysis was the integrated design package I-DEAS, produced and marketed by SDRC.

4.1 Description of Model

The finite element evaluation and experimentation discussed in this thesis are based on a cantilever plate, used as a typical structure. The prototype of the plate is illustrated schematically in Figure 4.1.

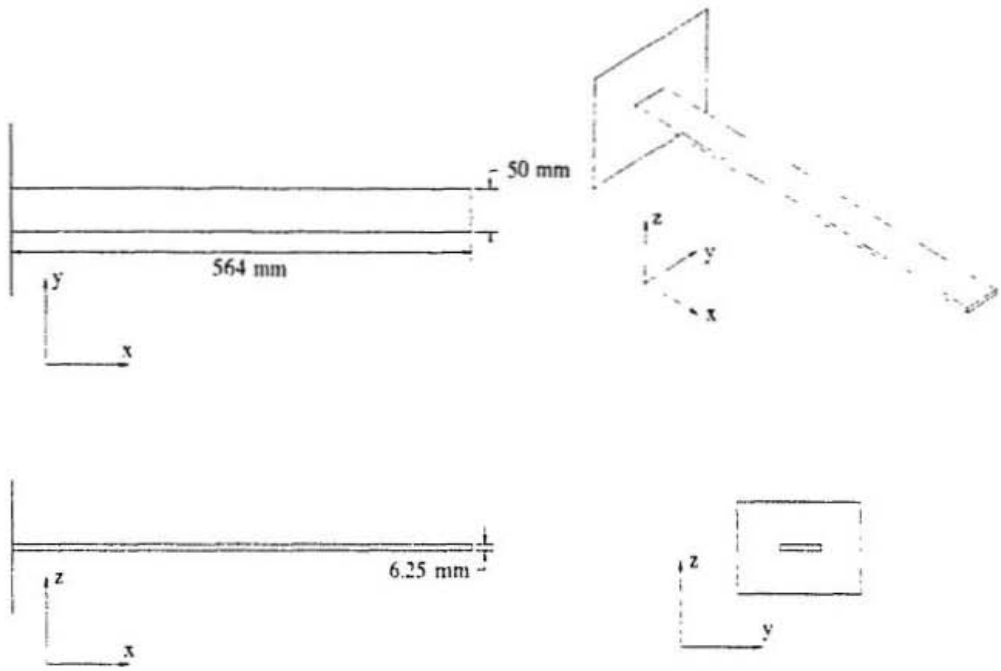

FIGURE 4.1 - SCHEMATIC DIAGRAM OF ANALYZED CANTILEVER PLATE

The physical characteristics of the prototype are given as follows:

Material Properties:

Material:	Mild Steel
Mass Density:	7850 kg/m^3
Elastic Modulus:	200.0 × 10^9 Pa
Shear Modulus:	77.0 × 10^9 Pa

Dimensions:

Width:	50.0 mm
Depth:	6.35 mm
Overall Length:	564 mm

Calculated Values (uncracked):

Total Volume:	1.7907×10^{-4} m^3
Total Mass:	1.4057 kg
Mass per unit length:	2.4924 kg/m
Moment of Inertia y-y:	1.0669×10^{-9} m^4
Moment of Inertia z-z:	6.6146×10^{-8} m^4

In order to simulate naturally occurring fatigue cracks, a rectangular notch 4 mm wide was cut into each of the 4 prototypes, used for experimentation. The crack location and crack cross-sections are illustrated in Figure 4.2. The analytical models used to describe these prototypes are discussed in the following section.

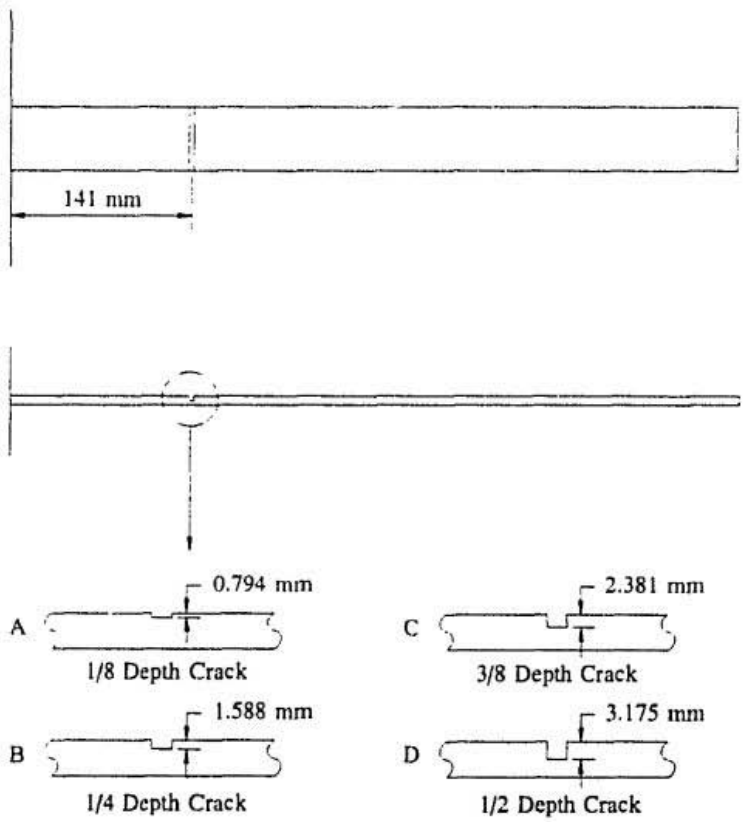

FIGURE 4.2 - CRACK LOCATION AND CRACK DEPTH CASES CONSIDERED

4.2 Development of the Finite Element Model

The procedures followed in the development of a model to be solved by a particular finite element software package, is somewhat dependant on the particular package being used. The differences between programs, however, are generally limited to specific input syntax as required by the software. The fundamentals of model development are the same regardless of the software being used, and can be summarized by the following list.

- Considering the geometry of the prototype, and the objectives of the finite element evaluation, choose basic parameters such as coordinate system, element type, and discretization procedures.
- Layout the geometry of the system to be evaluated and determine the coordinates of the nodes to be used in the model. Ensure that at minimum, nodes are placed wherever geometric, physical, or material inconsistencies occur.
- Define all elements in the model according to standard finite element procedure for the specific element type being used. For example ensure that two dimensional elements such as plates have width to height ratios which fall into the range of 0.5 to 2.
- Define all physical element properties required for the type of solution to be performed. The properties required are dependant upon the element type used, plate elements require a thickness specification, while beam elements require moments of inertia, area, etc.
- Define all material properties for each material used in the structure. The parameters required include density, modulus of elasticity, shear

modulus, etc. These parameters are not dependant upon element type and must be specified for all element cases.

- Define boundary conditions for the model which are representative of actual physical restraints. Make use of the ability to restrain redundant degrees of freedom to reduce model size and improve solution times.
- Input data in the format specified by the particular software package being used.
- Run the model solution and interpret the results.

The solution of the eigenvector/eigenvalue problem of concern here, was attempted by considering a model made up of plate like (thin shell) elements. This model was deemed appropriate due to the flat/slender geometry of the cantilever plate considered here (see Figure 4.1).

The basic finite element model is shown in Figure 4.3. It is made up of a series of nodes which define the boundaries of its elements. For this analysis, a parabolic thin (shallow) shell element was chosen due to its favourable combination of simplicity and effectiveness. The node arrangement associated with these types of elements are shown in Figure 4.4. Using this element, the effects of crack depth could be simulated by setting the thickness of the smaller rectangular elements (shown in Figure 4.3) to values equal to the remaining material thickness under the notched crack. All others are set equal to the original thickness of the plate. Table 4.1 lists information pertinent to the model used in this analysis.

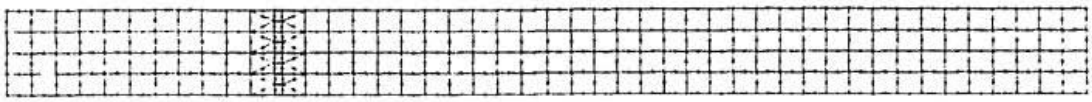

FIGURE 4.3 - FINITE ELEMENT MESH OF CANTILEVER PLATE

TABLE 4.1: FINITE ELEMENT MODEL INFORMATION

No. of Nodes	689	
No. of Ele·	216	
Plate Thickness (uncracked)	6.3500 mm	
Thickness of Crack Elements (defined as fraction of original plate tl.ickness)	0	6.3500
	1/8	5.5563
	1/4	4.7625
	3/8	3.9688
	1/2	3.1750
No. of Materials (per case)	1	
No. of Properties (per case)	2	

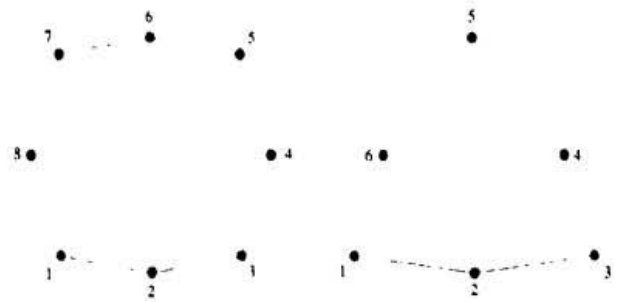

FIGURE 4.4 - THIN SHELL ELEMENTS

4.3 Results of Finite Element Analysis

The solution of the finite element model yielded the first 20 mode shapes and natural frequencies of each of the plates considered. Those of primary importance, were the bending modes about the weaker axis (y-y), whose frequencies were less than 1000 Hz. This limitation was set as a practical upper limit for the experimental analysis (discussed in Chapter 5) and was, therefore, used for the analytical results as well.

Considering first, the uncracked (reference) plate, the modes that occurred below 1000 Hz are listed in Table 4.2. For completeness, all the modes are listed along with an indication of the mode type. Shown as well, for comparison, are frequency values derived from the Euler beam equation (see Thomson (1981) Chapter 7).

TABLE 4.2 - FIRST 9 FREQUENCIES OF UNCRACKED CANTILEVER TEST PLATE

Mode & Type[3]	Finite Element Frequency (Hz)	Euler Beam Equation Frequency (Hz)	Percent Discrepancy (w.r.t. FE. Values)
1 B	16.04	16.28	1.50
2 B	100.36	102.00	1.64
1 H	127.48	128.15	0.53
3 B	280.78	285.64	1.73
1 T	323.10	n.a.	n.a.
4 B	549.62	559.75	1.84
2 H	769.98	803.17	4.31
5 B	906.86	925.21	2.02
2 T	973.99	n.a.	n.a.

[3] Mode types are designated as; B = Bending about y-y (vertical plane), H = Bending about z-z (horizontal plane), and T = Torsion about x-x.

Similar data for the cracked plates is shown in Table 4.3, along with an indication of the degree to which the frequency dropped.

TABLE 4.3 - FIRST 9 FREQUENCIES OF CRACKED CANTILEVER TEST PLATES

Mode & Type	1/8 Depth Crack		1/4 Depth Crack		3/8 Depth Crack		1/2 Depth Crack	
	Frequency (Hz)	% Change[4]	Frequency (Hz)	% Change	Frequency (Hz)	% Change	Frequency (Hz)	% Change
1 B	15.99	-0.31	15.91	-0.81	15.75	-1.81	15.43	-3.80
2 B	100.38	0.02	100.39	0.03	100.39	0.03	100.34	-0.02
1 H	127.38	-0.08	127.23	-0.20	127.03	-0.35	126.74	-0.58
3 B	280.41	-0.13	279.62	-1.01	277.94	-1.01	274.18	-2.35
1 T	322.35	-0.23	321.52	-0.76	320.65	-0.76	319.76	-1.03
4 B	548.66	-0.17	546.77	-1.20	543.01	-1.20	535.26	-2.61
2 H	770.15	0.02	770.30	0.05	770.40	0.05	770.45	0.06
5 B	906.55	-0.03	905.96	-0.22	904.82	-0.22	902.53	-0.48
2 T	974.07	0.01	974.07	0.01	974.02	0.00	973.94	-0.01

As shown, within the range of 0 to 1000 Hz, there exists for this structure 5 primary bending modes, two transverse bending modes, and two torsion modes. In addition to the natural frequencies, the analysis produced mode shapes for each of these modes. A multi-view graphical representation of the nine modes listed in the preceding tables, is given in Appendix A. For discussion here, Figure 4.5 shows a normalized representation of the first five vertical displacement bending modes of the plate.

The term *mode shape* is used almost exclusively when referring to the deformation pattern of a structure as it vibrates at its resonant frequencies. In other words, it is the time invariant displacement pattern of the vibrating structure. There are, however, other definitions which differ from the classical definition in that they consider response parameters other than displacement.

[4] % Change is always with respect to the uncracked plate.

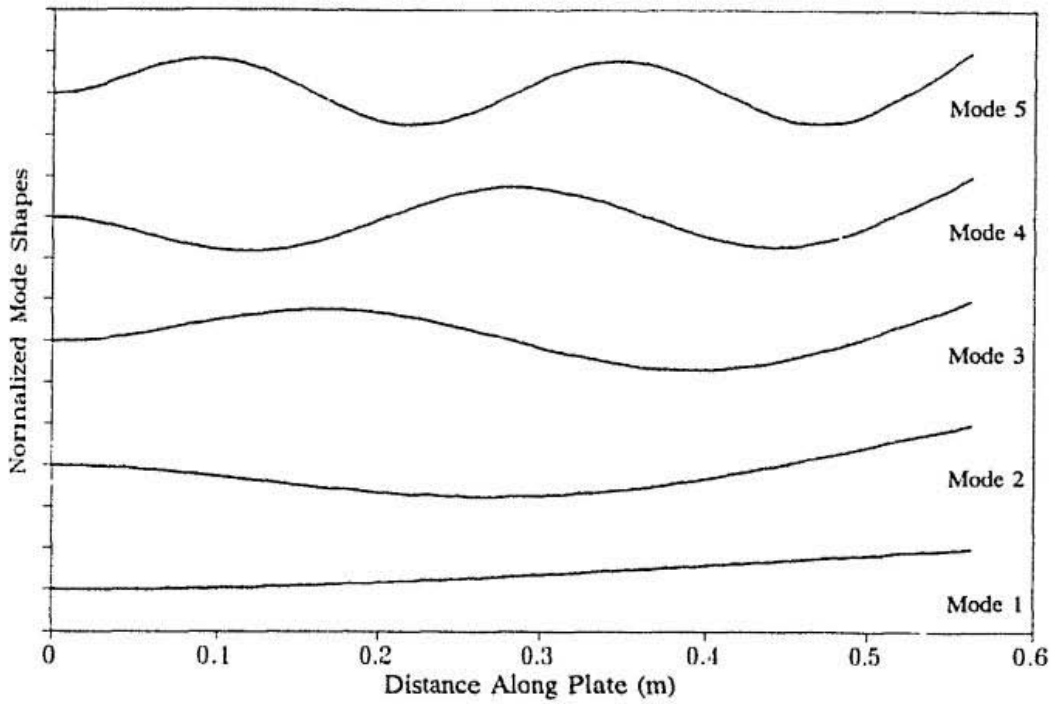

FIGURE 4.5 - FIRST FIVE DISPLACEMENT MODE SHAPES OF CANTILEVER PLATE (BENDING ABOUT THE PRIMARY AXIS)

These include slope and curvature mode shapes and while not a true representation of the deformed structure, they are represented in a similar manner and help to describe more completely, the actions of the structure being analyzed. These too, can be derived from the results of a finite element analysis, as illustrated in Figure 4.6, which shows the first five slope mode shapes derived from rotation data.

Results of the eigenvalue analysis, presented in Tables 4.2 and 4.3, clearly show that the depth of the crack strongly influences several of the natural frequencies of the plate. The differing degree to which various modes were affected can be attributed to the curvature of the corresponding mode shape at the crack location.

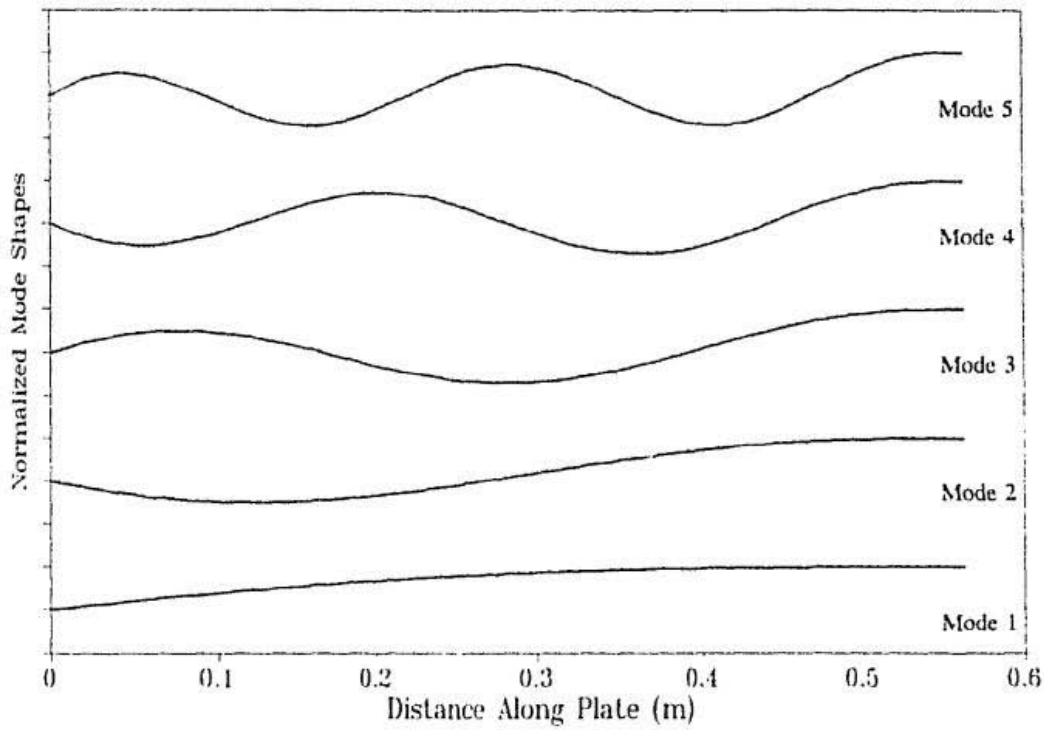

FIGURE 4.6 - FIRST FIVE ROTATION (SLOPE) MODE SHAPES OF CANTILEVER PLATE

It appears, then, that observing natural frequency is a useful procedure for the determination of crack existence. Further discussion of these phenomena is reserved for Chapter 5, where the results are compared with those obtained through experimentation.

The knowledge of crack existence, while fundamentally important is not extremely useful without having some idea of where the crack is located. One very useful ability of finite element analysis is the ability to discretize a structure into many small elements, thereby enabling close observation of very small segments. Changes in calculated quantities such as modal displacement which may on a global scale be invisible, can be extracted to yield very clear indications of the location of a crack or structural fault.

Such was the case in this analysis, where it was found that by observing the response of a strip of 90 nodes along one edge of the plate, it was possible to derive differences in mode shape patterns for the cracked versus the uncracked plates. While the observations should parallel the true structural response, the arrangement of measurement points on the experimental plates was not conducive to this type of detailed analysis and thus it can only be shown from results of the analytical solutions.

The basic premise of the method, is that for the cracked model, there will occur at the crack location an inconsistency in mode shape that does not occur in the uncracked model. As the depth of the crack increases, the inconsistency becomes more pronounced, even for modes that exhibited little, if any, frequency shift. To illustrate, both the displacement mode shapes (of Figure 4.5) and the rotation (slope)[5] mode shapes (of Figure 4.6) for the cracked models, were compared with their corresponding uncracked model. Figures 4.7 through 4.16 illustrate the difference (ie., $\phi_{cracked} - \phi_{reference}$) in normalized units[6] for the first five primary bending mode shapes, for both displacement, and rotation.

---

[5] Node rotation is an output parameter of the finite element analysis. Since slope is derived from rotation simply by taking its tangent and since for small angles, $tan(\alpha) = \alpha$, little error is introduced by considering the two to be equivalent.

[6] Mode shapes are normalized by scaling the output parameter to allow the maximum value to be equal to 1. This allows comparison of differential between modes on an equal basis. In all cases shown here, the value of displacement/rotation at the free-end of the plate is the local maximum and hence is given a value of unity.

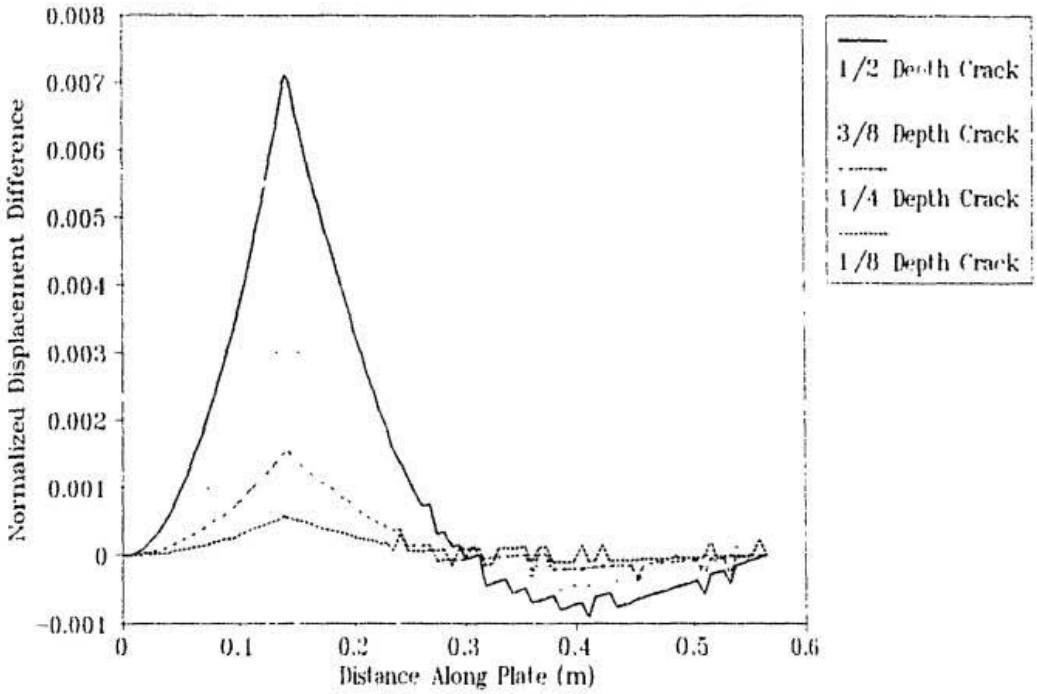

FIGURE 4.7 - DISPLACEMENT MODE SHAPE DIFFERENCE W.R.T REFERENCE PLATE, MODE 1

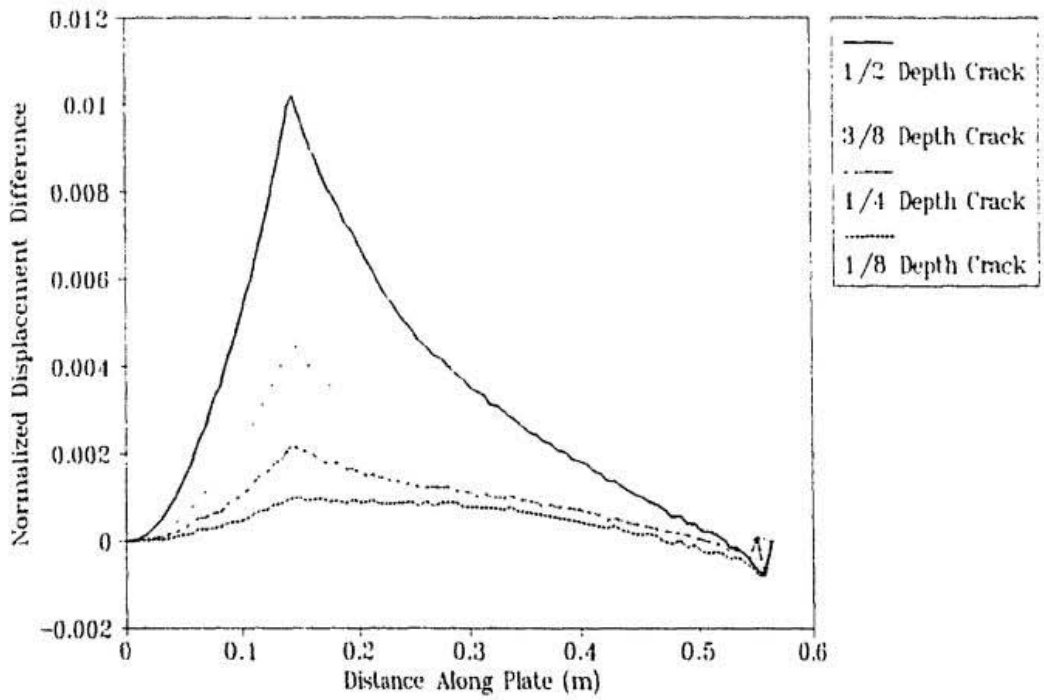

FIGURE 4.8 - DISPLACEMENT MODE SHAPE DIFFERENCE W.R.T REFERENCE PLATE, MODE 2

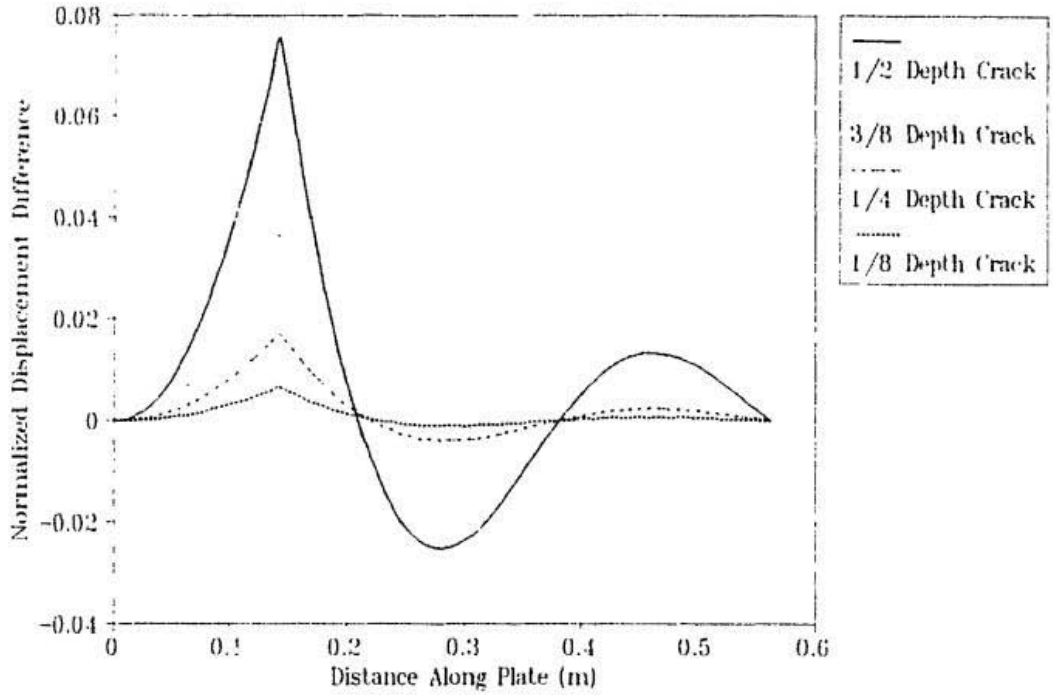

FIGURE 4.9 - DISPLACEMENT MODE SHAPE DIFFERENCE W.R.T REFERENCE PLATE, MODE 3

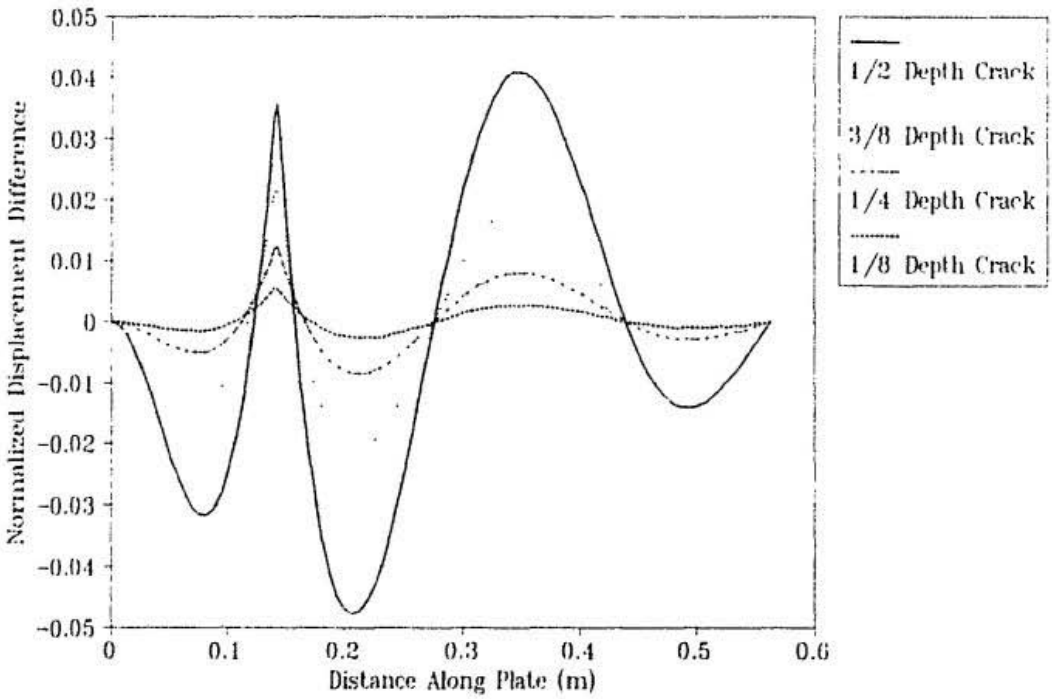

FIGURE 4.10 - DISPLACEMENT MODE SHAPE DIFFERENCE W.R.T REFERENCE PLATE, MODE 4

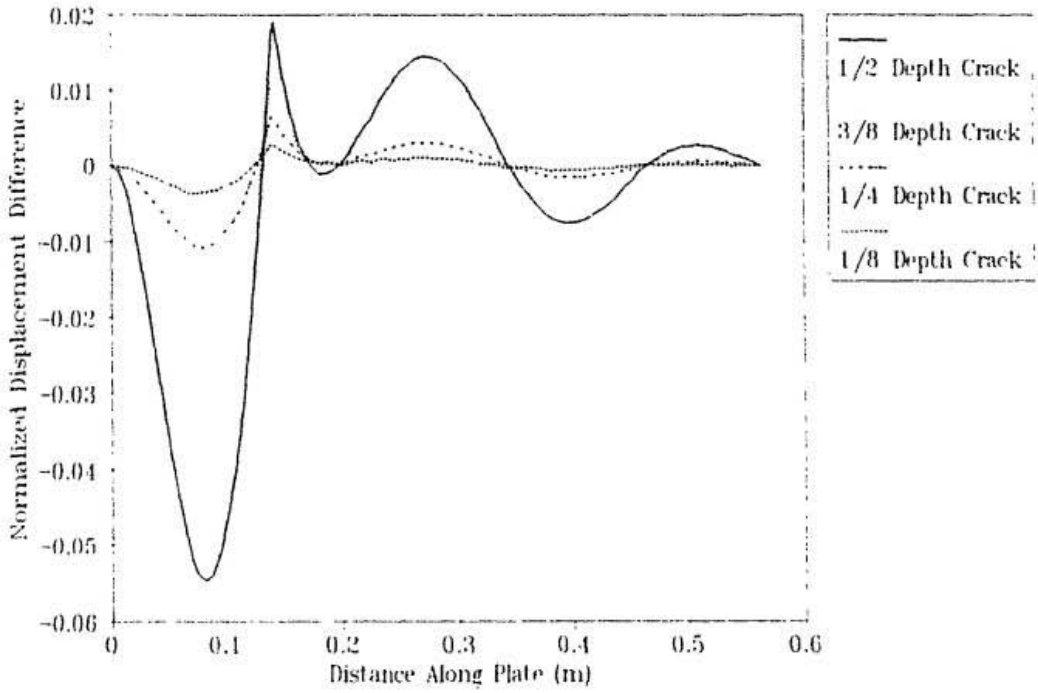

FIGURE 4.11 - DISPLACEMENT MODE SHAPE DIFFERENCE W.R.T REFERENCE PLATE, MODE 5

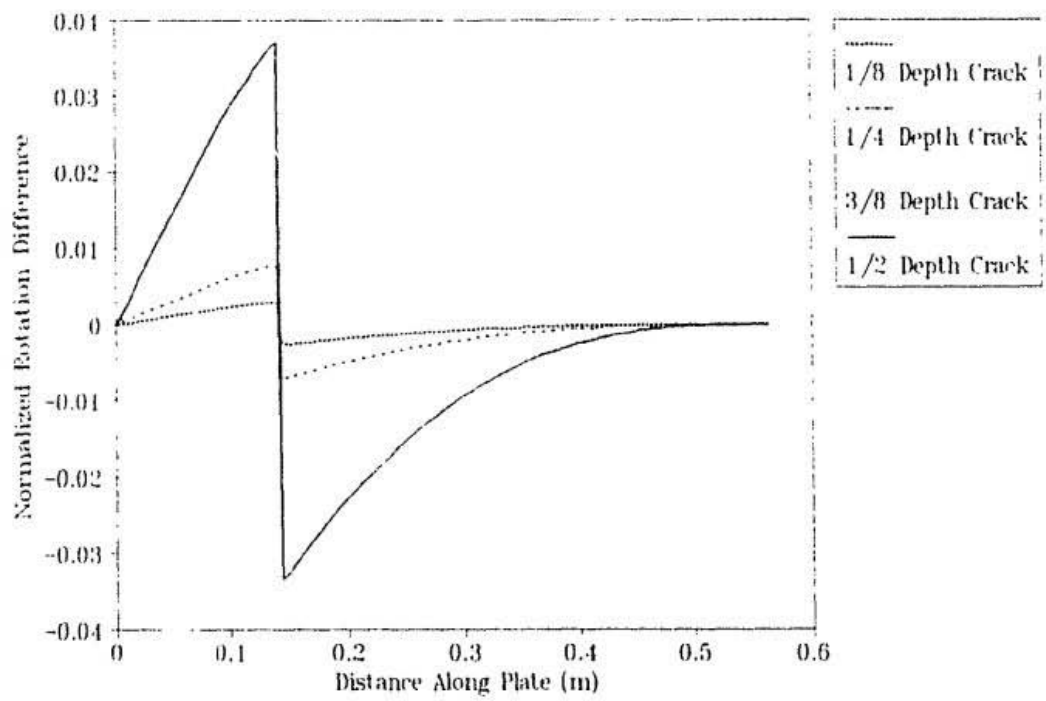

FIGURE 4.12 - ROTATION MODE SHAPE DIFFERENCE W.R.T REFERENCE PLATE, MODE 1

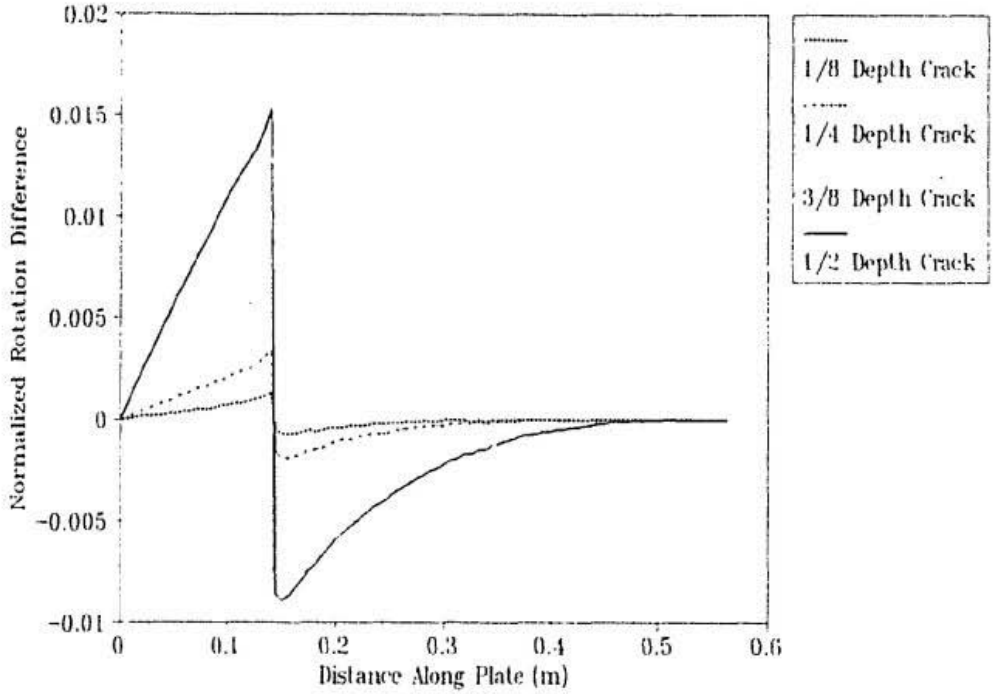

FIGURE 4.13 - ROTATION MODE SHAPE DIFFERENCE W.R.T REFERENCE PLATE, MODE 2

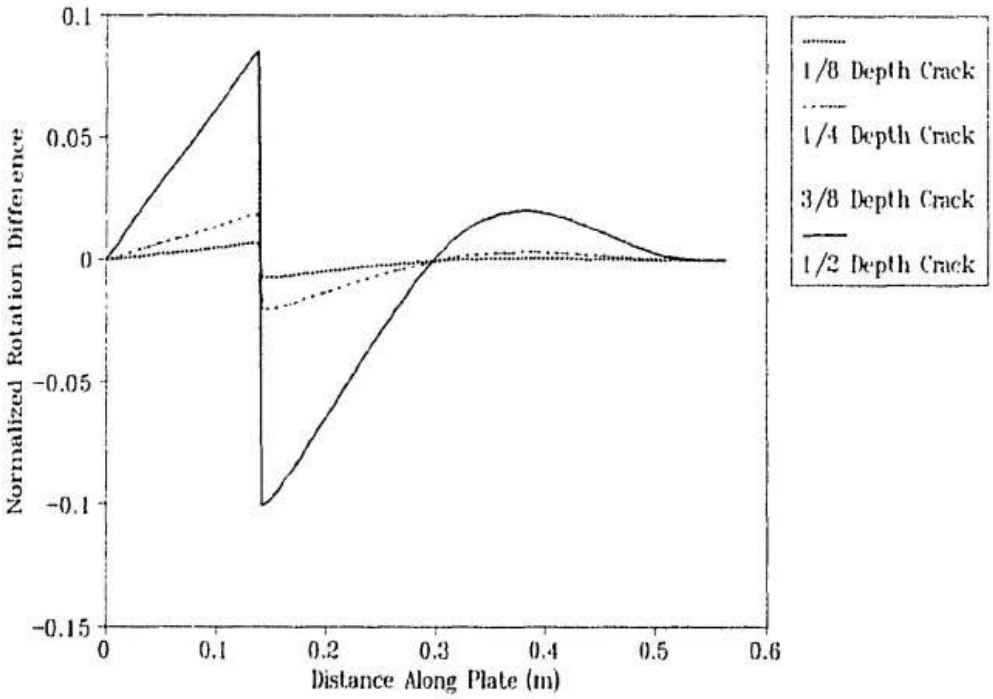

FIGURE 4.14 - ROTATION MODE SHAPE DIFFERENCE W.R.T REFERENCE PLATE, MODE 3

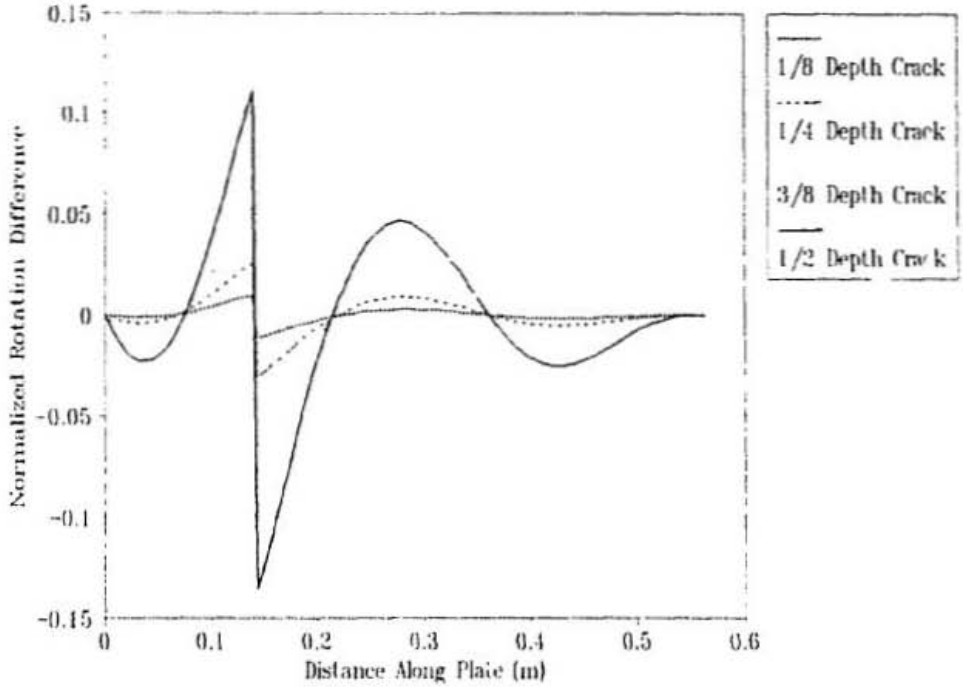

FIGURE 4.15 - ROTATION MODE SHAPE DIFFERENCE W.R.T REFERENCE PLATE, MODE 4

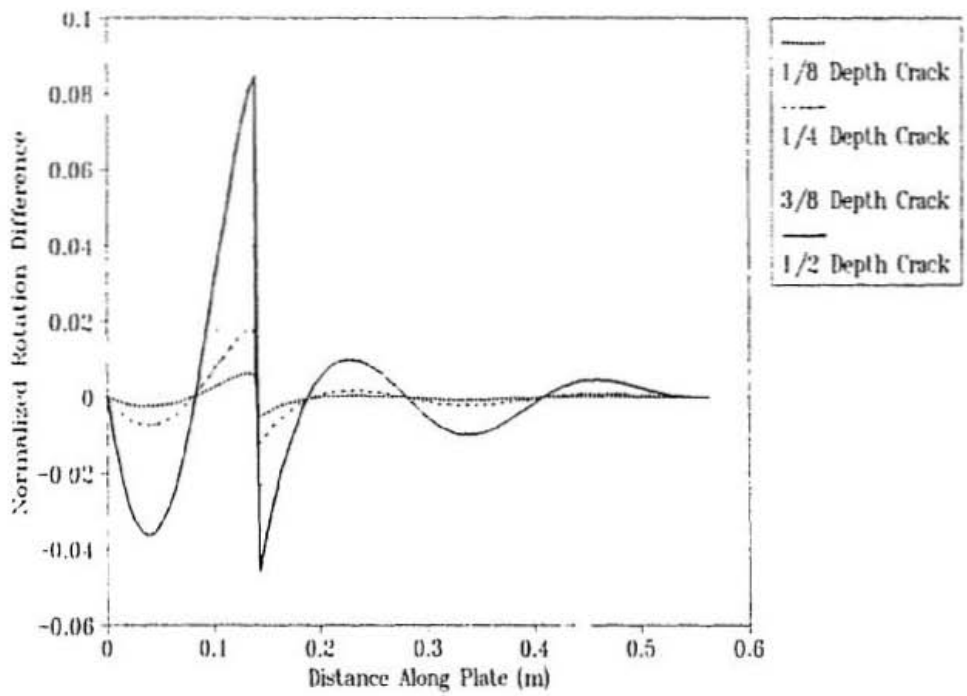

FIGURE 4.16 - ROTATION MODE SHAPE DIFFERENCE W.R.T REFERENCE PLATE, MODE 5

These plots show that this technique, of closely observing changes in the slope and displacement mode shapes, is a clear indicator of crack location. It is seen that for the lower modes the discontinuity of the plot of mode shape difference, at the location of the crack, is distinct and of a much larger magnitude than at any other location on the plate. The higher modes tend to lose the magnitude aspect since crack induced differences at other plate locations, tend to approach and surpass the magnitude of those at the crack. The qualitative aspect of the plot, however, remains distinctive due to the sharpness of the peak at the crack location. Other local maxima along the plate length, are much more gently curved and are easily distinguished from the crack maxima.

This method is a clear indicator of crack location for the structure evaluated here, namely, a cantilever plate. Its applicability to real structures, however, with their inherent complexity, is not necessarily assured, and remains to be determined. Additionally, the usefulness of this method, from an experimental aspect, is questionable due to the high degree of refinement that is required.

While the results of the method are notable, significant research remains to be conducted, in order to determine how to most appropriately apply the method to the development of the ultimate objective, that of a non-destructive evaluation scheme, using modal analysis.

4.4 Summary

There is a strong link between analytical and physical models in modal analysis and in general they must be used in conjunction with each other to form a valid system of prediction, modelling and testing. The analytical evaluation performed here, illustrated a number of useful phenomena, that might not have been observed from experimentation alone. It also provided a basis for comparison and verification of experimental results.

The analysis/prediction procedure is often iterative and requires consistent attention to results obtained both through analysis and experimentation. In an attempt to illustrate this link, this research considered both forms of analysis, the analytical, presented here, and the experimental, presented as follows, in Chapter 5.

Chapter 5

Experimental Results

A major part of the research conducted during this course of study involved experimentation to determine what effect, if any, the presence of a crack has on the modal properties of a typical vibrating structure. The structure of concern here, is of course, the cantilever plate that has been described in the previous section.

The experiments conducted for this study are grouped into two categories as determined by the type of output transducer used (ie., the type of response parameter measured). The first of these groups used accelerometers as the output transducers and is discussed in Section 5.1. The second used strain gauges as transducers and is discussed in Section 5.2. While each set of results was analyzed independently to determine how each could be put to effective use, a second underlying objective was to compare the relative merits of each type of transducer for response measurement.

In reality a structure that is subject to a cyclic loading regime of sufficient magnitude will develop fatigue cracks at points of extreme stress. In this initial experimentation scheme, it was deemed too complicated to develop fatigue cracks in the test specimens, so in its place, a number of specimens were manufactured with simulated cracks. To simulate these naturally occurring fatigue cracks, a rectangular notch was cut across the entire width of each plate with a milling machine. Five specimens were used for the accelerometer testing,

one without any notch, and four with notches of varying depth cut at the 1/4 span location of each, ie., 141 mm from the fixed end. The notch depths that were used varied from a minimum of 1/8 the plate thickness (0.794 mm) to a maximum of 1/2 the plate thickness (3.175 mm), in increments equal to 1/8 the plate thickness. An additional two specimens were used in the strain gauge testing, both with 1/2 depth cracks, one cut at the 1/2 span point (282 mm from the fixed end), and the other at the 2/3 span point (376 mm from the fixed end).

It was decided that to adequately determine the global response of the plate, response measurements using accelerometers would be conducted at 18 nodes on the plate. These response nodes are shown diagrammatically in Figure 5.1. Due to equipment limitations, however, it was not possible to measure all 18 nodes simultaneously. As a compromise the test was conducted by measuring 3 response nodes at a time. This meant that for a given plate it was necessary to move the accelerometers to 6 different locations. The mode of measurement was to move the accelerometers along the length of the plate, keeping them in line. The first test, therefore, measured the response at nodes 1, 2, and 3, the second at nodes 4, 5 and 6, and so on along the plate to test 6 which measured the response at nodes 16, 17, and 18. To ensure that the mass of the accelerometers (in the order of 10 grams each) would not affect the modal parameters as they were moved along the plate, small weights of similar mass to that of the accelerometers, were placed at all measurement points except the three occupied by the accelerometers. This ensured that there was no relative change in added masses for different locations from one test to the next.

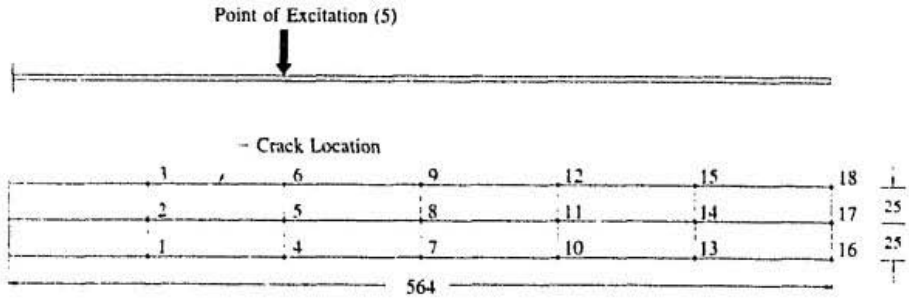

FIGURE 5.1 - LOCATION OF RESPONSE NODES ON TEST PLATES

It was found that it was impossible, given the resolution of the data acquisition system (DAC), to adequately measure response over a large frequency band. This was due to the fact that as with all similar systems, the data acquisition input voltage was limited to a relatively small value. To ensure that this value was not exceeded, it was necessary to adjust the input level so that the peak output from the accelerometer amplifiers was less than that permitted by the DAC. This in turn meant that the response level at the most dominant resonant frequency was the governing factor in determining the input level and gain factors. As a result the very low output signal at off-peak frequencies often fell below the level noise in the system and was undistinguishable from it. As a result, the transformed frequency domain functions were then very noisy at anti-resonance locations. To overcome this problem, the test was divided into seven frequency bands. This permitted the input level to be adjusted higher for low output regions thus giving a strong clean signal well above the level of noise. Each band was analyzed individually, and the global response function over the entire frequency range was created by assembling pieces from each of the individual tests. Table 5.1 lists these seven frequency bands, and the type of excitation input used for each.

TABLE 5.1 - TEST FREQUENCY RANGES

Band Number	Frequency Band (Hz)	Type of Excitation
1	1 - 100	Log Sweep
2	35 - 350	Log Sweep
3	280 - 420	Linear Sweep
4	380 - 520	Linear Sweep
5	480 - 770	Linear Sweep
6	730 - 890	Linear Sweep
7	870 - 1020	Linear Sweep

The individual tests recorded five seconds of response and excitation data at a sampling frequency of 4000 Hz. As a result each channel of input collected 20000 time history data points. Performing the tests over the seven frequency bands, for each of 24 channels per plate (18 response & 6 input) for the 5 plates, produced 16.8 million data points, for subsequent analysis. Appendix B contains plots of several typical time histories recorded during the course of this experiment.

All data acquisition was performed using a Keithley 570 data acquisition system mated to a 386 (25 MHz) personal computer, running a control program developed at Memorial University. After acquisition the raw ascii data was converted to universal files[7] using an author written program and transferred to a VAX 8530 computer for processing using the test data analysis module of the software package I-DEAS. Each of the time history data sets were analyzed individually to generate frequency response functions (FRF's), valid over the frequency range of the excitation force used during the test. These small band FRF's were then assembled to create a single FRF for each node, valid over a frequency

---

7 Universal files are special format ascii files used by I-DEAS for inputting data generated outside the program.

range from 0 to 1000 Hz. These calculations used the Fast Fourier Transform algorithms and as such the resulting frequency domain functions are restricted in terms of data resolution ($\Delta\omega$) and maximum frequency (ω_{max}), to values determined from the expressions

$$\Delta\omega = \frac{\omega_s}{N} = \frac{2\pi}{T} \tag{5.1}$$

$$\omega_{max} = \frac{\omega_s}{2} = \frac{2\pi N}{T} \tag{5.2}$$

where

ω_s = the sampling frequency

N = the number of data points

The FRF's for this experiment, were generated using 12000 point averaging ensembles, recorded using a 4000 Hz sampling rate. As a result the frequency resolution of the FRF data from Equation 5.1 is 0.333 Hz, and the valid maximum frequency from Equation 5.2 is 2000 Hz (twice the desired range of consideration).

The entire set of FRF's (90 in all) generated from the test data is included at the end of this document in Appendix C.

5.1 Discussion of Accelerometer Results

The task of FRF generation from time history data, while computationally intensive, is considered only to be primary processing. The procedure does not yield results which are in any way indicative of the modal parameters of the system. These are determined via a second phase of processing, one which uses as input the results of the primary processing, ie., the frequency response functions. This secondary processing is the modal analysis

phase, where the objective is to evaluate the modal parameters of the system from the frequency domain data previously derived. The modal parameters include: natural frequencies of the system (eigenvalues), their associated mode shapes (eigenvectors), structural damping associated with these modes, and amplitudes of vibration in terms of the output parameter measured (ie. acceleration, velocity or displacement). It is these values which are of primary interest to this experimentation.

5.1.1 Frequency Shifts Resulting from Cracks in The Plates

The successful development of a monitoring system which uses dynamic response as an indicator of loss of structural integrity, will rely heavily on its ability to monitor the natural frequencies of the structural system. This investigation attempted to reveal how the imposed structural defects affected the natural modes of a vibrating cantilever plate. From the analysis discussed in Chapter 4, and from the closed form solution of a cantilever beam, the theoretical modes of the plate being considered were well known prior to commencement of testing. It was decided that considering the frequency range from 0 to 1000 Hz, would be sufficient to illustrate the potential changes in modal parameters. In this frequency range there are 5 primary bending modes (which are of primary interest here), two torsional modes, and two transverse bending modes. Due to the orientation of the response transducers, only the primary bending and torsion modes could be measured from experimentation. The transverse bending modes were not expected to show much change due to the orientation of the crack and were, therefore, not considered in the analysis.

The initial phase of this investigation simply focused on determining the natural frequencies of each of the five plates. This is of course one of the output parameters associated with curve fitting (to be discussed later in this section) but can most accurately be determined from a global perspective through the generation of Mode Indicator Functions (MIF's). There are two primary types of MIFs, both of which are intended to visually locate frequencies associated with the natural modes of the system. They do not, however, give any indication as to the other parameters of the system (ie., damping and amplitude). The first type of MIF is called the Normal Mode Indicator Function. This function has a maximum value of unity and a number of local valleys where structural modes exist. The function is the ratio of the sum of the products of the real part of a series of frequency response functions and their magnitudes to the sum of the squares of the magnitudes of these functions. This is written in equation form as

$$\frac{\sum(|\Re(H)|\cdot|H|)}{\sum(|H|^2)} \tag{5.3}$$

The second type of MIF is called the Power Spectra Mode Indicator Function, and is simply a conjugate summation of selected functions derived by multiplying each function by its complex conjugate and summing the result. This type of MIF calculates peaks where structural modes exist, rather than valleys. In equation form this is written as follows:

$$\sum(H\cdot H^*) \tag{5.4}$$

This author found that after comparing the two, the second type of function, ie., the power spectra, provided the clearest indication of where the modes were located.

Mode indicator functions were generated for each of the five plates used in the accelerometer testing. The input included all 18 FRF's for each plate to ensure that average values were obtained. The resulting functions are shown in Figures 5.2 through 5.6. Table 5.2 lists the results obtained from these functions.

TABLE 5.2 - NATURAL FREQUENCIES FROM MODAL TEST (HZ)

Mode	Reference Plate	1/8 Depth Crack	1/4 Depth Crack	3/8 Depth Crack	1/2 Depth Crack
1 B	15.67	15.55	15.53	15.45	14.60
2 B	97.00	97.16	96.33	97.00	97.96
3 B	272.67	271.82	269.16	267.66	258.18
1 T	334.67	332.67	330.34	329.99	328.98
4 B	541.67	539.06	532.95	529.95	518.12
5 B	889.00	886.71	880.67	884.95	881.43
2 T	990.67	989.83	987.29	990.79	990.00

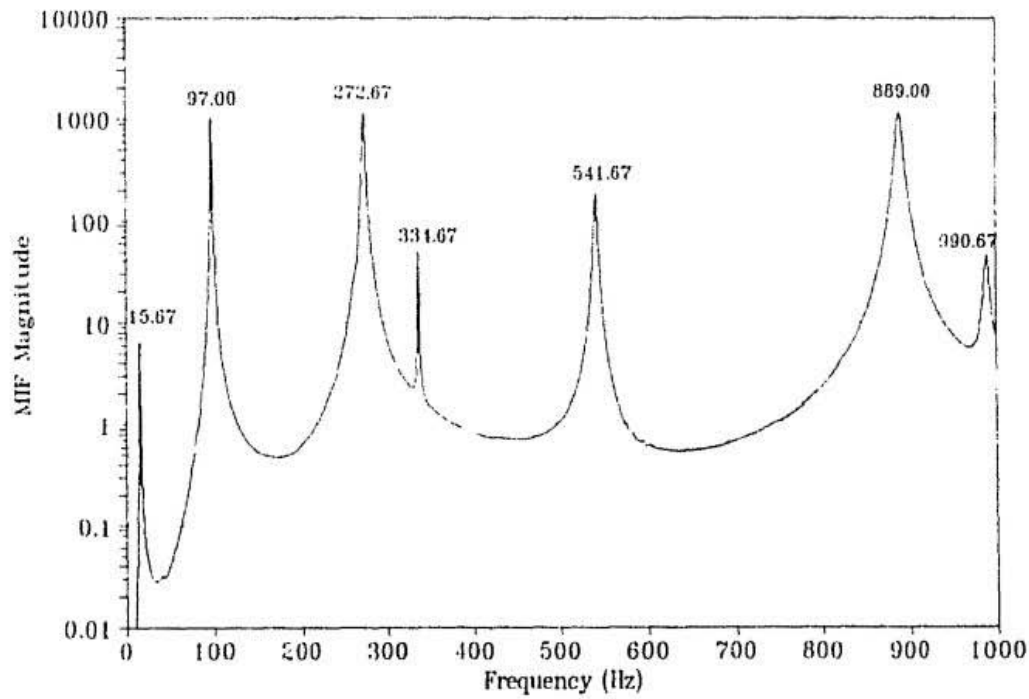

FIGURE 5.7 - POWER SPECTRA MIF, REFERENCE PLATE (NO CRACK)

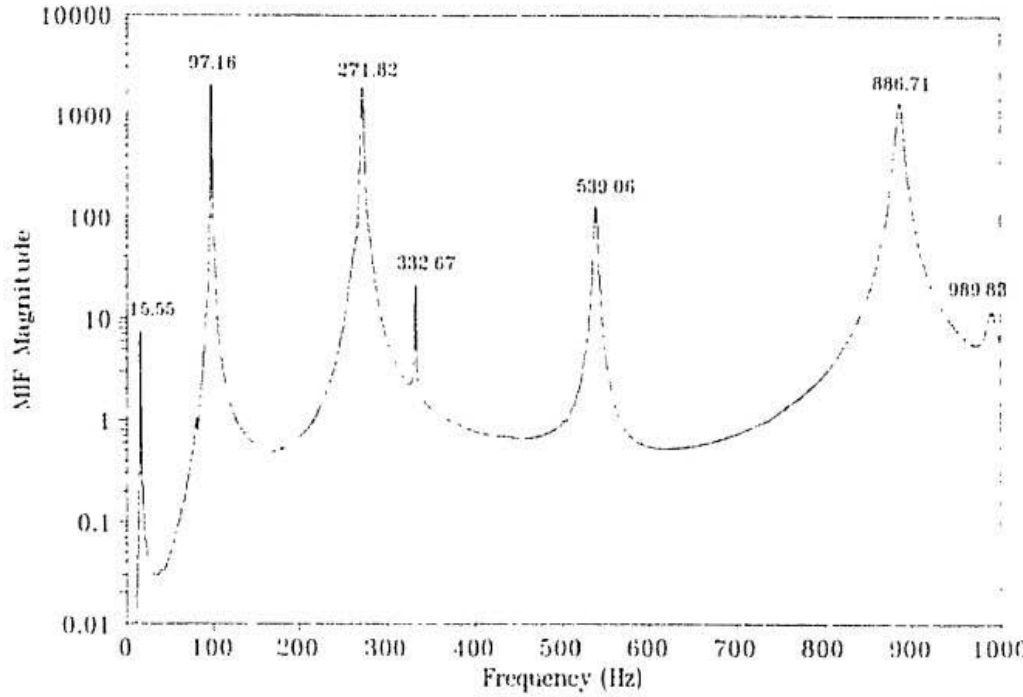

FIGURE 5.3 - POWER SPECTRA MIF, 1/8 DEPTH CRACK

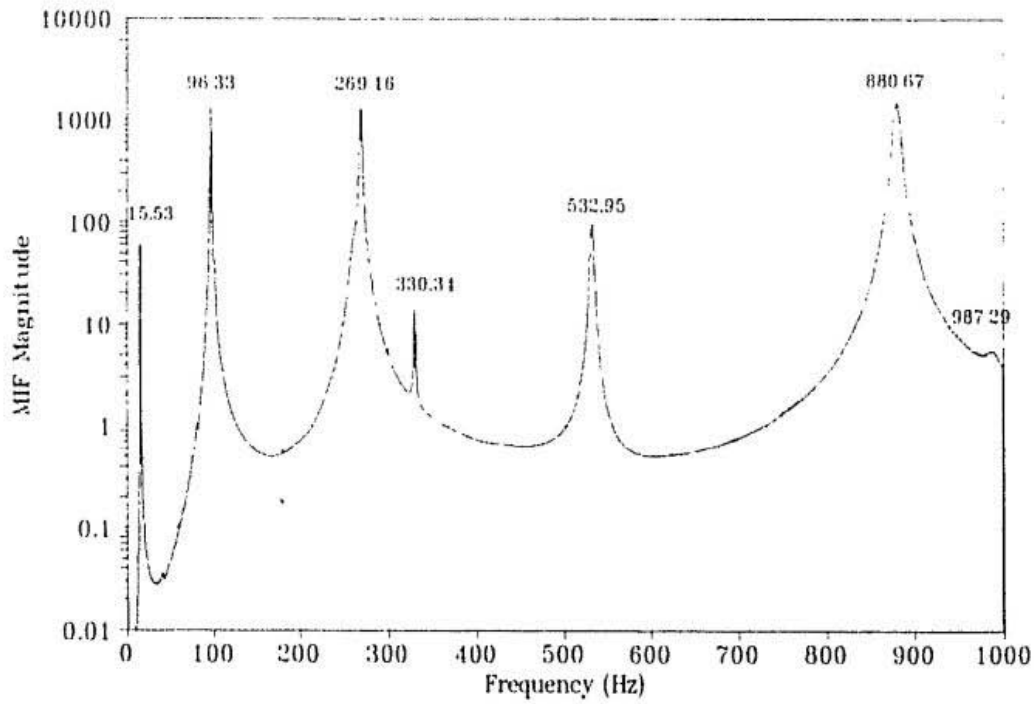

FIGURE 5.4 - POWER SPECTRA MIF, 1/4 DEPTH CRACK

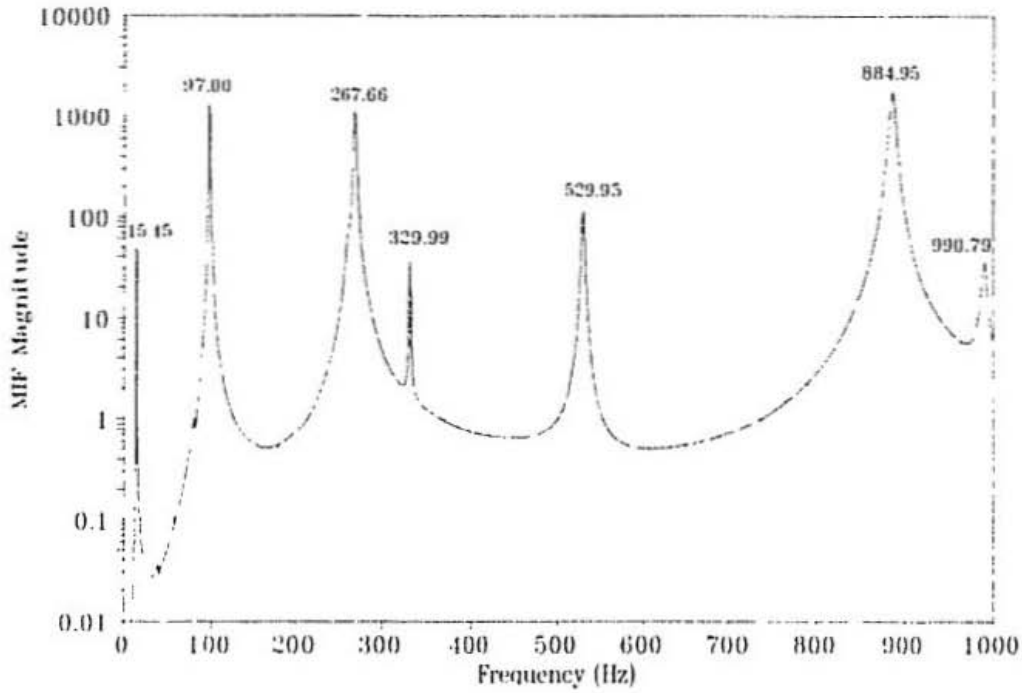

FIGURE 5.5 - POWER SPECTRA MIF, 3/8 DEPTH CRACK

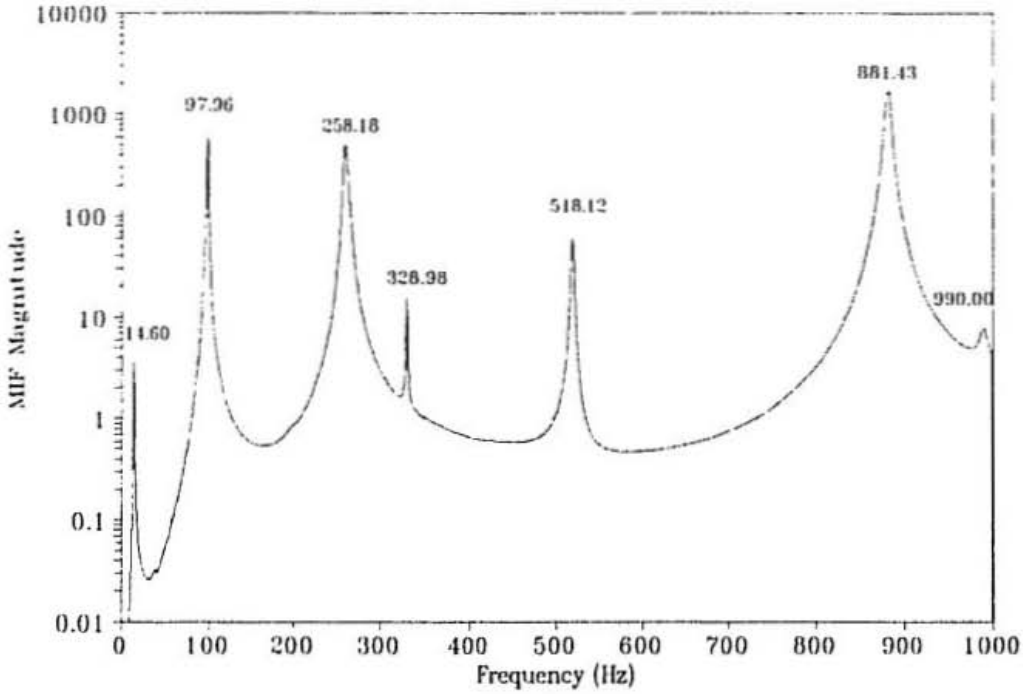

FIGURE 5.6 - POWER SPECTRA MIF, 1/2 DEPTH CRACK

It appears from perusing these results that for specific modes, there is a downward shift in frequency associated with an increasing crack depth. To fully illustrate this effect on resonant frequencies the following discussion will consider each mode individually.

The shift in frequency for mode 1 shows a clear dov nward trend as the depth of the crack increases. The results, however, do not show as smooth a downward trend as expected from the results of the finite element analysis. Additionally, the net downward shift for the largest crack is 6.8 percent, a value larger than expected, since the finite element model results showed only a 3.8 percent drop. This can probably be attributed to experimental error, mesh limitations in modelling the crack for the finite element analysis, and limitations in the experimental test equipment. These are further elaborated upon in the following paragraphs.

The aforementioned equipment limitations concerned the accelerometers that were used for the testing. These were very light so as not to affect the true modes of the plate to any large extent. This, however, compromised the usable lower frequency limit, since light accelerometers are not suitable for measurement of low frequencies. These particular accelerometers were found to produce a readable signal at around 10 Hz, a value not far removed from the first natural frequency. The results for mode 1 are, therefore, suspect since they are located just barely inside this lower frequency limit.

The errors alluded to concerning the finite element results deal with the manner in which the crack section was modelled. The method adopted for this investigation, as described in Chapter 4, consisted of reducing the element thickness at the crack location and

considering the crack as a set of separate elements. This method would tend to produce a somewhat stiffer response, resulting in frequency values higher than those derived from experimentation. Notwithstanding the discrepancy, the shift is quite obvious, and in the direction expected.

The shift in frequency for mode 2 was random and of no significant magnitude. The values show both upward and downward movement for various crack depths. This is not considered an error, however, since no trend was evident for this mode from the finite element analysis either. Considering the location of the crack with respect to the mode shape for this frequency, as shown in Figure 5.7, it is obvious that the crack will have little effect since it lies almost directly on a point of inflection (zero bending moment) of the deformed plate. The shifts that did occur were of little consequence and can be attributed to experimental inconsistencies. Of more importance in these observations, is the lack of a notable trend in the frequency shifts.

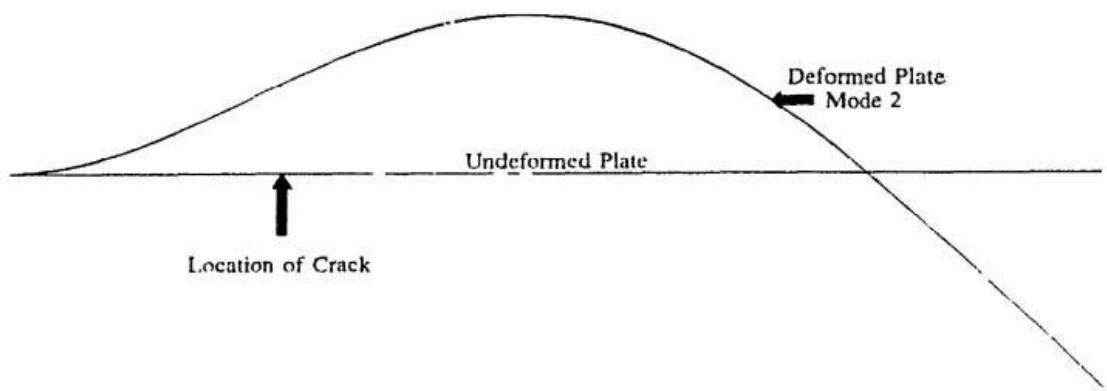

FIGURE 5.7 - MODE SHAPE FOR SECOND MODE

The shift in mode 3 is very obvious from 272.67 Hz for the uncracked specimen to 258.18 Hz for the 1/2 depth crack specimen, a 5.31 percent shift. The results are similar to that

expected from the analytical results, but are in fact more severe. The predicted shift was only 2.35 percent. This discrepancy, is most likely attributable to the modelling characteristics of the mesh used in the finite element analysis, as previously explained for mode 1. The extent of the decrease is not surprising considering the fact that this frequency's associated mode shape, exhibits a high degree of curvature in the region of the crack. The obvious loss of stiffness in this region has resulted in the significant drop in the frequency, observed for this mode.

The next mode is the first torsional mode of the plate. This mode would not be expected to be affected by the presence of a crack to the same degree that a bending mode would. This is due largely to its dependence on the torsional stiffness of the section rather than the bending stiffness. Since the existence of a crack would not significantly change the torsional stiffness it would likewise not significantly change a torsional natural frequency to any large extent. Notwithstanding this explanation, there was a noticeable shift in frequency of the first torsion mode. The frequency shifted by 1.69 percent over the range of crack depths. This correlates quite well with the results of the analytical model, which predicted a 1.03 percent shift for this mode. It is noteworthy that the finite element results tended to overpredict the frequencies for the bending modes, but was conservative on its prediction of the torsional modes frequencies.

The fourth bending mode like the third, showed a significant downward shift as a result of the crack. Here, the frequency shifted from a high of 541.67 Hz to a low of 518.12 Hz. A shift of 4.35 percent. Once again the shift is expected due to the high degree of curvature in the vicinity of the crack. Analytical results correlated quite well, predicting

a downward trend, but of lesser magnitude. The predicted shift was only 2.61 percent.

The fifth bending mode did not produce results which closely reflected those derived from the analytical model. The overall shift was downward but the trend was not consistent due to a shift for the 1/4 depth plate, which was larger than that observed for either the 3/8 depth plate or the 1/2 depth plate. The trend is apparent, however, if the data for this specimen is not included. The analytical model did not predict a large shift, only in the order of 0.5 percent. In comparison, the experimental frequency shifted by 0.85 percent. This lack of significant shift, combined with high frequency sensitivity to experimental error would more than account for a single outlier in the results.

The final mode, the second torsion mode, showed no trend and very little shift, either up or down. Once again the torsion modes would not be expected to be significantly affected, due to the type of defect imposed. This prediction was shared by the analytical model, which likewise showed little in the way of frequency shift.

Additional illustration of the preceding discussion is provided in Figure 5.8 through 5.14 which show graphically the results of Table 5.2. For comparison, as in the text, the results of the finite element analysis are included in these figures.

For a detailed graphical comparison of the shifts in frequency along with a visual representation of the effects of changes in the other modal parameters, the reader is referred to Appendix D. The figures there, were obtained by comparing FRF's for each of the center-line nodes (ie. 2, 5, 8, 11, 15 and 17). Data is given for each of the 5 plates over a limited frequency range centred on the 5 bending mode frequencies.

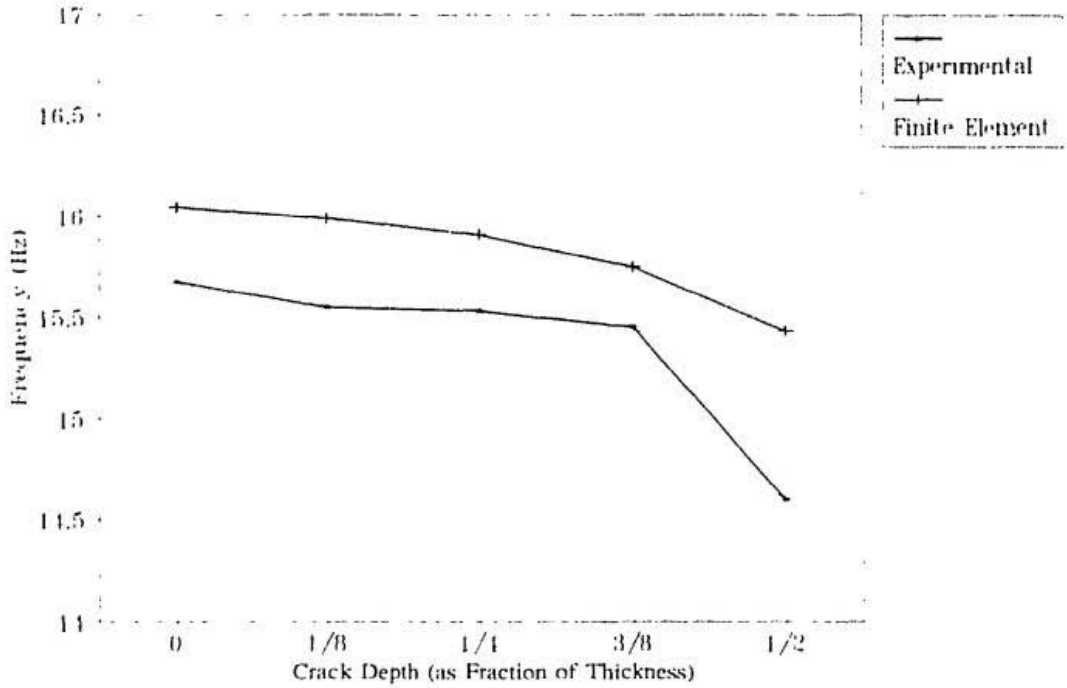

FIGURE 5.8 - FREQUENCY VARIATION WITH INCREASING CRACK DEPTH FOR BENDING MODE 1

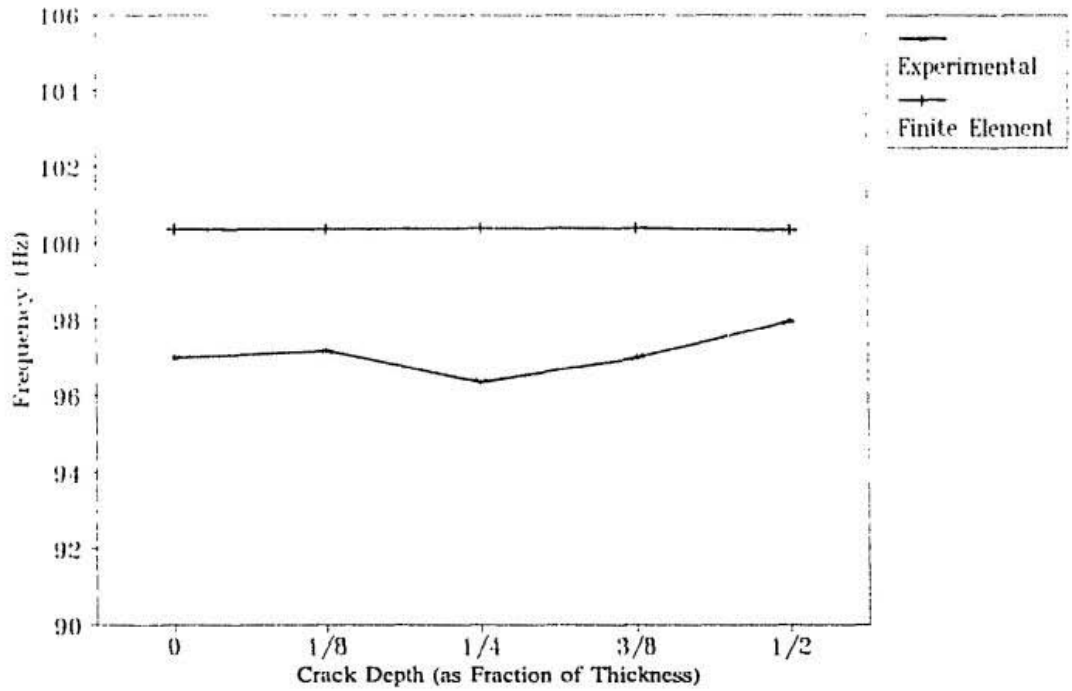

FIGURE 5.9 - FREQUENCY VARIATION WITH INCREASING CRACK DEPTH FOR BENDING MODE 2

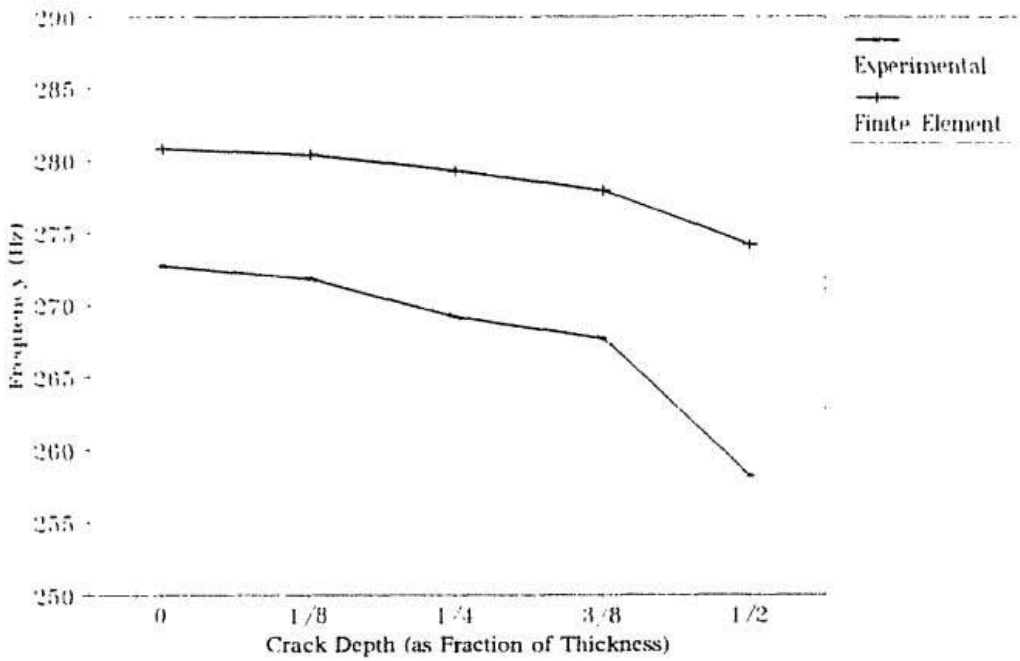

FIGURE 5.10 - FREQUENCY VARIATION WITH INCREASING CRACK DEPTH FOR BENDING MODE 3

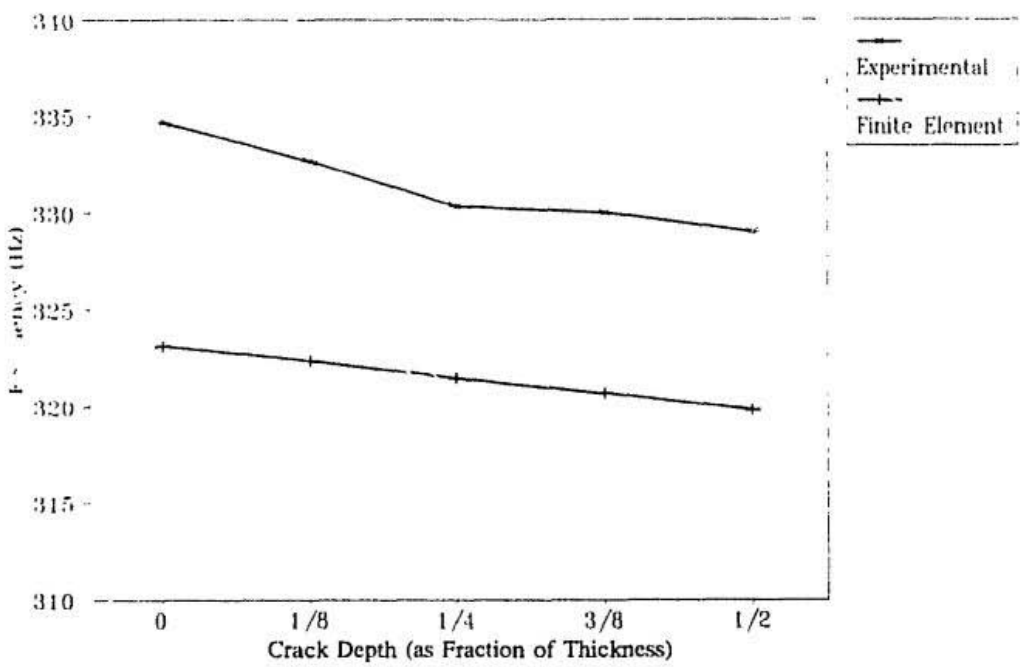

FIGURE 5.11 - FREQUENCY VARIATION WITH INCREASING CRACK DEPTH FOR TORSION MODE 1

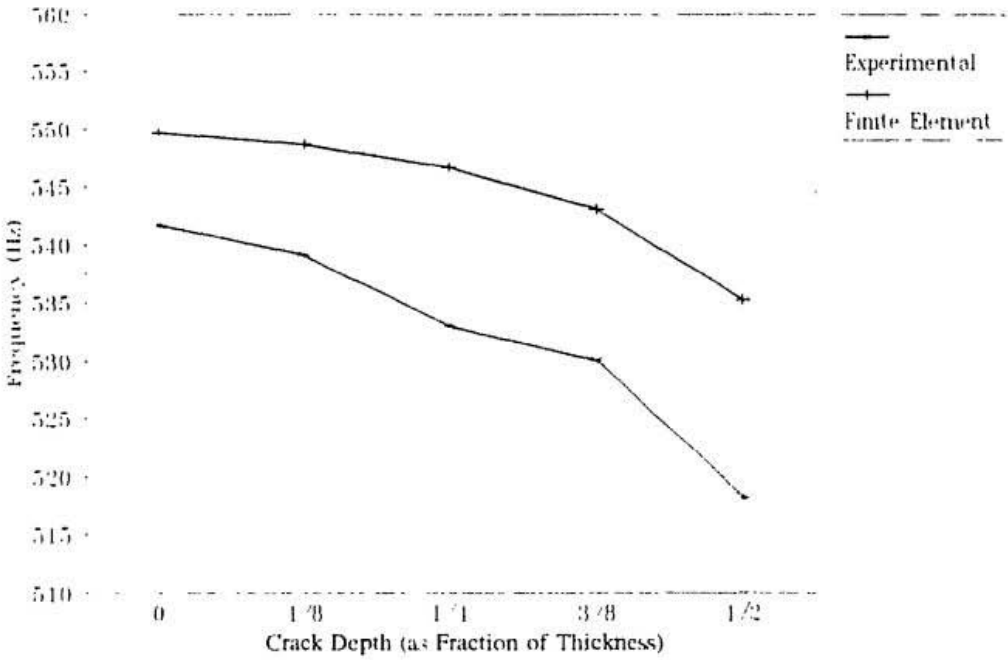

FIGURE 5.12 - FREQUENCY VARIATION WITH INCREASING CRACK DEPTH FOR BENDING MODE 4

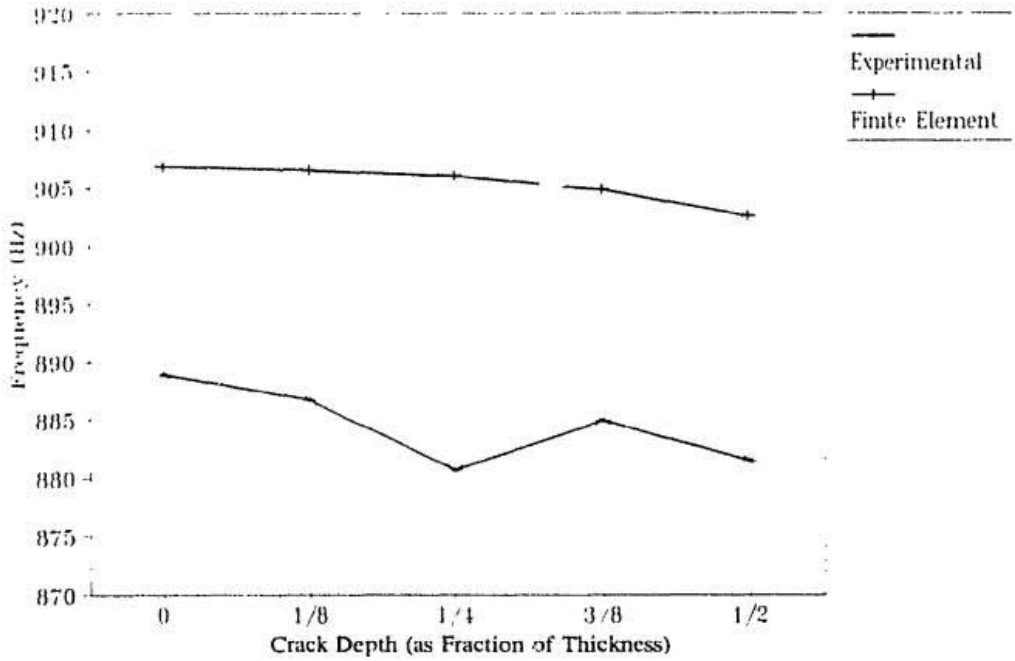

FIGURE 5.13 - FREQUENCY VARIATION WITH INCREASING CRACK DEPTH FOR BENDING MODE 5

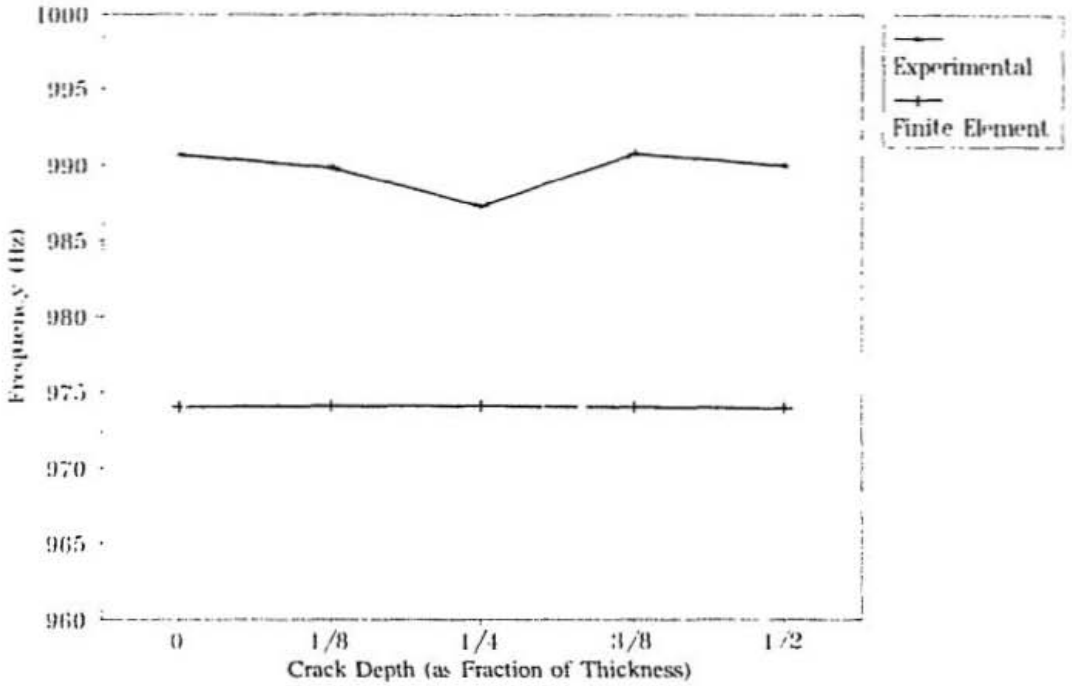

FIGURE 5.14 - FREQUENCY VARIATION WITH INCREASING CRACK DEPTH FOR TORSION MODE 2

5.1.2 Damping Changes Resulting from Cracks in Plates

The task of modal parameter estimation, also known as modal curvefitting, was alluded to at the start of the previous section. While it may not be the only method for estimating frequencies it is necessary for the calculation of damping values as well as modal residues. This task attempts to construct a mathematical model of vibration properties and physical deformations which represent the behaviour of a tested structure. For insight into the mathematical theory behind several popular parameter estimation techniques, the reader is referred to Chapter 3. The discussion which follows illustrates the modal curvefitting procedure generally followed in the analysis of experimental results.

Due to the similarity of results between nodes on a given plate, it was deemed unnecessary to perform parameter estimation for more than a representative number of nodes. Three nodes were chosen: 2, 11, and 17, along the center-line of the plate. Center-line nodes were chosen so as to eliminate the torsion modes from the FRF's, since torsion modes were not to be considered in this phase of the analysis.

The program I-DEAS by SDRC, was used to perform the task of modal curvefitting. From the perspective of this program, the general process of modal curve fitting and mode shape generation can best be described diagrammatically as shown in Figure 5.15.

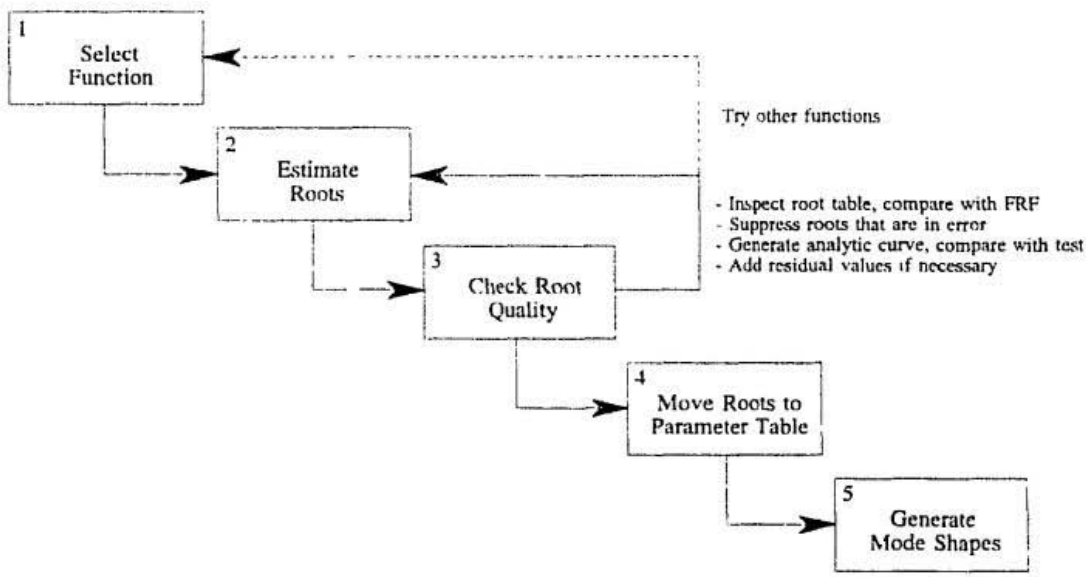

FIGURE 5.15 - MODAL CURVEFITTING PROCESS

From this diagram it is apparent that this is an iterative procedure which can require a number of adjustments before a suitable fit is achieved. Often, even after adjustment a good fit cannot be achieved and a compromise must be accepted. To accelerate the process this

author developed a procedure which used in conjunction with I-DEAS produced as close a fit as could be expected in a short period of time. Considering one peak at a time, this procedure simply produced a single degree of freedom analytical curve from the general expression for a FRF, written as

$$H(\omega) = \left[\frac{1}{k}\right] \frac{1}{1 - \left[\frac{\omega}{\omega_n}\right]^2 + i2\zeta\left[\frac{\omega}{\omega_n}\right]} \tag{5.5}$$

which can be written in the form $a + ib$ as:

$$kH(\omega) = \frac{1-\beta^2 - i2\zeta\beta}{\gamma} \tag{5.6}$$

where

$$\gamma = 1 + (4\zeta^2 - 2)\beta^2 + \beta^4$$

$$\beta = \frac{\omega}{\omega_n}$$

User input was requested for frequency and damping and inserted in the above equation. The generated curve was automatically scaled (in effect adjusting 1/k) so that the amplitude at the peak matched that of the experimentally derived function. Overlaying the two functions produced a visual indication of the correctness of the assumed values. These values could then be modified and another analytical curve generated until a reasonable fit was achieved. I-DEAS was then invoked to evaluate the analytical curve using its Circle Fit algorithm[8], to derive any missing parameters (ie., modal residue). As a final

[8] While the Circle Fit Technique was used predominantly for this purpose, the Complex Exponential Method was also used on occasion for verification of results and for evaluation of coupled modes.

comparison, an analytic curve was generated by I-DEAS and compared to the test curve to indicate the curve fit quality.

In this manner, the damping values, along with the other modal parameters, were derived for the first five bending modes of the three selected nodes on each of the five plates. These values are listed in Table 5.3, and compared graphically in Figures 5.16 through 5.20.

TABLE 5.3 - DAMPING VALUES (%) FOR SELECTED NODES

Mode	Node	Reference Plate	1/8 Depth Crack	1/4 Depth Crack	3/8 Depth Crack	1/2 Depth Crack
1	2	2.111	2.200	0.731	0.600	2.200
	11	2.200	2.200	0.680	0.660	2.700
	17	2.300	2.300	0.700	0.900	2.800
2	2	0.690	0.500	0.450	0.550	0.630
	11	0.550	0.380	0.500	0.550	0.650
	17	0.650	0.420	0.500	0.600	0.800
3	2	0.630	0.456	0.496	0.542	1.319
	11	0.600	0.400	0.500	0.542	1.100
	17	0.650	0.520	0.600	0.600	1.000
4	2	0.704	0.600	0.422	0.300	0.300
	11	0.300	0.340	0.350	0.360	0.310
	17	0.400	0.390	0.390	0.380	0.350
5	2	0.491	0.545	0.550	0.371	0.380
	11	0.450	0.400	0.470	0.390	0.420
	17	0.550	0.500	0.500	0.500	0.540

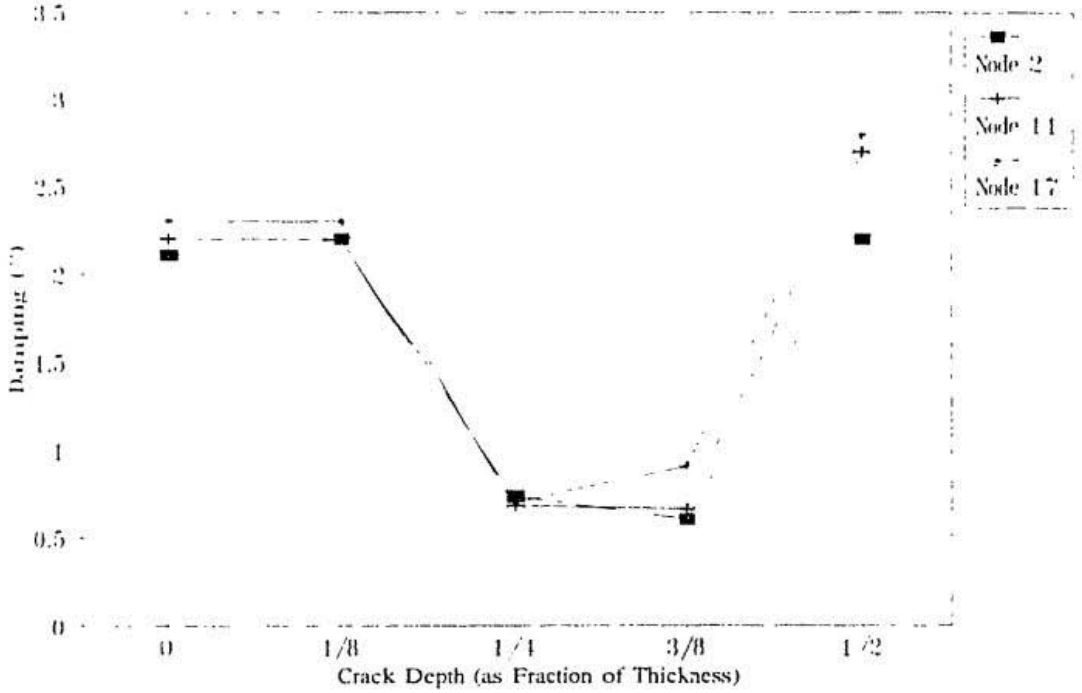

FIGURE 5.16 - DAMPING VARIATION WITH INCREASING CRACK DEPTH FOR BENDING MODE 1

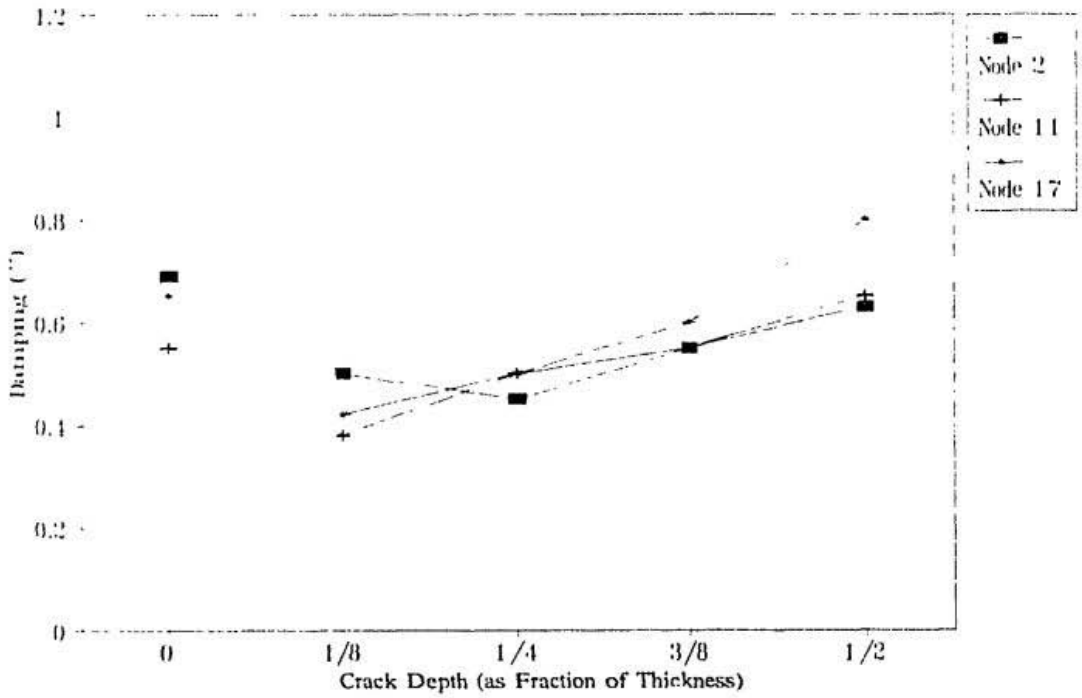

FIGURE 5.17 - DAMPING VARIATION WITH INCREASING CRACK DEPTH FOR BENDING MODE 2

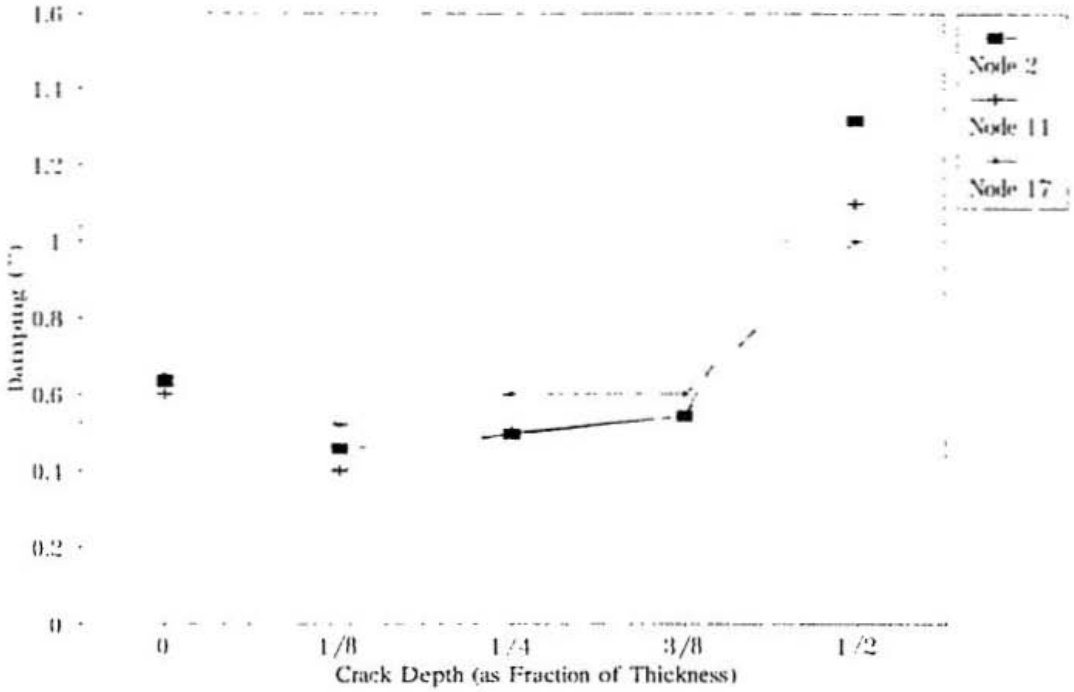

FIGURE 5.18 - DAMPING VARIATION WITH INCREASING CRACK DEPTH FOR BENDING MODE 3

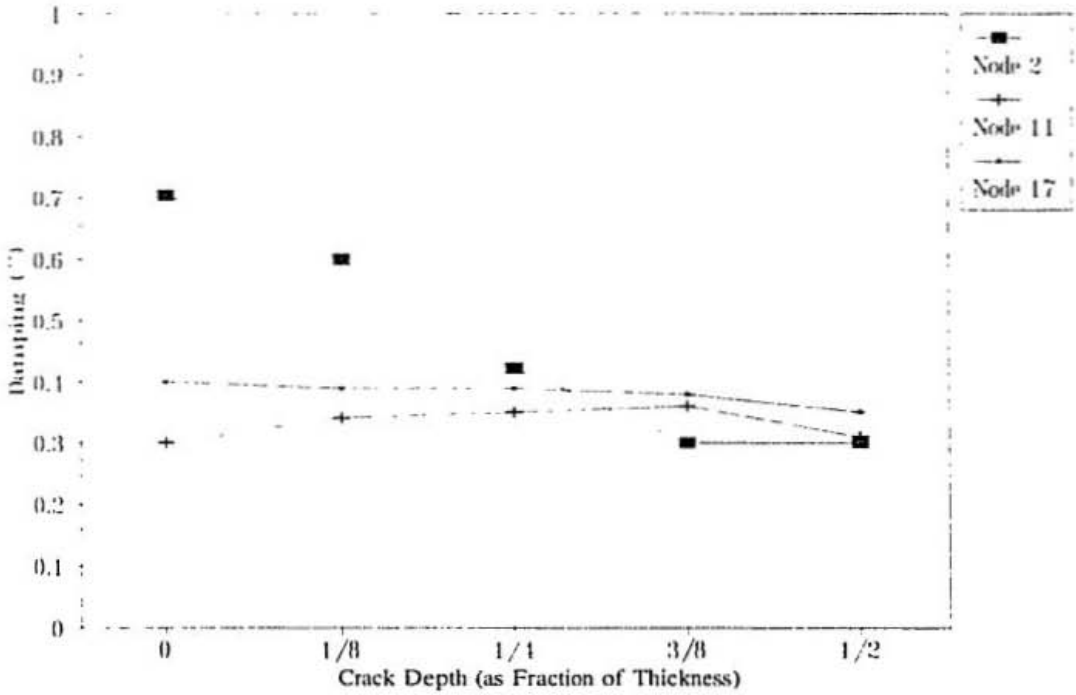

FIGURE 5.19 - DAMPING VARIATION WITH INCREASING CRACK DEPTH FOR BENDING MODE 4

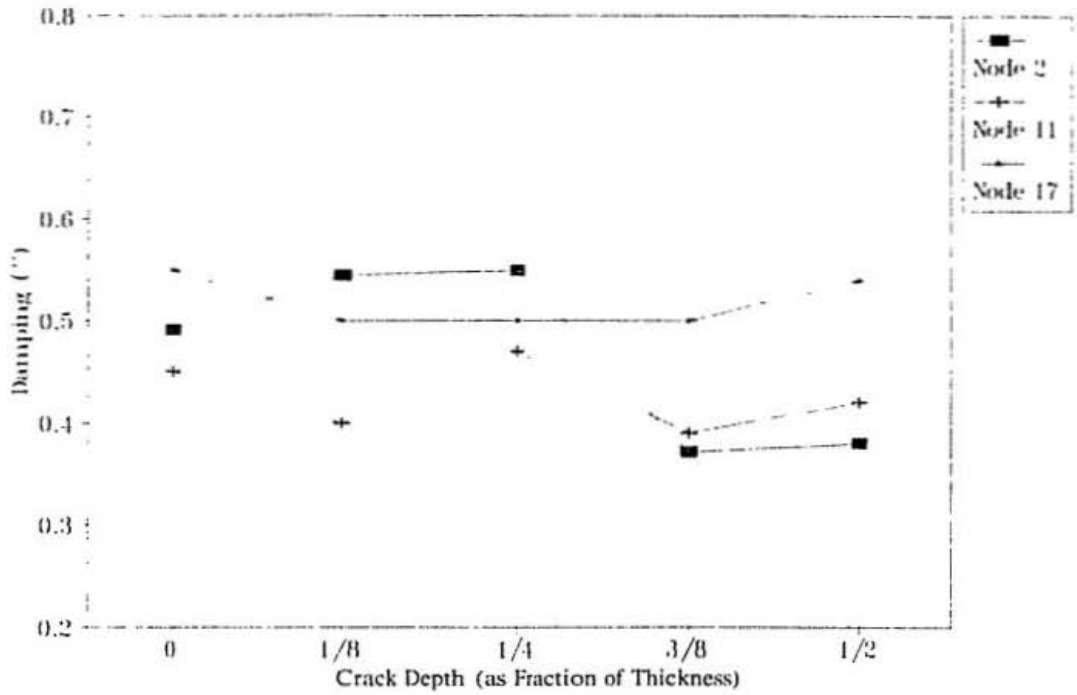

FIGURE 5.20 - DAMPING VARIATION WITH INCREASING CRACK DEPTH FOR BENDING MODE 5

The trends for damping are not quite as obvious as those discovered for frequency. There is some evidence, however, that seems to indicate a causal relationship. Of the five bending modes considered two appear to show an upward trend. Consider, for instance, the change in damping for mode 2. There is a drop in damping for the initial crack but a consistent increase for each of the others. The overall trend appears to show an increase in damping associated with an increase in crack depth. It is interesting to note, though, that this mode was little affected in terms of frequency shift. Mode 3, as well, shows a distinct upward trend correlated with increased crack depth. Here, though, a major frequency shift accompanies the increased damping.

Evidence of a trend is not apparent in the damping plots for the other three modes. In actuality there is probably no physical phenomena here to cause it. One investigation presented in Sanliturk and Imregun (1991), showed that for fatigue cracks a mathematical relationship could be derived to predict damping increases due to fatigue cracks. The principle action of concern here, is the friction between the surfaces in the crack. In this experiment, however, the cracks are simulated by rectangular notches and as such have a relatively wide separation between the sides of the crack. As a result, friction is definitely not a factor.

A definitive statement concerning damping cannot be made with the evidence presented here. Further research is necessary in this area, encompassing many more modes and considering a greater variety of cracks. In addition natural fatigue cracks should be used as the failure mode to insure realistic effects on damping.

5.1.3 Amplitude Changes Resulting from Cracks in Plates

The consideration of amplitude as it applies to vibrating structures is at times a confusing issue as a result of the various definitions that can be placed on this term. The classical definition of amplitude for a harmonically excited single degree of freedom system is generally calculated by the following non-dimensional expression:

$$\frac{Xk}{Fo} = \frac{1}{\sqrt{(1 - \beta^2)^2 + (2\zeta\beta)^2}} \qquad (5.7)$$

and its phase by:

$$\phi = \tan^{-1}\left[\frac{2\zeta\beta}{1-\beta^2}\right] \tag{5.8}$$

where

β = ω/ω_n.
X = dynamic displacement (m)
k = spring stiffness (N/m)
F = dynamic force (N)

This is the expression for a SDOF frequency response function, that yields the output displacement per unit of force input. It is apparent from the numerator of the right side of Equation 5.7, that the damping ratio ζ, strongly influences the output value in the vicinity of $\omega=\omega_n$.

In a test situation it is very difficult to measure displacements directly. As a result, the output response typically measured is acceleration due to the reliability and versatility of the ubiquitous accelerometer. If desired there are methods that can be used to transform the output into displacement, one of which is to electrically alter the measured signal by filtering it through one or two capacitors and applying a calibrated resistance. This method in effect performs numerical integration on the analogue response signal before recording it through data acquisition. A second method is to record strictly acceleration data, generate acceleration frequency response functions, and subsequently perform a double numerical integration to obtain a displacement frequency response function. While these methods work they are not typically used due to increased computational effort resulting from diminishing numerical values, and lack of beneficial output. In general the response parameter used is inconsequential since one is analogous to another and changes that occur in one will similarly occur in the others. In addition the procedures involved introduce

additional sources of error into the results. In the first of the methods mentioned above, this error is caused by the introduction of additional circuitry and the inherent noise associated with it, and in the second method, by computational errors as a result of the rounding off of very small numbers[9]

The results of this experimentation express amplitude in terms of acceleration. The accelerometer output was calibrated and recorded using the standard unit, meters per second squared (m/s^2). All subsequent analysis used this unit for amplitude calculations.

In Chapter 3, the theory of modal analysis was discussed and a term known as the *modal constant* or *residue* was mentioned. This term is sometimes referred to as the amplitude and for this reason, the issue becomes somewhat confused. The analysis software I-DEAS, used in this analysis, is one such example. To avoid confusion in the following discussion, the term *amplitude* will only be used when referring to FRF amplitude (ie., physical amplitude) and the term *residue* will be used in reference to the modal factor described in Chapter 3.

The value of residue for a specific mode at a given location on the structure, along with damping and frequency, is one of the output modal parameters derived from the parameter estimation procedure. To begin discussion of the topic of amplitude, the residue values of the three nodes considered in the parameter estimation procedure will be compared. The calculated residues for the three nodes analyzed (2, 11 and 17) are given in Table 5.4. As before, the discussion values have been plotted for further illustration. These plots are given in Figures 5.21 through 5.25.

---

[9] Most digital computers are capable of performing calculations on double precision level, ie., to 14 decimal places. Amplitude of displacement in vibrating structures can be very small, often in the order of 10^{-7} or smaller (for this experiment at least). At this magnitude round off errors can become significant even at double precision.

TABLE 5.4 - RESIDUE VALUES FOR SELECTED NODES

Mode	Node	Reference Plate	1/8 Depth Crack	1/4 Depth Crack	3/8 Depth Crack	1/2 Depth Crack
1	2	0.050	0.197	0.211	0.146	0.080
	11	1.171	1.302	1.351	1.087	1.097
	17	2.379	2.561	2.369	2.227	2.193
2	2	12.547	12.544	12.362	12.313	12.902
	11	20.677	18.244	18.849	20.491	19.700
	17	45.000	46.214	45.269	46.247	53.413
3	2	76.077	68.711	67.737	68.629	100.030
	11	97.915	87.461	86.899	84.121	105.710
	17	132.760	129.110	118.340	124.070	143.890
4	2	57.708	43.846	38.453	34.094	22.976
	11	12.09	12.70	10.19	11.05	7.88
	17	60.503	55.211	44.406	46.566	32.535
5	2	274.330	296.140	307.300	283.860	285.600
	11	184.160	176.070	190.980	184.790	200.910
	17	269.410	359.400	344.660	342.500	359.410

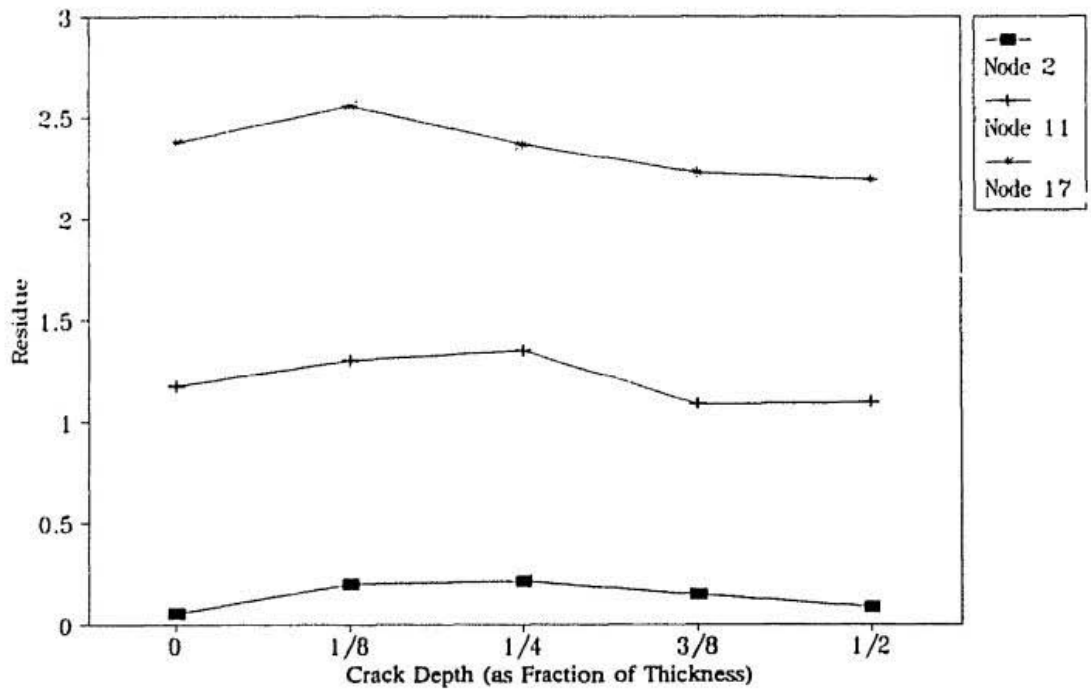

FIGURE 5.21 - RESIDUE VARIATION WITH INCREASING CRACK DEPTH FOR BENDING MODE 1

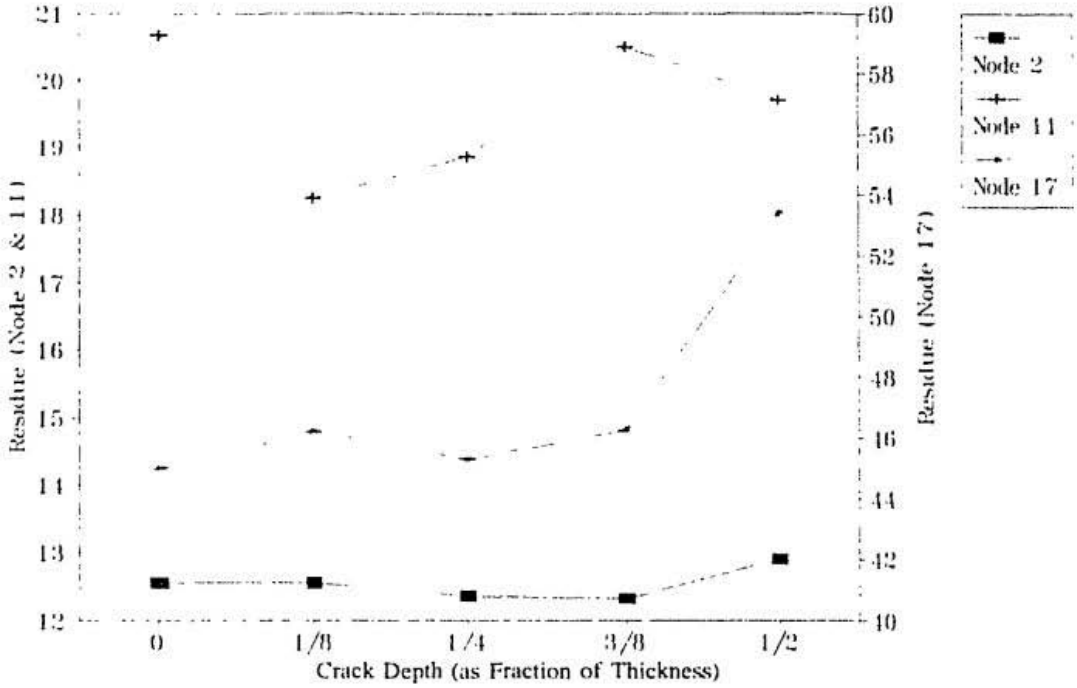

FIGURE 5.22 - RESIDUE VARIATION WITH INCREASING CRACK DEPTH FOR BENDING MODE 2

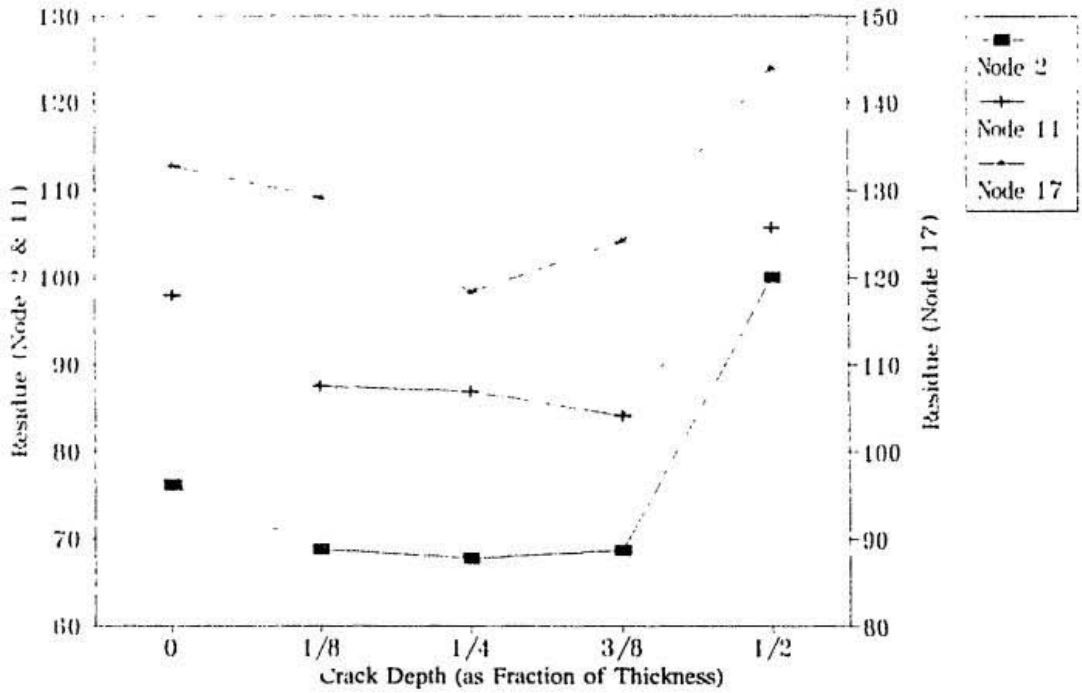

FIGURE 5.23 - RESIDUE VARIATION WITH INCREASING CRACK DEPTH FOR BENDING MODE 3

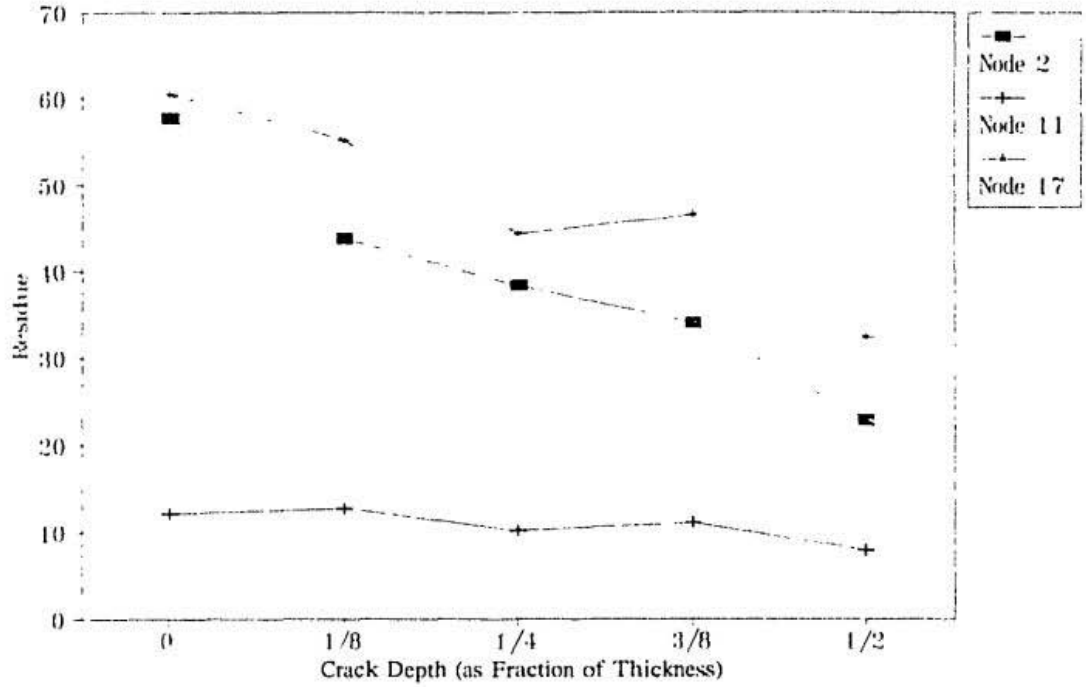

FIGURE 5.24 - RESIDUE VARIATION WITH INCREASING CRACK DEPTH FOR BENDING MODE 4

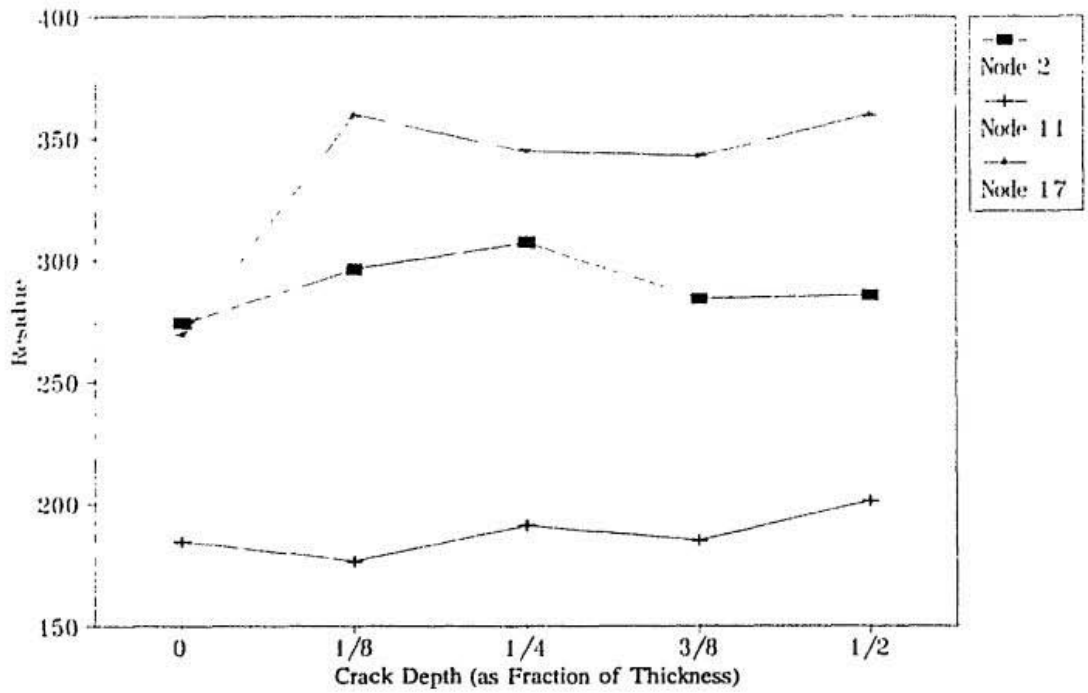

FIGURE 5.25 - RESIDUE VARIATION WITH INCREASING CRACK DEPTH FOR BENDING MODE 5

The preceding results would seem to suggest that there is little evidence of an observable trend associated with modal residue as crack depth increases. The patterns of these figures show that changes that did occur were marginal and behaved in a random fashion. This is not entirely unexpected considering the dependence of this parameter on the other two. From theory the general expression for a frequency response function at node k due to excitation at node i is given as

$$H_{ik} = \sum_{r=1}^{N} \frac{A^r_{ik}}{j\omega + \zeta_r\omega_r - j\omega_r\sqrt{1-\zeta_r^2}} + \frac{A^{r*}_{ik}}{j\omega + \zeta_r\omega_r + j\omega_r\sqrt{1-\zeta_r^2}} \qquad (5.10)$$

This expression shows that modal residue, denoted by A, is inversely related to both damping and frequency. If it is then assumed that for increasing crack depth, there will be a general decrease in frequency, combined with a smaller increase in damping, then it is logical to assume that modal residue will be affected very little if the FRF peak values are not significantly changed.

This logically leads to a question concerning change in FRF amplitudes, which, although related to change in residue, varies independently and may or may not follow the residue trend (ie., no trend at all). In observing the various FRF peaks shown in Appendix D it was noted that in many cases there appeared to be a decrease in the magnitude of the peak values as the crack depth increased. The shift, however, was small and not a global observation. In fact, some peaks showed almost no shift, while others did, but did not follow a trend.

Further observations reveal a more significant trend in the magnitude of the FRF at frequencies whose abscissa values are slightly offset from the peak value. The pattern of decreasing magnitude at these locations, is much more obvious and consistent than at the peaks. To further illustrate this phenomena consider a comparison of function magnitudes for node 17 at points offset above and below the FRF peak frequencies for each of the 5 bending modes.

The offset frequency values used for this comparison along with their associated FRF amplitudes (at node 17) for each of the tested plates is listed in Table 5.5. Additional illustration is provided by the graphical representation of this data in Figures 5.26 through 5.35.

TABLE 5.5 - COMPARISON OF OFF-PEAK FRF AMPLITUDES

Bending Mode	Hi / Low Frequency Offset Values	FRF Magnitude at Hi and Low Offset				
		Reference Plate	1/8 Depth Crack	1/4 Depth Crack	3/8 Depth Crack	1/2 Depth Crack
1 Low	12	0.05413	0.05859	0.06001	0.06439	0.07581
1 Hi	17	0.2955	0.2924	0.2574	0.2353	0.1871
2 Low	90	0.8478	0.9963	1.082	0.9078	1.111
2 Hi	103	1.478	1.636	1.509	1.605	1.442
3 Low	250	1.024	1.119	1.271	1.407	2.446
3 Hi	277	4.357	3.712	2.362	2.322	1.218
4 Low	513	0.5098	0.4786	0.4956	0.5773	0.9993
4 Hi	550	1.038	0.6392	0.2508	0.2195	0.02858
5 Low	875	2.802	4.901	9.657	4.749	7.885
5 Hi	893	6.714	6.718	3.991	6.239	4.328

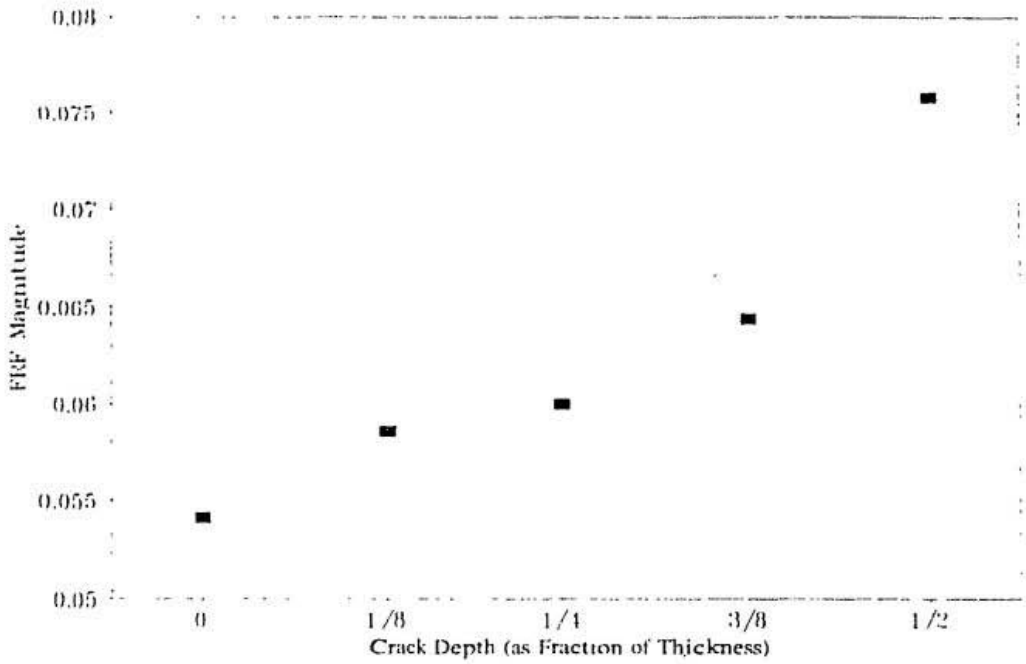

FIGURE 5.26 - FRF AMPLITUDE VARIATION WITH INCREASING CRACK DEPTH FOR NODE 17 AT LOWER OFFSET OF BENDING MODE 1 (12 HZ)

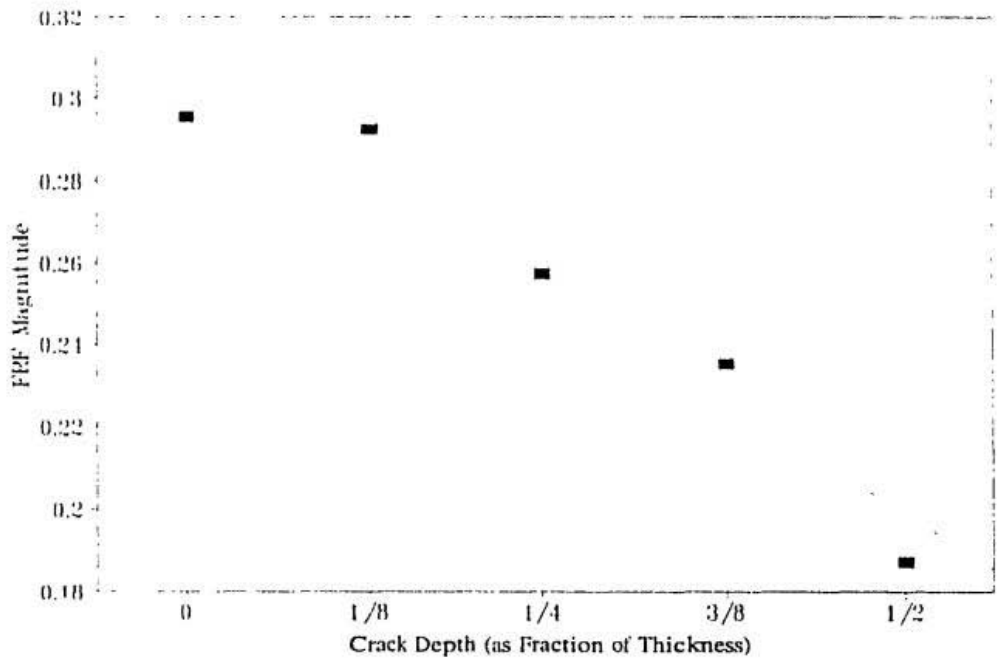

FIGURE 5.27 - FRF AMPLITUDE VARIATION WITH INCREASING CRACK DEPTH FOR NODE 17 AT UPPER OFFSET OF BENDING MODE 1 (17 HZ)

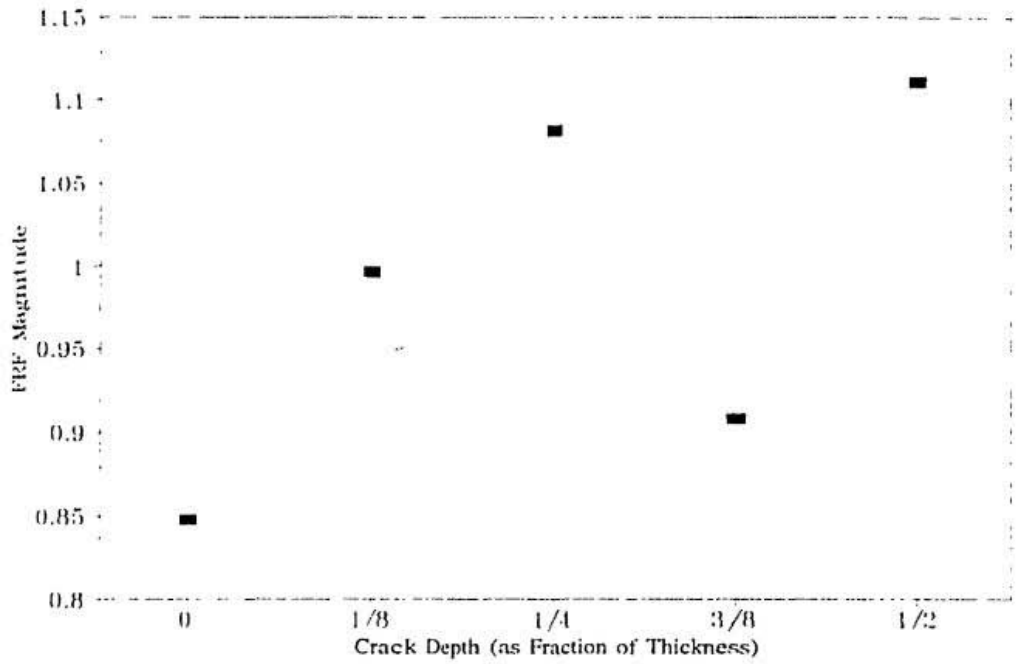

FIGURE 5.28 - FRF AMPLITUDE VARIATION WITH INCREASING CRACK DEPTH FOR NODE 17 AT LOWER OFFSET OF BENDING MODE 2 (90 HZ)

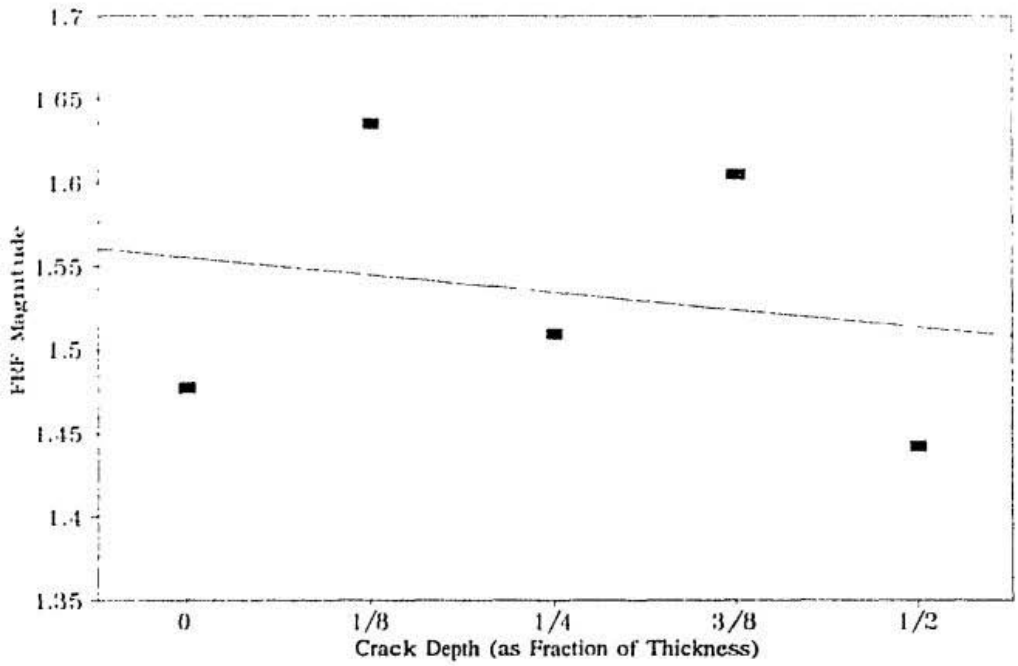

FIGURE 5.29 - FRF AMPLITUDE VARIATION WITH INCREASING CRACK DEPTH FOR NODE 17 AT UPPER OFFSET OF BENDING MODE 2 (103 HZ)

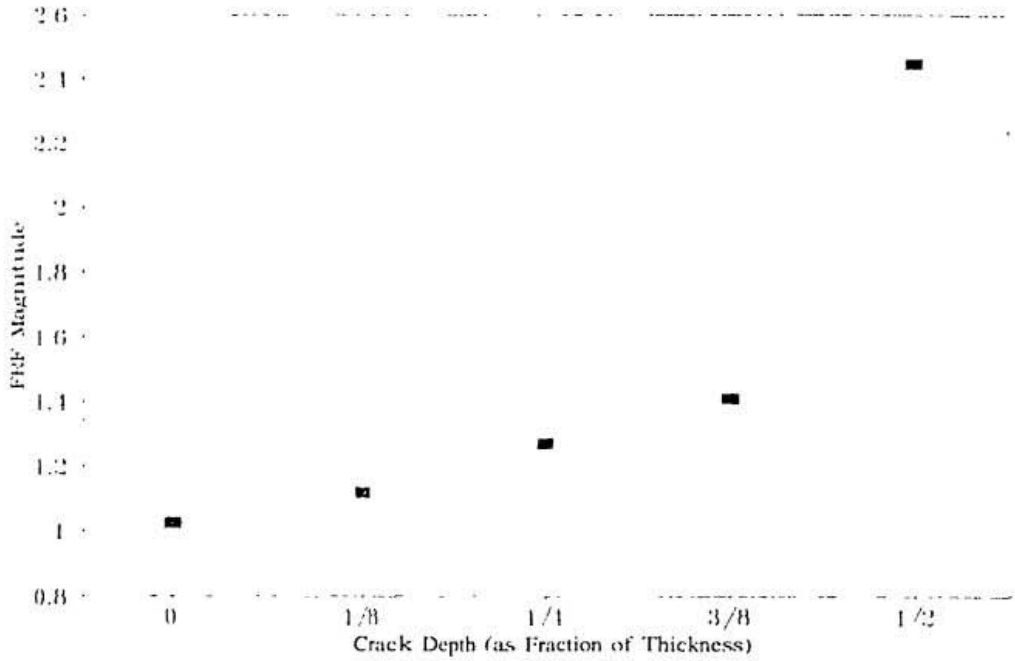

FIGURE 5.30 - FRF AMPLITUDE VARIATION WITH INCREASING CRACK DEPTH FOR NODE 17 AT LOWER OFFSET OF BENDING MODE 3 (250 HZ)

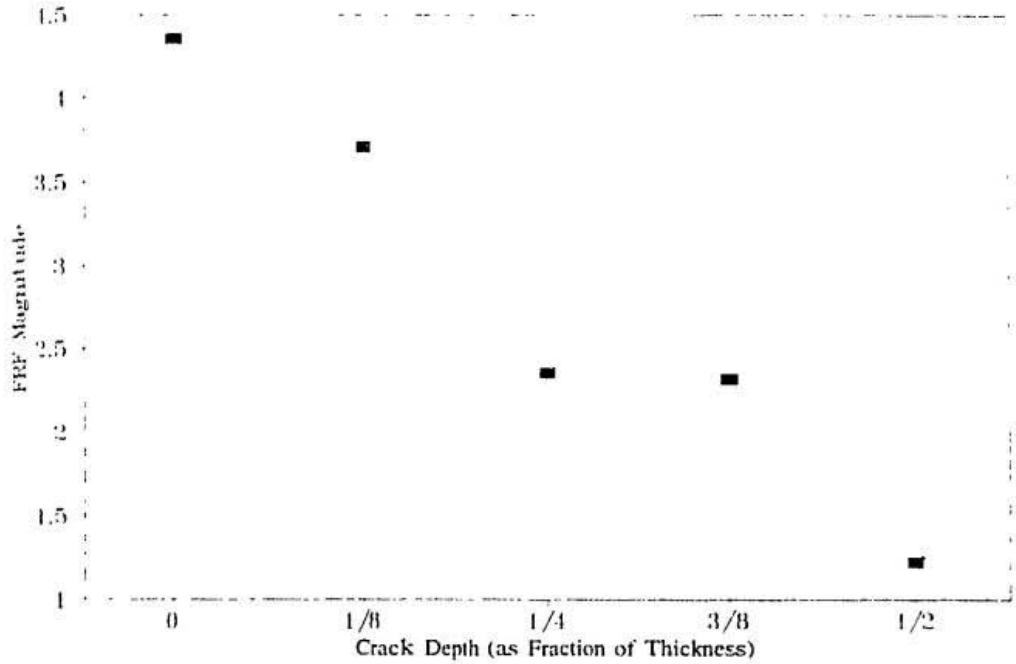

FIGURE 5.31 - FRF AMPLITUDE VARIATION WITH INCREASING CRACK DEPTH FOR NODE 17 AT UPPER OFFSET OF BENDING MODE 3 (277 HZ)

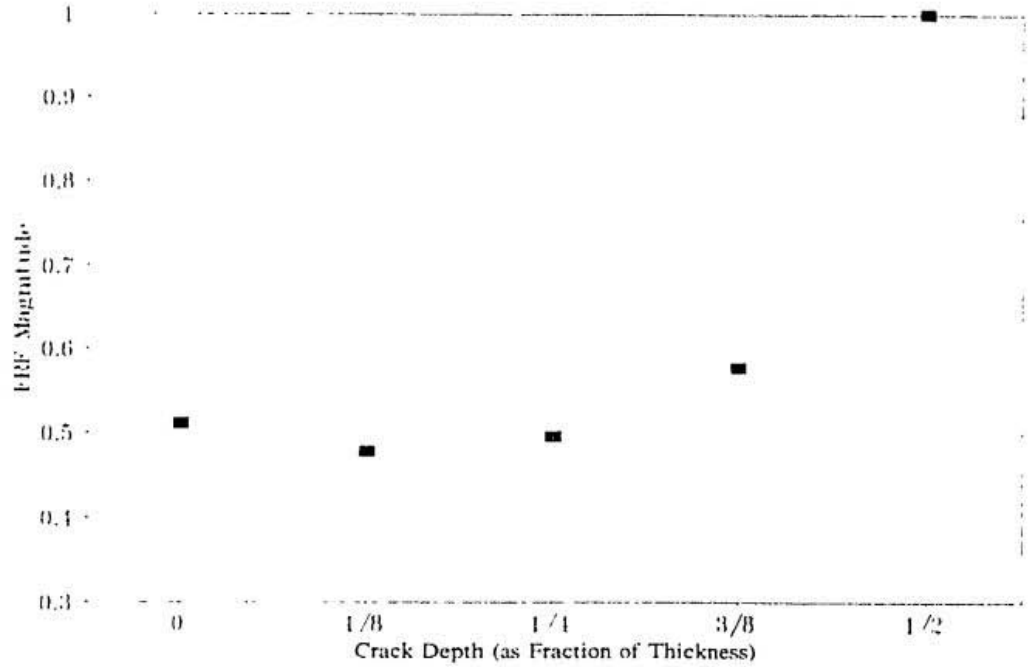

FIGURE 5.32 - FRF AMPLITUDE VARIATION WITH INCREASING CRACK DEPTH FOR NODE 17 AT LOWER OFFSET OF BENDING MODE 4 (513 HZ)

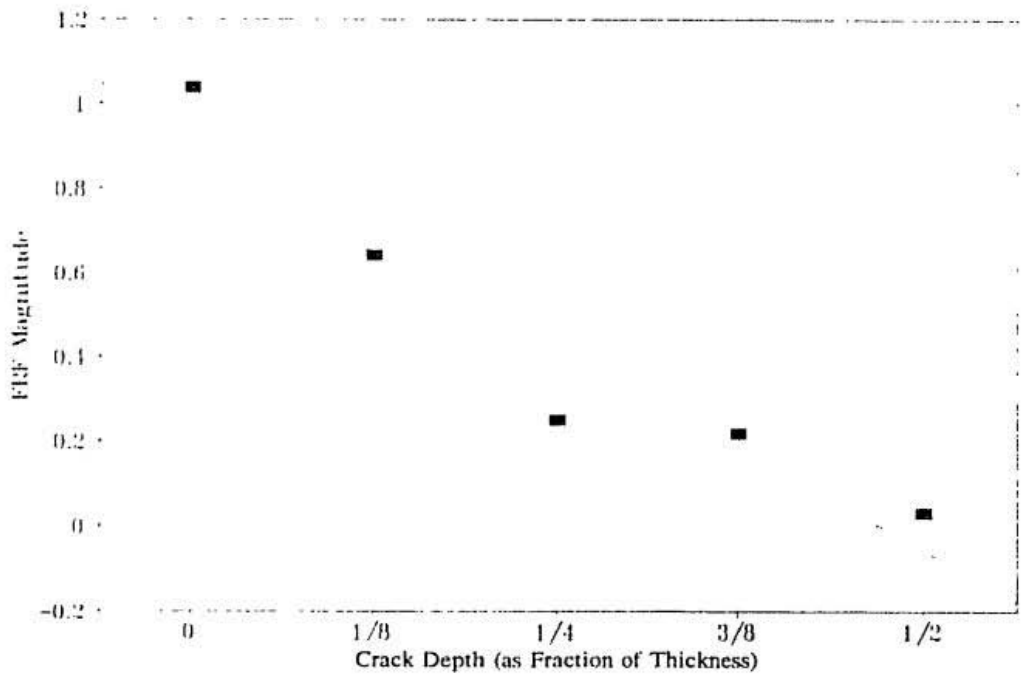

FIGURE 5.33 - FRF AMPLITUDE VARIATION WITH INCREASING CRACK DEPTH FOR NODE 17 AT UPPER OFFSET OF BENDING MODE 4 (550 HZ)

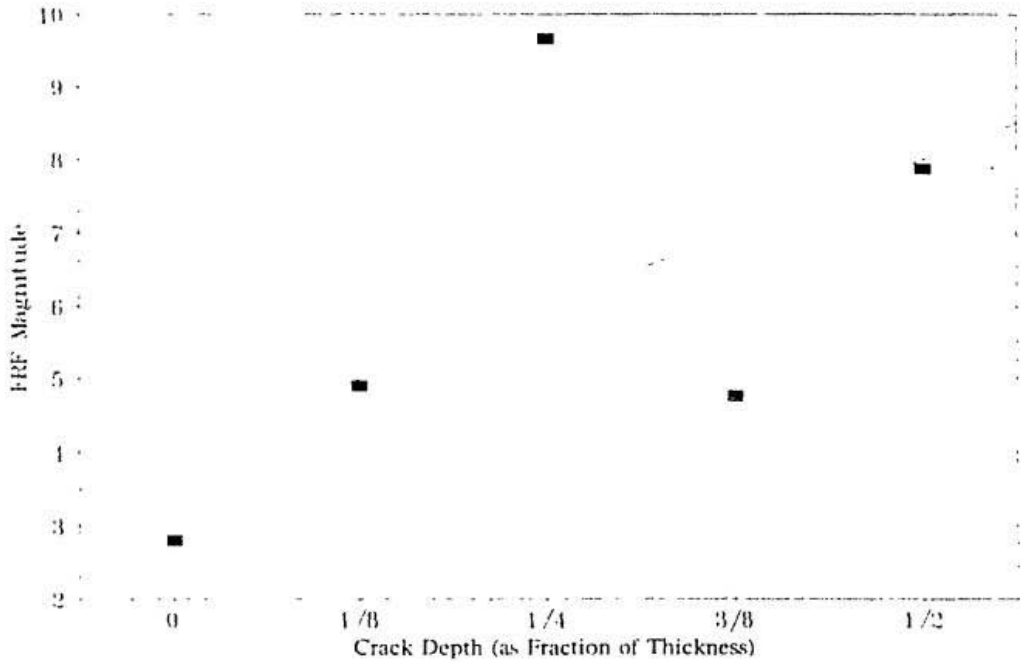

FIGURE 5.34 - FRF AMPLITUDE VARIATION WITH INCREASING CRACK DEPTH FOR NODE 17 AT LOWER OFFSET OF BENDING MODE 5 (875 HZ)

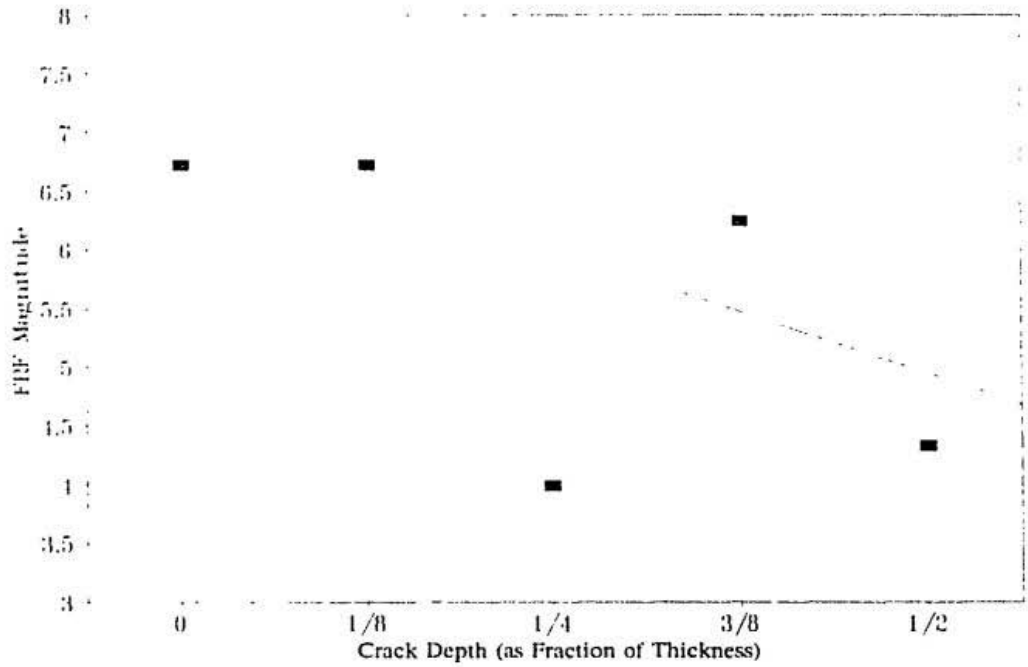

FIGURE 5.35 - FRF AMPLITUDE VARIATION WITH INCREASING CRACK DEPTH FOR NODE 17 AT UPPER OFFSET OF BENDING MODE 5 (893 HZ)

The trend in this data is quite obvious, even for mode 1 where the frequency shift was difficult to see, and for mode 5 which had non-conforming data for the 1/4 crack specimen. Amplitude values increase consistently and by significant amounts at the low frequency offset. Similarly with inverted trend the values decrease at the high frequency offset. One possible reason why this trend is more obvious here than at peak location may be that the effect of damping on amplitudes is moderated greatly at values away from the peaks. At the peaks, even the slightest change in damping, which may or may not be attributable to defects (ie., possibly attributable to system inconsistencies) can cause unexpected changes in amplitudes. This phenomena can be illustrated by considering a plot of SDOF response given as Equations (5.7) and (5.8), shown in Figures 5.36 and 5.37.

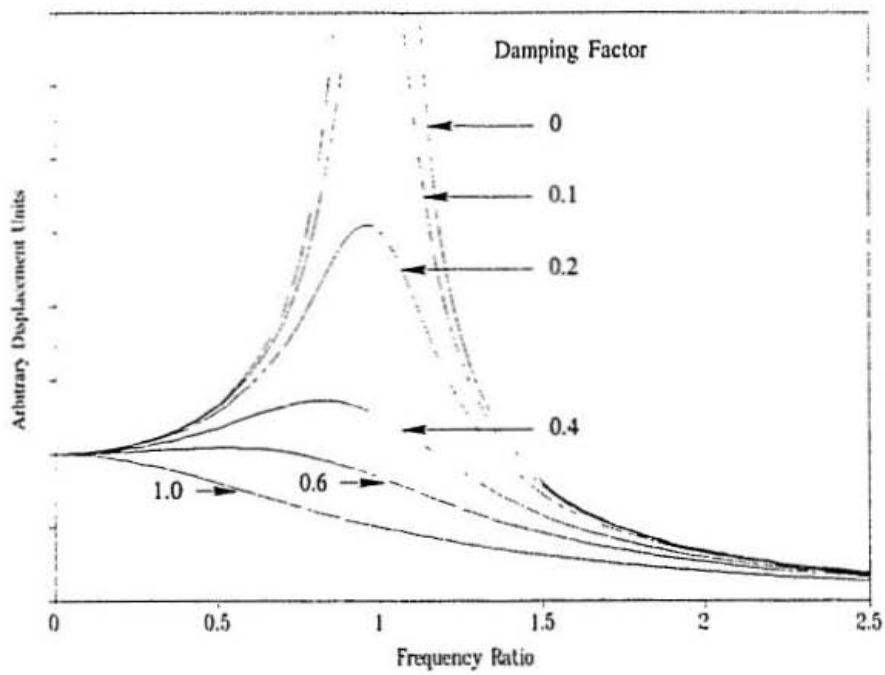

FIGURE 5.36 - CHANGES IN SDOF RESPONSE AMPLITUDE RESULTING FROM DAMPING VARIATION

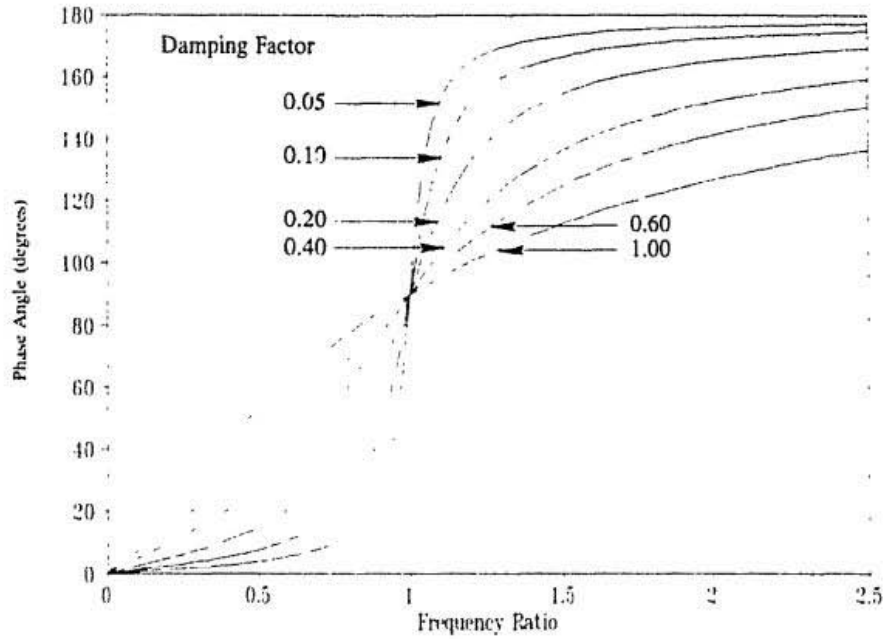

FIGURE 5.37 - CHANGES IN SDOF RESPONSE PHASE RESULTING FROM DAMPING VARIATION

Figure 5.36 shows that the effect of damping on peak amplitude is much more pronounced at peak locations than at off-peak locations. So while the variation in peak amplitude is noteworthy, it would seem that a much more reliable indicator is the amplitude changes associated with off-peak frequencies.

To illustrate this theory further consider the expression used to derive Figure 5.36, Equation (5.7). If a range of frequency ratios are considered, grouped around the unity value and a random damping factor (in the range from 0.13 to 0.18) is applied to the various ranges, the result is a plot similar to that shown in Figure 5.38. As can be clearly seen, the peak values vary randomly due to the random damping changes, but on either

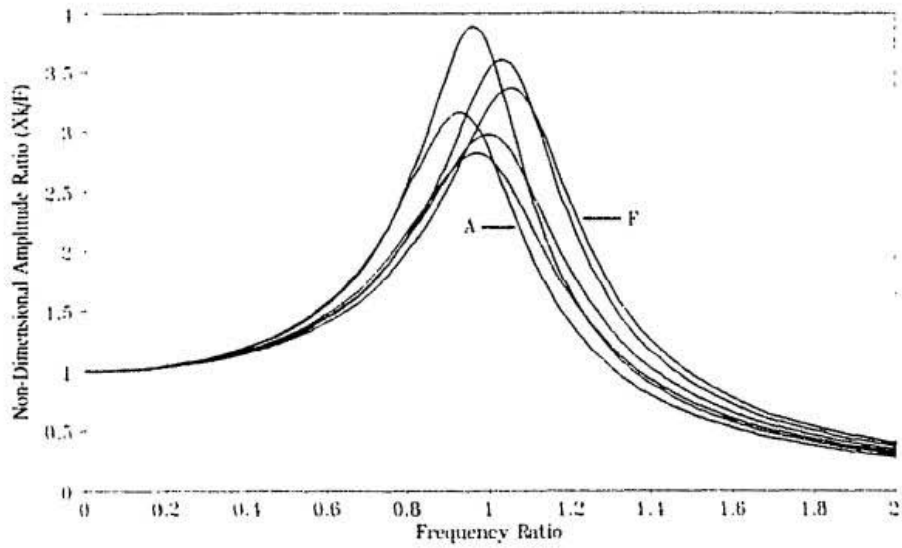

FIGURE 5.38 - AMPLITUDE VARIATION FOR SYNTHESIZED FRF SUBJECTED TO RANDOM VARIATIONS IN DAMPING)

side of the peak, the amplitude returns to the trend seen in the experimental results, viz., clear amplitude ranking, directly corresponding to frequency ranking. Illustration of this trend is provided by plotting the amplitudes from both sides of the peak for each of the curves shown in Figure 5.38. The results, given in Figures 5.39 and 5.40, show that the trend at positive and negative offsets is far more consistent than at the peaks.

It must be noted that the amplitude trends observed, would not have occurred without an associated frequency shift. It seems then, that the application of these observations would best be suited to complimenting observed frequency changes. The amplitude trends, however, appear to be more sensitive to increasing crack depth than does the trend in frequency, and therefore, appear to be a better indicator than the frequency shifts alone. Used in conjunction with each other, they are quite conclusive in indicating the loss of structural integrity associated with the imposed cracks of the tested specimens.

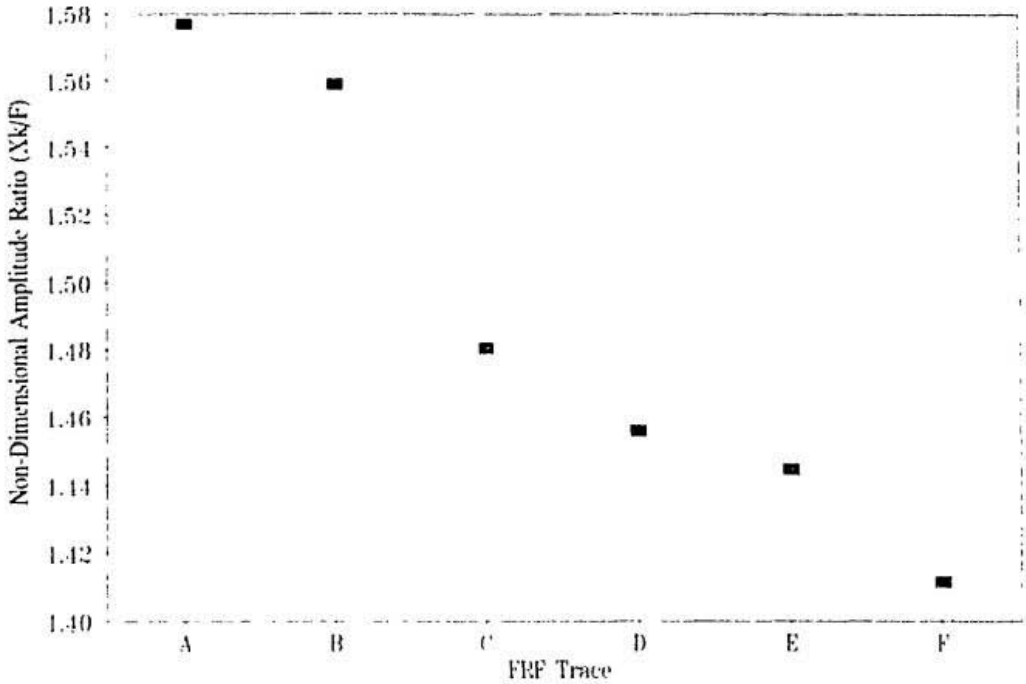

FIGURE 5.39 - AMPLITUDE VARIATION AT LOWER OFFSET OF SYNTHESIZED FRF (F.R. = 0.6)

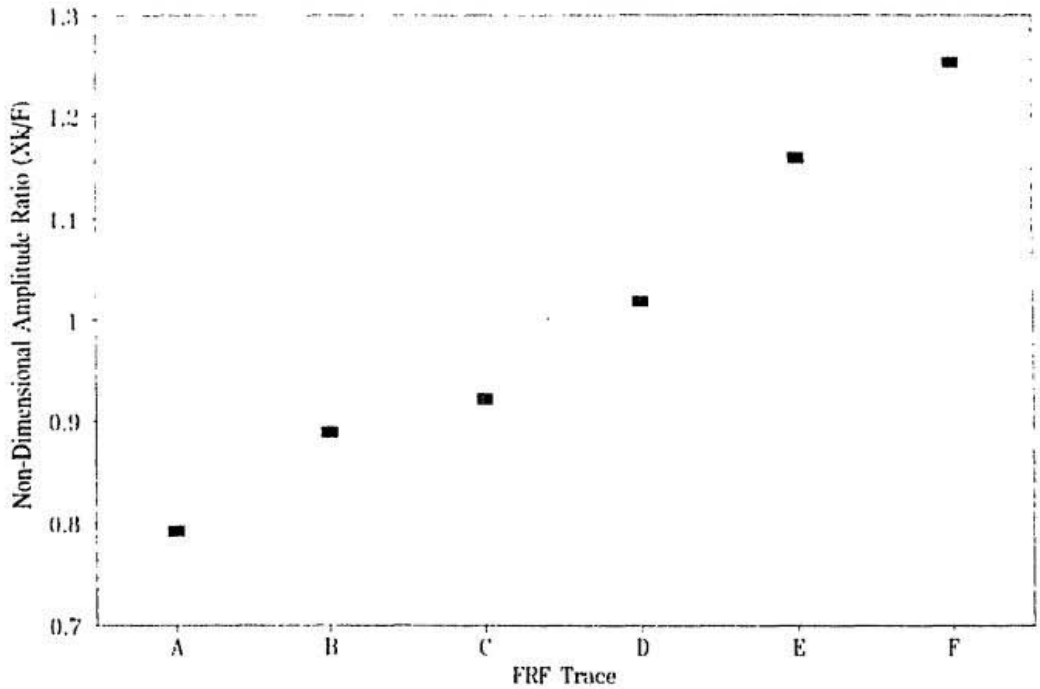

FIGURE 5.40 - AMPLITUDE VARIATION AT UPPER OFFSET OF SYNTHESIZED FRF (F.R. = 1.4)

The results discussed thus far have shown that modal analysis using accelerometers does provide a number of techniques which can be used to indicate the existence of surface defects such as cracks. As discussed earlier a second phase of experimentation was performed to determine if strain gauges were suitable response transducers for performing modal analysis and if so what observations can be made from the results. This topic will form the focus of discussion in the next section.

5.2 Discussion of Strain Gauge Results

It the past the vast majority of vibrational experimentation has used the accelerometer to determine structural response. As pointed out in Chapter 2, a number of modern researchers have begun to look at the strain gauge as an alternative response transducer in the field of modal analysis.

There are some advantages and disadvantages in using the strain gauge over the accelerometer. The primary disadvantages are listed as follows:

- Installation is more difficult than the accelerometer and cannot be performed in a short period of time (ie., mounting fluids need time to dry). Once mounted, the strain gauge cannot be moved, or easily removed.
- More electronic apparatus is required to obtain a readable voltage signal that can be correlated with surface strain. This adds noise to the measured signal and complexity to the experimental set-up.

- The output signal diminishes rapidly with increasing frequency requiring special care to distinguish the signal from the system noise during high frequency measurements (a task not always achievable).
- The results of modal testing using strain gauges cannot be used to plot displacement mode shapes, often a useful tool in verifying proper experimental procedure.
- Since strain is a local phenomena rather than a global one, strain gauges must be located close to the suspected location of a defect in order to be effective.

There are, however, some advantages to using strain gauges as response transducers. The most significant of these are listed as follows:

- The strain gauge is light enough to be considered of negligible mass. This allows the measurement of *true* structural properties, rather than the modified properties which result after the added mass of the accelerometers has been considered.
- There is little possibility of a strain gauge coming loose after it has been mounted. This effectively removes a common source of error associated with accelerometers (ie., mounting variations and associated limitations).

In this experimentation four different plates were used in the strain gauge phase of testing. One of the plates was the reference plate (uncracked) that was used for the first phase of testing. The other three plates had simulated cracks, all of equal depth (1/2 the plate thickness), but in three different locations as illustrated in Figure 5.41. The first location was at 1/4 the plate span, the second at 1/2 span and the third at 2/3 span. On each of the

cracked plates a strain gauge was mounted directly under the crack and for comparison on the reference plate three strain gauges were mounted at similar locations so that direct comparisons could be made between the cracked and uncracked plates.

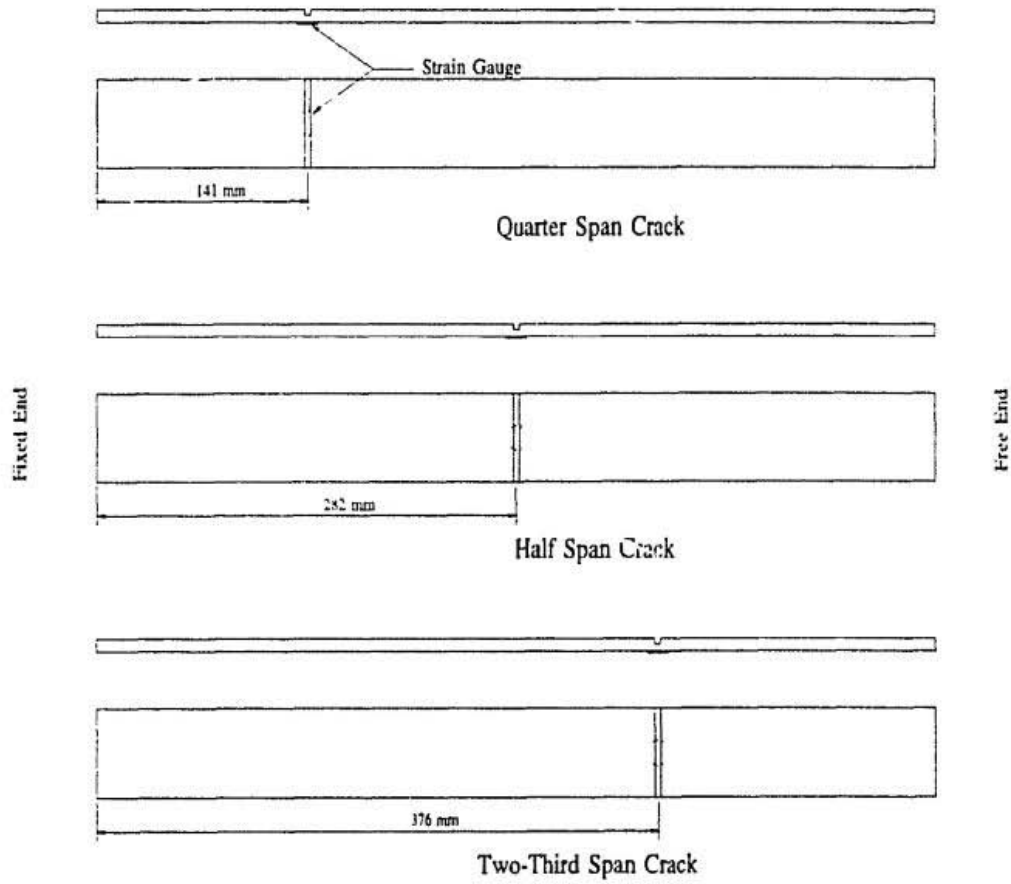

FIGURE 5.41 - LOCATIONS OF STRAIN GAUGES AND CRACKS FOR SECOND PHASE OF EXPERIMENT

The primary objective of this phase of testing was to determine the effect that a crack has on the strain properties of the cantilever plates. Ideally a series of crack depths would have been investigated to determine the trend but due to time and equipment restrictions it was decided that only the worst degree of cracking would be investigated. Considering the action taking place as a crack appears in a flexed plate the trend of strain changes could

be logically predicted. The questions here concerned the magnitude of the change and to what dynamic limits the results could be accurately measured. In other words how well do strain gauges perform in a high frequency test environment and assuming adequate response, to what degree is dynamic strain increased by the presence of a crack.

The parameters of a modal test using strain gauges are similar to those obtained with accelerometers except that here the FRF amplitudes are in strain units. The other parameters, damping and frequency, should be directly comparable to the accelerometer results. As a result other than listing their values as derived from the strain measurements, these latter two will not be discussed here.

5.2.1 Parameter Changes as Derived from Strain Gauge Results

After completing the installation of strain gauges and all associated hardware, the methodology of acquiring data from a dynamic test using strain gauges is very similar to that used in accelerometer testing. Likewise, generation of frequency response functions and performing modal parameter estimation is accomplished in a similar manner. The interpretation of the results, however, is a different matter altogether as will be illustrated in the following discussion.

The results obtained through the typical modal parameter estimation procedures on strain gauge data are given below in Tables 5.6 through 5.8, and are separated according to the location of the crack and its associated gauges. For further illustration of the results, the

full band FRF's (0 to 1000 Hz), derived from strain time histories, are shown in Figures 5.42 through 5.44.

The results clearly show that there is a dramatic increase in the measured strain level of the cracked plate as compared to the uncracked plate. The most significant increase in strain level (as given by the amplitudes of the FRF peaks) was achieved in the 1/2 span crack where for the first mode, the strain level increased by a factor of almost 13. Additionally, several of the other peaks showed considerable increases, with factors ranging from 3 to 7. These results seem to indicate rather convincingly that the measurement of strain is a very good indicator of crack existence and that strain gauges are indeed appropriate and useful in a dynamic test environment.

TABLE 5.6 - STRAIN PARAMETERS FOR PLATE WITH 1/4 SPAN CRACK

Mode	Uncracked Plate				Cracked Plate			
	Frequency (Hz)	Damping (%)	Residue	FRF Peak Amplitude	Frequency (Hz)	Damping (%)	Residue	FRF Peak Amplitude
1	15.35	2.40	69.47	29.96	14.33	2.50	231.96	104.24
2	98.92	0.80	65.33	13.22	98.35	0.80	173.91	35.59
3	273.41	0.55	192.12	20.39	257.76	1.00	619.77	38.37
4	541.93	0.26	41.37	4.68	518.25	0.30	59.51	6.26
5	889.35	0.47	35.97	1.37	880.68	0.50	151.18	5.48

TABLE 5.7 - STRAIN PARAMETERS FOR PLATE WITH 1/2 SPAN CRACK

Mode	Uncracked Plate				Cracked Plate			
	Frequency (Hz)	Damping (%)	Residue	FRF Peak Amplitude	Frequency (Hz)	Damping (%)	Residue	FRF Peak Amplitude
1	15.48	[10]	[10]	15.85	15.31	0.90	177.40	203.43
2	99.08	[10]	[10]	38.39	90.22	0.80	772.83	170.59
3	273.31	[10]	[10]	1.12	271.10	0.75	70.22	5.46
4	542.76	[10]	[10]	4.86	505.53	0.50	4.54	12.85
5	888.32	[10]	[10]	0.38	882.23	0.48	64.09	2.40

TABLE 5.8 - STRAIN PARAMETERS FOR PLATE WITH 2/3 SPAN CRACK

Mode	Uncracked Plate				Cracked Plate			
	Frequency (Hz)	Damping (%)	Residue	FRF Peak Amplitude	Frequency (Hz)	Damping (%)	Residue	FRF Peak Amplitude
1	15.50	2.40	19.52	8.35	15.49	2.00	94.67	48.54
2	98.80	0.85	191.60	36.52	91.86	0.80	607.23	132.61
3	273.33	0.65	258.82	23.11	254.84	0.90	749.16	52.39
4	542.13	0.35	18.14	1.52	539.77	0.40	20.45	1.51
5	889.62	0.43	161.98	6.62	851.52	0.48	446.96	21.22

While these results are remarkable, it must be remembered that a major factor in the magnitude of strain level increase is the position of the strain gauge with respect to the crack. Having the gauge placed directly under the crack is the ideal location and will yield the most notable results. The amount of change would decrease rapidly if the gauge were moved away from the crack.

[10] It was not possible to calculate these parameters due to a loss of time-history data from a storage tape.

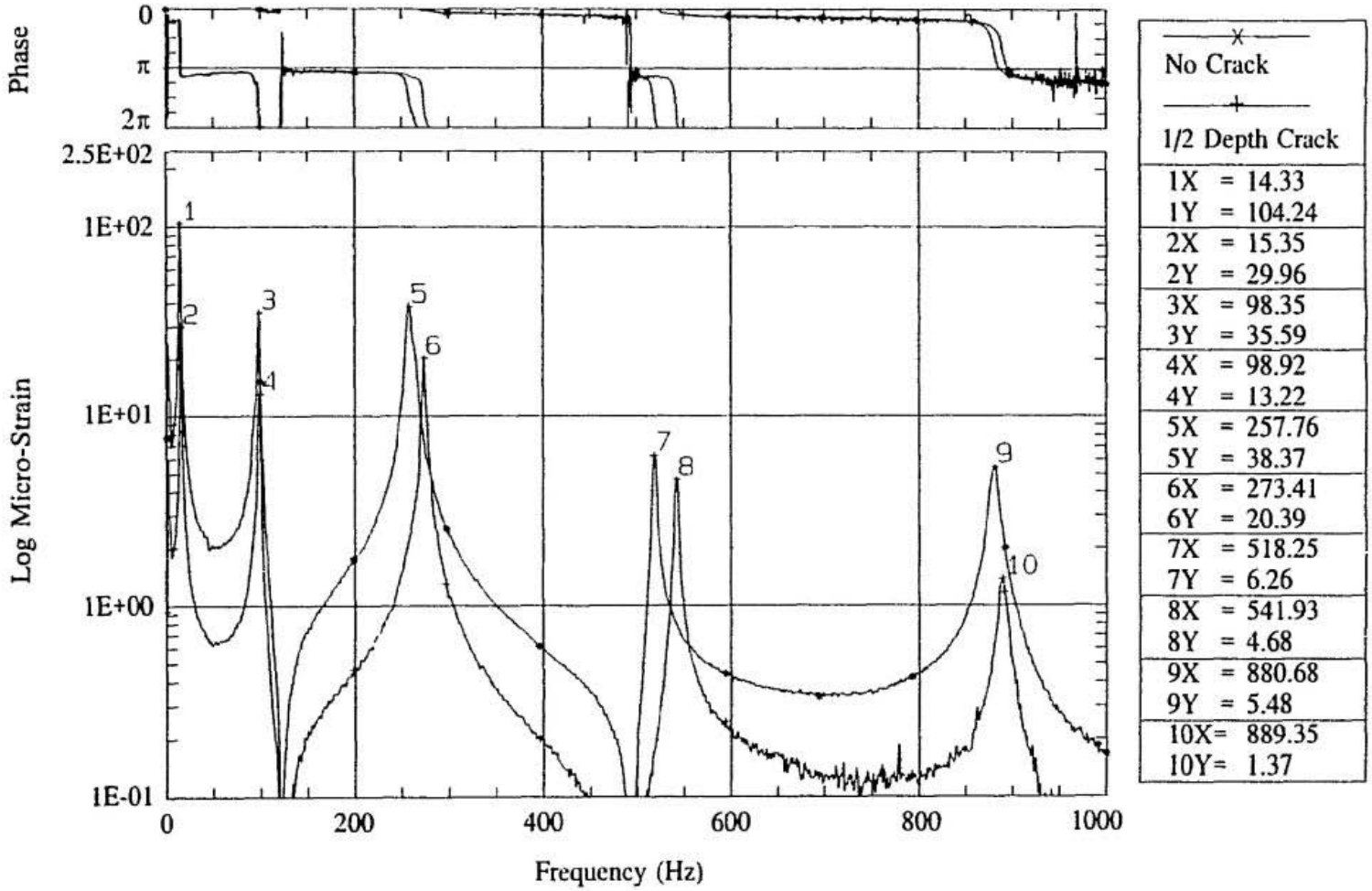

FIGURE 5.42 - STRAIN FRF FOR CRACK LOCATED AT 1/4 SPAN

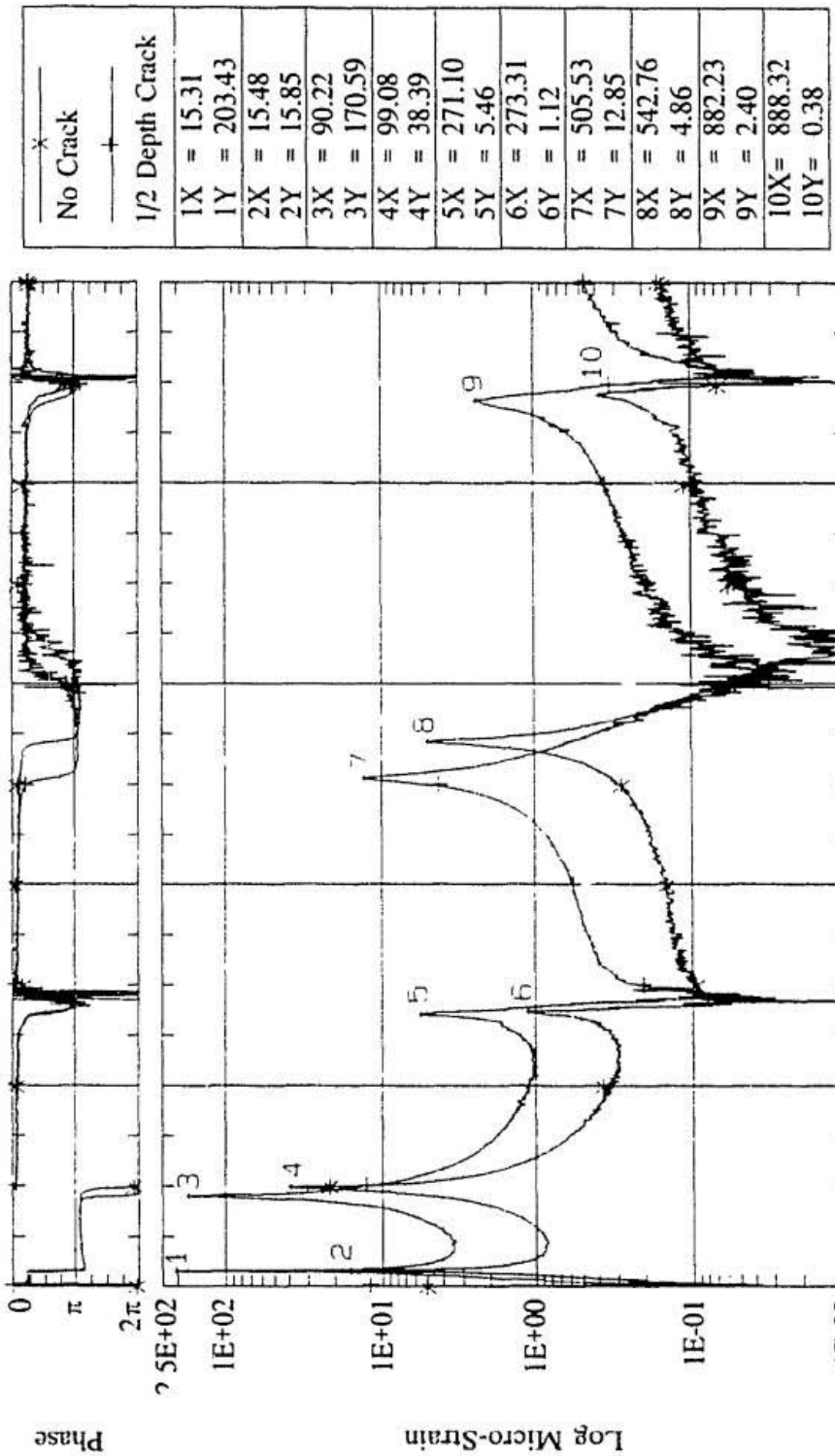

FIGURE 5.43 - STRAIN FRF FOR CRACK LOCATED AT 1/2 SPAN

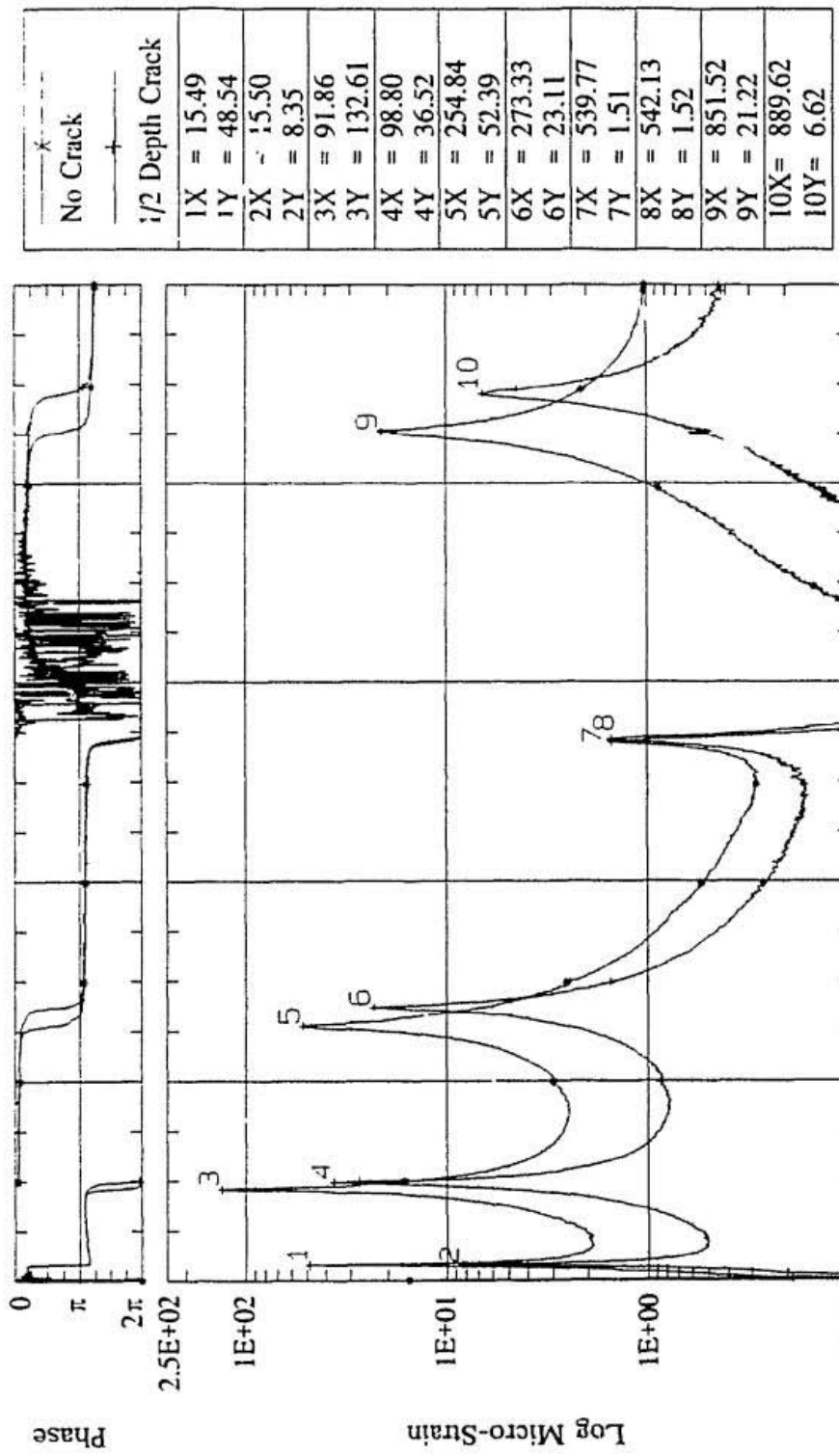

FIGURE 5.44 - STRAIN FRF FOR CRACK LOCATED AT 2/3 SPAN

This imposes a restriction on the usefulness of strain measurement as a tool in structural integrity monitoring. An effective system would require that many gauges be used, placed adjacent to all areas that cracks would be likely to initiate. These areas would include; all high stress welds, bends in structural members, member intersections and rigid connections among others. This is not meant to imply that such a system would be impractical to construct; only that as compared to the measurement of global parameters (ie. displacement, acceleration etc.) the initial system installation would be more complicated and the system itself would be more complex. Considering the sensitivity of strain measurements, however, the added complexity might be worth while.

5.3 Errors in Experimental Data

Any program of research which uses experimentally derived data must concede that no matter how much attention is paid to the setup of the experiment, there will always be sources of error which are not found in corresponding analytical models. The experimentation performed here, was an early attempt at modal analysis research in this faculty and as such is a little more prone to errors, since it is only through experience that many of the finer points of dynamic testing become apparent. While the data presented in this chapter does illustrate a number of useful phenomena, some of the unexplained or unexpected results could certainly be attributable to experimental error. In the context of this and other similar test environments, the following points highlight some of the problem areas of experimentation.

- The assumption of fixity at the clamped end can never truly be made, especially without making a very concerted effort to achieve this result. Through the course of this experiment numerous modifications were made to improve clamp fixation but in the end it still remained as the most likely source of error in the experimental data.

- Improperly attached transducers can lead to errors in measured data. Accelerometer mounting can be achieved through the use of wax (used here), magnets, or studs. Each has its own characteristics and downfalls. Wax in particular is not considered ideal, but given the large number of measurement points, it was the only acceptable alternative for this experiment.

- Attachment of the excitation device can change loading conditions if it is not carefully monitored. Here, the exciter was suspended above the specimen by using elastic cords. Relaxation of these elastic cords could result in application of a pre-load at the point of attachment. Care was taken, however, to ensure that at the beginning of each test the elastics were adjusted so that contact was made without imposing load.

- Electrical noise and interference can at times over-ride the true signal. This can be a problem for low level signals as was evident in the strain measurement. If care is taken, however, to calibrate devices and to use error reducing filters and procedures, this type of error can be minimized.

- The digitizing of analogue signals can result in aliasing and leakage errors if care is not taken to avoid them. These type of errors have become well defined and are fairly easy to resolve. Generally, the use of anti-aliasing filters, the windowing of data before transformation into frequency domain, and averaging of results, are the remedies used here.

- All the specimens used here, were manufactured from a single mill order. There were, however, inevitable variations from one plate to the next which could not be controlled. As insignificant as these might be, they could have affected the dynamic behaviour, and caused otherwise unexplained discrepancies. Additionally, the mounting and dismounting of specimens, while carefully performed, could never be exact, thus resulting in changes in dynamic properties simply as a result of geometric changes. The ideal solution to this type of error would be to mount a single specimen, fatigue it to develop "real" cracks, and perform all tests on it over a period of time without removing it from its mount.

Errors are an inherent part of experimentation but if a systematic approach is taken in performing experiments and a great deal of care and attention is given to the construction of the experimental model, these errors can be minimized to a level of relative insignificance. Drawing on the experience of others who have performed similar work is also very helpful since many of these problem areas only present themselves after many long hours have already been spent in set-up and calibration.

5.4 Summary

This concludes discussion of the experimentation conducted during this course of study. While noteworthy, the results are only to be considered a small part of the research necessary to fully understand the interaction between the modal properties of a structural system, and system integrity, or lack thereof. Chapter 6, which follows, concludes this thesis by summarizing its contents and making recommendations for further research.

Chapter 6

Conclusions and Recommendations

6.1 Conclusions Based on Results

Based on the results of the research presented in this thesis, the following conclusions have been mad.

- The use of modal analysis in the development of an structural integrity monitoring system, with the objective of early unaided detection of structural faults, is still in its initial development stage. Research conducted to date, though, has showed that methods developed using modal analysis are showing merit. With continued development and refinement, it is expected that the many branches of this work will begin to assemble into a unified methodology that will greatly modify non-destructive evaluation as it now exists.
- The use of analytical modelling through finite element analysis is an invaluable tool which is an integral part of modal analysis, specifically in the realm of crack detection. Analytical results of a refined finite element model predict with a high degree of accuracy the effects of structural faults on the natural frequencies and mode shapes of a real structure. It was found that the existence and severity of the crack, could be determined by observing frequency reduction, and its location on the structure, through inspection of mode shape variation.

- Results from analytical and experimental analysis showed that for a cantilever plate, the existence of a crack caused a reduction in the natural frequency for a number of modes, especially for those modes whose mode shapes exhibited a high degree of curvature in the vicinity of the crack. The extent of the drop was found to correlate well with the crack depth, showing that it could be used as an effective indicator of crack extent.

- A notable method for determining the crack location was derived from the analytical results. Observing changes in the displacement and slope mode shapes illustrated that a significant discontinuity occurs in the plot of mode shape difference, at the crack location, for all analyzed modes. The method clearly shows the crack location for the cantilever plate, but its effectiveness for real structures is somewhat questionable.

- Observation of modal parameters derived through experimentation showed that while crack induced frequency changes could be easily observed, noted changes in damping, and residue were not conclusive, and showed little in the way of trend.

- Subsequent investigation of the experimental FRF's showed that the comparing of off-peak amplitudes resulted in a clear trend, indicative of crack existence. The results appeared quite sensitive and provided more consistent results than did the observation of frequency shift alone.

- Investigation into the usefulness of strain gauges as a dynamic response transducer showed that while the signals were more prone to noise, they were still quite usable. It was found that the peak magnitudes of the resulting FRF's were very sensitive to cracking. These were observed to shift by more that a full order of magnitude in some cases.

6.2 Recommendations for Future Investigations

The investigation conducted here have illustrated a number of useful phenomena; it is, however, only a small part of what is needed to significantly contribute to the development of theory leading to a modal analysis based, non-destructive evaluation technique. The next generation of research might consider the following recommendations when deciding on the course of investigation into crack detection;

- The is a need for more research focusing on real structures or models of real structures. While simple structures yield useful information, only a complex structure will truly represent the actions of those for which this technique is intended.
- Any work on simple structures should implement a technique of creating real fatigue cracks, rather than artificial ones. Limitations in cutting devices would never allow the milling or cutting of notches to truly represent the action of a fatigue crack.
- Modelling of representative support conditions is of utmost importance, and probably the most likely part of any model to introduce error. An investigation into support limitations themselves might produce interesting and useful results.
- An intensive investigation into methods of analytical modelling is necessary to determine the most applicable modelling procedures for this type of analysis. It is clear, that there is much room for refinement of analytical results, by as yet there appears to be little consensus on how to best achieve this outcome.

There are many other aspects of crack detection using modal analysis which could greatly benefit from additional investigation. Since this area of research has attracted much attention over the past few years, it is likely that these and other topics will not have to wait long before being investigated. Much progress is being made in this area of research and it appears likely that before long a workable method of defect detection will result from efforts now being made.

References

Araújo Gomes, A.J.M. and Montalvão e Silva, J.M. (1990). "On the Use of Modal Analysis for Crack Identification." *Proceedings of the 8th Modal Analysis Conference*, Kissimmee, Florida, USA, pp. 1108-1115.

Araújo Gomes, A.J.M. and Montalvão e Silva, J.M. (1991). "Theoretical and Experimental Data on Crack Depth Effects in the Dynamic Behaviour of Free-Free Beams," *Proceedings of the 9th Modal Analysis Conference*, Florence, Italy, 1991, pp. 274-283.

Araújo Gomes, A.J.M. and Montalvão e Silva, J.M. (1992). "Dynamic Analysis of Clamped-Free Cracked Beams Subjected to Axial Loads," *Proceedings of the 10th Modal Analysis Conference*, San Diego, California, USA.

Blakely, L.L. (1984). "Comparison of Modal Analysis, Energy Methods, and Finite Element Analysis for Estimation of Natural Frequencies," *Proceedings of the 2nd Modal Analysis Conference*, Orlando Florida, USA, pp. 580-584.

Chiarito, V.P. and Mlakar, P.F. (1984). "Modal Test of a Concrete Gravity Dam," *Proceedings of the 2nd Modal Analysis Conference*, Orlando Florida, USA, pp. 142-148.

Chondros, T.G. and Dimarogonas, A.D. (1980). "Identification of Cracks in Welded Joints of Complex Structures," *Journal of Sound and Vibration*, Vol. 69, No. 4, pp. 531-538.

Clarkson, B.L. (1965). "The Propagation of Fatigue Cracks in a Tensioned Plate Subjected to Acoustic Loads." *Acoustical Fatigue in Aerospace Structures*, Syracuse University Press., p. 361.

Cole, H.A. (1973). "On Line Failure Detection and Damping Measurement of Aerospace Structures by Random Decrement Signatures." NASA CR 2205.

Debao, L., Zhaochang, Z., Ke, H. and Bo, W. (1992). "Damage Detection in Offshore Structures by the FRF Method." *Proceedings OMAE*, Calgary, Canada, Vol. 1, Part B, pp. 601-604.

Dobson, B.J. (1984). "Modification of Finite Element Models using Experimental Modal Analysis." *Proceedings of the 2nd Modal Analysis Conference*, Orlando Florida, USA, pp. 593-601.

Ewins, D.J. (1984). *Modal Testing: Theory and Practice*, Research Studies Press Ltd. Letchworth, England.

Ewins, D.J. (1987). "Uses and Abuses of Modal Testing," *SV Sound and Vibration*, Vol. 21, No. 1, pp. 32-39.

Haynes, F.D. (1986). "Vibration Analysis of the Yamachiche Lightpier." *Proceedings of the 4th Modal Analysis Conference*, Los Angeles, California, USA, pp. 238-244.

Ju, F.D. (1982). "Modal Methods in Diagnosis of Fracture Damage in Simple Structures." *Productive Applications of Mechanical Vibrations*, ASME AMD Vol. 52, pp. 113-126.

Ju, F.D. and Mimovich, M. (1986). "Modal Frequency Method in Diagnosis of Fracture Damage in Structures," *Proceedings of the 4th Modal Analysis Conference*, Los Angeles, California, USA, pp. 1168-1174.

Kennedy, C.C. and Pancu C.D.P. (1947). "Use of Vectors in Vibration Measurement and Analysis," *Journal of Aeronautical Science*, Vol. 14, No. 11.

Kopff, P. (1987). "Experimental Modal Analysis for Structural Damage Assessment - The Case of natural Convection Cooling Towers," *Proceedings of the 5th Modal Analysis Conference*, London, England, pp. 122-125.

Li-Chung, L. (1985). "Randomdec Analysis of Multi-Degree-of-Freedom Systems," *Proceedings of the 3rd Modal Analysis Conference*, Orlando Florida, USA, pp. 101-107.

Lopes, T.A.P. and Raposo, C.V. (1991). "A Correlation between Experimental and Numerical Data Applied to Fixed Offshore Structures," *Proceedings of the 9th Modal Analysis Conference*, Florence, Italy, pp. 455-461.

Mannan, M.A. and Richardson, M.H. (1990). "Detection and Location of Structural Cracks using FRF Measurements," *Proceedings of the 8th Modal Analysis Conference*, Kissimmee, Florida, USA, pp. 652-657.

Montalvão e Silva, J.M. and Araújo Gomes, A.J.M. (1992). "On the Use of Modal Analysis for Fatigue Crack Detection in Simple Structural Elements," *Proceedings of the 10th Modal Analysis Conference*, San Diego, California, USA, pp. 595-600.

Ohlsson, S. (1986). "Modal Testing of the Tjörn Bridge," *Proceedings of the 4th Modal Analysis Conference*, Los Angeles, California, USA, pp. 599-605.

Pandey, A.K., Biswas, M. and Samman, M.M., (1991). "Damage Detection from Changes in Curvature Mode Shapes," *Journal of Sound and Vibration*, Vol. 145, No. 2, pp. 321-332.

Petyt, M. (1968). "The Vibration Characteristics of a Tensioned Plate Containing a Fatigue Crack," *Journal of Sound and Vibration*, Vol. 8, No. 3, pp. 377-389.

Powell, C.D. and Goldberger, S. (1991). "Modal Analysis and Strain Gauge Testing of Finned-Tube Heat Exchanger," *Proceedings of the 9th Modal Analysis Conference*, Florence, Italy, pp. 12-16.

Ramsey, K.A. and Firmin A. (1982). "Experimental Modal analysis, Structural Modifications and FEM Analysis - Combining Forces on a Desktop Computer," *Proceedings of the 1st Modal Analysis Conference*, Orlando Florida, USA, pp. 443-455.

Richardson M.H. and Mannan, M.A. (1991). "Determination of Modal Sensitivity Functions for Location of Structural Faults," *Proceedings of the 9th Modal Analysis Conference*, Florence, Italy, pp. 670-676.

Sanliturk, K.Y. and Imregun, M. (1990). "Theoretical Modelling of the Damping Produced by Fatigue Cracks," *Proceedings of the 8th Modal Analysis Conference*, Kissimmee, Florida, USA, pp. 1370-1374.

Sidhu, J. and Ewins, D.J. (1984). "Correlation of Finite Element and Modal Test Studies of a Practical Structure," *Proceedings of the 2nd Modal Analysis Conference*, Orlando Florida, USA, pp. 756-762.

Shahrivar, F. and Bouwkamp, J.G. (1986). "Damage Detection in Offshore Platforms Using Vibration Information," *Journal of Energy Resources Technology*, Vol. 108, pp. 97-106.

Solecki, R. (1980). "Bending Vibration of Simply Supported Rectangular Plates with Internal Rigid Supports," *International Journal of Engineering Science*, Vol. 18, pp. 1309-1318.

Solecki, R. (1983). "Bending Vibration of a Simply Supported Rectangular Plate with a Crack Parallel to One Edge," *Engineering Fracture Mechanics*, Vol. 18, No. 6, pp. 1111-1118.

Solecki, R. (1985). "Bending Vibration of a Rectangular Plate with Arbitrarily Located Rectilinear Crack," *Engineering Fracture Mechanics*, Vol. 22, No. 4, pp. 687-695.

Springer, W.T., Stuff, S.A., Coleman, A.D., and Driskell, T.A. (1990). "Simulating the Presence of Damage in a Vibrating Structure with Finite Element and Structural Dynamics Modifications Techniques," *Proceedings of the 8th Modal Analysis Conference*, Kissimmee, Florida, USA, pp. 1108-1109.

Stimpson, J.B. and Griffith, D.T. (1982). "Finite Element Model Validation via Modal Testing," *Proceedings of the 1st Modal Analysis Conference*, Orlando Florida, USA, pp. 456-461.

Stubbs, N. (1990). "Global Non-Destructive Damage Evaluation in Solids." *The International Journal of Analytical & Experimental Modal Analysis*, Vol. 5, No. 2, pp. 67-79.

Swamidas, A.S.J. and Chen, Y. (1992). "Damage Detection in a Tripod Tower Platform (TTP) using Modal Analysis." *Proceedings OMAE*, Calgary, Canada, Vol. 1, Part B, pp. 577-583.

Thomson, W.T. (1981). *Theory of Vibration with Applications*, Prentice-Hall Inc., Englewood Cliffs, New Jersey.

Tsang, W.F. (1990). "Use of Dynamic Strain Measurements for the Modelling of Structures." *Proceedings of the 8th Modal Analysis Conference*, Kissimmee, Florida, USA, pp. 1246-1251.

White, J.M. and Pardoen, G.C. (1987). "Modal Identification of the Golden Gate Bridge Tower Using Ambient Vibration Data." *Proceedings of the 5th Modal Analysis Conference*, London, England, pp. 16-20.

Zhang, P.Q., Song T.X., and Huang, T.C. (1986). "Modal Analysis of a Cantilever with Changing Stiffness and with Added Concentrated Mass." *Proceedings of the 4th Modal Analysis Conference*, Los Angeles, California, USA, pp. 787-793.

Appendix A

First Nine Mode Shapes for Cantilever Plate

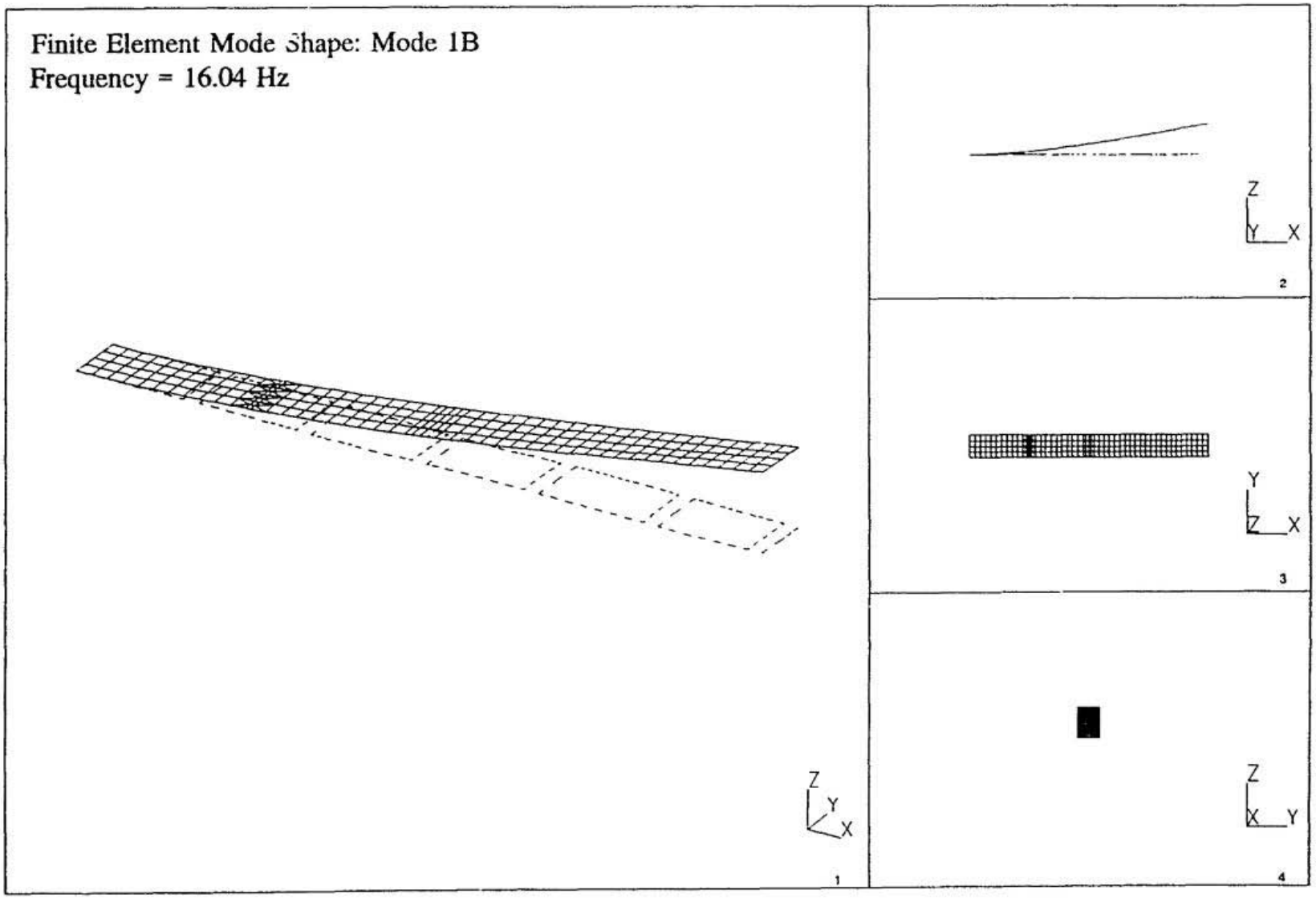
Finite Element Mode Shape: Mode 1B
Frequency = 16.04 Hz
Z
Y
X
1
Z
Y
X
2
Y
Z
X
3
Z
X
Y
4

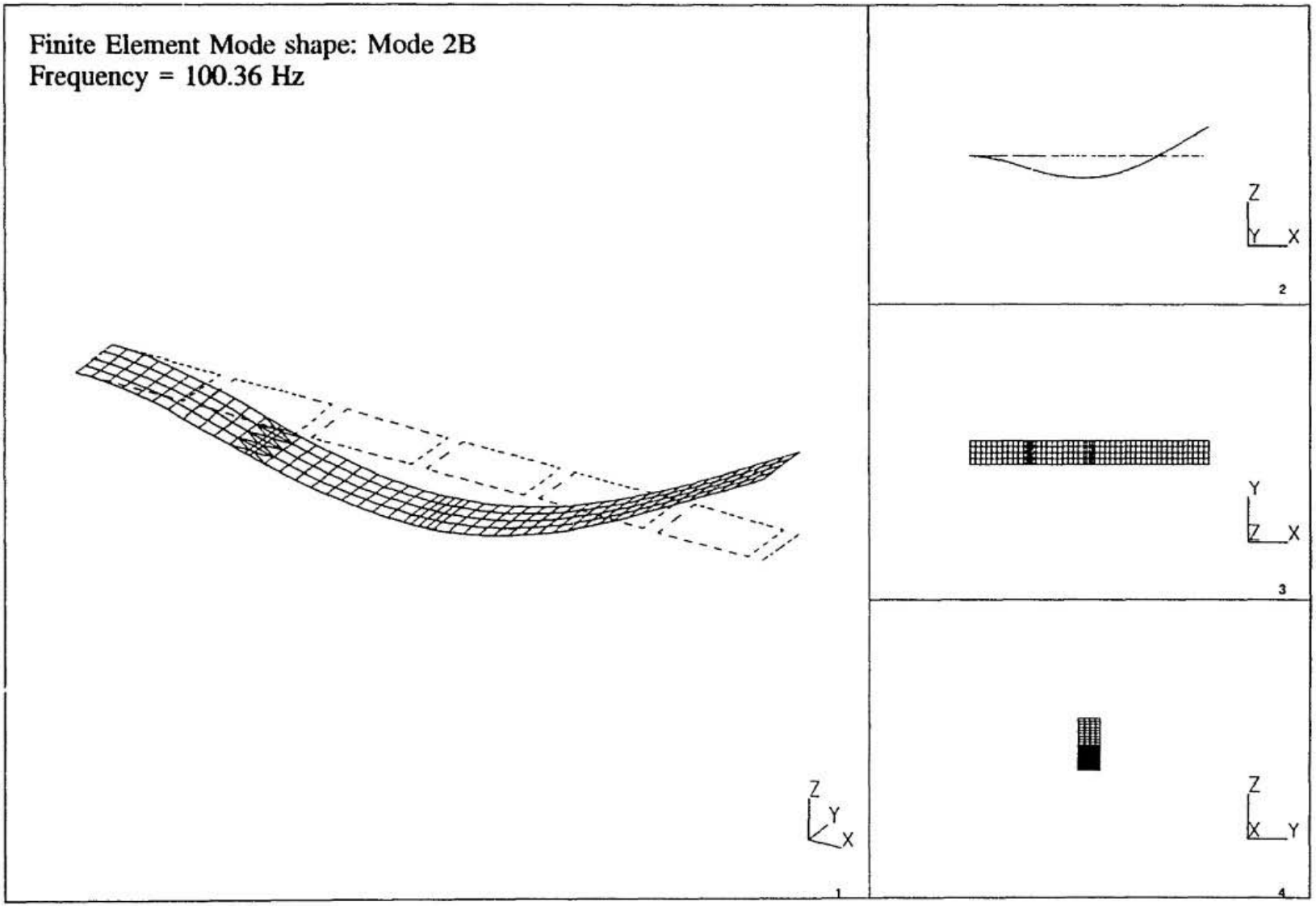
Finite Element Mode shape: Mode 2B
Frequency = 100.36 Hz
Z
Y
X
1
Z
Y
X
2
Y
Z
X
3
Z
X
Y
4

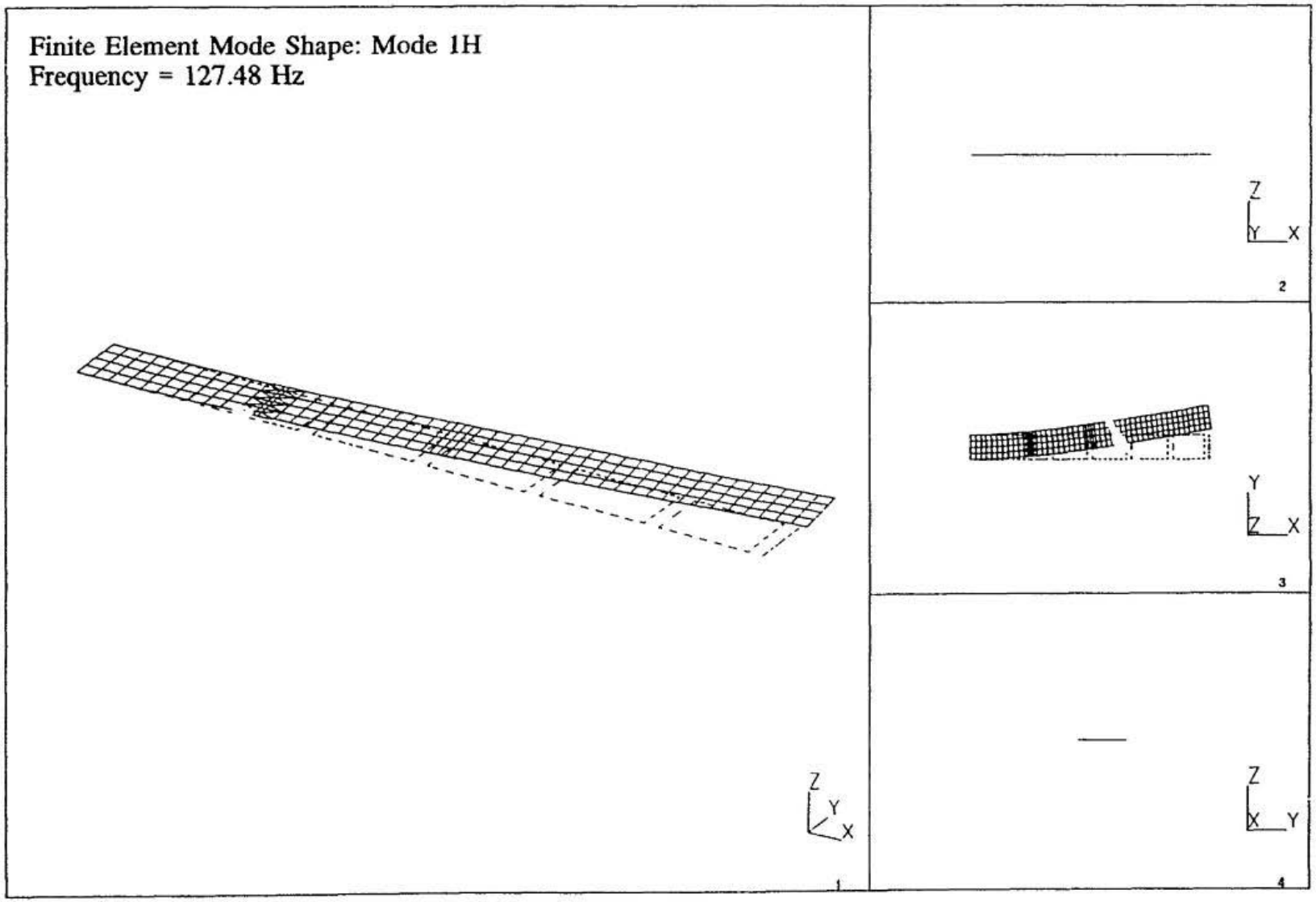
Finite Element Mode Shape: Mode 1H
Frequency = 127.48 Hz
Z
Y
X
1
Z
Y
X
2
Y
Z
X
3
Z
X
Y
4

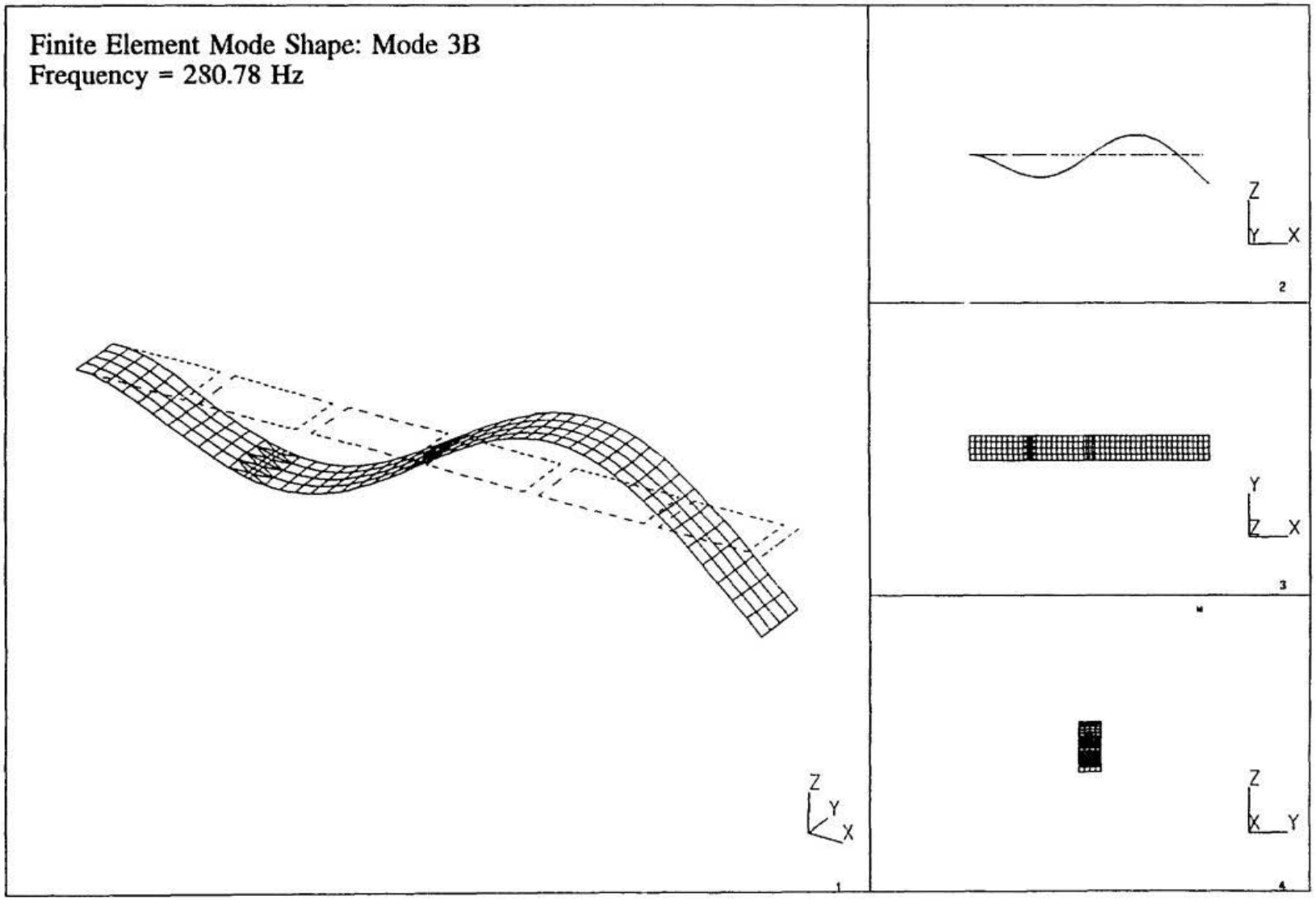
Finite Element Mode Shape: Mode 3B
Frequency = 280.78 Hz
Z
Y
X
1
Z
Y
X
2
Y
Z
X
3
Z
X
Y
4

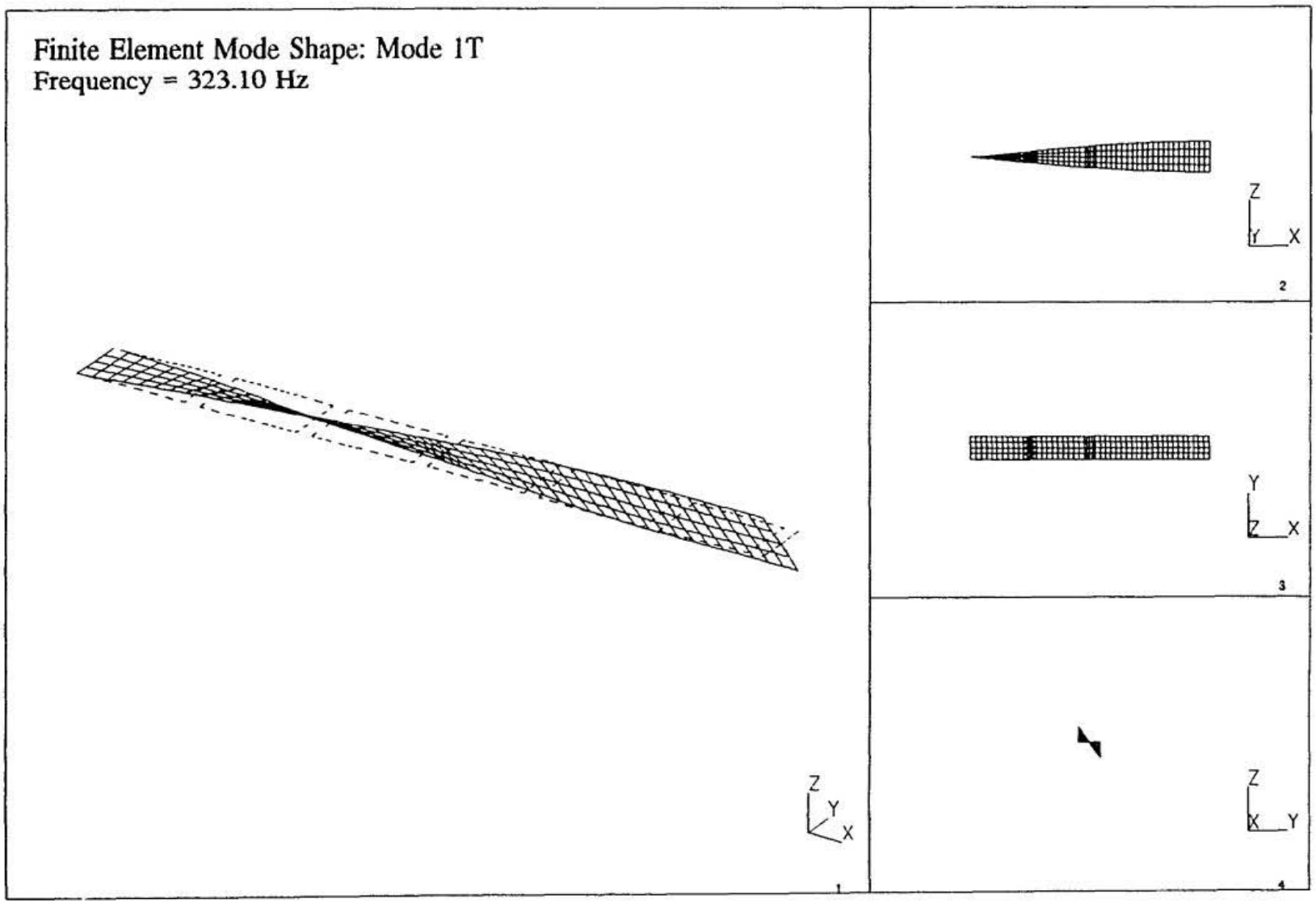
Finite Element Mode Shape: Mode 1T
Frequency = 323.10 Hz
Z
Y
X
1
Z
Y
X
2
Y
Z
X
3
Z
X
Y
4

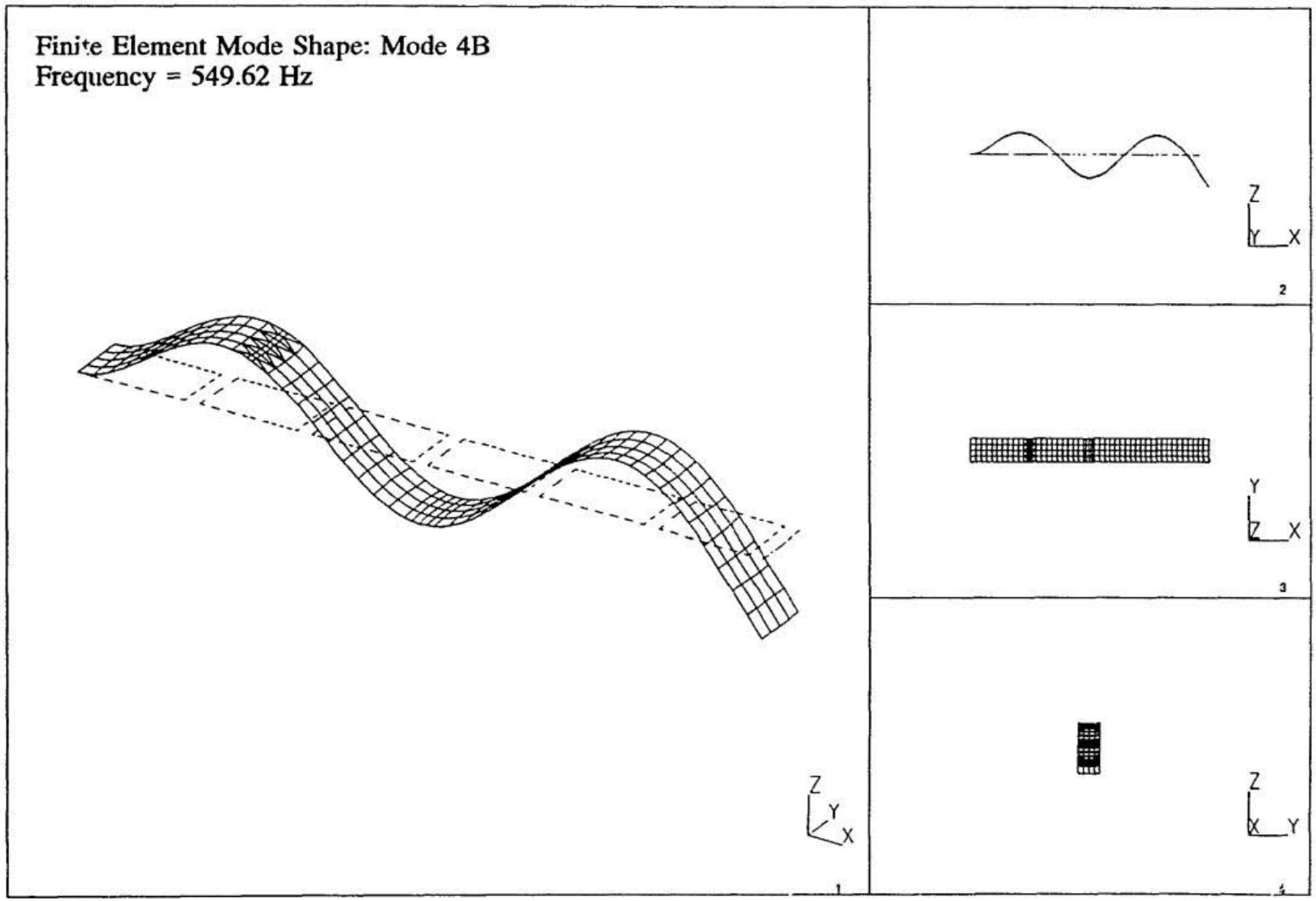
Finite Element Mode Shape: Mode 4B
Frequency = 549.62 Hz
Z
Y
X
1
Z
Y
X
2
Y
Z
X
3
Z
X
Y
4

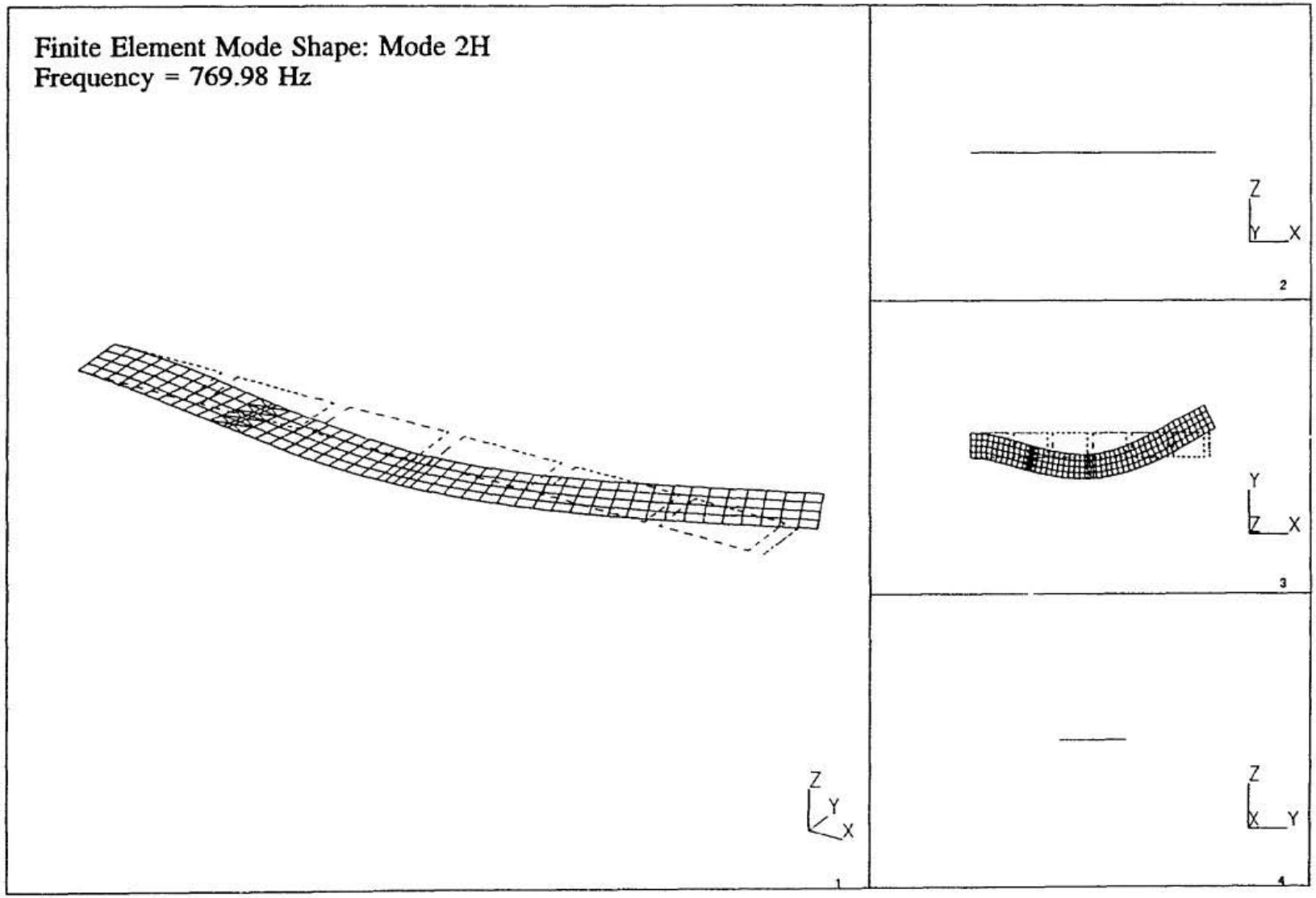
Finite Element Mode Shape: Mode 2H
Frequency = 769.98 Hz
Z
Y
X
1
Z
Y
X
2
Y
Z
X
3
Z
X
Y
4

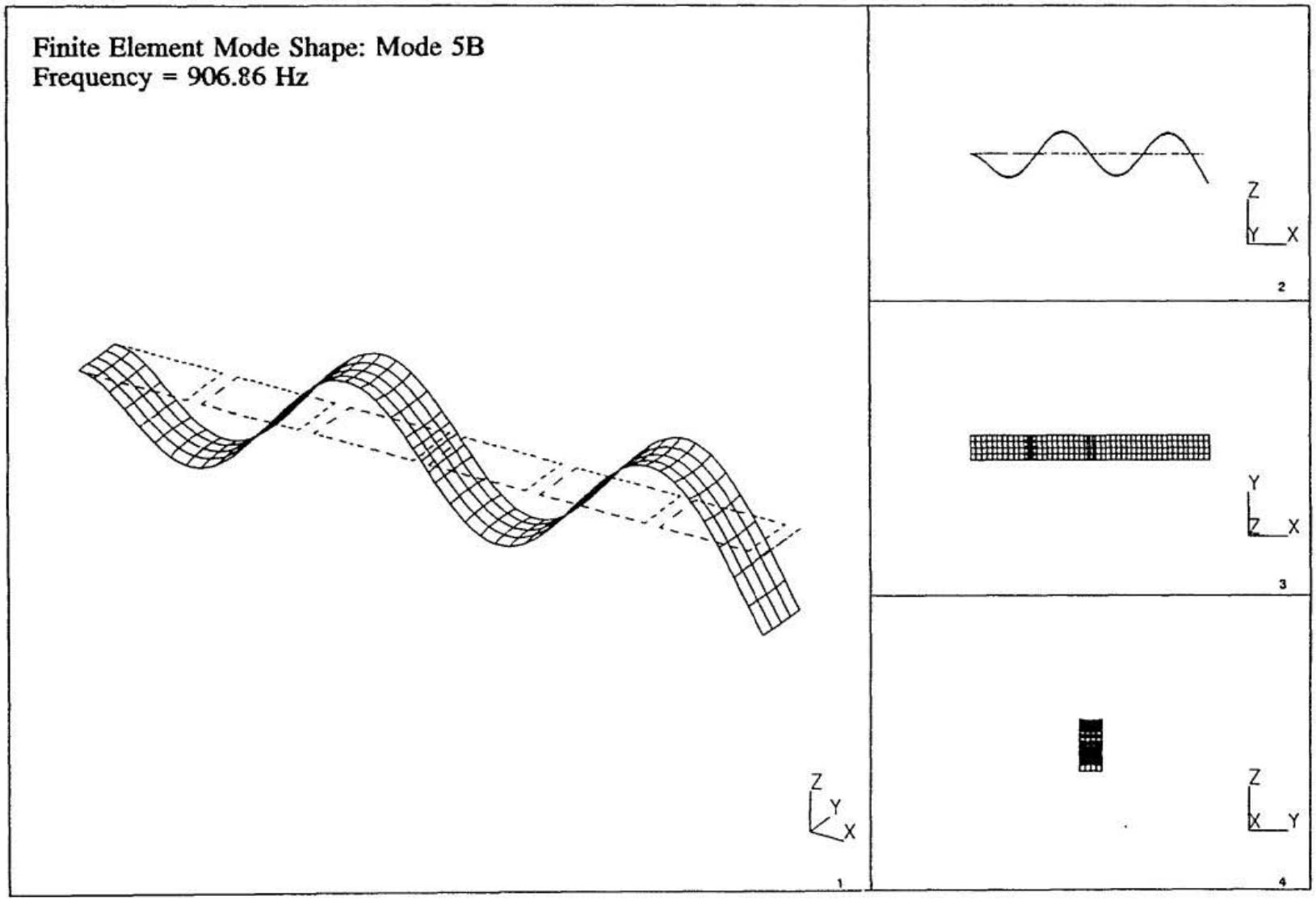
Finite Element Mode Shape: Mode 5B
Frequency = 906.86 Hz
Z
Y
X
1
Z
Y
X
2
Y
Z
X
3
Z
X
Y
4

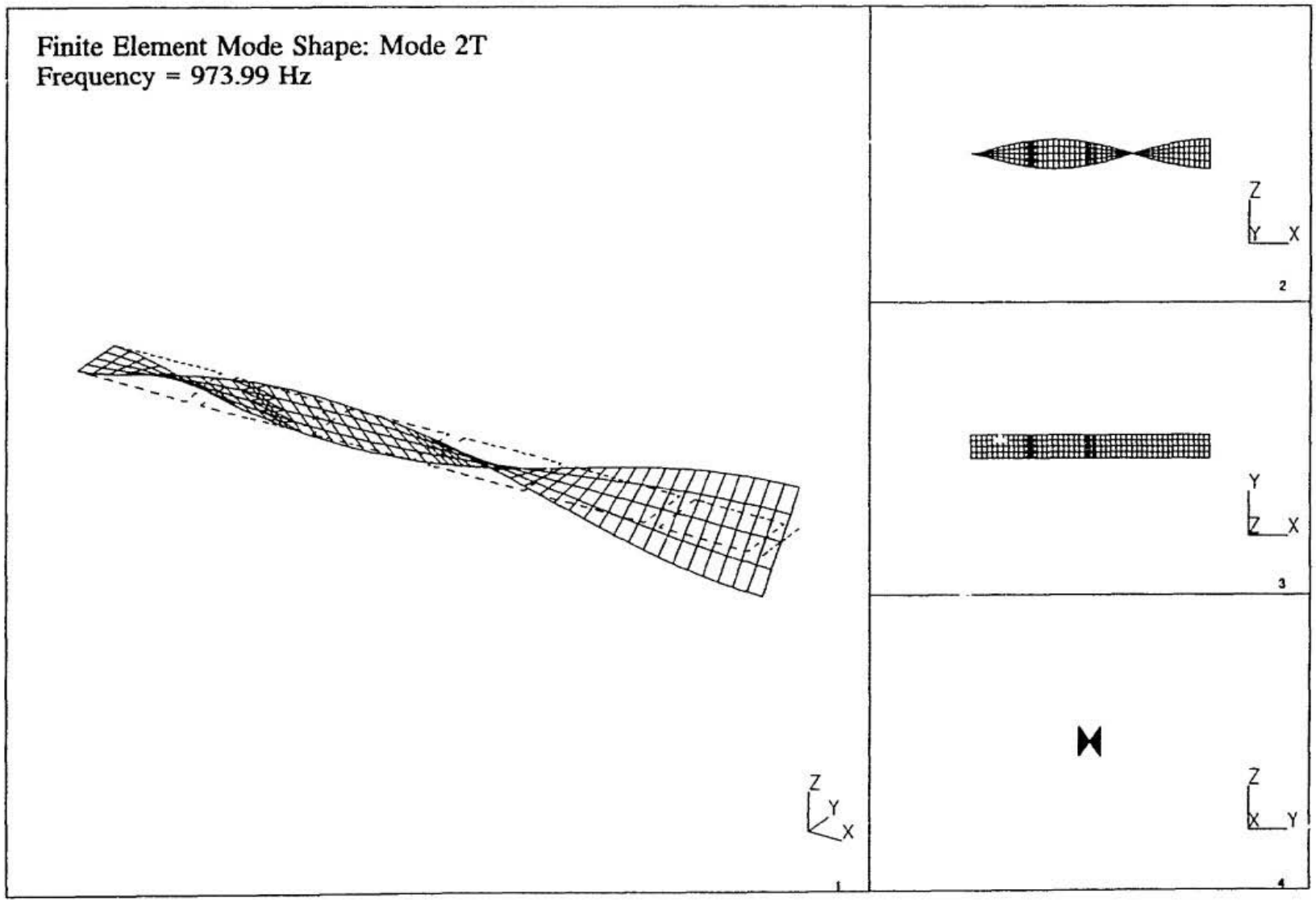
Finite Element Mode Shape: Mode 2T
Frequency = 973.99 Hz
Z
Y
X
1
Z
Y
X
2
Y
Z
X
3
Z
X
Y
4

Appendix B

Sample Time Histories from Experiment

Note: In the following plots, the units for the ordinate quantities are not included with the axis label. The units for acceleration are meters per second squared (m/s^2), and the units for force are newtons (N).

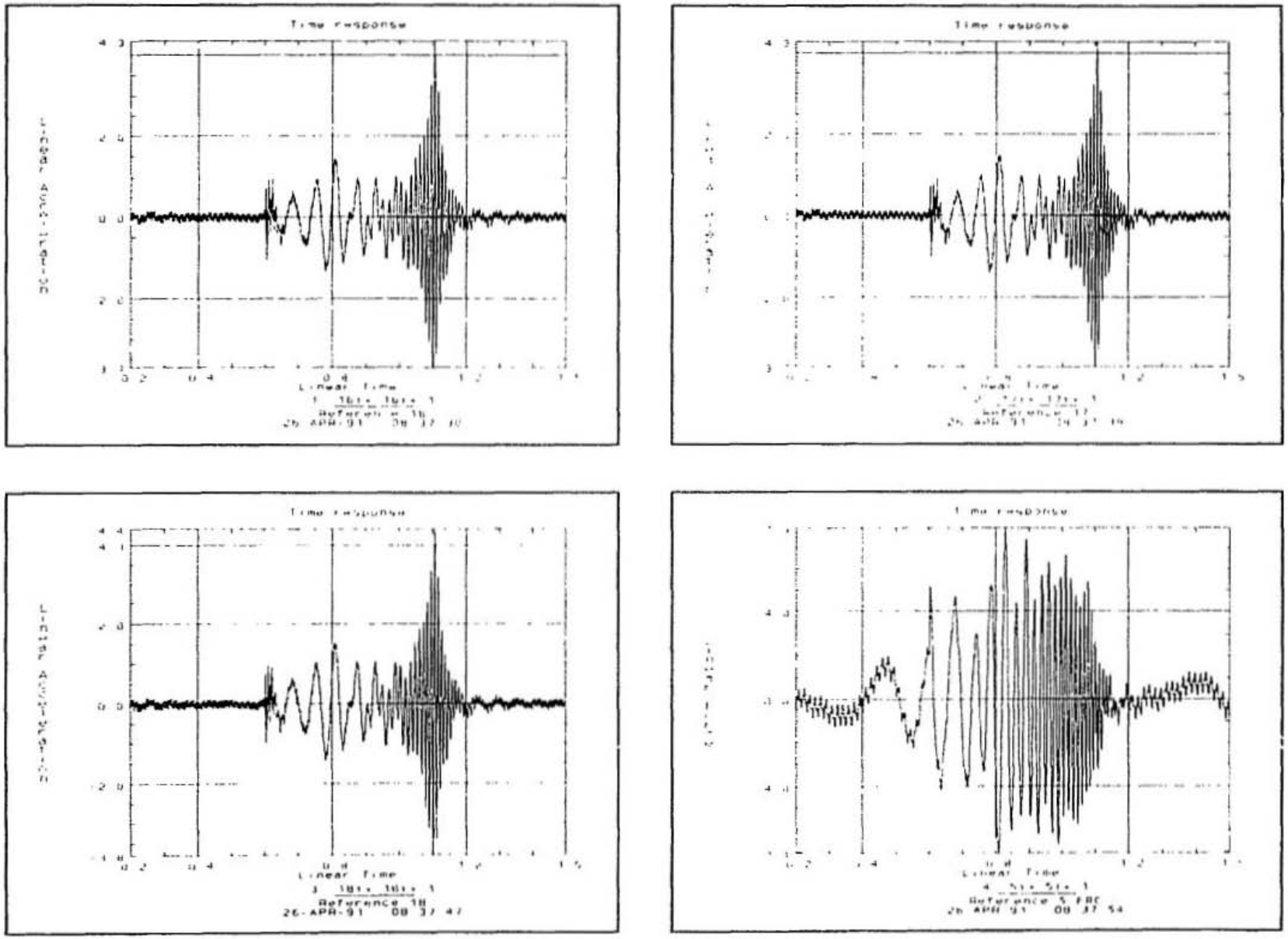

Typical Time Histories Nodes 16, 17, & 18 Accel. Node 5 Force, Phase A - 1-100 Hz Log Sweep

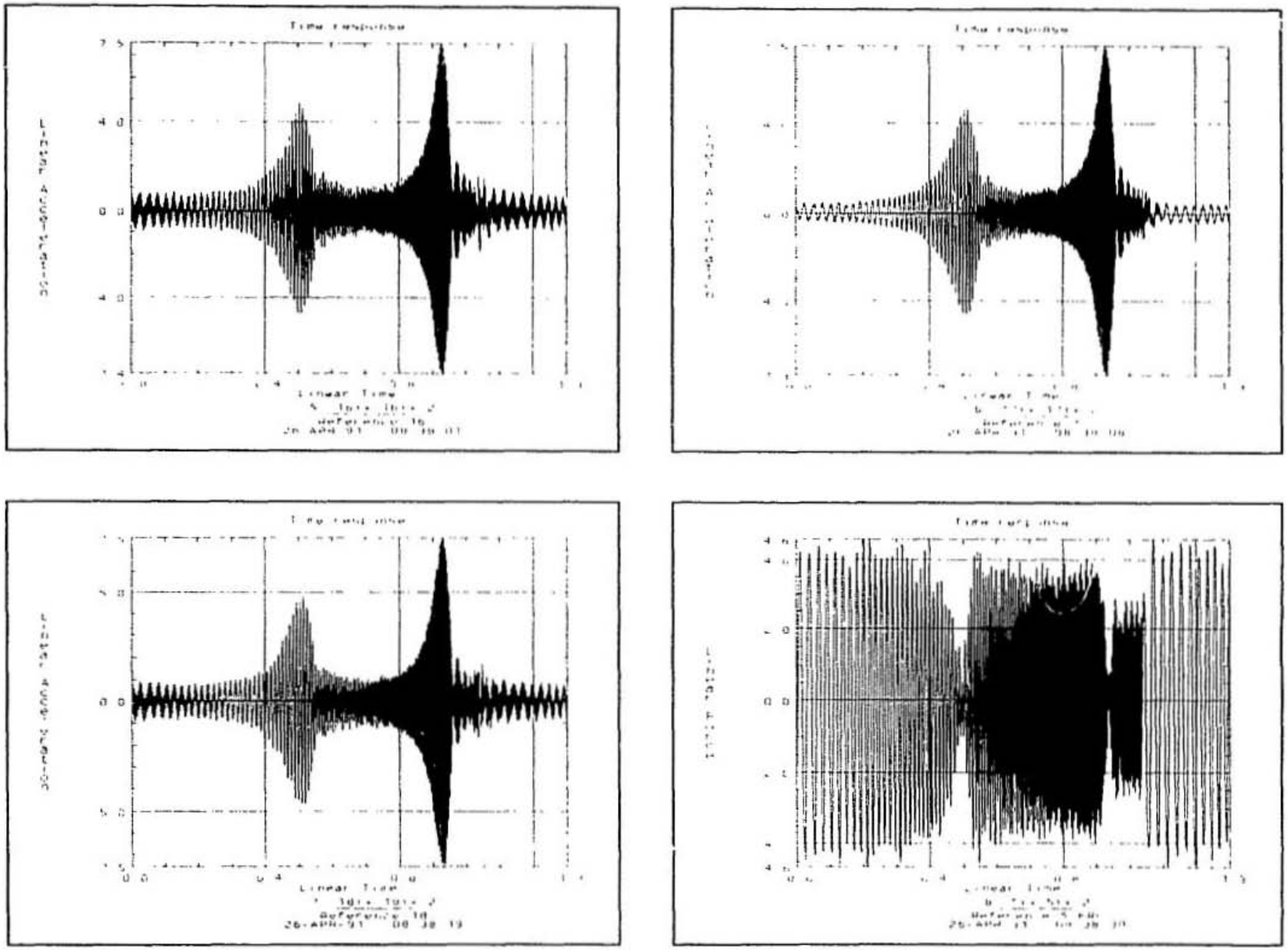

Typical Time Histories Nodes 16, 17, & 18 Accel. Node 5 Force, Phase B - 35-350 Hz Log Sweep

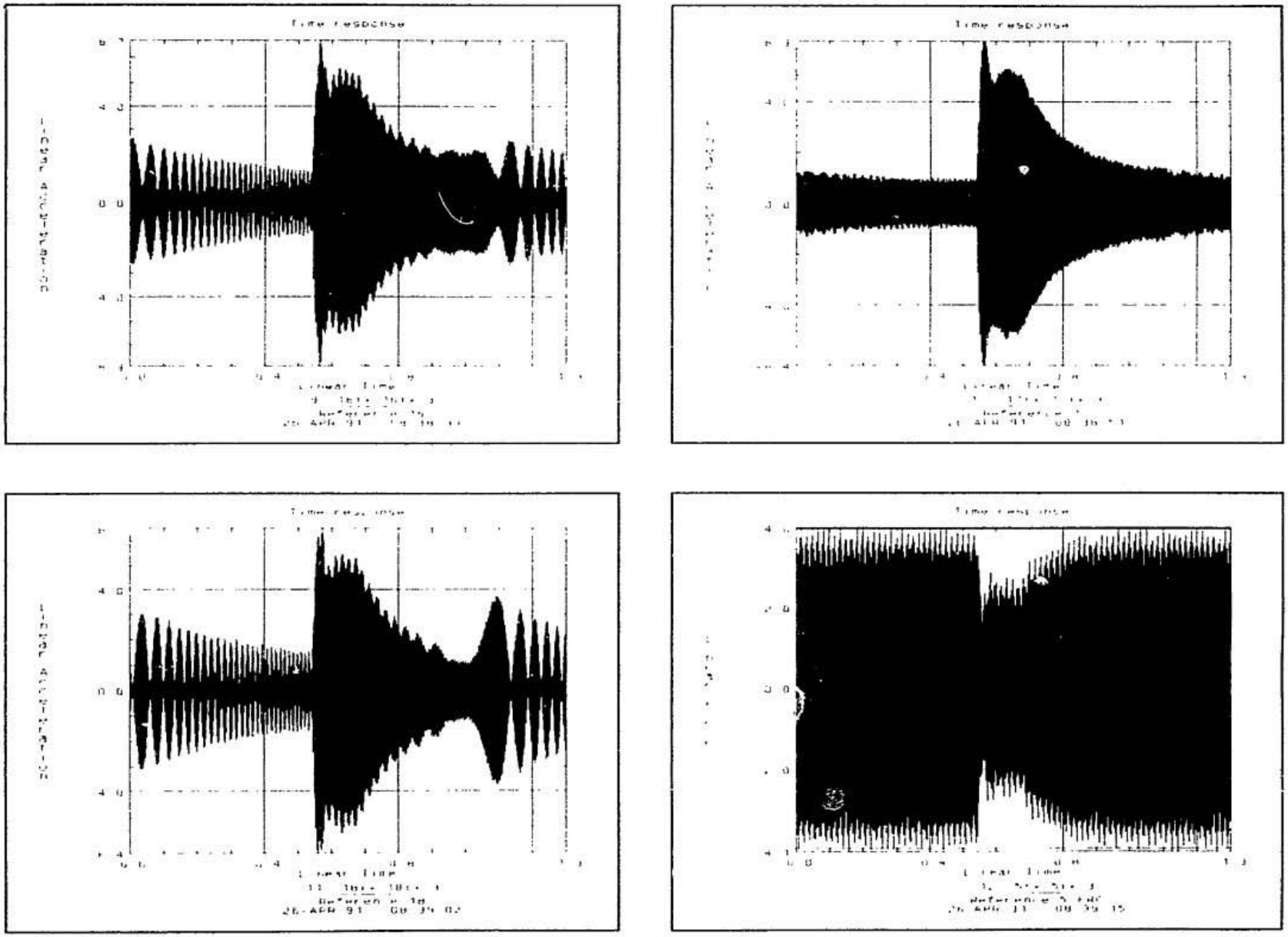

Typical Time Histories Nodes 16, 17, & 18 Accel. Node 5 Force, Phase C - 280-420 Hz Linear Sweep

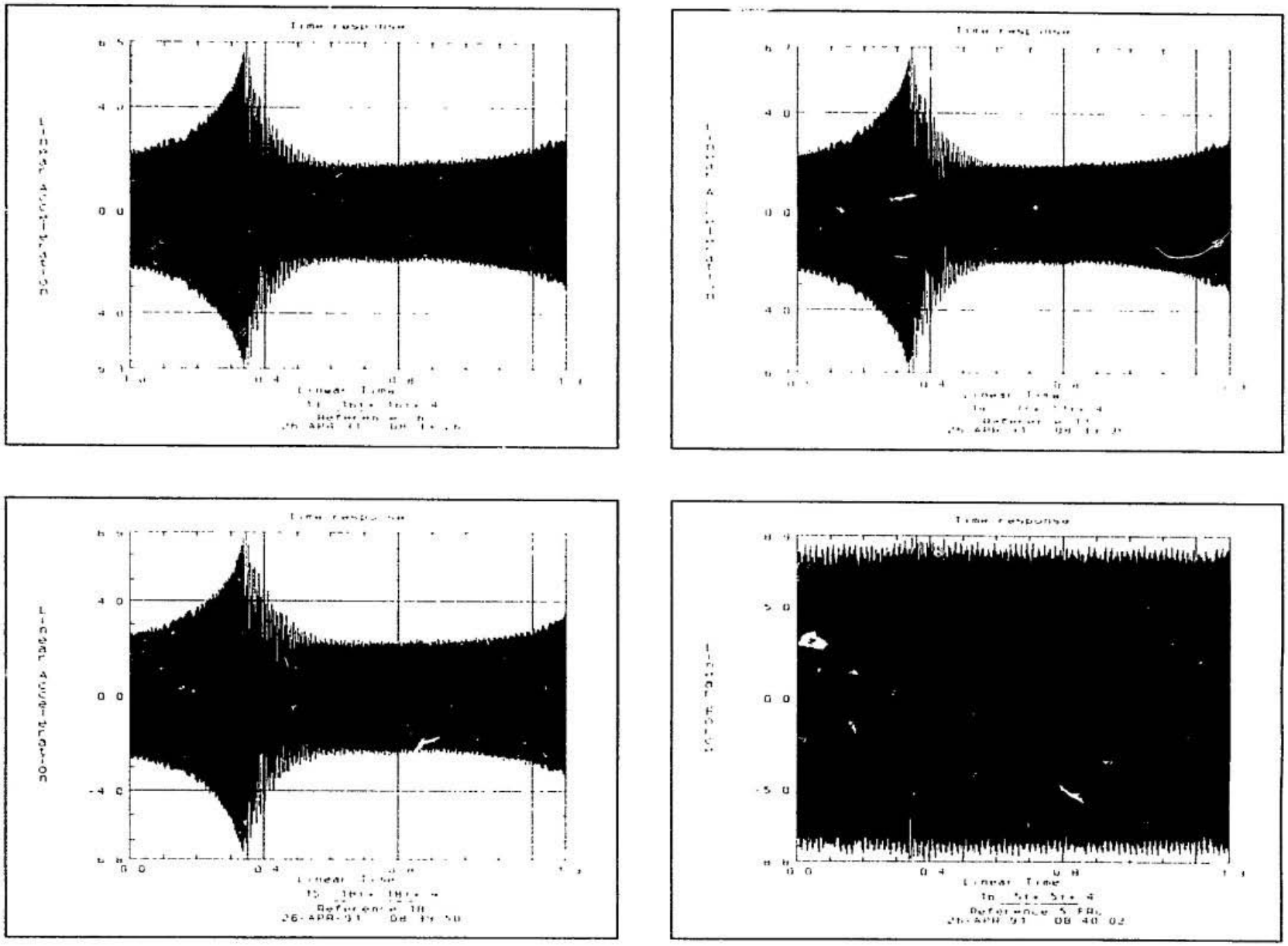

Typical Time Histories Nodes 16, 17, & 18 Accel. Node 5 Force, Phase D - 380-520 Hz Linear Sweep

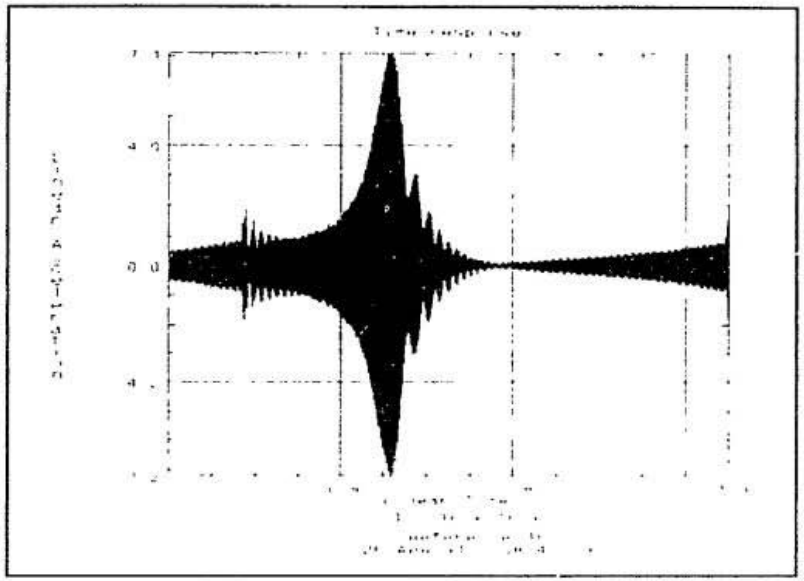

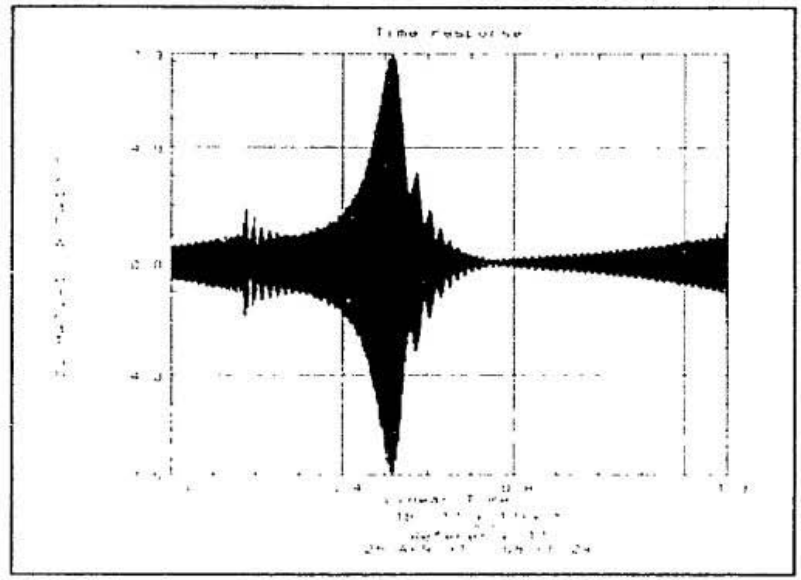

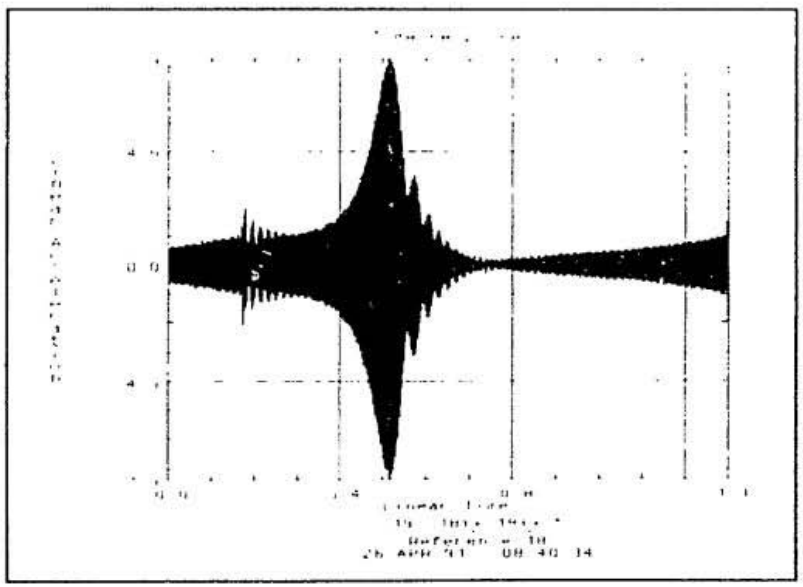

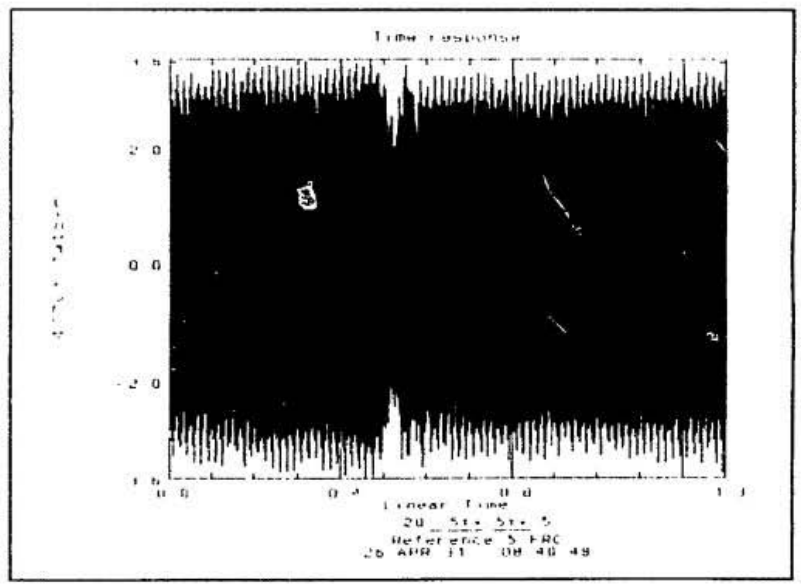

Typical Time Histories Nodes 16, 17, & 18 Accel. Node 5 Force, Phase E - 480-770 Hz Linear Sweep

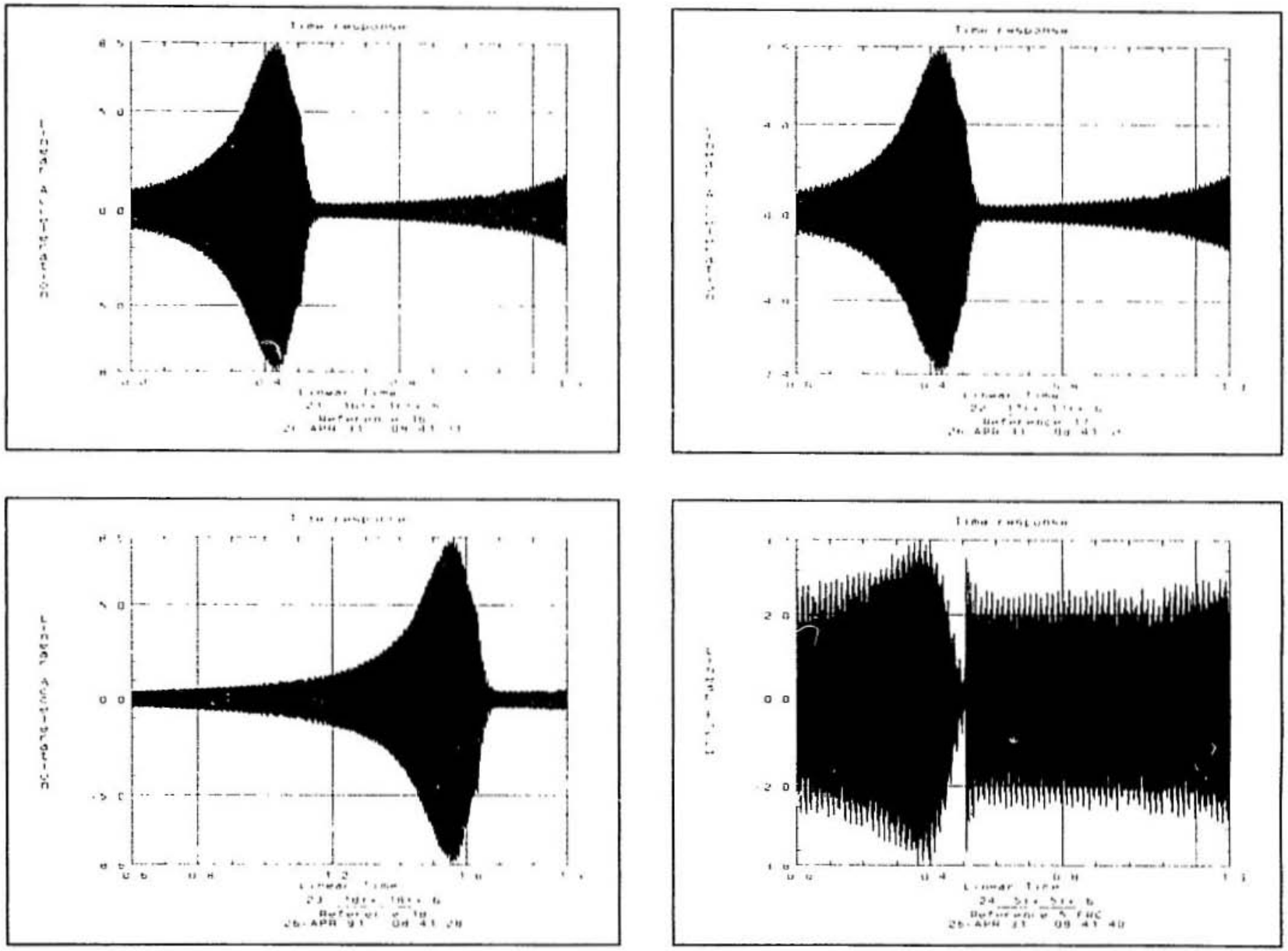

Typical Time Histories Nodes 16, 17, & 18 Accel. Node 5 Force, Phase F - 730-890 Hz Linear Sweep

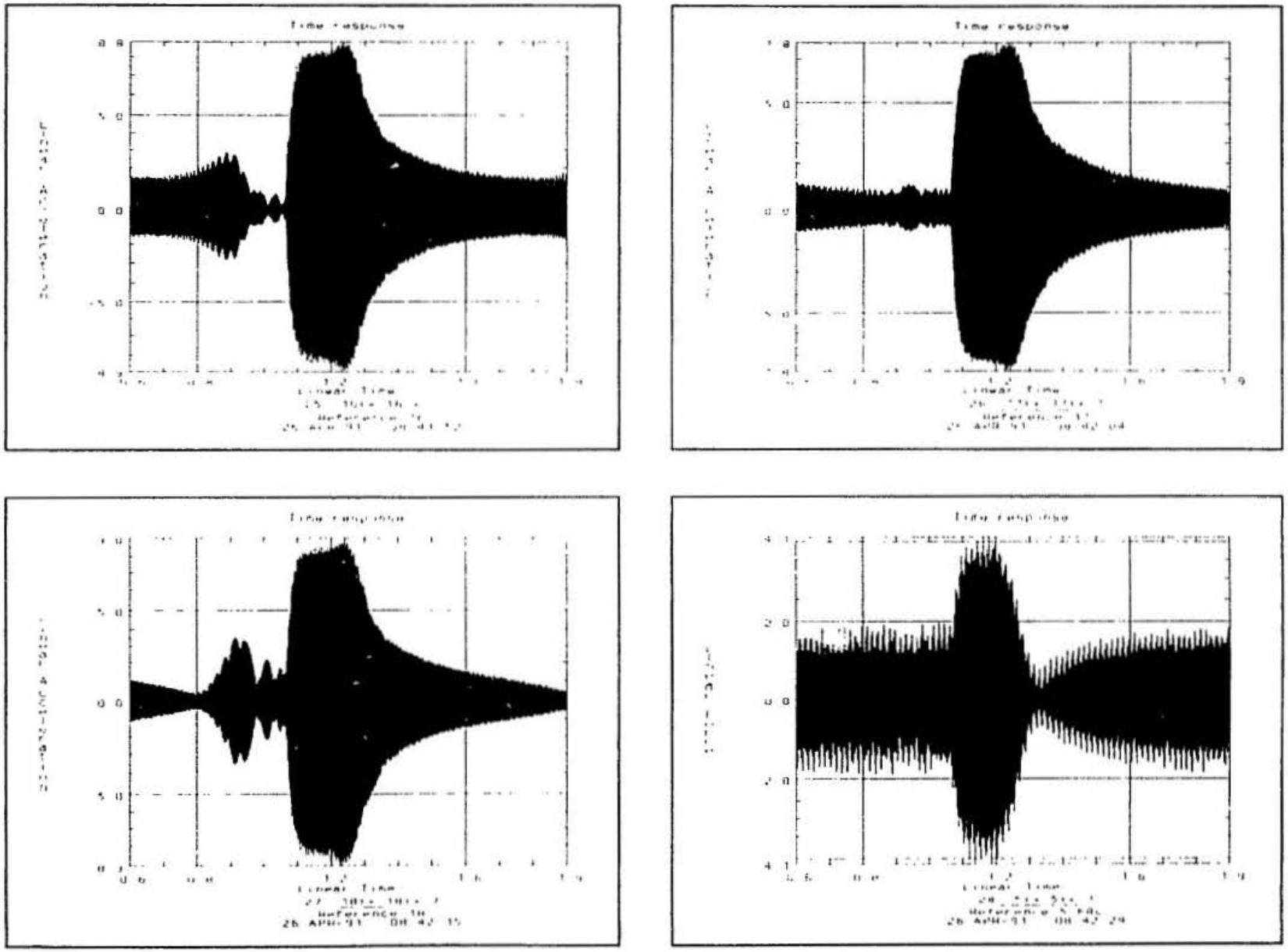

Typical Time Histories Nodes 16, 17, & 18 Accel. Node 5 Force, Phase G - 870-1020 Hz Linear Sweep

Appendix C

FRF's for All 18 Nodes on 5 Plates

Note: To determine the particular point of analysis for each FRF, observe the second to last line of the caption under each figure. The numeric value to the right of this line is the response node evaluated, the term to the left, indicates the particular plate on which the node is located: reference, indicates the zero crack plate, all others are indicated by a Q or q followed by the crack depth ratio (eg . q1-8 n2 = Node 2 on plate with 1 8 depth crack). The ordinate label of an FRF is usually indicative of the response parameter measured and does not include its unit. For these FRF's the magnitude of the FRF is a ratio of acceleration output to force input and hence, has the unit [(m/s^2)/N].

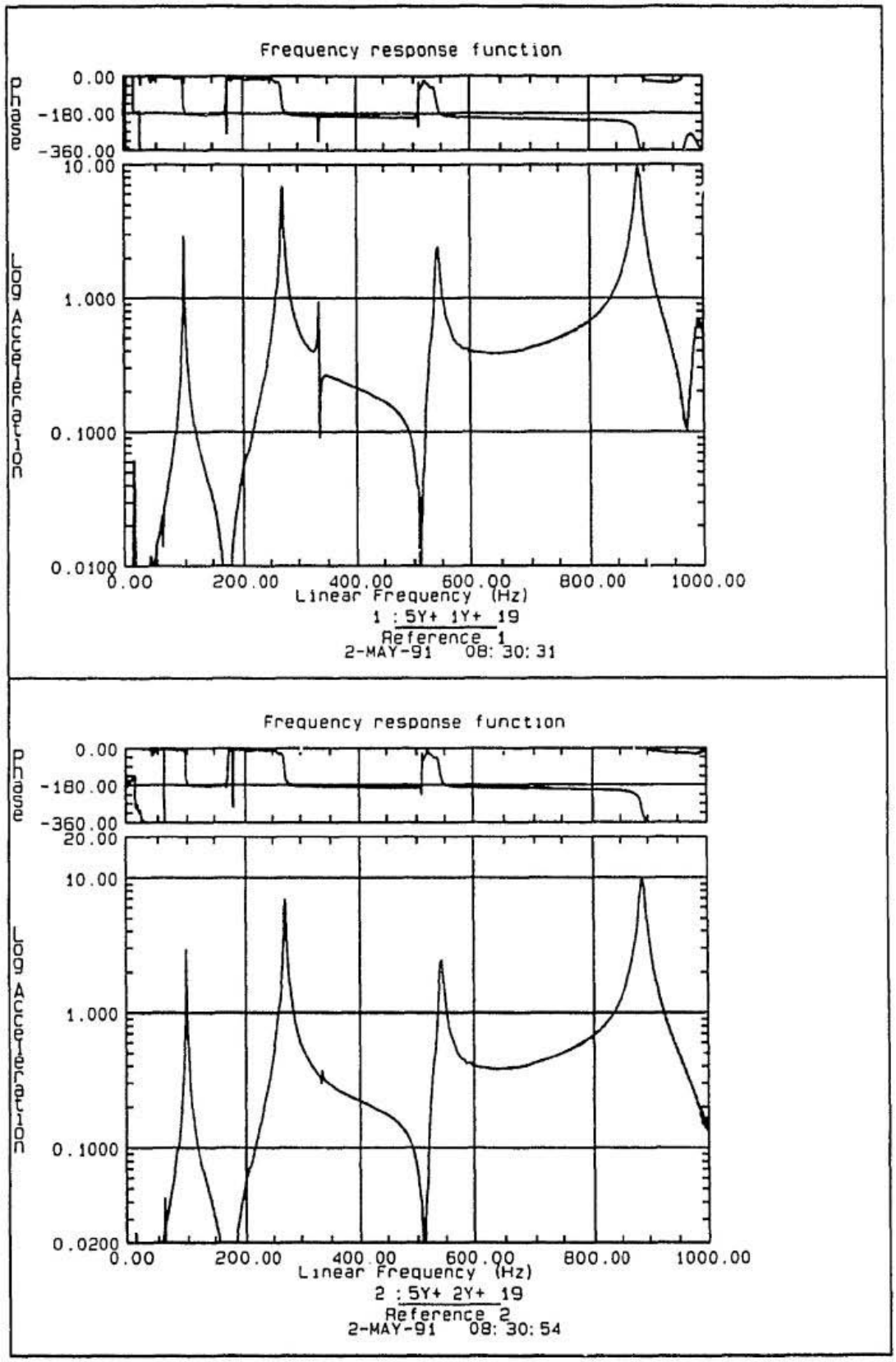
Frequency response function
Phase
0.00
-180.00
-360.00
Log Acceleration
10.00
1.000
0.1000
0.0100
0.00
200.00
400.00
600.00
800.00
1000.00
Linear Frequency (Hz)
1 : 5Y+ 1Y+ 19
Reference 1
2-MAY-91 08:30:31
Frequency response function
Phase
0.00
-180.00
-360.00
Log Acceleration
20.00
10.00
1.000
0.1000
0.0200
0.00
200.00
400.00
600.00
800.00
1000.00
Linear Frequency (Hz)
2 : 5Y+ 2Y+ 19
Reference 2
2-MAY-91 08:30:54

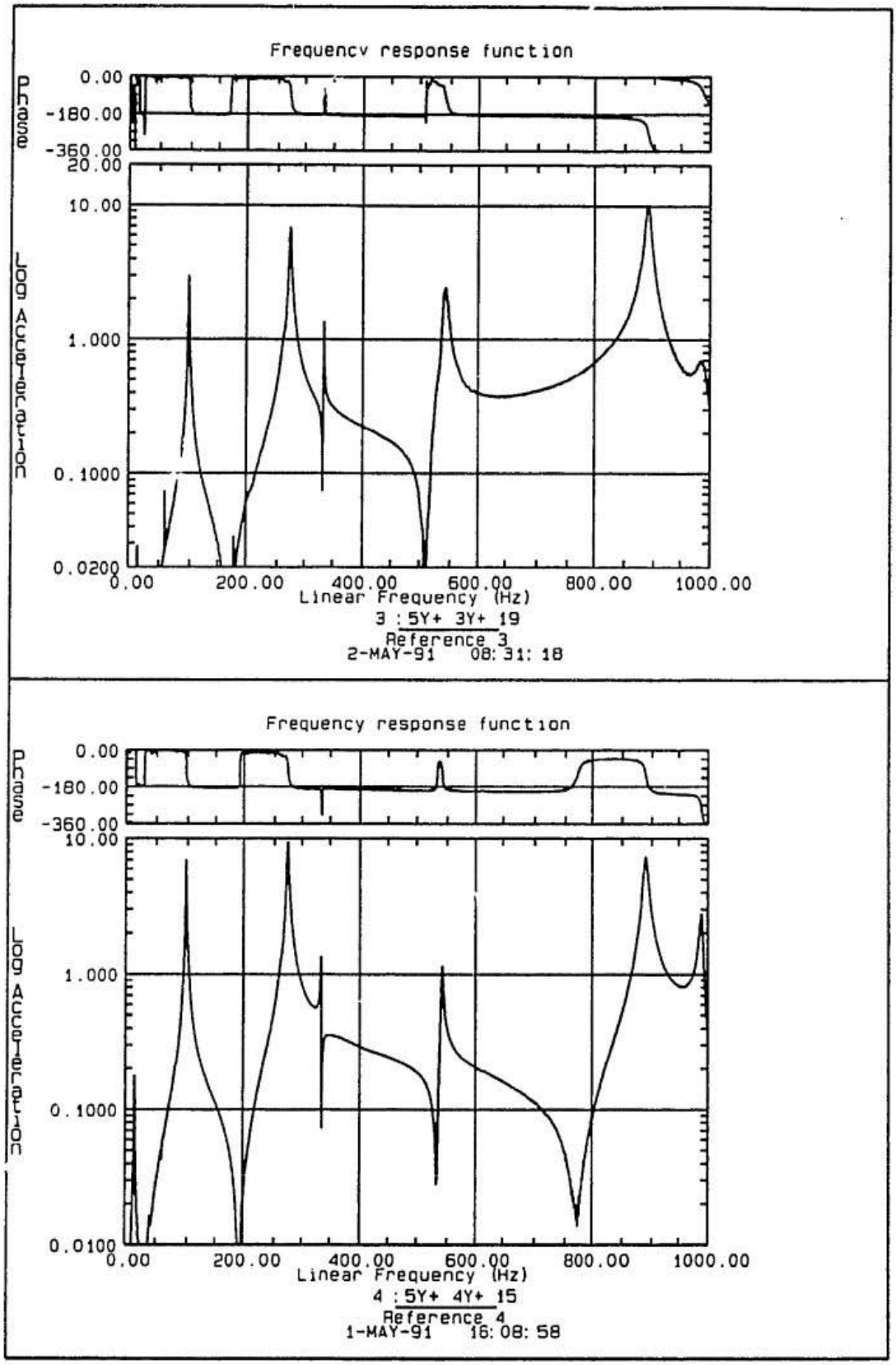
Frequency response function
Phase
0.00
-180.00
-360.00
Log Acceleration
20.00
10.00
1.000
0.1000
0.0200
0.00
200.00
400.00
600.00
800.00
1000.00
Linear Frequency (Hz)
3 : 5Y+ 3Y+ 19
Reference 3
2-MAY-91 08:31:18
Frequency response function
Phase
0.00
-180.00
-360.00
Log Acceleration
10.00
1.000
0.1000
0.0100
0.00
200.00
400.00
600.00
800.00
1000.00
Linear Frequency (Hz)
4 : 5Y+ 4Y+ 15
Reference 4
1-MAY-91 16:08:58

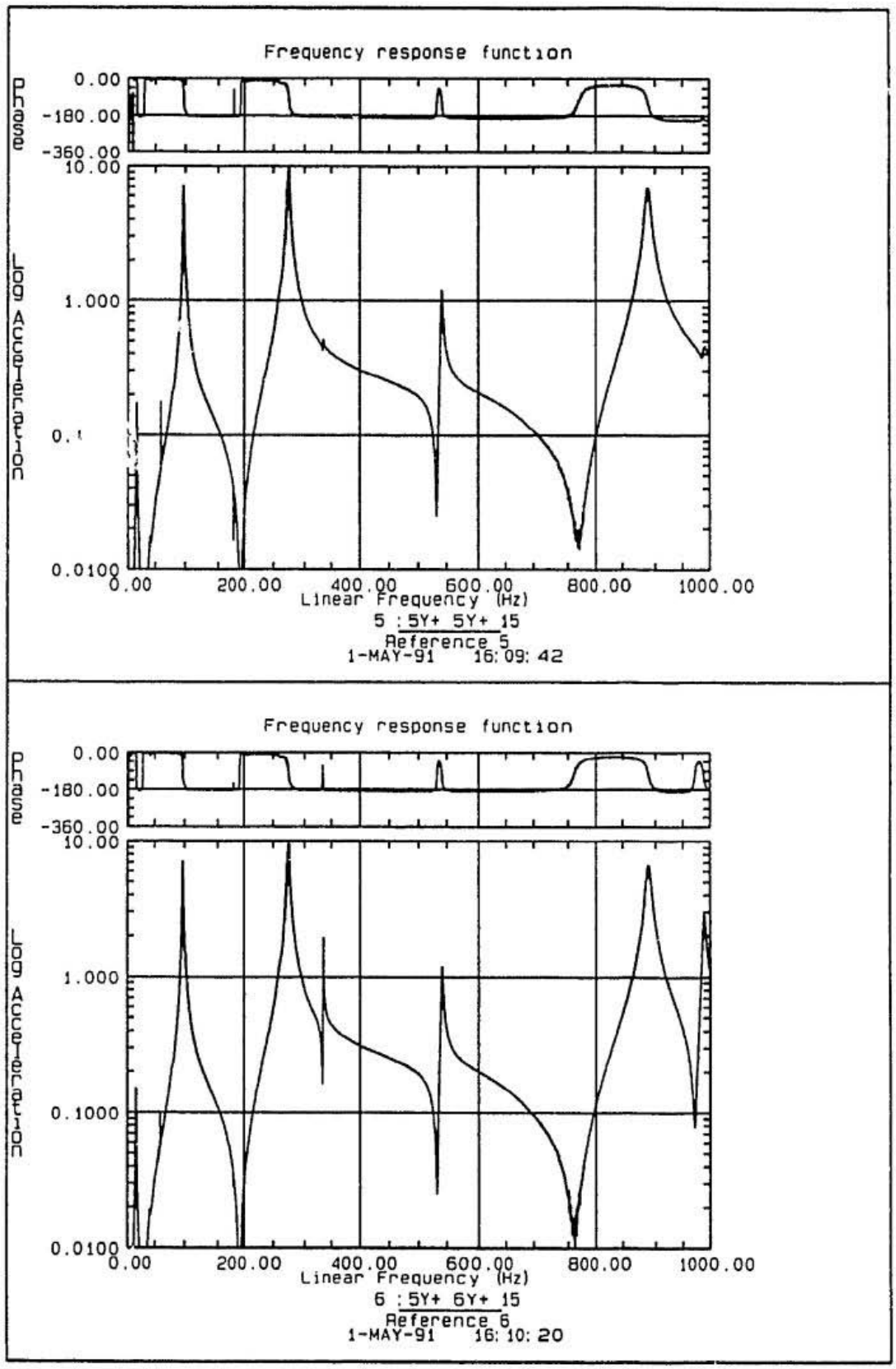
Frequency response function
Phase
0.00
-180.00
-360.00
Log Acceleration
10.00
1.000
0.1
0.0100
0.00
200.00
400.00
600.00
800.00
1000.00
Linear Frequency (Hz)
5 : 5Y+ 5Y+ 15
Reference 5
1-MAY-91 16:09:42
Frequency response function
Phase
0.00
-180.00
-360.00
Log Acceleration
10.00
1.000
0.1000
0.0100
0.00
200.00
400.00
600.00
800.00
1000.00
Linear Frequency (Hz)
6 : 5Y+ 6Y+ 15
Reference 6
1-MAY-91 16:10:20

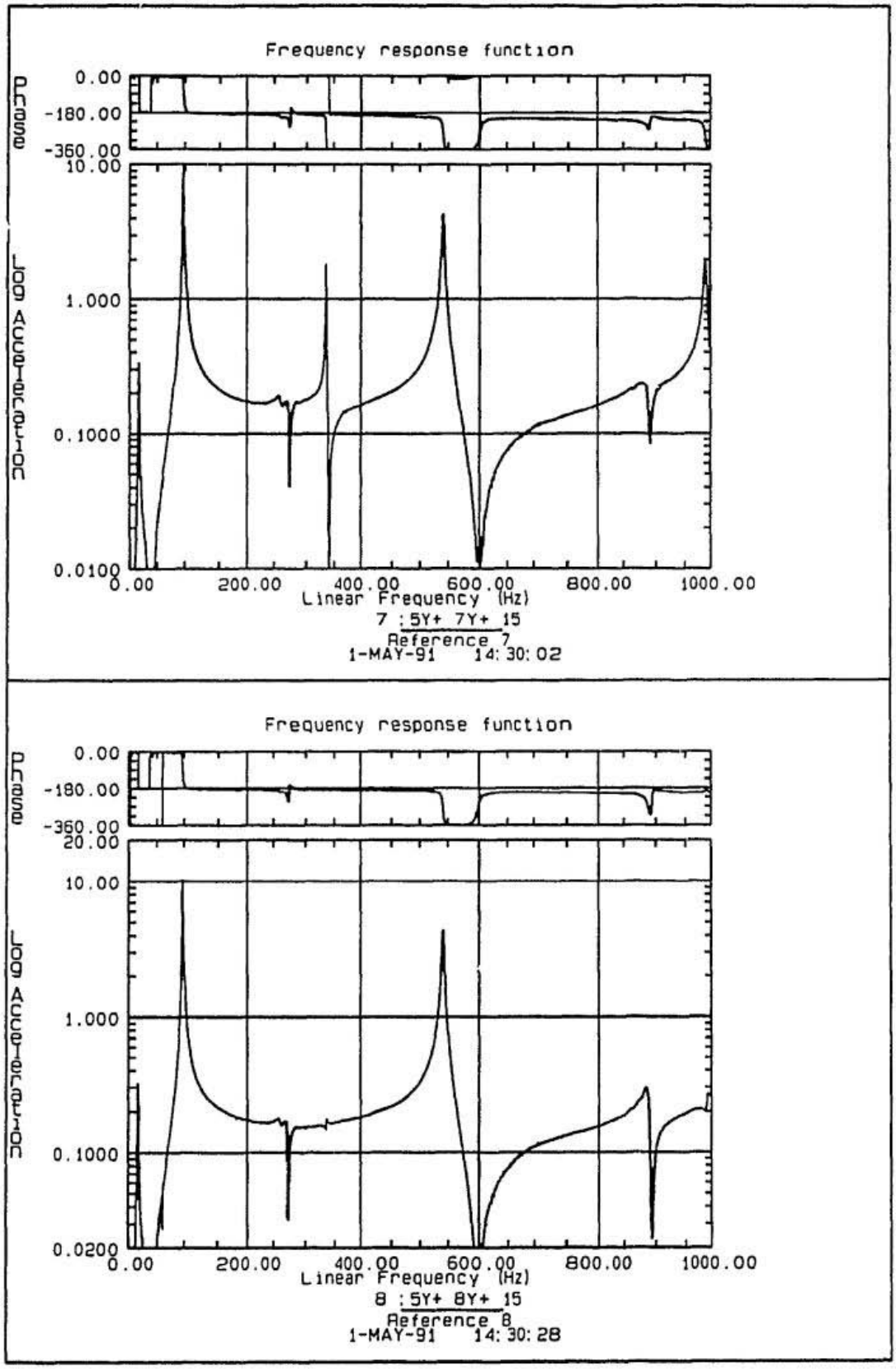
Frequency response function
Phase
0.00
-180.00
-360.00
Log Acceleration
10.00
1.000
0.1000
0.0100
0.00
200.00
400.00
600.00
800.00
1000.00
Linear Frequency (Hz)
7 :5Y+ 7Y+ 15
Reference 7
1-MAY-91 14:30:02
Frequency response function
Phase
0.00
-180.00
-360.00
Log Acceleration
20.00
10.00
1.000
0.1000
0.0200
0.00
200.00
400.00
600.00
800.00
1000.00
Linear Frequency (Hz)
8 :5Y+ 8Y+ 15
Reference 8
1-MAY-91 14:30:28

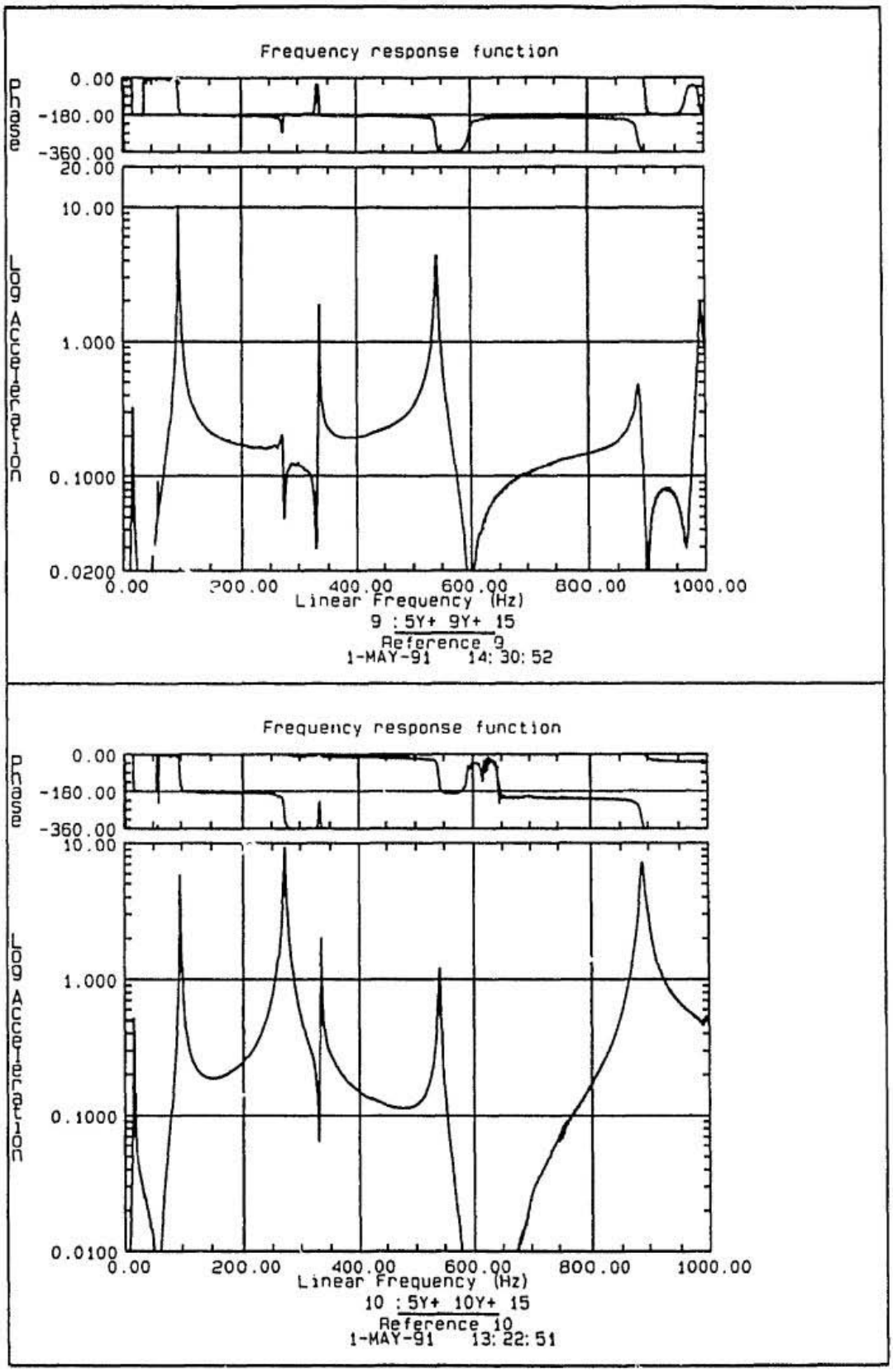
Frequency response function
Phase
0.00
-180.00
-360.00
Log Acceleration
20.00
10.00
1.000
0.1000
0.0200
0.00
200.00
400.00
600.00
800.00
1000.00
Linear Frequency (Hz)
9 : 5Y+ 9Y+ 15
Reference 9
1-MAY-91 14:30:52
Frequency response function
Phase
0.00
-180.00
-360.00
Log Acceleration
10.00
1.000
0.1000
0.0100
0.00
200.00
400.00
600.00
800.00
1000.00
Linear Frequency (Hz)
10 : 5Y+ 10Y+ 15
Reference 10
1-MAY-91 13:22:51

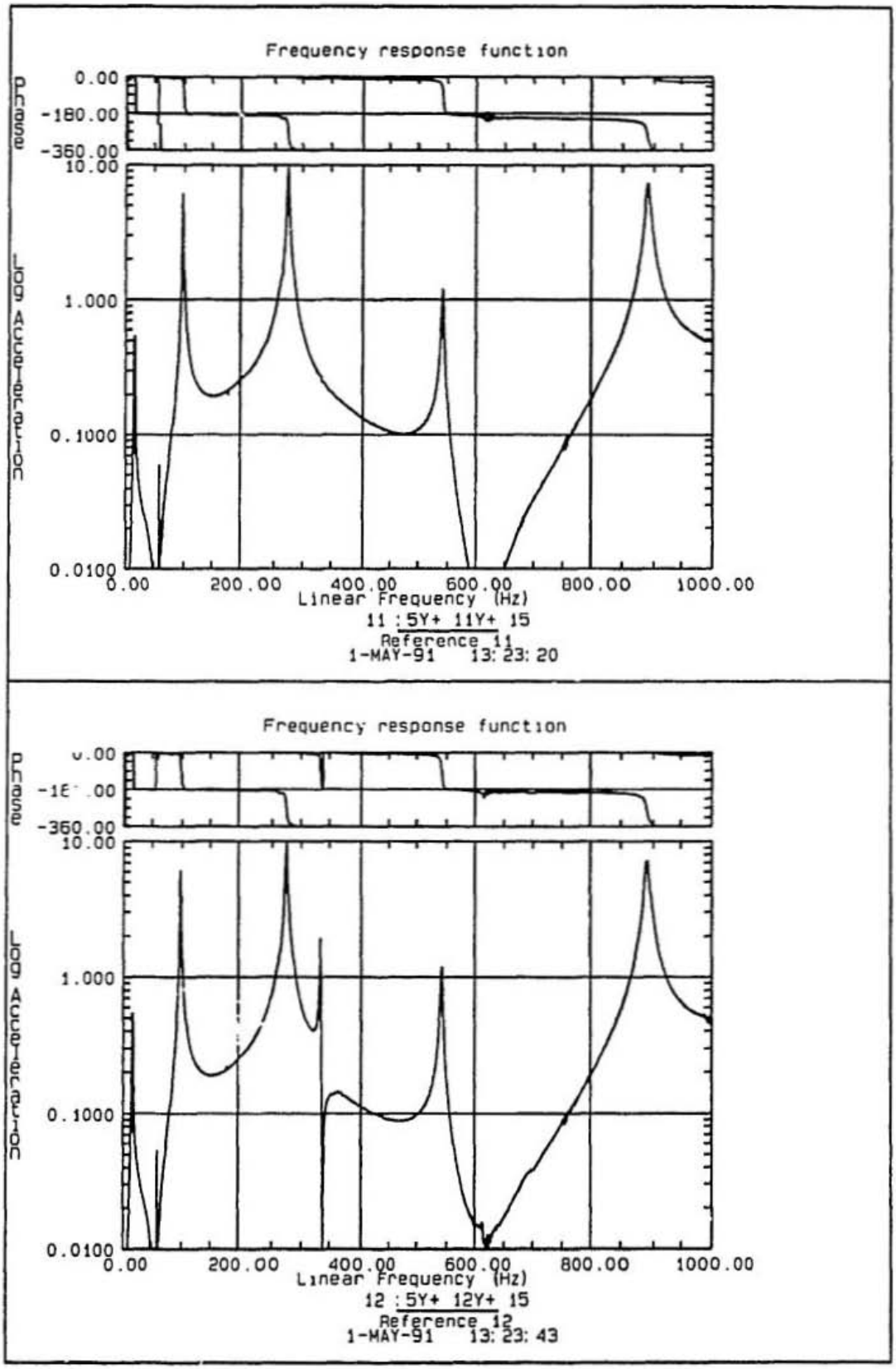
Frequency response function
0.00
-180.00
-360.00
10.00
1.000
0.1000
0.0100
0.00
200.00
400.00
600.00
800.00
1000.00
Linear Frequency (Hz)
11 :5Y+ 11Y+ 15
Reference 11
1-MAY-91 13:23:20
Frequency response function
-360.00
10.00
1.000
0.1000
0.0100
0.00
200.00
400.00
600.00
800.00
1000.00
Linear Frequency (Hz)
12 :5Y+ 12Y+ 15
Reference 12
1-MAY-91 13:23:43

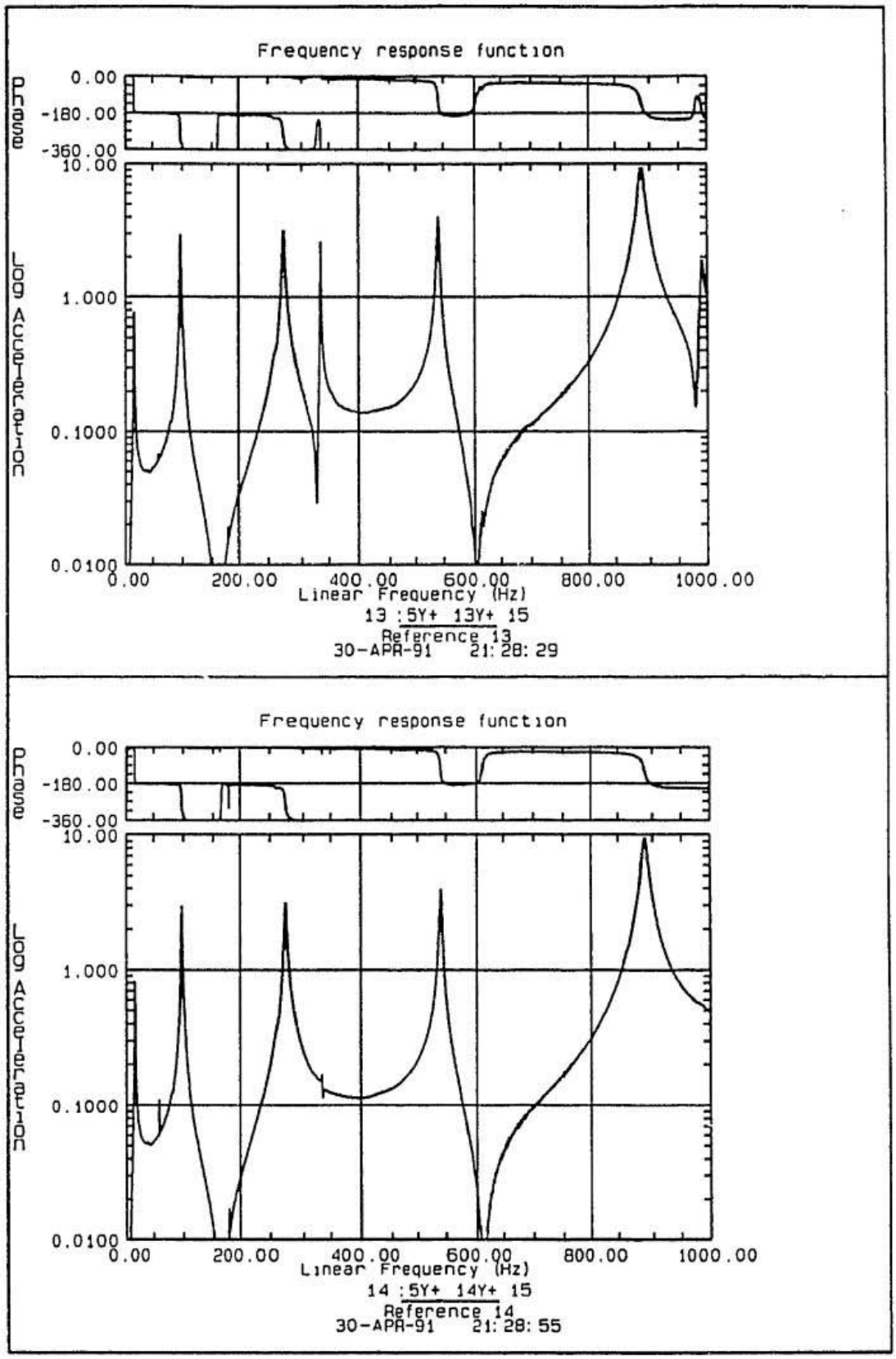
Frequency response function
Phase
0.00
-180.00
-360.00
Log Acceleration
10.00
1.000
0.1000
0.0100
0.00
200.00
400.00
600.00
800.00
1000.00
Linear Frequency (Hz)
13 :5Y+ 13Y+ 15
Reference 13
30-APR-91 21:28:29
Frequency response function
Phase
0.00
-180.00
-360.00
Log Acceleration
10.00
1.000
0.1000
0.0100
0.00
200.00
400.00
600.00
800.00
1000.00
Linear Frequency (Hz)
14 :5Y+ 14Y+ 15
Reference 14
30-APR-91 21:28:55

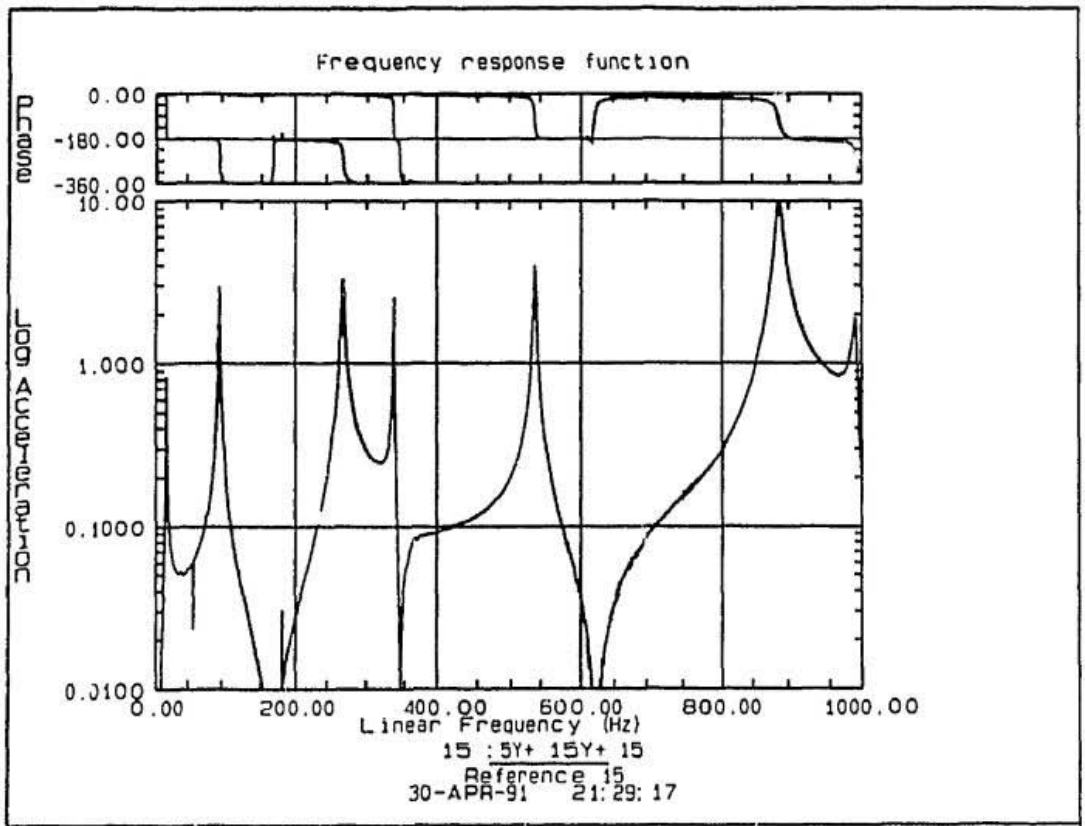
Frequency response function
Phase
0.00
-180.00
-360.00
Log Acceleration
10.00
1.000
0.1000
0.0100
0.00
200.00
400.00
600.00
800.00
1000.00
Linear Frequency (Hz)
15 :5Y+ 15Y+ 15
Reference 15
30-APR-91 21:29:17

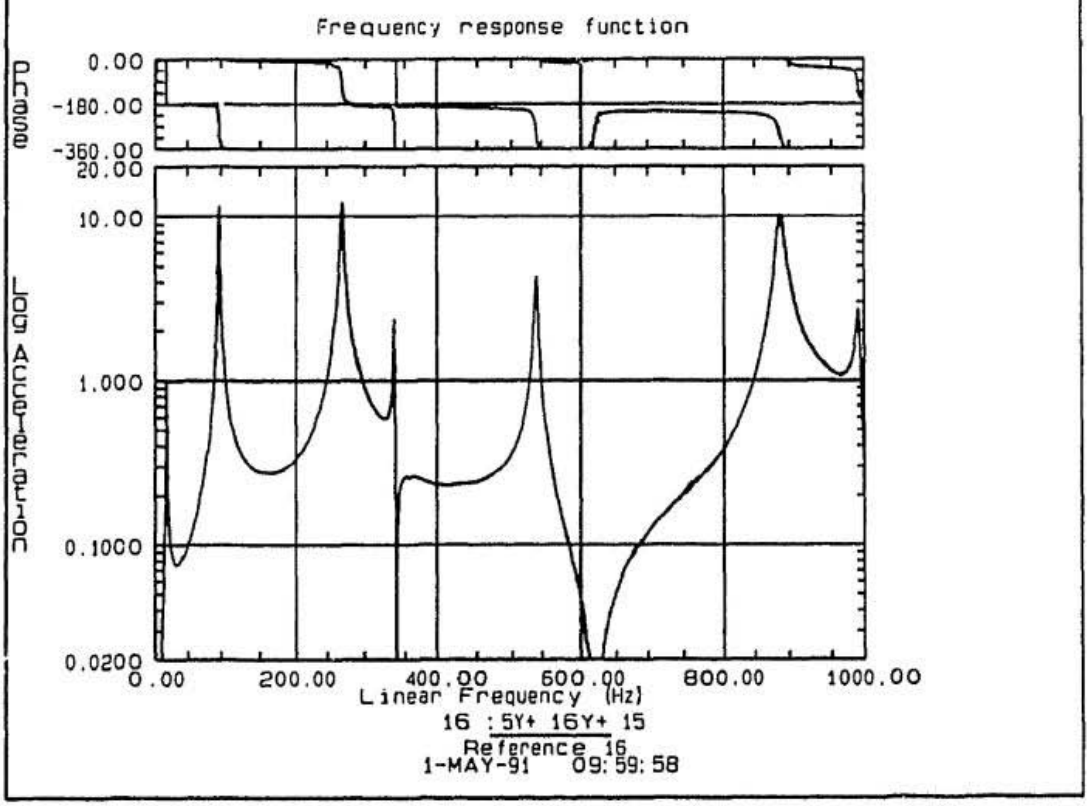
Frequency response function
Phase
0.00
-180.00
-360.00
Log Acceleration
20.00
10.00
1.000
0.1000
0.0200
0.00
200.00
400.00
600.00
800.00
1000.00
Linear Frequency (Hz)
16 :5Y+ 16Y+ 15
Reference 16
1-MAY-91 09:59:58

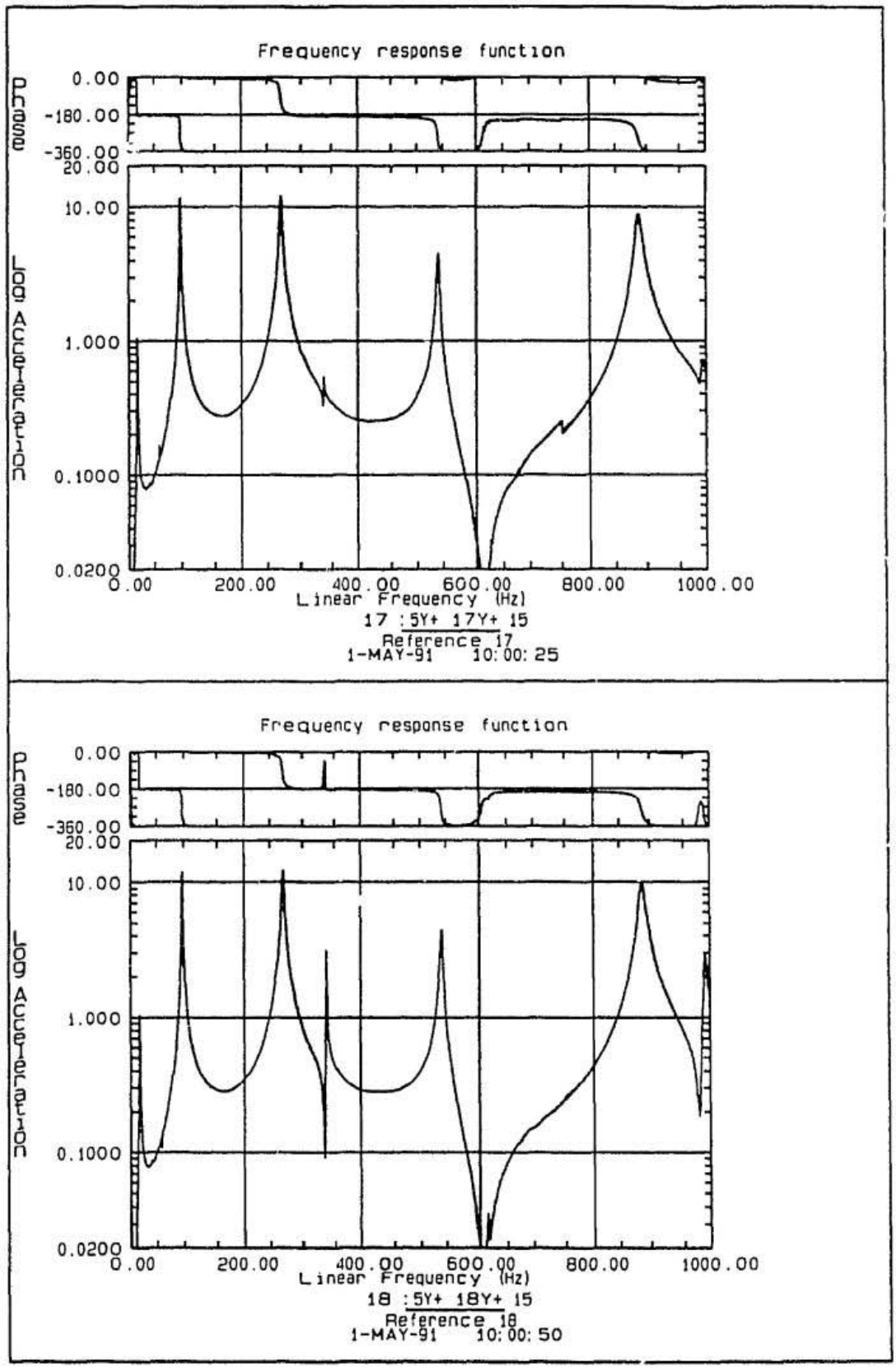
Frequency response function
Phase
0.00
-180.00
-360.00
Log Acceleration
20.00
10.00
1.000
0.1000
0.0200
0.00
200.00
400.00
600.00
800.00
1000.00
Linear Frequency (Hz)
17 :5Y+ 17Y+ 15
Reference 17
1-MAY-91 10:00:25
Frequency response function
Phase
0.00
-180.00
-360.00
Log Acceleration
20.00
10.00
1.000
0.1000
0.0200
0.00
200.00
400.00
600.00
800.00
1000.00
Linear Frequency (Hz)
18 :5Y+ 18Y+ 15
Reference 18
1-MAY-91 10:00:50

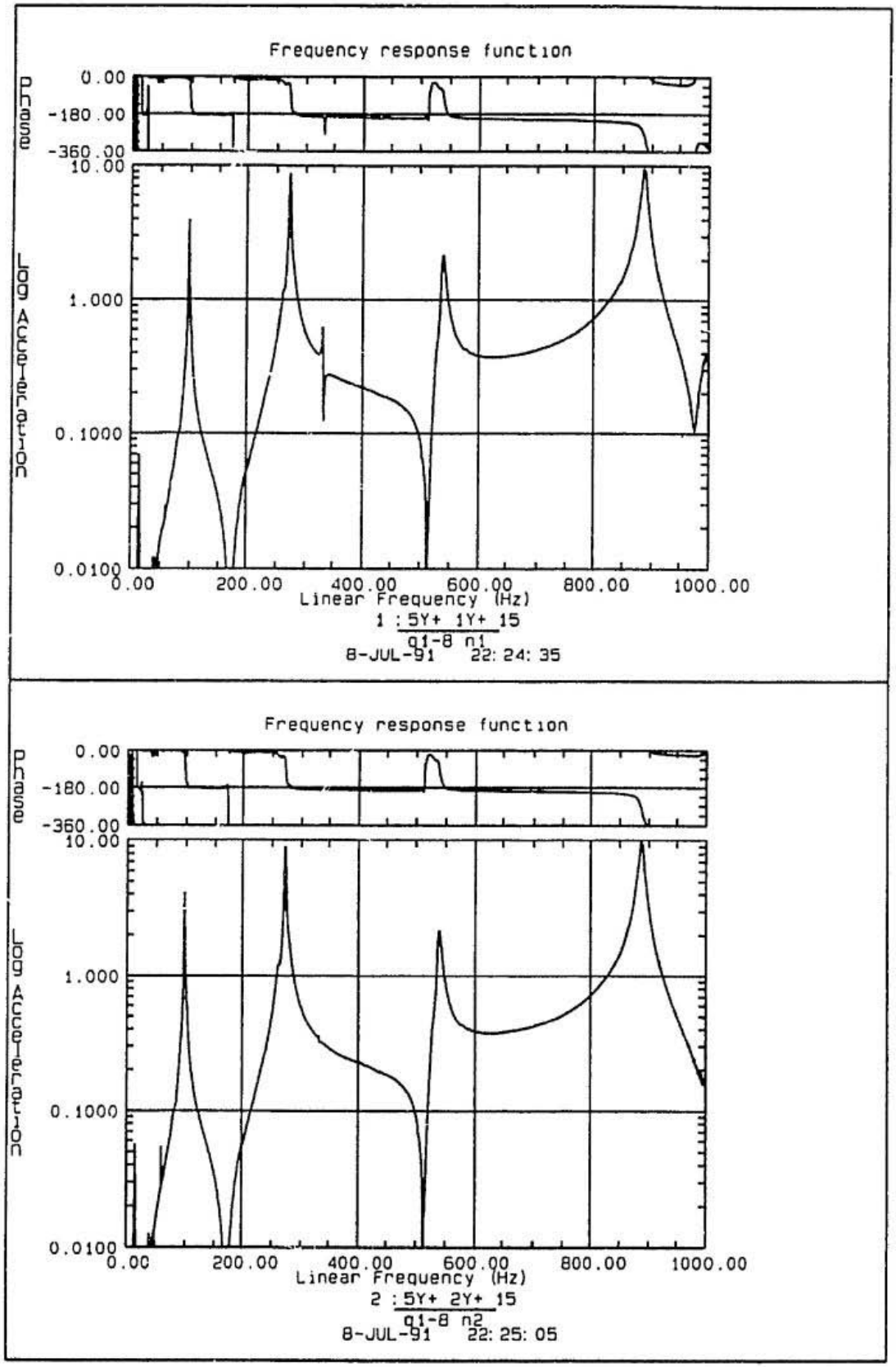
Frequency response function
Phase
0.00
-180.00
-360.00
Log Acceleration
10.00
1.000
0.1000
0.0100
0.00
200.00
400.00
600.00
800.00
1000.00
Linear Frequency (Hz)
1 :5Y+ 1Y+ 15
q1-8 n1
8-JUL-91 22:24:35
Frequency response function
Phase
0.00
-180.00
-360.00
Log Acceleration
10.00
1.000
0.1000
0.0100
0.00
200.00
400.00
600.00
800.00
1000.00
Linear Frequency (Hz)
2 :5Y+ 2Y+ 15
q1-8 n2
8-JUL-91 22:25:05

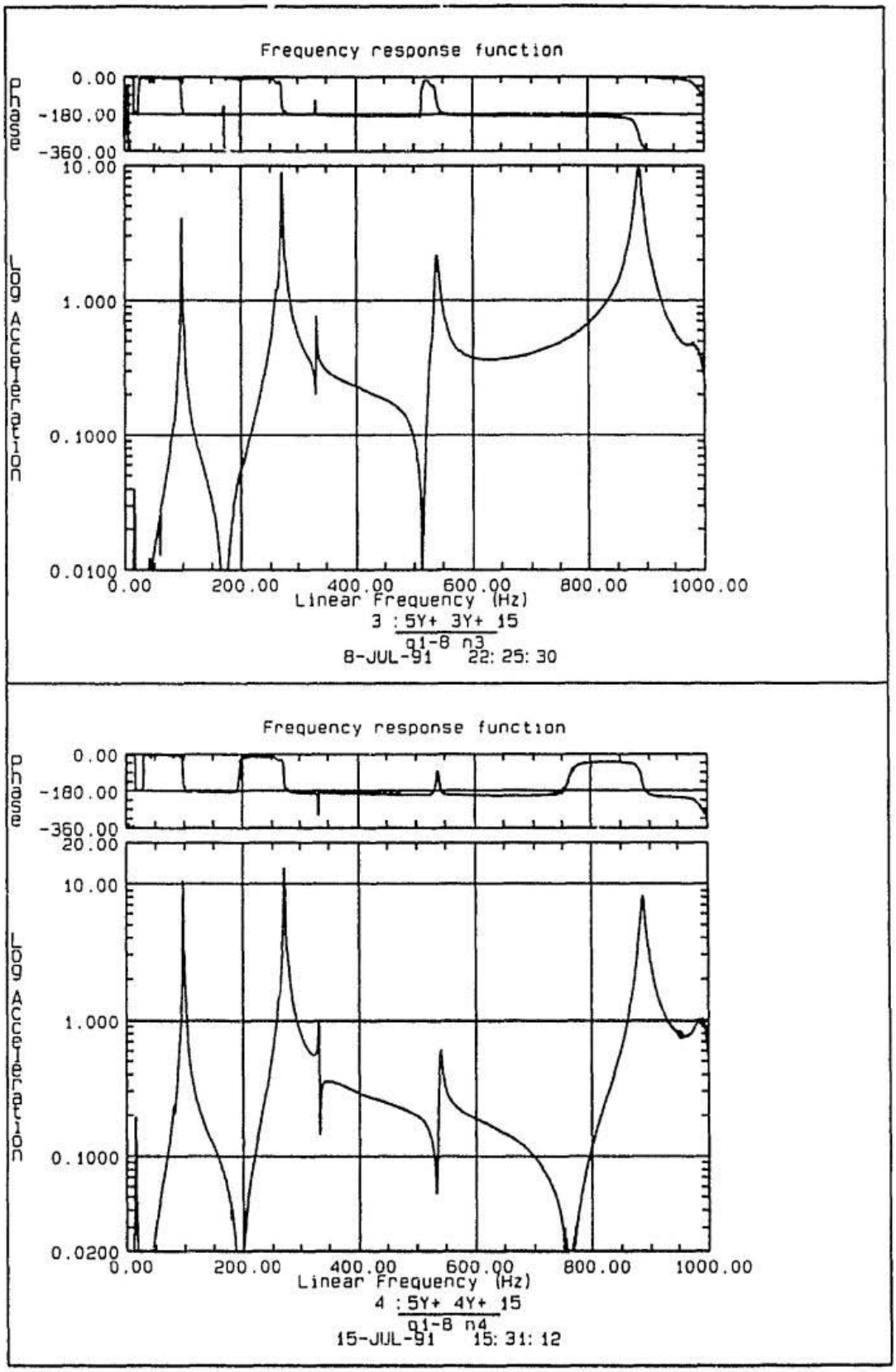
Frequency response function
Phase
0.00
-180.00
-360.00
Log Acceleration
10.00
1.000
0.1000
0.0100
0.00
200.00
400.00
600.00
800.00
1000.00
Linear Frequency (Hz)
3 : 5Y+ 3Y+ 15
q1-8 n3
8-JUL-91 22:25:30
Frequency response function
Phase
0.00
-180.00
-360.00
Log Acceleration
20.00
10.00
1.000
0.1000
0.0200
0.00
200.00
400.00
600.00
800.00
1000.00
Linear Frequency (Hz)
4 : 5Y+ 4Y+ 15
q1-8 n4
15-JUL-91 15:31:12

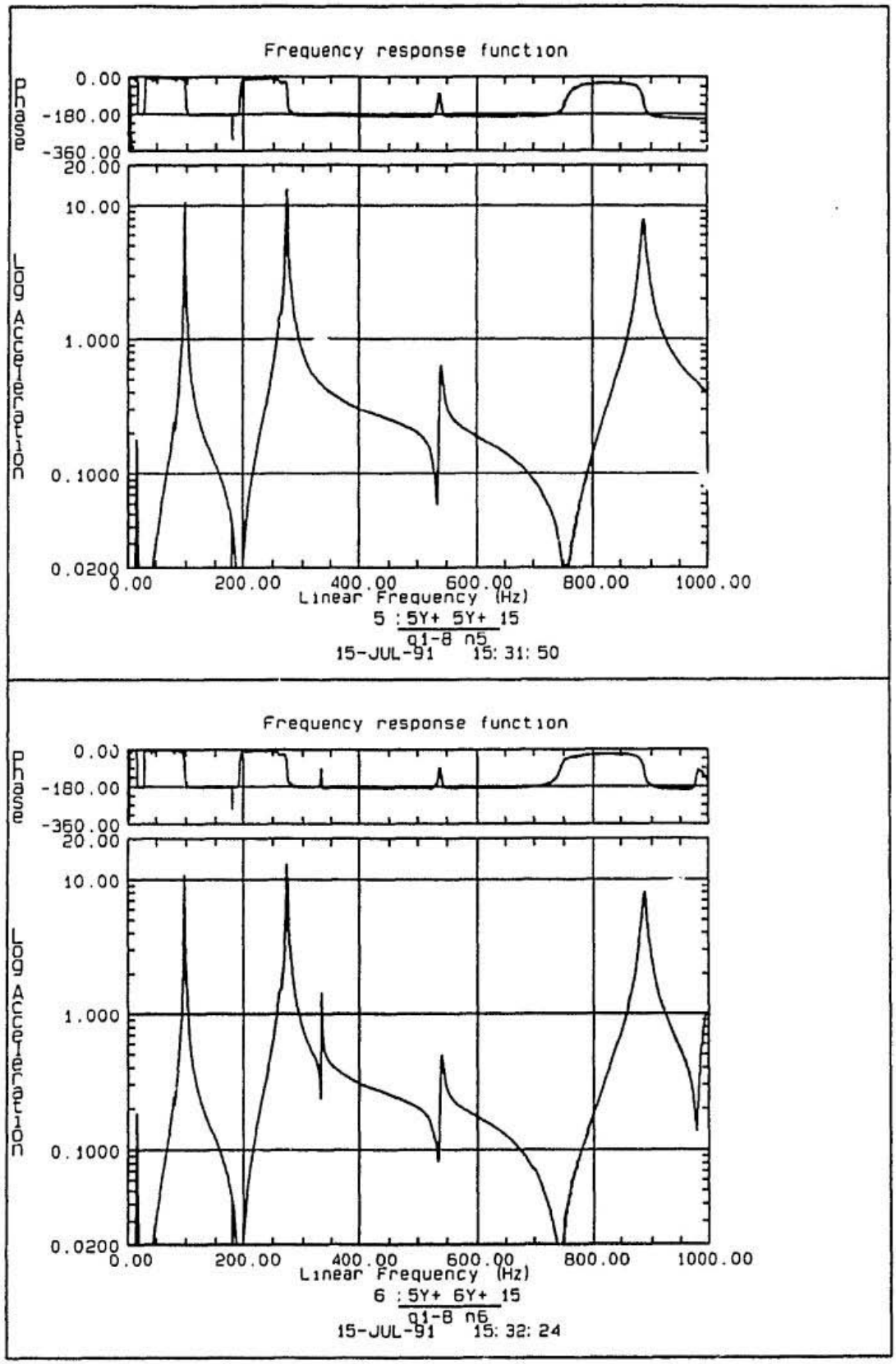
Frequency response function
Phase
0.00
-180.00
-360.00
Log Acceleration
20.00
10.00
1.000
0.1000
0.0200
0.00
200.00
400.00
600.00
800.00
1000.00
Linear Frequency (Hz)
5 : 5Y+ 5Y+ 15
q1-8 n5
15-JUL-91 15:31:50
Frequency response function
Phase
0.00
-180.00
-360.00
Log Acceleration
20.00
10.00
1.000
0.1000
0.0200
0.00
200.00
400.00
600.00
800.00
1000.00
Linear Frequency (Hz)
6 : 5Y+ 6Y+ 15
q1-8 n6
15-JUL-91 15:32:24

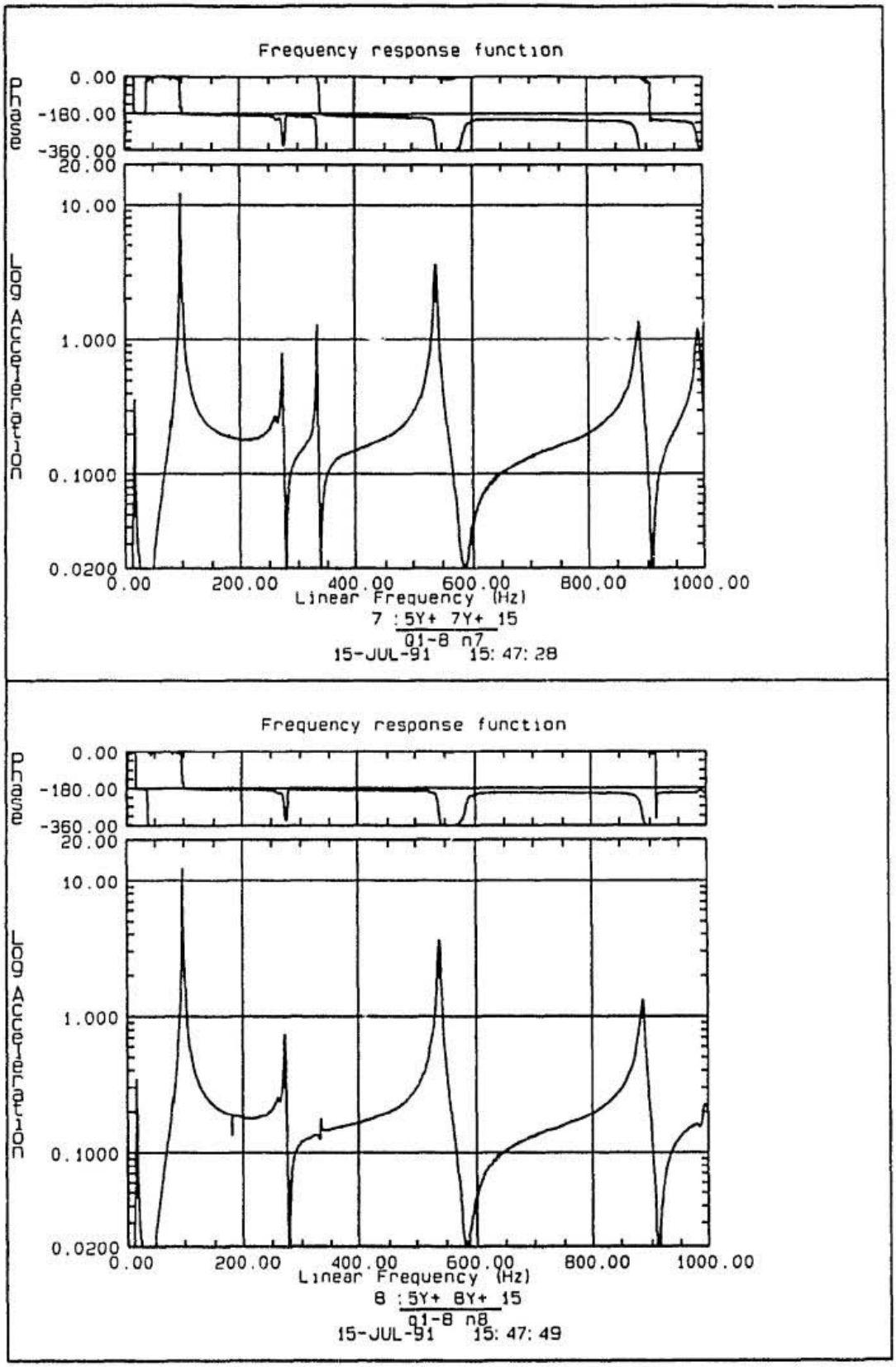
Frequency response function
Phase
0.00
-180.00
-360.00
Log Acceleration
20.00
10.00
1.000
0.1000
0.0200
0.00
200.00
400.00
600.00
800.00
1000.00
Linear Frequency (Hz)
7 :5Y+ 7Y+ 15
01-8 n7
15-JUL-91 15:47:28
Frequency response function
Phase
0.00
-180.00
-360.00
Log Acceleration
20.00
10.00
1.000
0.1000
0.0200
0.00
200.00
400.00
600.00
800.00
1000.00
Linear Frequency (Hz)
8 :5Y+ 8Y+ 15
01-8 n8
15-JUL-91 15:47:49

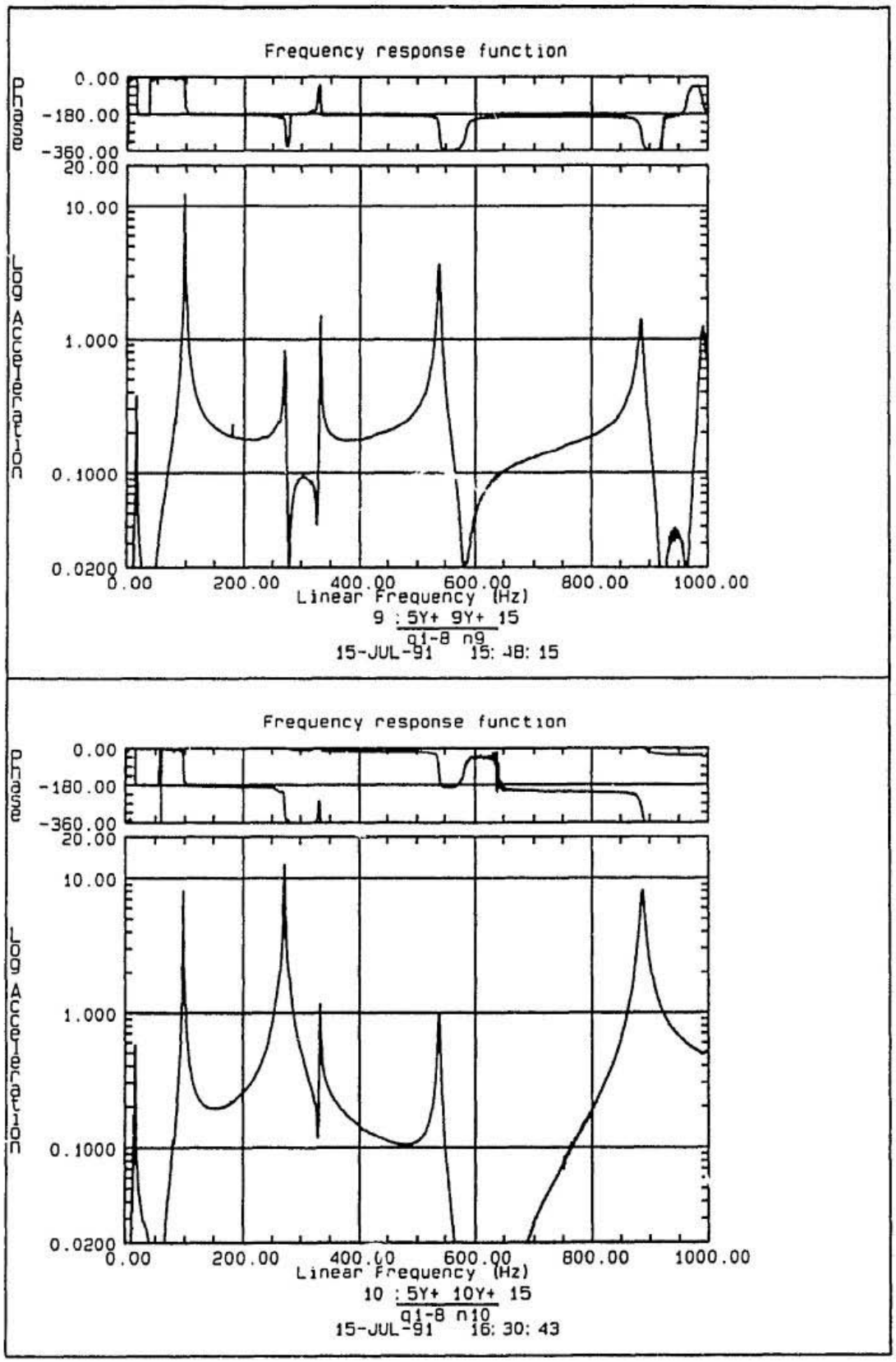
Frequency response function
Phase
0.00
-180.00
-360.00
Log Acceleration
20.00
10.00
1.000
0.1000
0.0200
0.00
200.00
400.00
600.00
800.00
1000.00
Linear Frequency (Hz)
9 : 5Y+ 9Y+ 15
q1-8 n9
15-JUL-91 15: 48: 15
Frequency response function
Phase
0.00
-180.00
-360.00
Log Acceleration
20.00
10.00
1.000
0.1000
0.0200
0.00
200.00
400.00
600.00
800.00
1000.00
Linear Frequency (Hz)
10 : 5Y+ 10Y+ 15
q1-8 n10
15-JUL-91 16: 30: 43

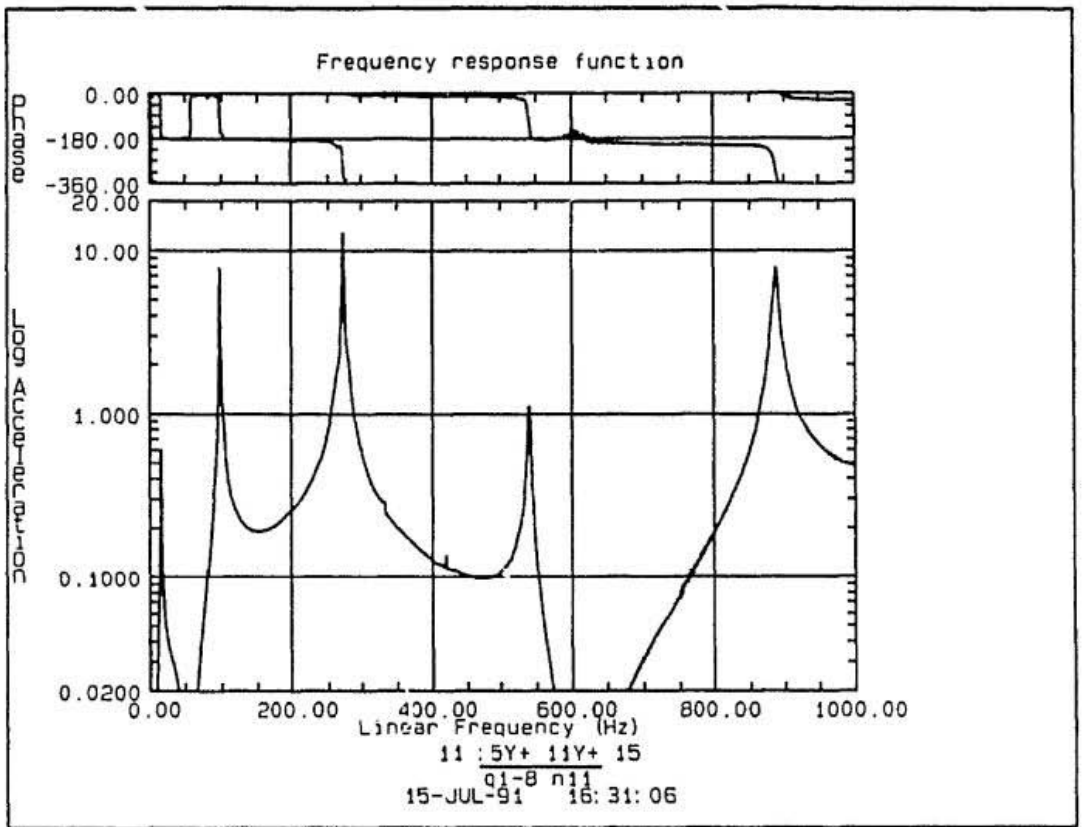
Frequency response function
Phase
0.00
-180.00
-360.00
Log Acceleration
20.00
10.00
1.000
0.1000
0.0200
0.00
200.00
400.00
600.00
800.00
1000.00
Linear Frequency (Hz)
11 :5Y+ 11Y+ 15
q1-8 n11
15-JUL-91 16:31:06

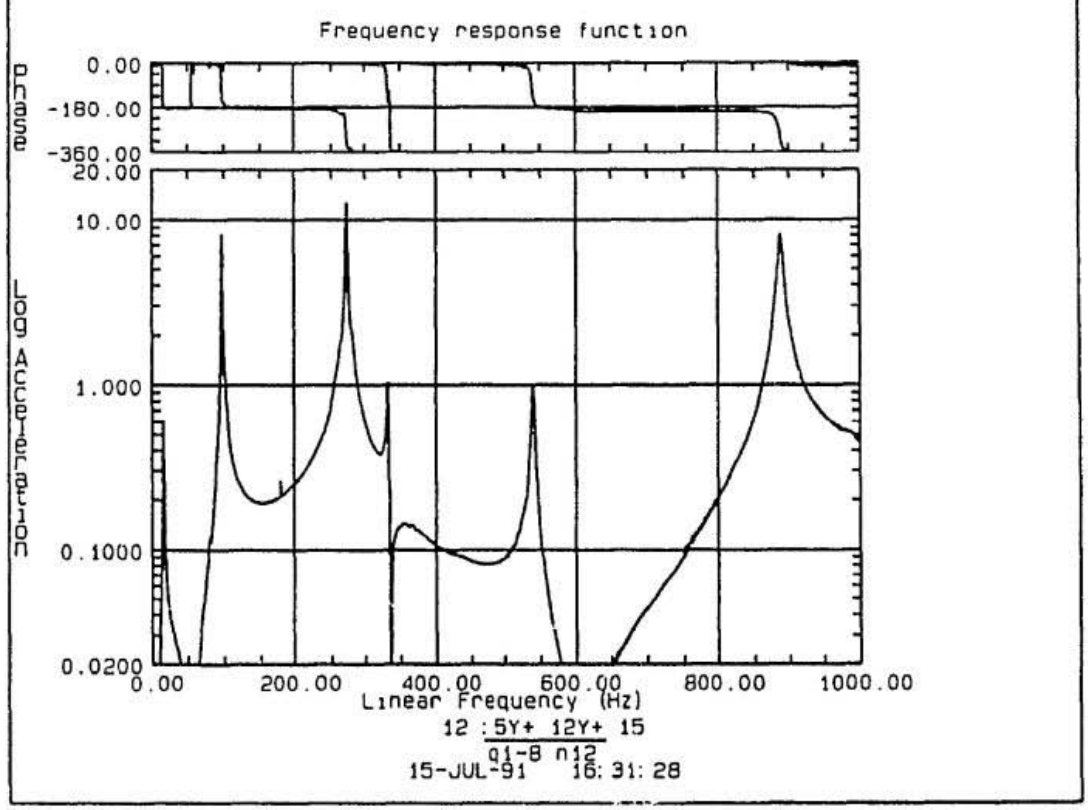
Frequency response function
Phase
0.00
-180.00
-360.00
Log Acceleration
20.00
10.00
1.000
0.1000
0.0200
0.00
200.00
400.00
600.00
800.00
1000.00
Linear Frequency (Hz)
12 :5Y+ 12Y+ 15
q1-8 n12
15-JUL-91 16:31:28

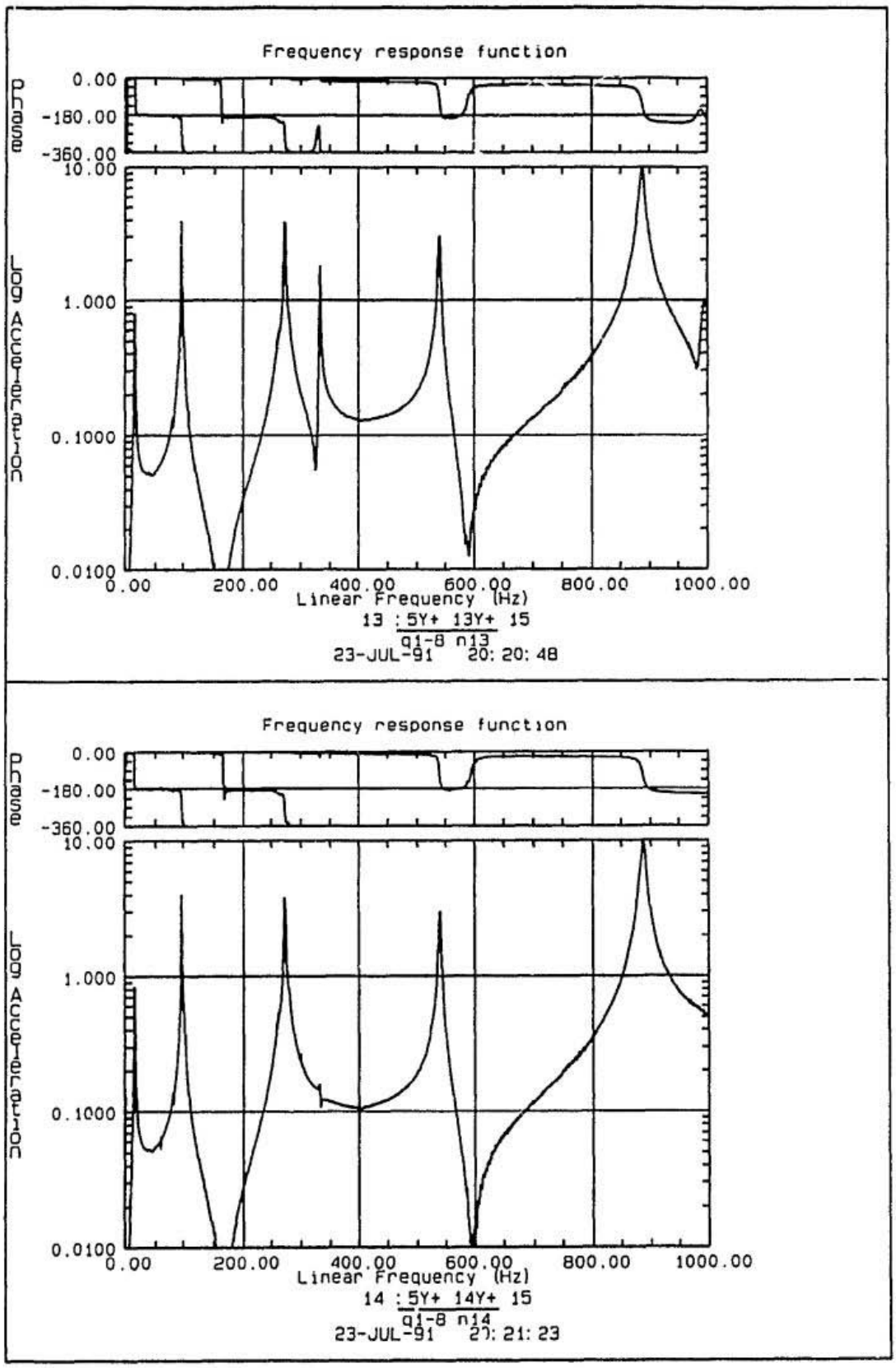
Frequency response function
Phase
0.00
-180.00
-360.00
Log Acceleration
10.00
1.000
0.1000
0.0100
0.00
200.00
400.00
600.00
800.00
1000.00
Linear Frequency (Hz)
13 : 5Y+ 13Y+ 15
q1-8 n13
23-JUL-91 20:20:48
Frequency response function
Phase
0.00
-180.00
-360.00
Log Acceleration
10.00
1.000
0.1000
0.0100
0.00
200.00
400.00
600.00
800.00
1000.00
Linear Frequency (Hz)
14 : 5Y+ 14Y+ 15
q1-8 n14
23-JUL-91 20:21:23

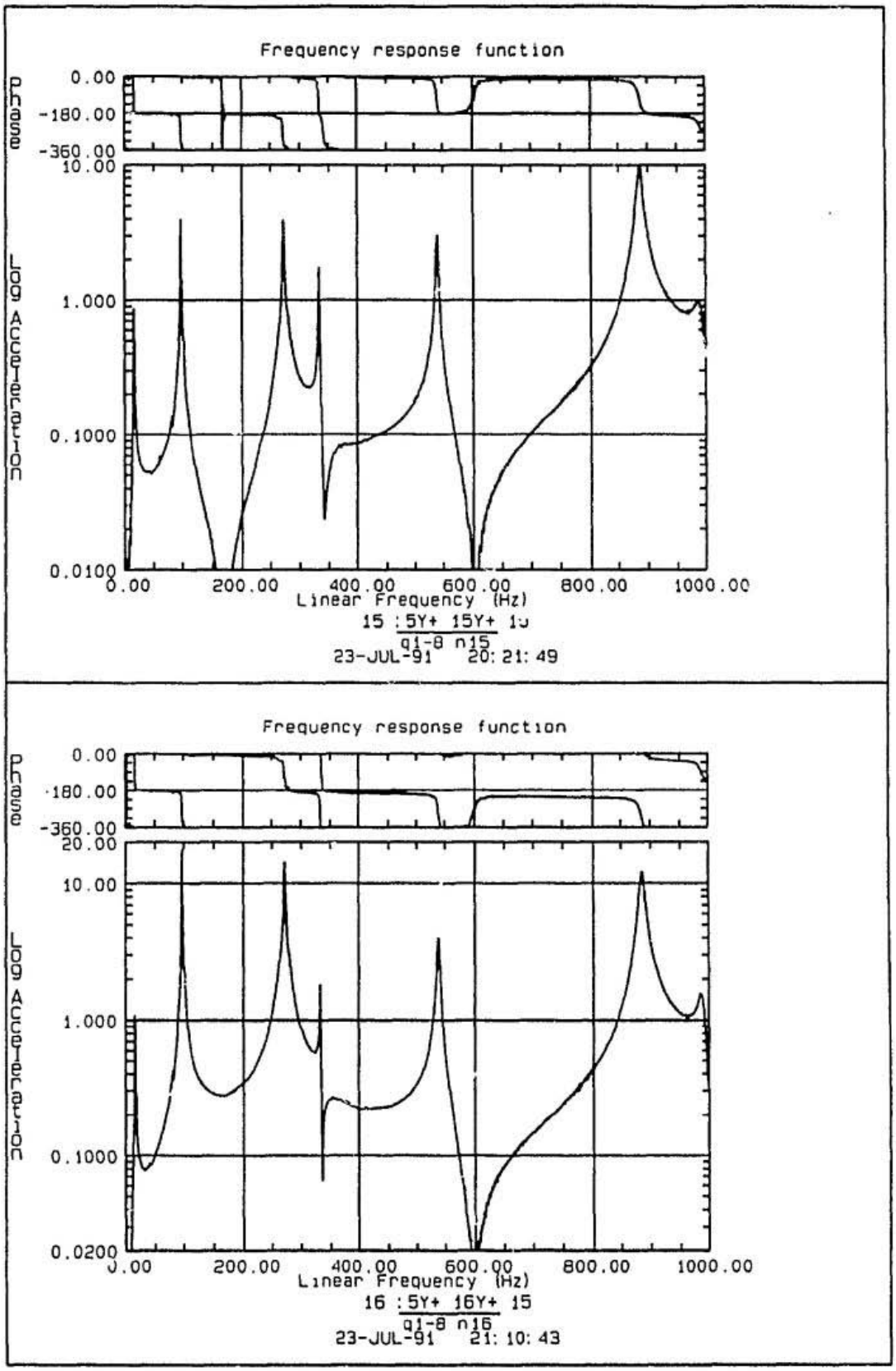
Frequency response function
Phase
0.00
-180.00
-360.00
Log Acceleration
10.00
1.000
0.1000
0.0100
0.00
200.00
400.00
600.00
800.00
1000.00
Linear Frequency (Hz)
15 :5Y+ 15Y+ 15
q1-8 n15
23-JUL-91 20:21:49
Frequency response function
Phase
0.00
-180.00
-360.00
Log Acceleration
20.00
10.00
1.000
0.1000
0.0200
0.00
200.00
400.00
600.00
800.00
1000.00
Linear Frequency (Hz)
16 :5Y+ 16Y+ 15
q1-8 n16
23-JUL-91 21:10:43

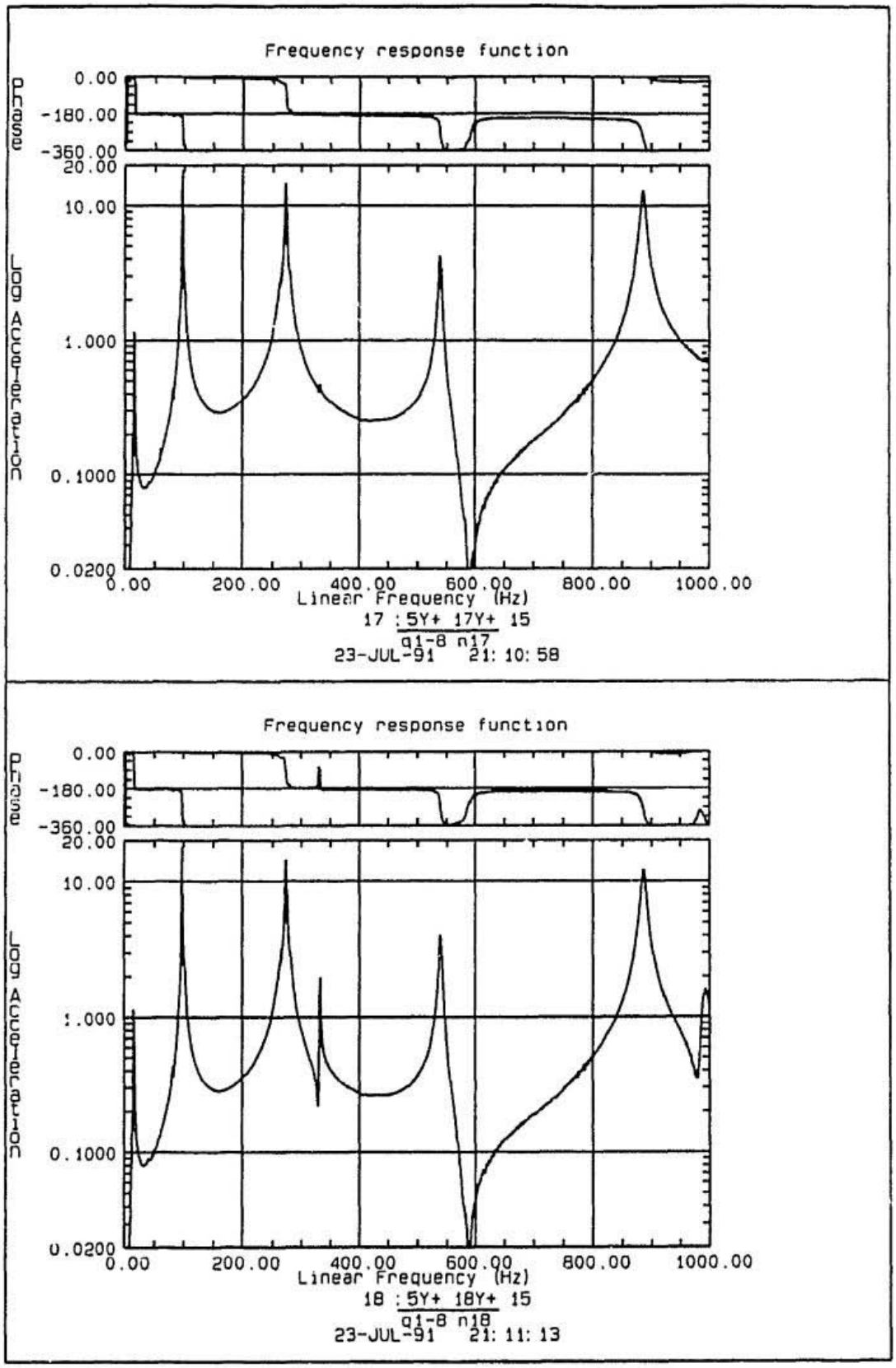
Frequency response function
Phase
0.00
-180.00
-360.00
Log Acceleration
20.00
10.00
1.000
0.1000
0.0200
0.00
200.00
400.00
600.00
800.00
1000.00
Linear Frequency (Hz)
17 : 5Y+ 17Y+ 15
a1-8 n17
23-JUL-91 21: 10: 58
Frequency response function
Phase
0.00
-180.00
-360.00
Log Acceleration
20.00
10.00
1.000
0.1000
0.0200
0.00
200.00
400.00
600.00
800.00
1000.00
Linear Frequency (Hz)
18 : 5Y+ 18Y+ 15
a1-8 n18
23-JUL-91 21: 11: 13

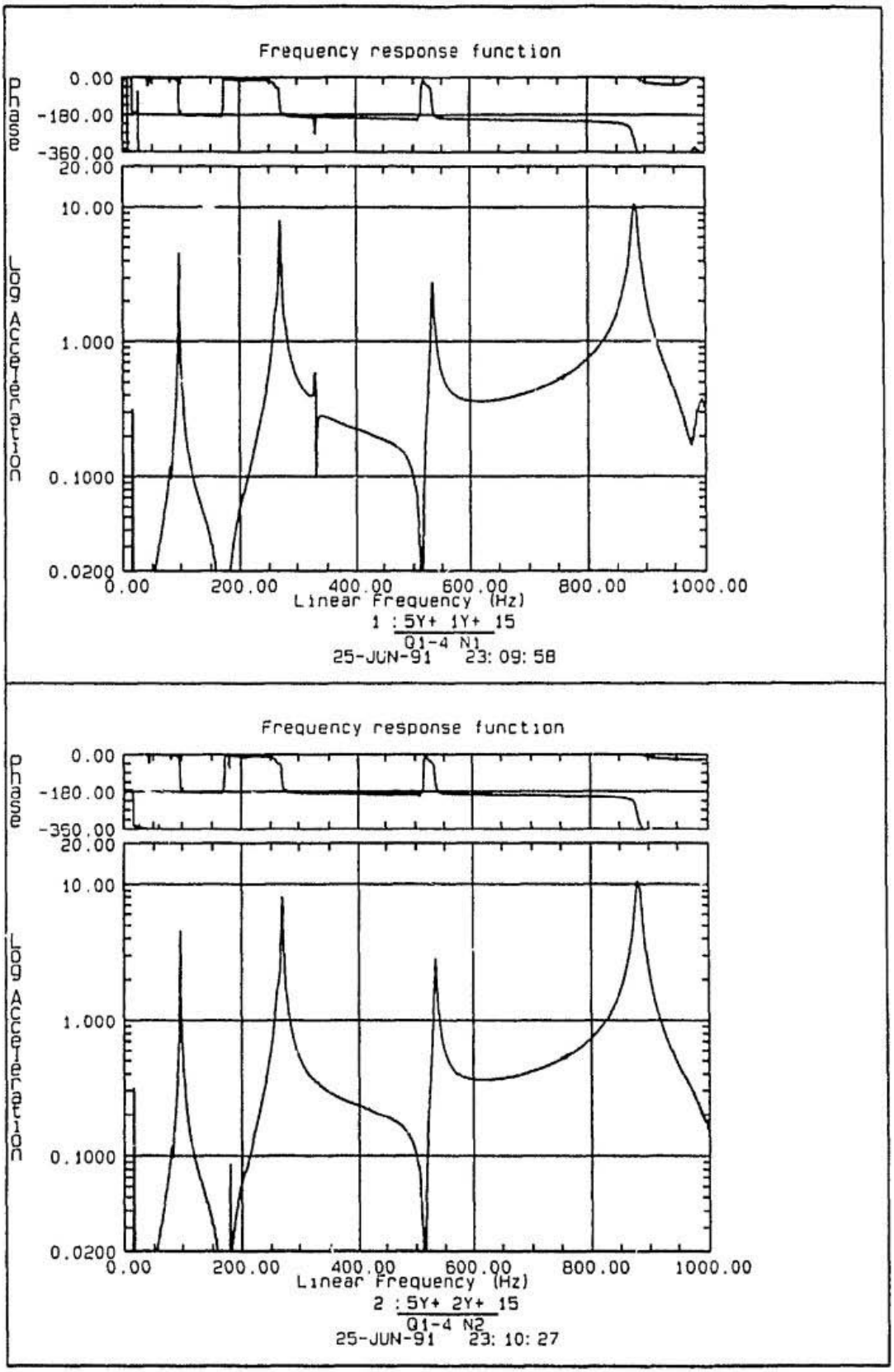
Frequency response function
Phase
0.00
-180.00
-360.00
Log Acceleration
20.00
10.00
1.000
0.1000
0.0200
0.00
200.00
400.00
600.00
800.00
1000.00
Linear Frequency (Hz)
1 : 5Y+ 1Y+ 15
Q1-4 N1
25-JUN-91 23:09:58
Frequency response function
Phase
0.00
-180.00
-350.00
Log Acceleration
20.00
10.00
1.000
0.1000
0.0200
0.00
200.00
400.00
600.00
800.00
1000.00
Linear Frequency (Hz)
2 : 5Y+ 2Y+ 15
Q1-4 N2
25-JUN-91 23:10:27

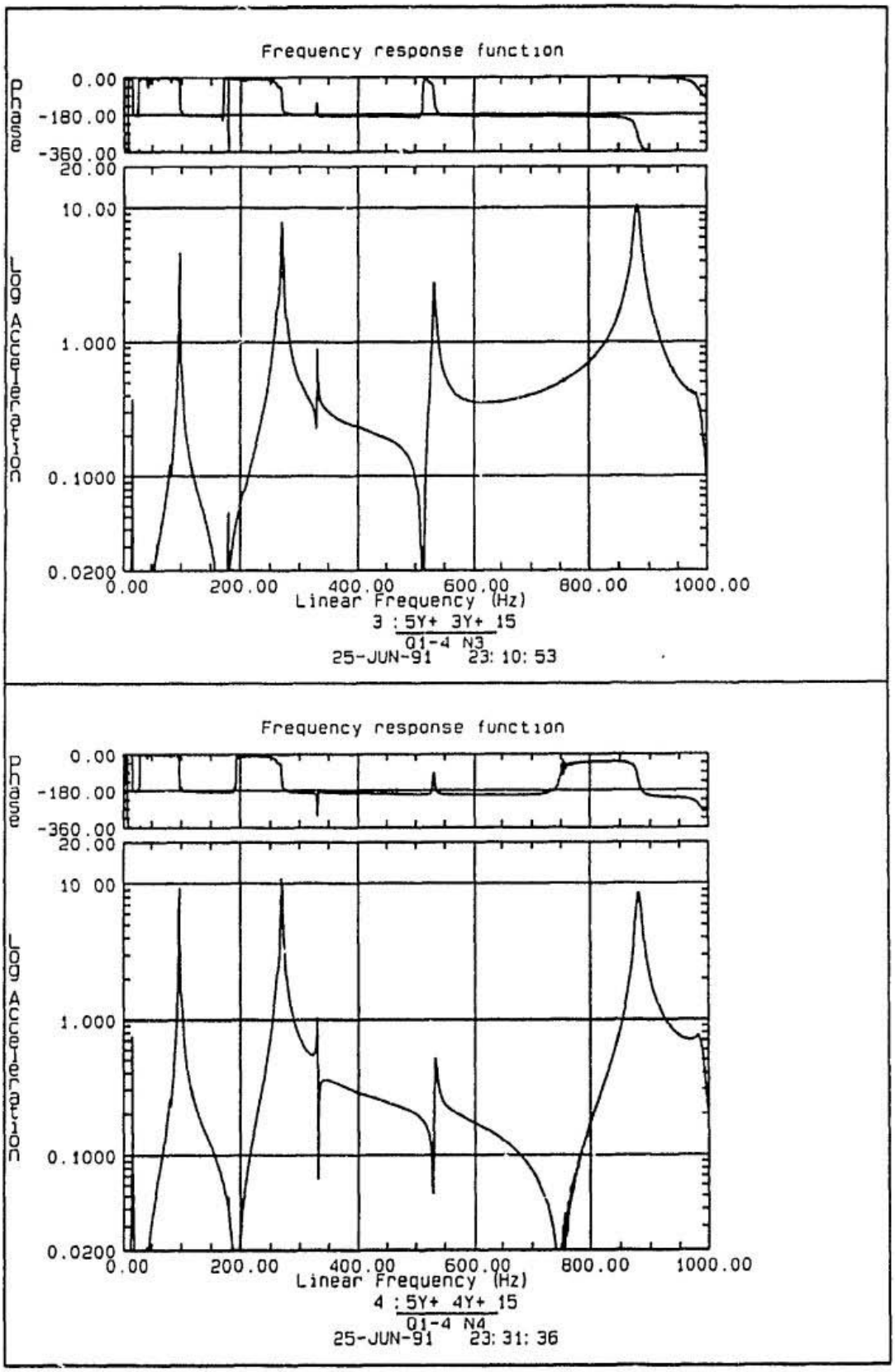
Frequency response function
Phase
0.00
-180.00
-360.00
Log Acceleration
20.00
10.00
1.000
0.1000
0.0200
0.00
200.00
400.00
600.00
800.00
1000.00
Linear Frequency (Hz)
3 : 5Y+ 3Y+ 15
Q1-4 N3
25-JUN-91 23: 10: 53
Frequency response function
Phase
0.00
-180.00
-360.00
Log Acceleration
20.00
10 00
1.000
0.1000
0.0200
0.00
200.00
400.00
600.00
800.00
1000.00
Linear Frequency (Hz)
4 : 5Y+ 4Y+ 15
Q1-4 N4
25-JUN-91 23: 31: 36

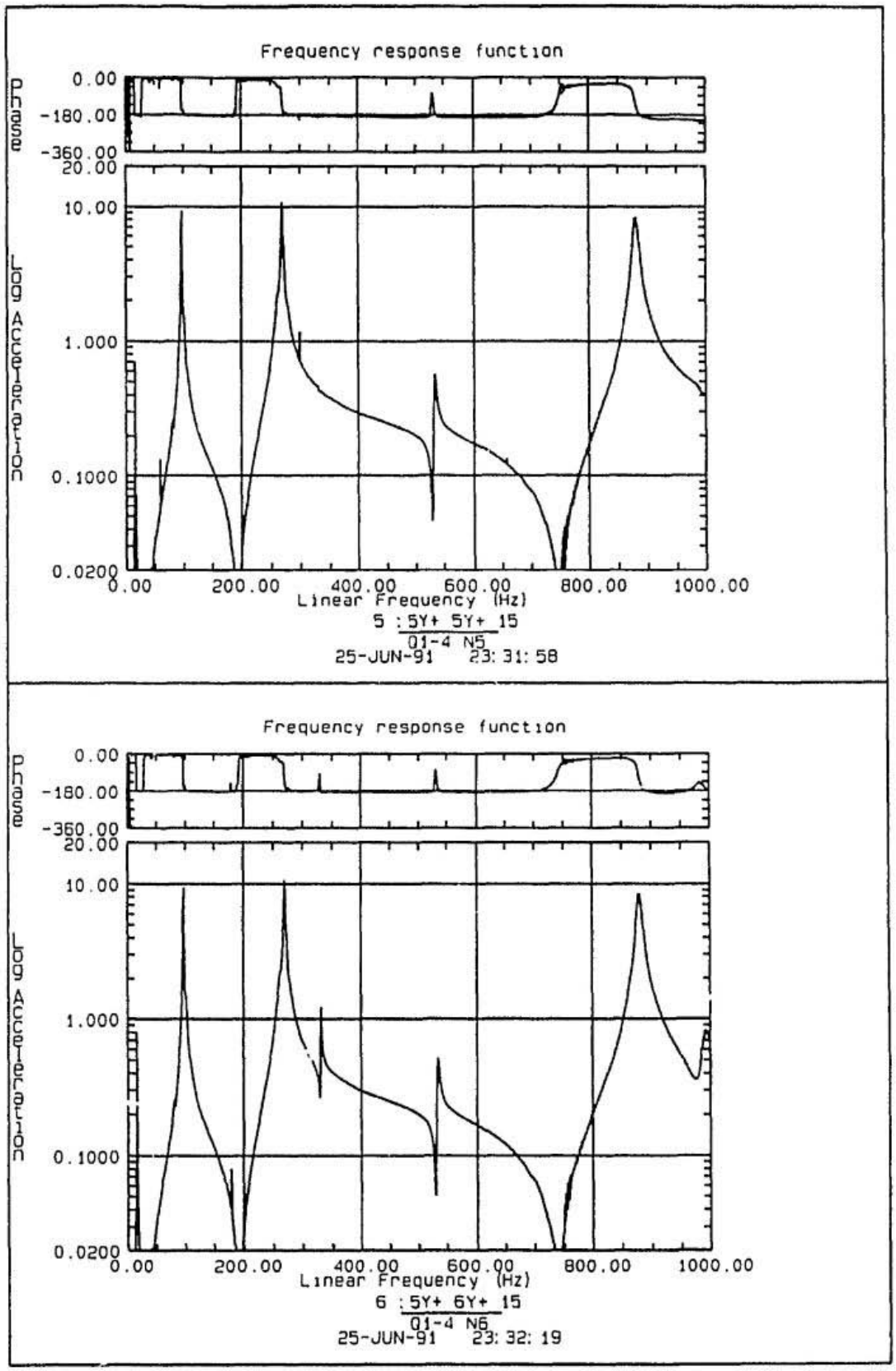
Frequency response function
Phase
0.00
-180.00
-360.00
Log Acceleration
20.00
10.00
1.000
0.1000
0.0200
0.00
200.00
400.00
600.00
800.00
1000.00
Linear Frequency (Hz)
5 :5Y+ 5Y+ 15
Q1-4 N5
25-JUN-91 23:31:58
Frequency response function
Phase
0.00
-180.00
-360.00
Log Acceleration
20.00
10.00
1.000
0.1000
0.0200
0.00
200.00
400.00
600.00
800.00
1000.00
Linear Frequency (Hz)
6 :5Y+ 6Y+ 15
Q1-4 N6
25-JUN-91 23:32:19

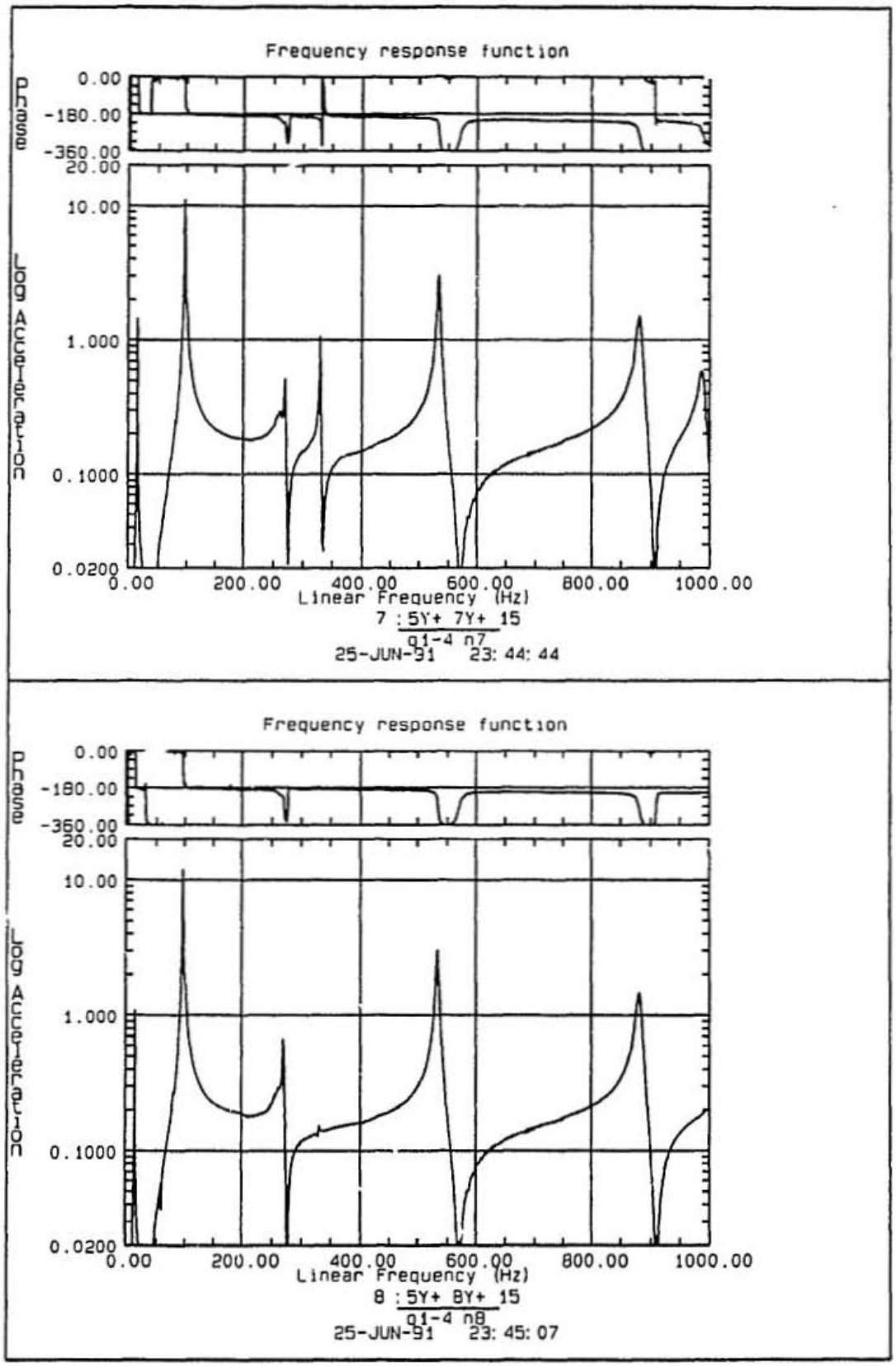
Frequency response function
Phase
0.00
-180.00
-360.00
Log Acceleration
20.00
10.00
1.000
0.1000
0.0200
0.00
200.00
400.00
600.00
800.00
1000.00
Linear Frequency (Hz)
7 :5Y+ 7Y+ 15
q1-4 n7
25-JUN-91 23: 44: 44
Frequency response function
Phase
0.00
-180.00
-360.00
Log Acceleration
20.00
10.00
1.000
0.1000
0.0200
0.00
200.00
400.00
600.00
800.00
1000.00
Linear Frequency (Hz)
8 :5Y+ 8Y+ 15
q1-4 n8
25-JUN-91 23: 45: 07

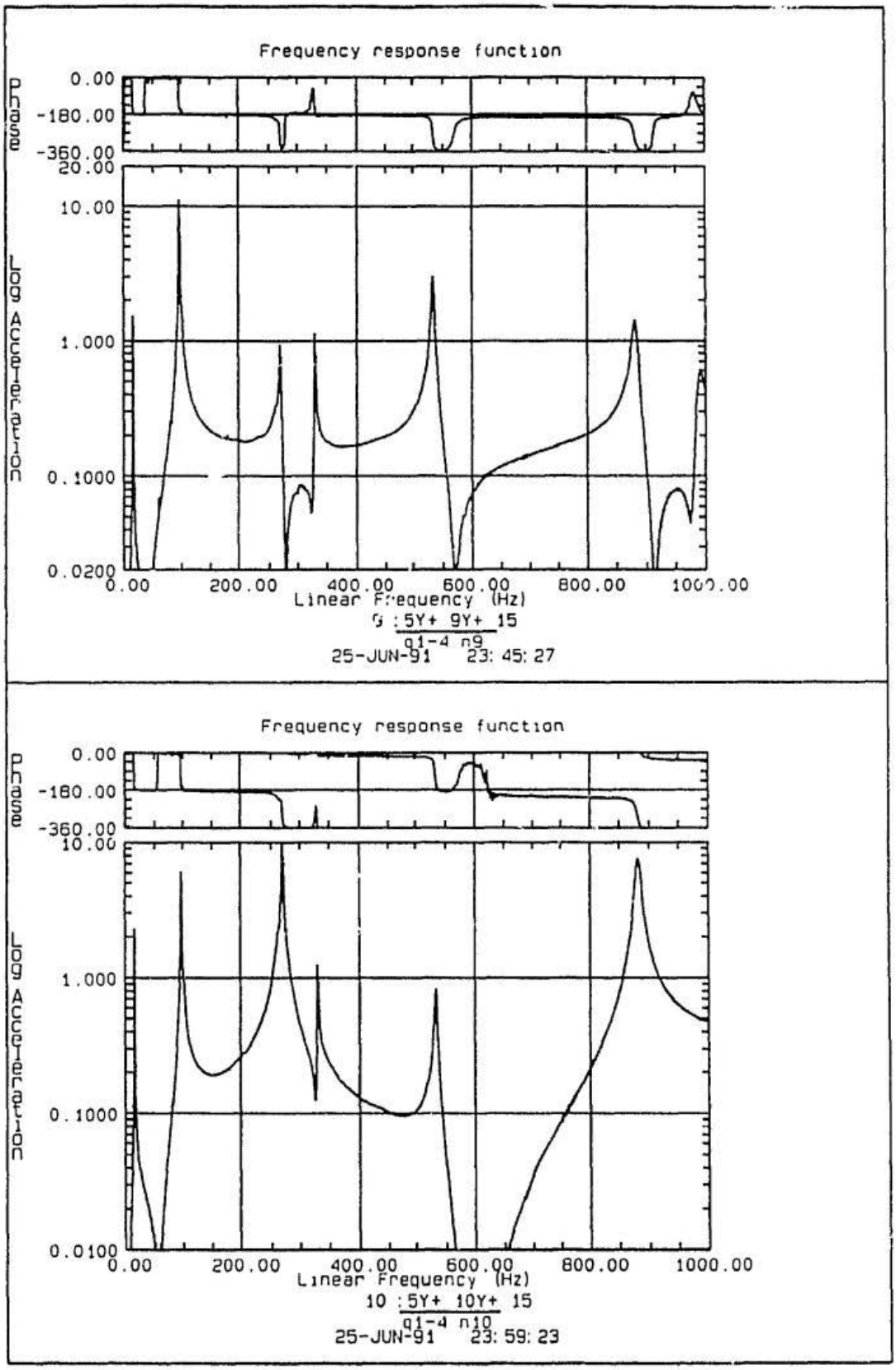
Frequency response function
Phase
0.00
-180.00
-360.00
Log Acceleration
20.00
10.00
1.000
0.1000
0.0200
0.00
200.00
400.00
600.00
800.00
1000.00
Linear Frequency (Hz)
9 :5Y+ 9Y+ 15
q1-4 n9
25-JUN-91 23:45:27
Frequency response function
Phase
0.00
-180.00
-360.00
Log Acceleration
10.00
1.000
0.1000
0.0100
0.00
200.00
400.00
600.00
800.00
1000.00
Linear Frequency (Hz)
10 :5Y+ 10Y+ 15
q1-4 n10
25-JUN-91 23:59:23

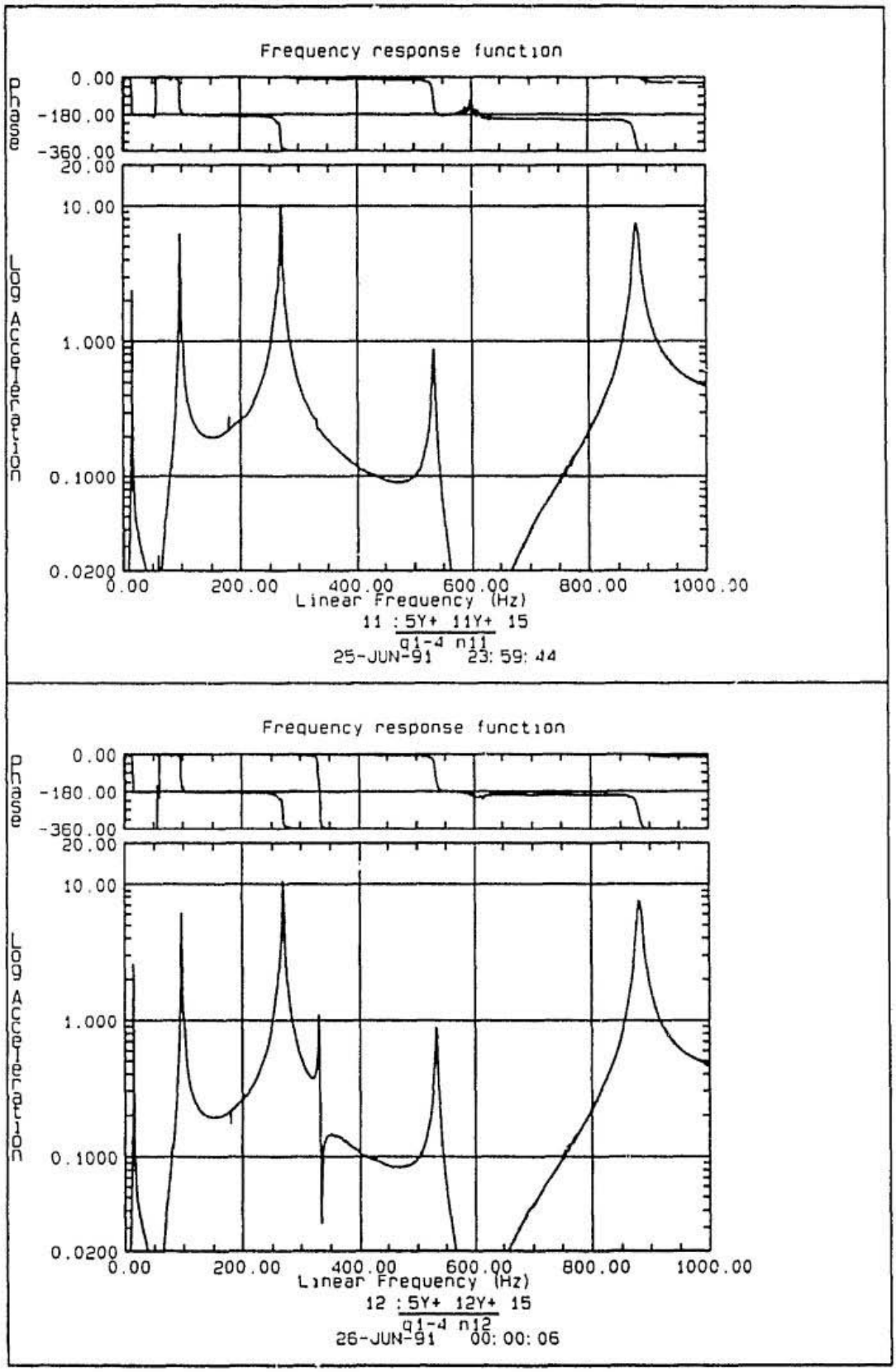
Frequency response function
Phase
0.00
-180.00
-360.00
Log Acceleration
20.00
10.00
1.000
0.1000
0.0200
0.00
200.00
400.00
600.00
800.00
1000.00
Linear Frequency (Hz)
11 : 5Y+ 11Y+ 15
q1-4 n11
25-JUN-91 23:59:44
Frequency response function
Phase
0.00
-180.00
-360.00
Log Acceleration
20.00
10.00
1.000
0.1000
0.0200
0.00
200.00
400.00
600.00
800.00
1000.00
Linear Frequency (Hz)
12 : 5Y+ 12Y+ 15
q1-4 n12
26-JUN-91 00:00:06

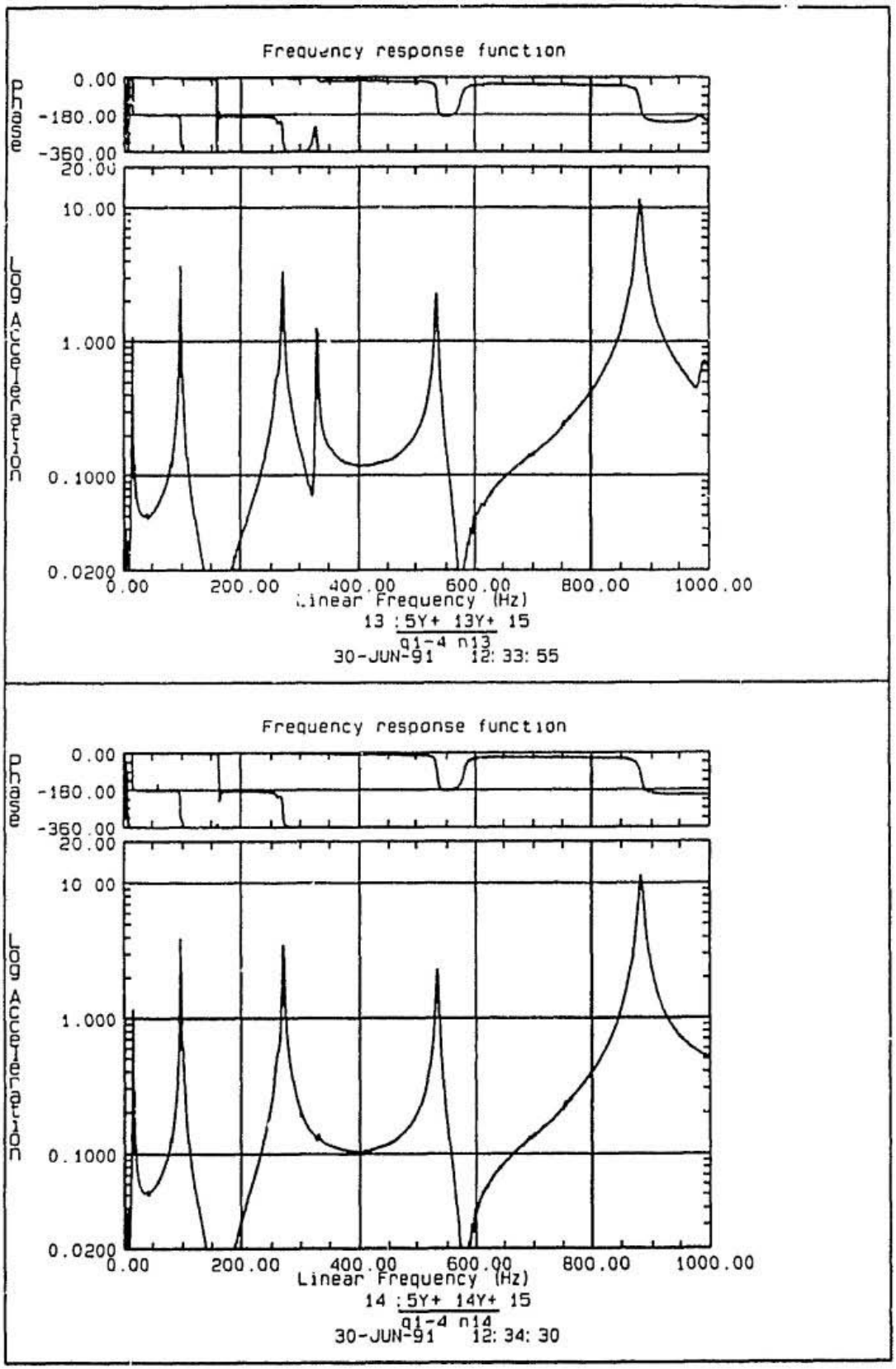
Frequency response function
Phase
0.00
-180.00
-360.00
Log Acceleration
20.00
10.00
1.000
0.1000
0.0200
0.00
200.00
400.00
600.00
800.00
1000.00
Linear Frequency (Hz)
13 :5Y+ 13Y+ 15
q1-4 n13
30-JUN-91 12:33:55
Frequency response function
Phase
0.00
-180.00
-360.00
Log Acceleration
20.00
10.00
1.000
0.1000
0.0200
0.00
200.00
400.00
600.00
800.00
1000.00
Linear Frequency (Hz)
14 :5Y+ 14Y+ 15
q1-4 n14
30-JUN-91 12:34:30

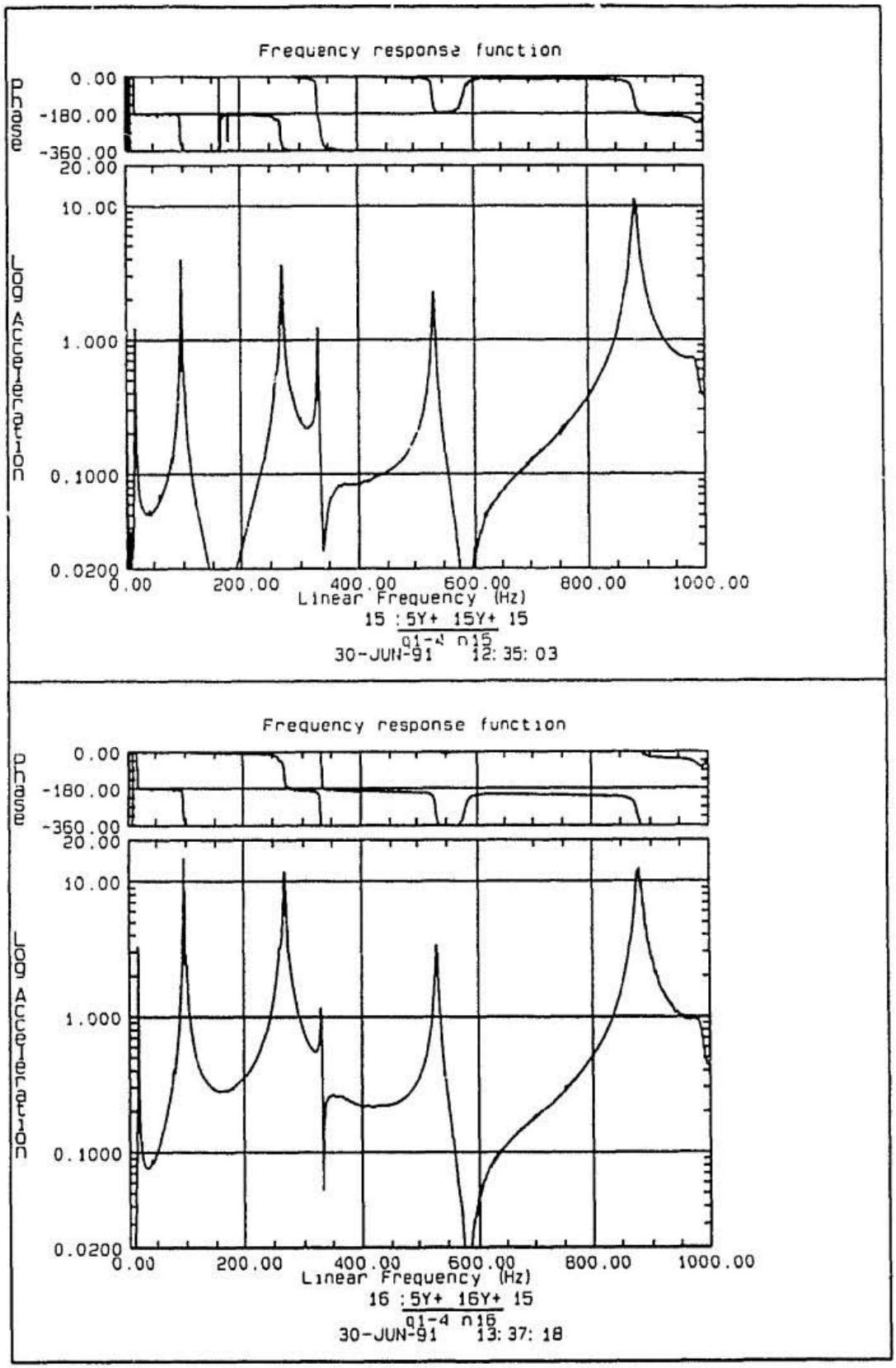
Frequency response function
Phase
0.00
-180.00
-360.00
Log Acceleration
20.00
10.00
1.000
0.1000
0.0200
0.00
200.00
400.00
600.00
800.00
1000.00
Linear Frequency (Hz)
15 :5Y+ 15Y+ 15
01-4 n15
30-JUN-91 12:35:03
Frequency response function
Phase
0.00
-180.00
-360.00
Log Acceleration
20.00
10.00
1.000
0.1000
0.0200
0.00
200.00
400.00
600.00
800.00
1000.00
Linear Frequency (Hz)
16 :5Y+ 16Y+ 15
01-4 n16
30-JUN-91 13:37:18

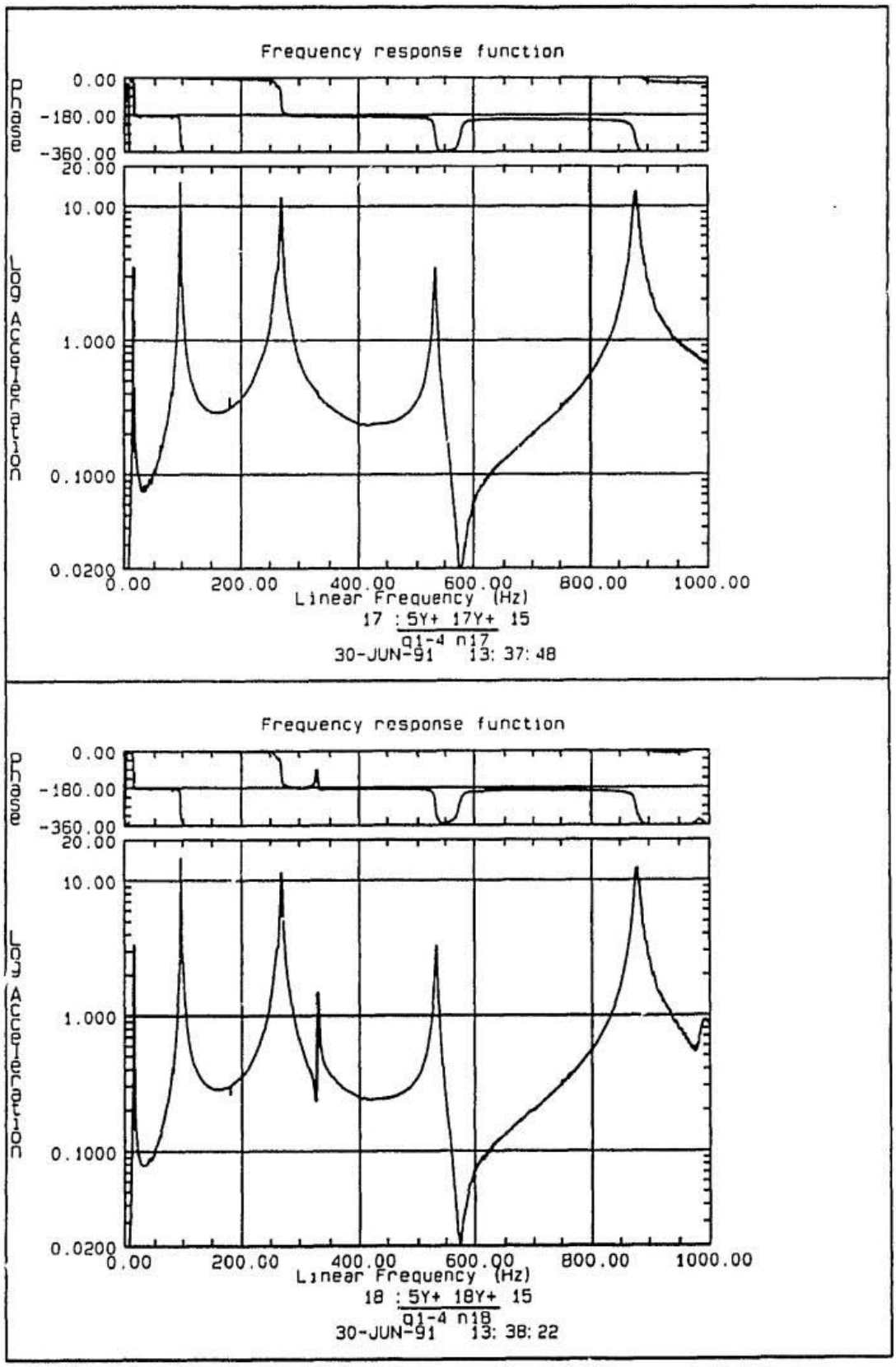
Frequency response function
Phase
0.00
-180.00
-360.00
Log Acceleration
20.00
10.00
1.000
0.1000
0.0200
0.00
200.00
400.00
600.00
800.00
1000.00
Linear Frequency (Hz)
17 : 5Y+ 17Y+ 15
q1-4 n17
30-JUN-91 13: 37: 48
Frequency response function
Phase
0.00
-180.00
-360.00
Log Acceleration
20.00
10.00
1.000
0.1000
0.0200
0.00
200.00
400.00
600.00
800.00
1000.00
Linear Frequency (Hz)
18 : 5Y+ 18Y+ 15
q1-4 n18
30-JUN-91 13: 38: 22

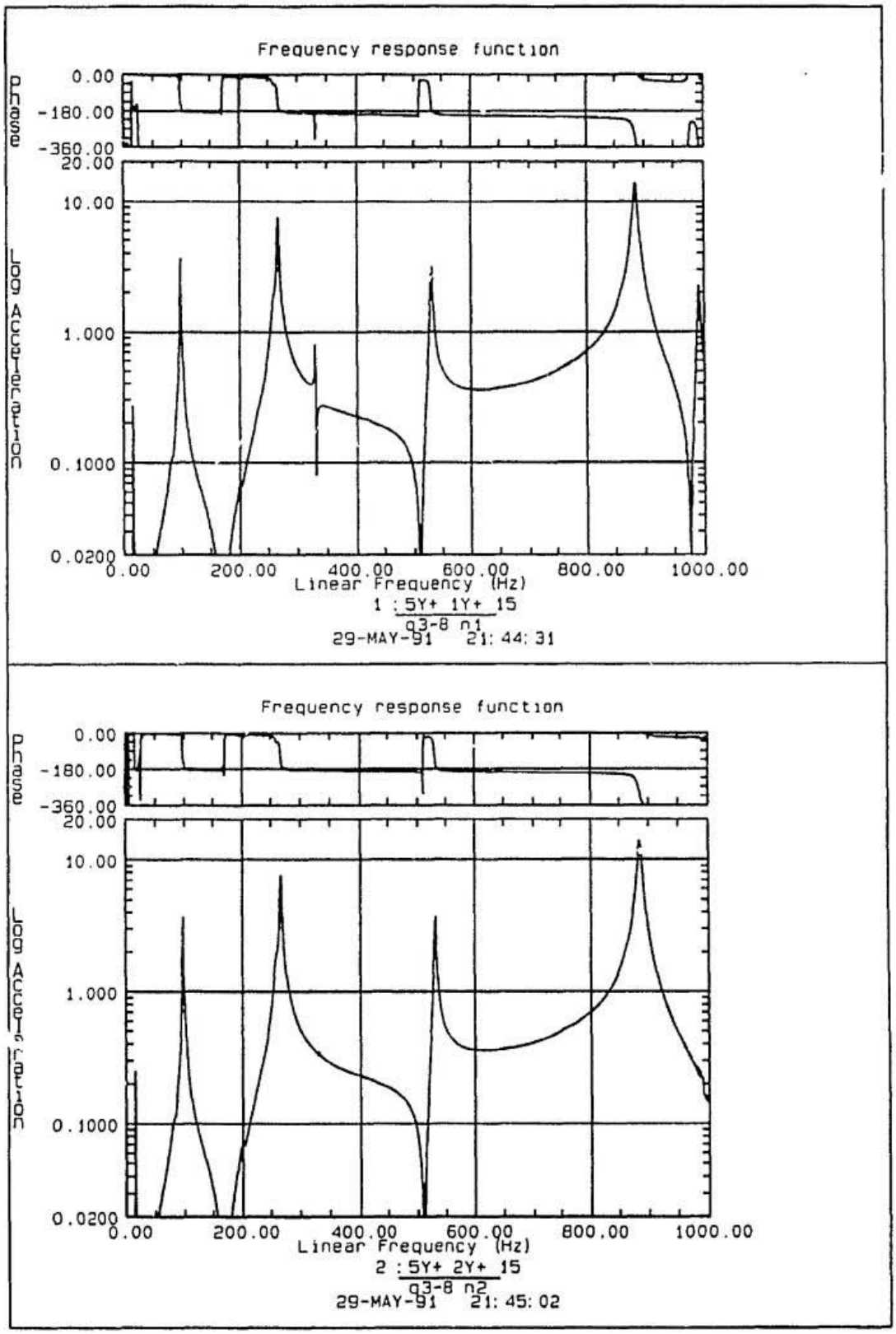
Frequency response function
Phase
0.00
-180.00
-360.00
Log Acceleration
20.00
10.00
1.000
0.1000
0.0200
0.00
200.00
400.00
600.00
800.00
1000.00
Linear Frequency (Hz)
1 : 5Y+ 1Y+ 15
q3-8 n1
29-MAY-91 21: 44: 31
Frequency response function
Phase
0.00
-180.00
-360.00
Log Acceleration
20.00
10.00
1.000
0.1000
0.0200
0.00
200.00
400.00
600.00
800.00
1000.00
Linear Frequency (Hz)
2 : 5Y+ 2Y+ 15
q3-8 n2
29-MAY-91 21: 45: 02

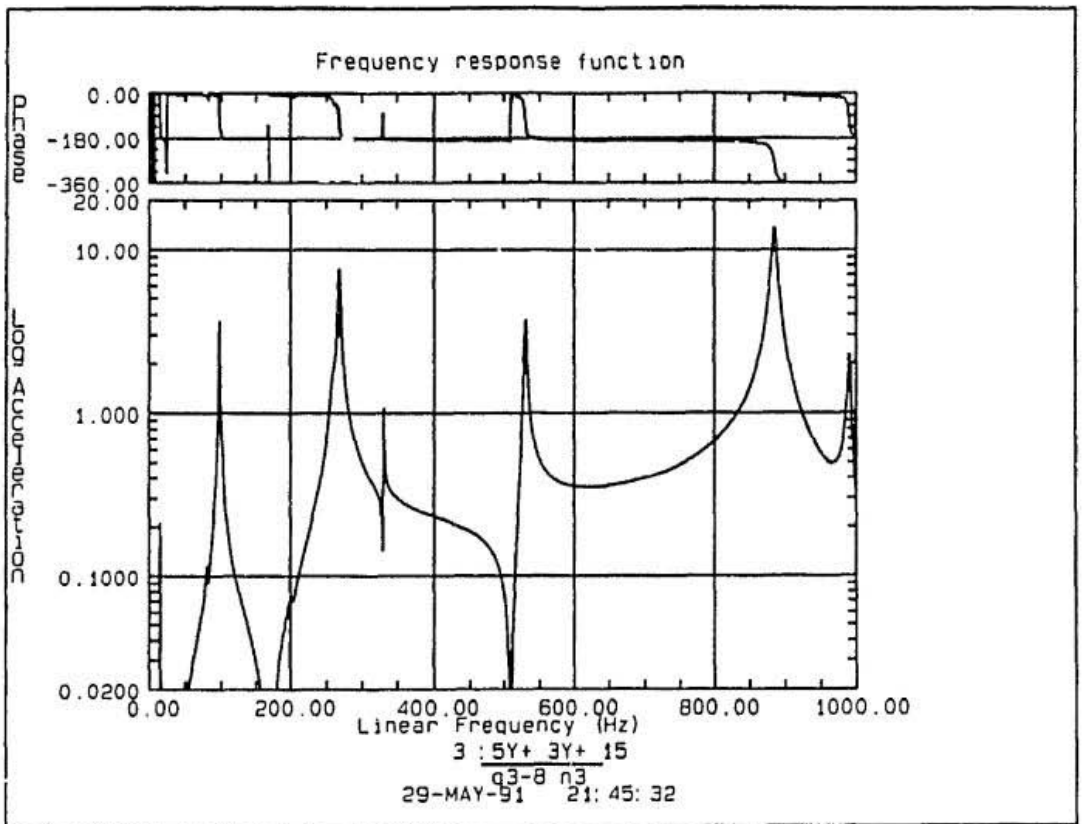
Frequency response function
Phase
0.00
-180.00
-360.00
Log Acceleration
20.00
10.00
1.000
0.1000
0.0200
0.00
200.00
400.00
600.00
800.00
1000.00
Linear Frequency (Hz)
3 :5Y+ 3Y+ 15
q3-8 n3
29-MAY-91 21:45:32

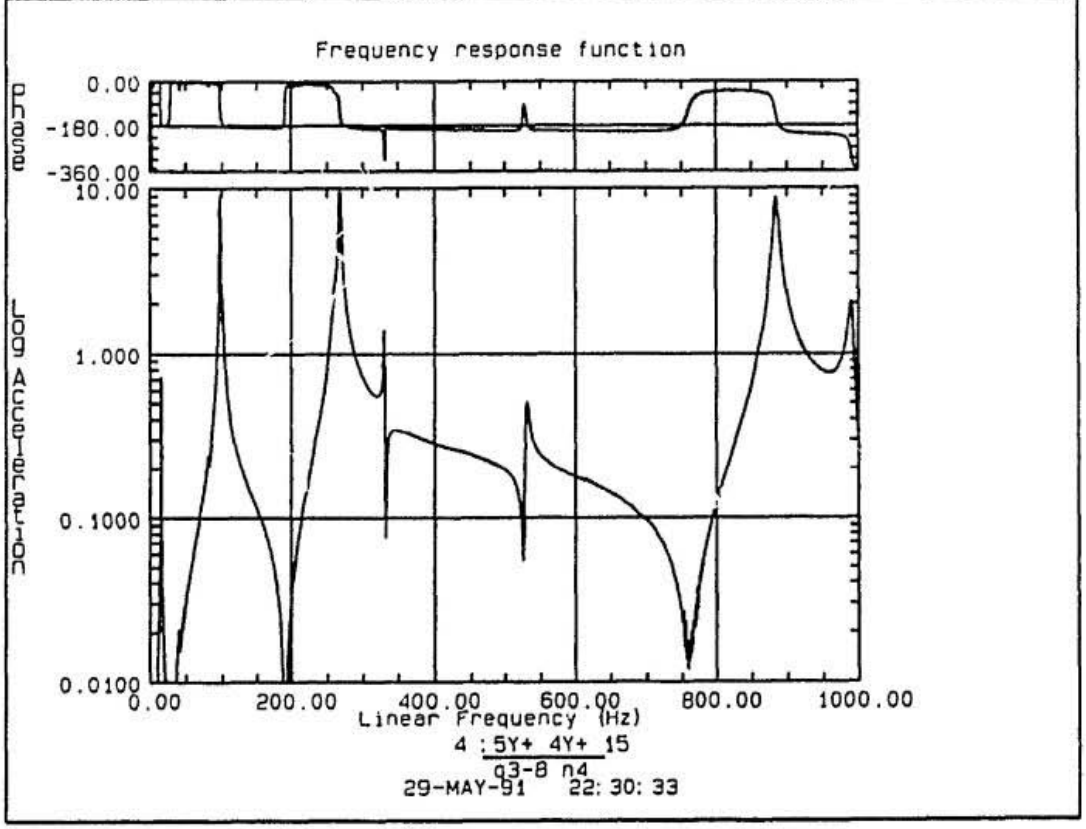
Frequency response function
Phase
0.00
-180.00
-360.00
Log Acceleration
10.00
1.000
0.1000
0.0100
0.00
200.00
400.00
600.00
800.00
1000.00
Linear Frequency (Hz)
4 :5Y+ 4Y+ 15
q3-8 n4
29-MAY-91 22:30:33

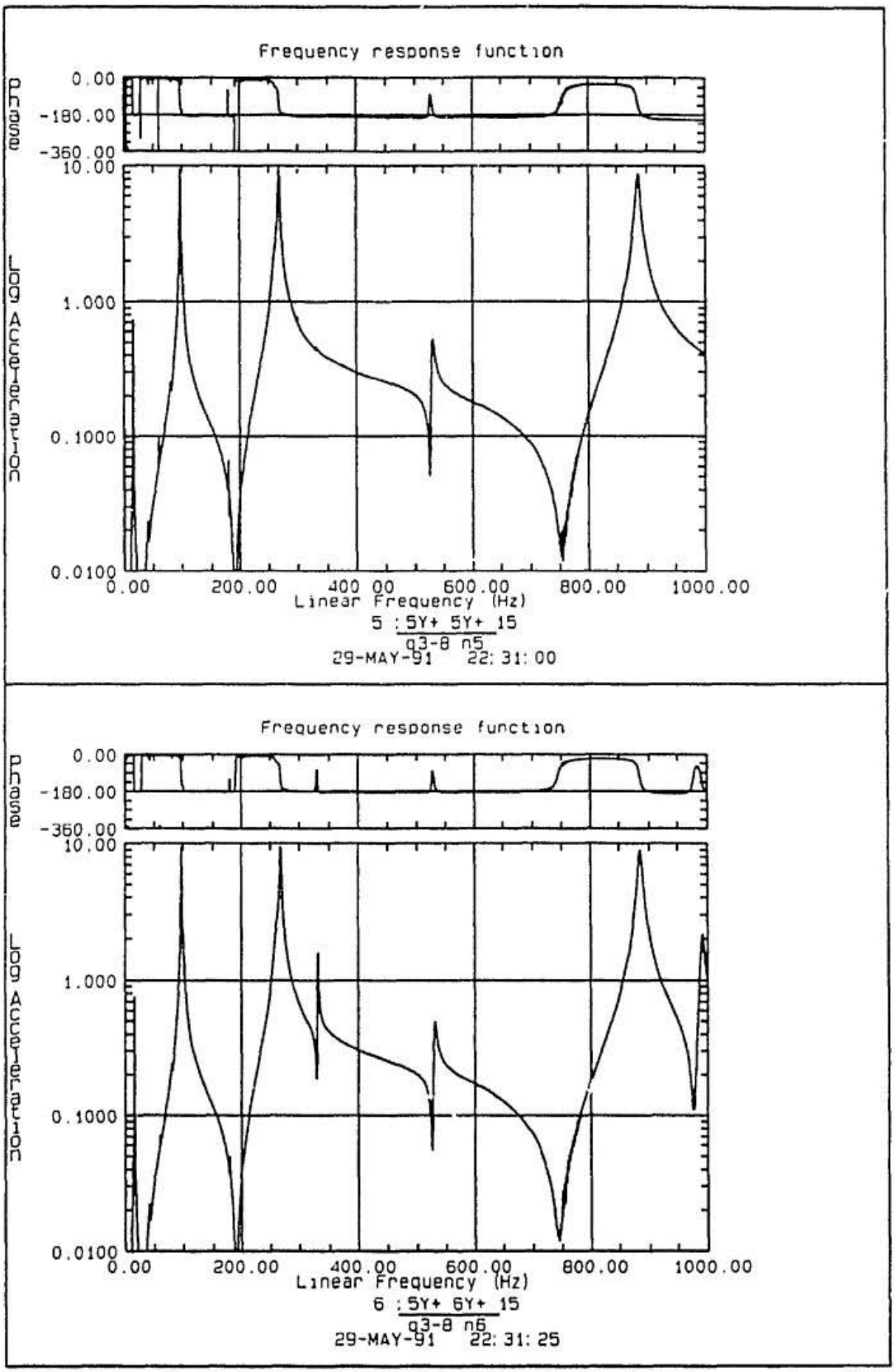
Frequency response function
Phase
0.00
-180.00
-360.00
Log Acceleration
10.00
1.000
0.1000
0.0100
0.00
200.00
400.00
600.00
800.00
1000.00
Linear Frequency (Hz)
5 : 5Y+ 5Y+ 15
q3-8 n5
29-MAY-91 22:31:00
Frequency response function
Phase
0.00
-180.00
-360.00
Log Acceleration
10.00
1.000
0.1000
0.0100
0.00
200.00
400.00
600.00
800.00
1000.00
Linear Frequency (Hz)
6 : 5Y+ 6Y+ 15
q3-8 n6
29-MAY-91 22:31:25

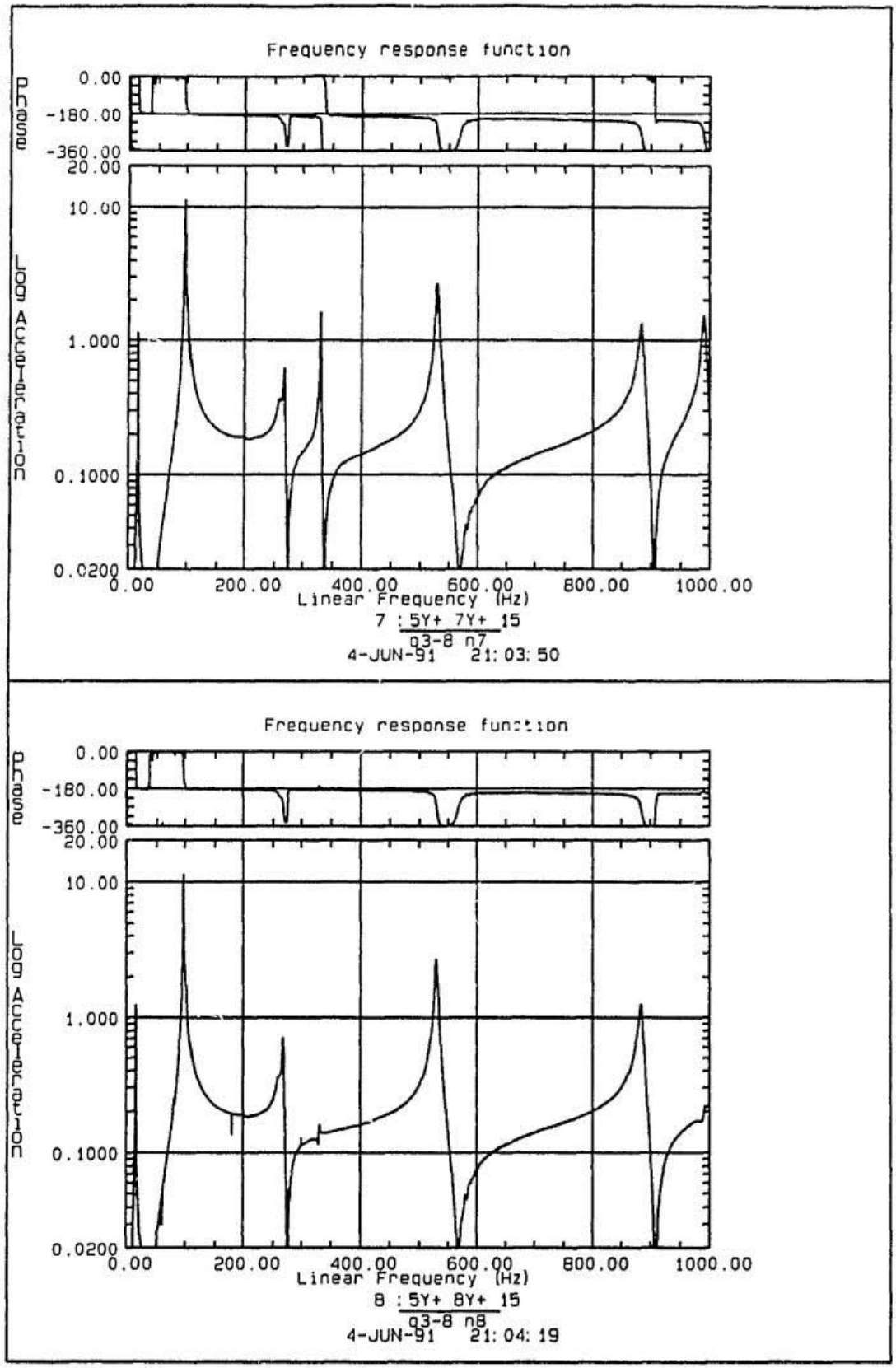
Frequency response function
Phase
0.00
-180.00
-360.00
Log Acceleration
20.00
10.00
1.000
0.1000
0.0200
0.00
200.00
400.00
600.00
800.00
1000.00
Linear Frequency (Hz)
7 : 5Y+ 7Y+ 15
q3-8 n7
4-JUN-91 21:03:50
Frequency response function
Phase
0.00
-180.00
-360.00
Log Acceleration
20.00
10.00
1.000
0.1000
0.0200
0.00
200.00
400.00
600.00
800.00
1000.00
Linear Frequency (Hz)
8 : 5Y+ 8Y+ 15
q3-8 n8
4-JUN-91 21:04:19

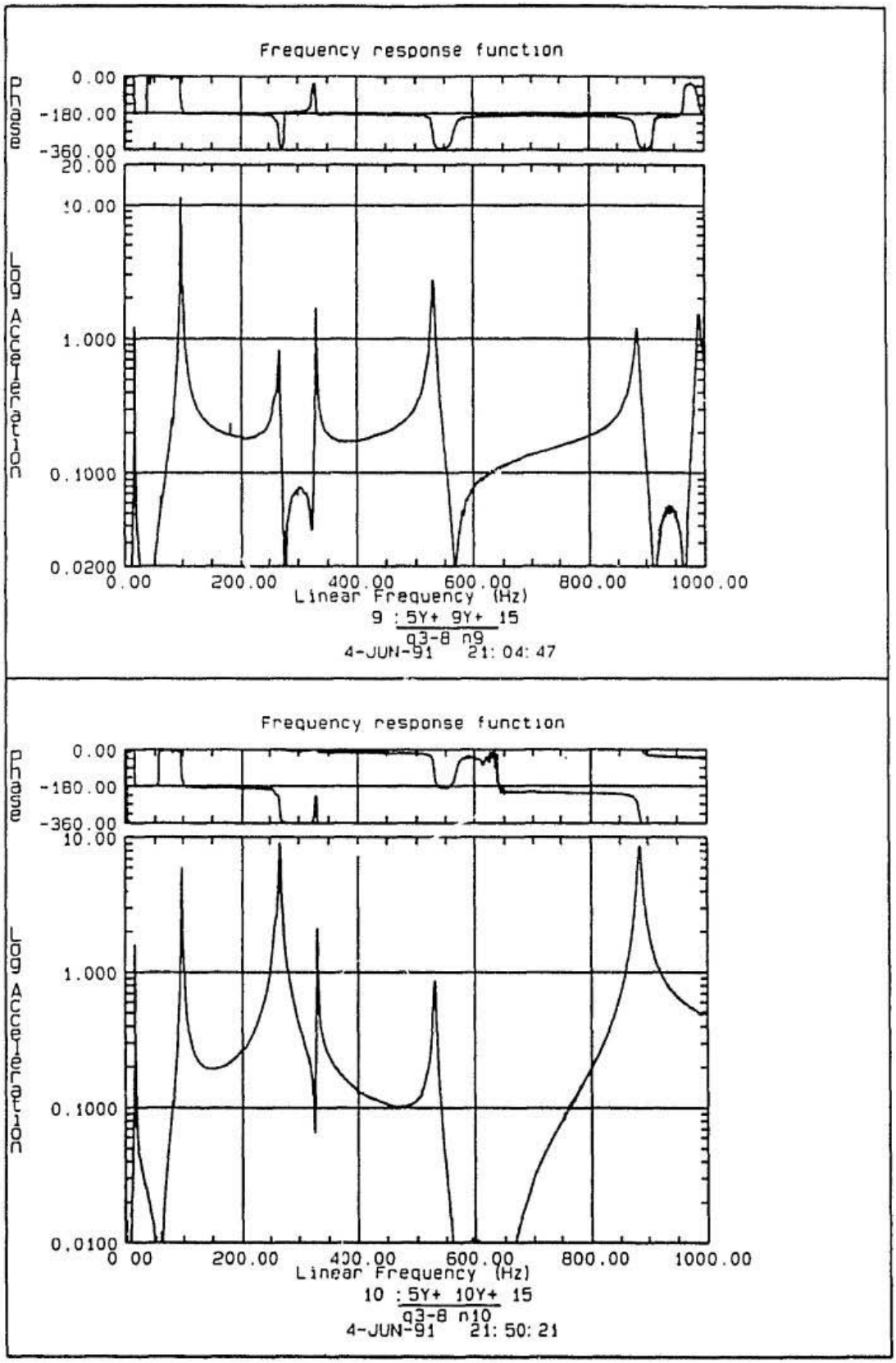
Frequency response function
Phase
0.00
-180.00
-360.00
Log Acceleration
20.00
10.00
1.000
0.1000
0.0200
0.00
200.00
400.00
600.00
800.00
1000.00
Linear Frequency (Hz)
9 : 5Y+ 9Y+ 15
q3-8 n9
4-JUN-91 21:04:47
Frequency response function
Phase
0.00
-180.00
-360.00
Log Acceleration
10.00
1.000
0.1000
0.0100
0.00
200.00
400.00
600.00
800.00
1000.00
Linear Frequency (Hz)
10 : 5Y+ 10Y+ 15
q3-8 n10
4-JUN-91 21:50:21

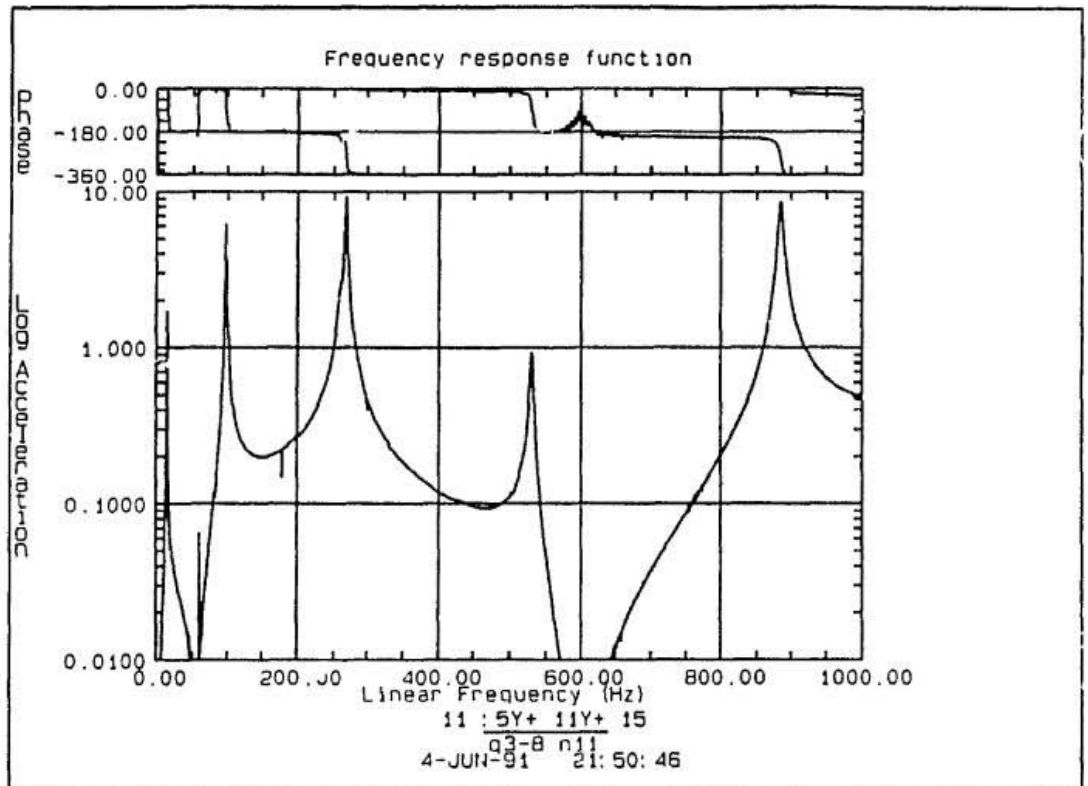
Frequency response function
Phase
0.00
-180.00
-360.00
Log Acceleration
10.00
1.000
0.1000
0.0100
0.00
200.00
400.00
600.00
800.00
1000.00
Linear Frequency (Hz)
11 : 5Y+ 11Y+ 15
q3-8 n11
4-JUN-91 21:50:46

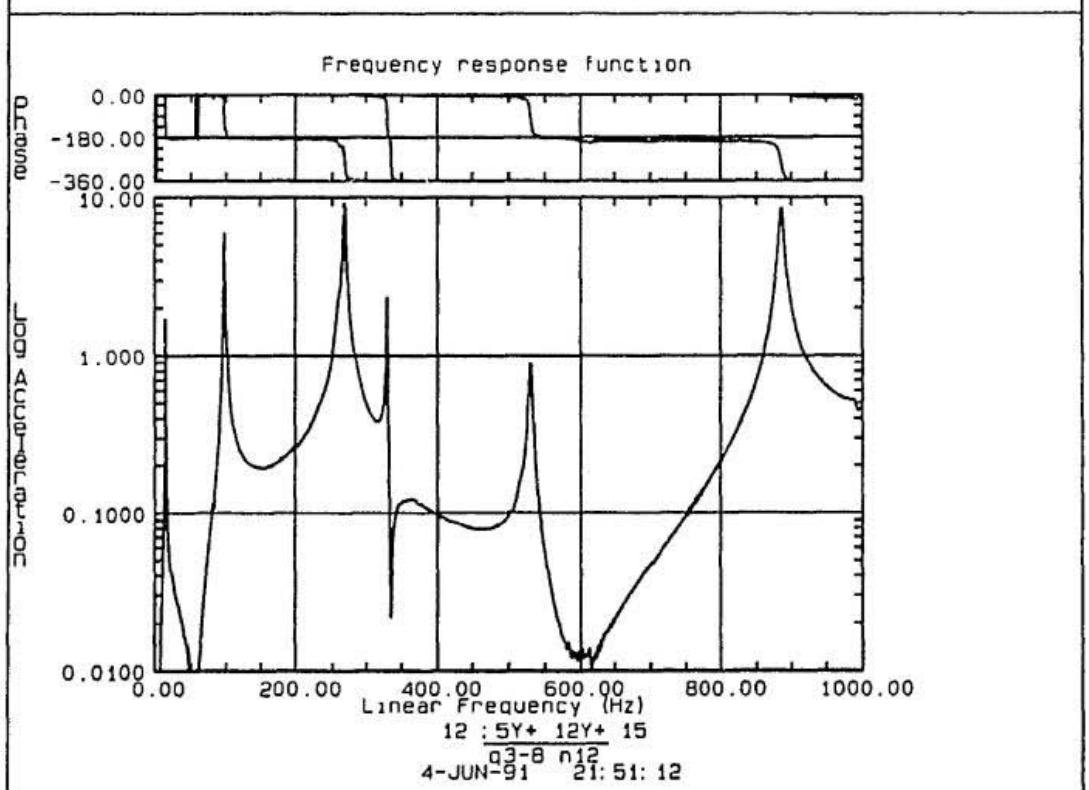
Frequency response function
Phase
0.00
-180.00
-360.00
Log Acceleration
10.00
1.000
0.1000
0.0100
0.00
200.00
400.00
600.00
800.00
1000.00
Linear Frequency (Hz)
12 : 5Y+ 12Y+ 15
q3-8 n12
4-JUN-91 21:51:12

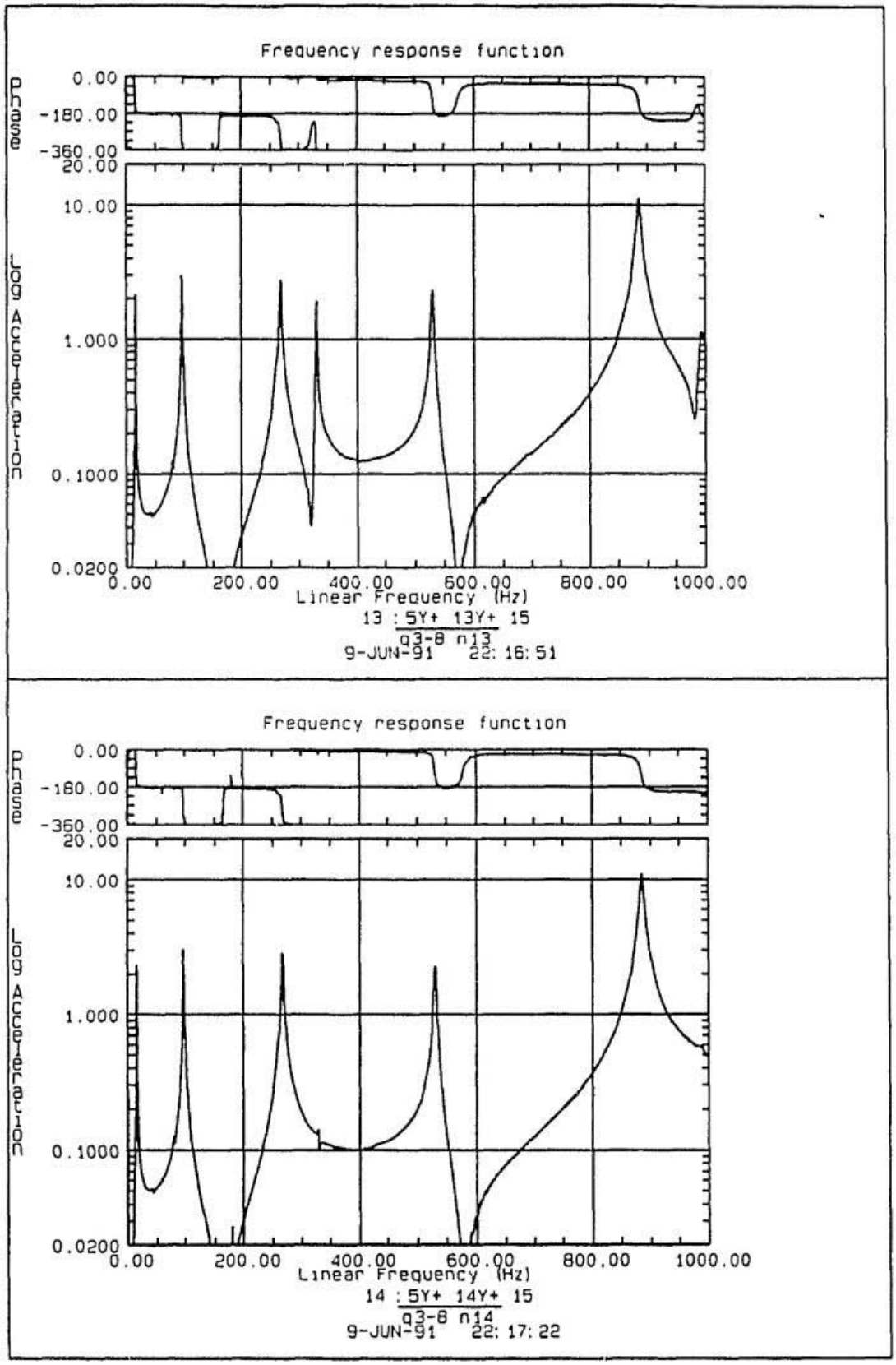
Frequency response function
Phase
0.00
-180.00
-360.00
Log Acceleration
20.00
10.00
1.000
0.1000
0.0200
0.00
200.00
400.00
600.00
800.00
1000.00
Linear Frequency (Hz)
13 : 5Y+ 13Y+ 15
q3-8 n13
9-JUN-91 22:16:51
Frequency response function
Phase
0.00
-180.00
-360.00
Log Acceleration
20.00
10.00
1.000
0.1000
0.0200
0.00
200.00
400.00
600.00
800.00
1000.00
Linear Frequency (Hz)
14 : 5Y+ 14Y+ 15
q3-8 n14
9-JUN-91 22:17:22

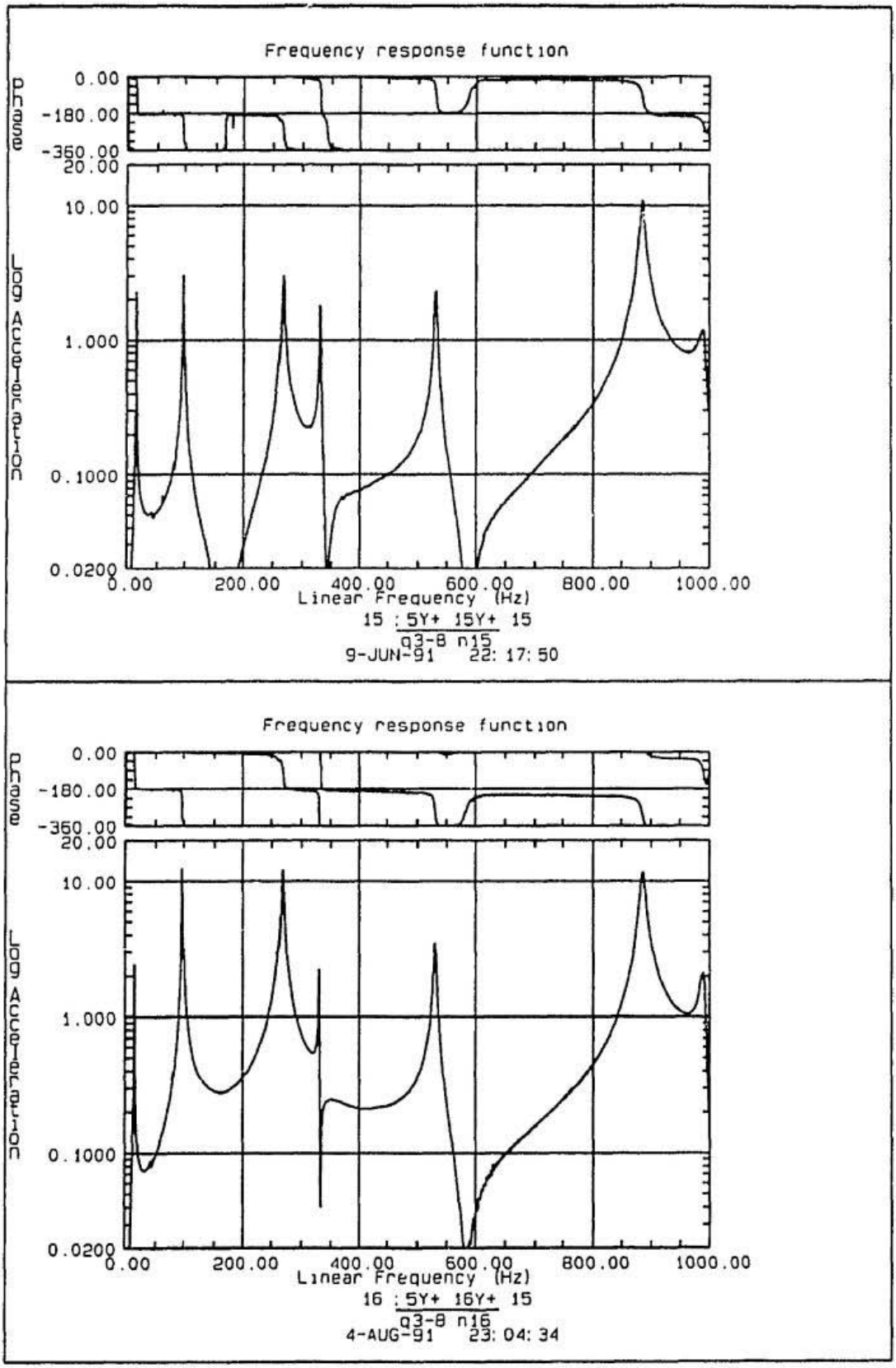
Frequency response function
Phase
0.00
-180.00
-360.00
Log Acceleration
20.00
10.00
1.000
0.1000
0.0200
0.00
200.00
400.00
600.00
800.00
1000.00
Linear Frequency (Hz)
15 : 5Y+ 15Y+ 15
q3-8 n15
9-JUN-91 22: 17: 50
Frequency response function
Phase
0.00
-180.00
-360.00
Log Acceleration
20.00
10.00
1.000
0.1000
0.0200
0.00
200.00
400.00
600.00
800.00
1000.00
Linear Frequency (Hz)
16 : 5Y+ 16Y+ 15
q3-8 n16
4-AUG-91 23: 04: 34

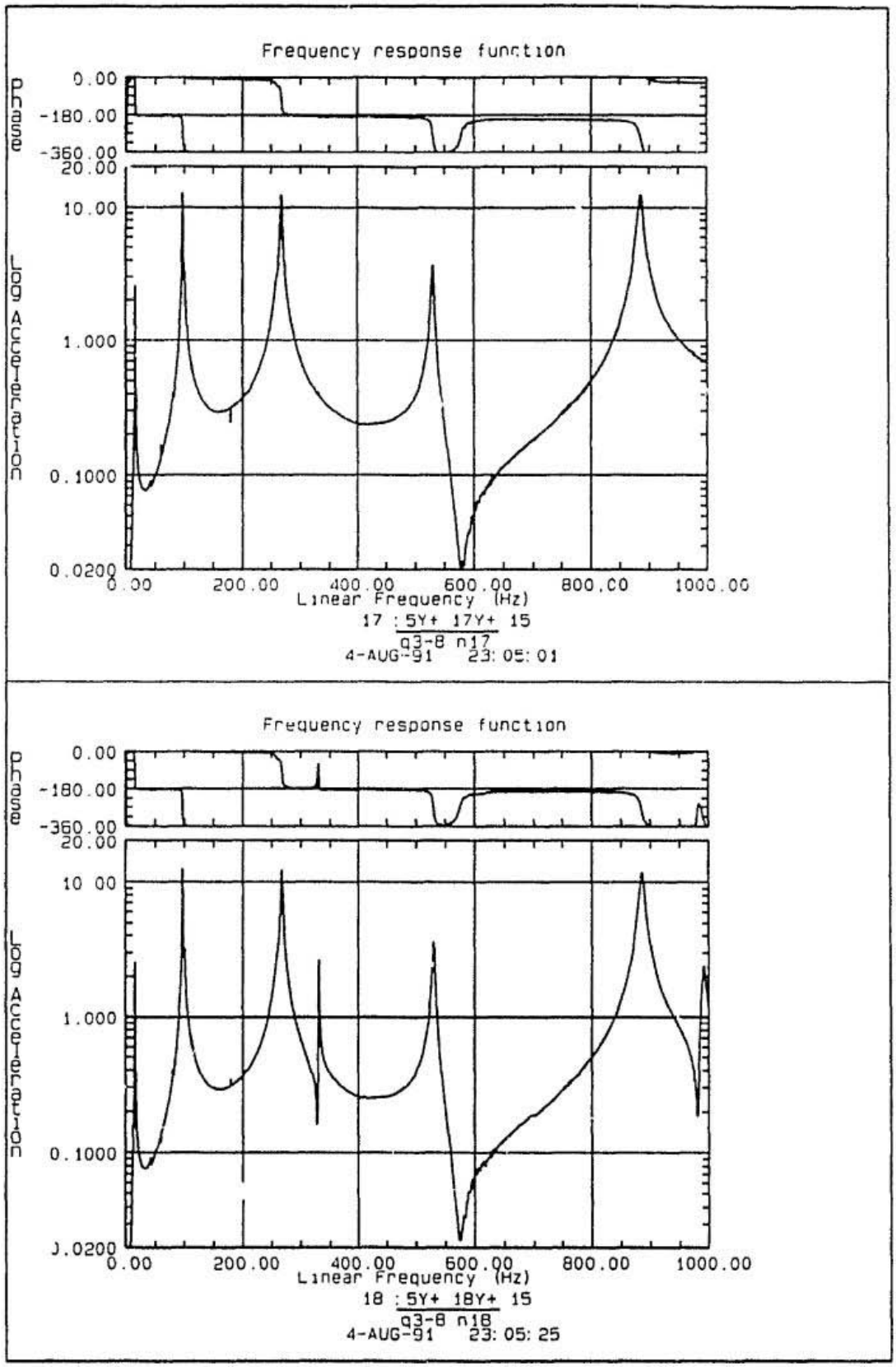
Frequency response function
Phase
0.00
-180.00
-360.00
Log Acceleration
20.00
10.00
1.000
0.1000
0.0200
0.00
200.00
400.00
600.00
800.00
1000.00
Linear Frequency (Hz)
17 : 5Y+ 17Y+ 15
q3-8 n17
4-AUG-91 23:05:01
Frequency response function
Phase
0.00
-180.00
-360.00
Log Acceleration
20.00
10.00
1.000
0.1000
0.0200
0.00
200.00
400.00
600.00
800.00
1000.00
Linear Frequency (Hz)
18 : 5Y+ 18Y+ 15
q3-8 n18
4-AUG-91 23:05:25

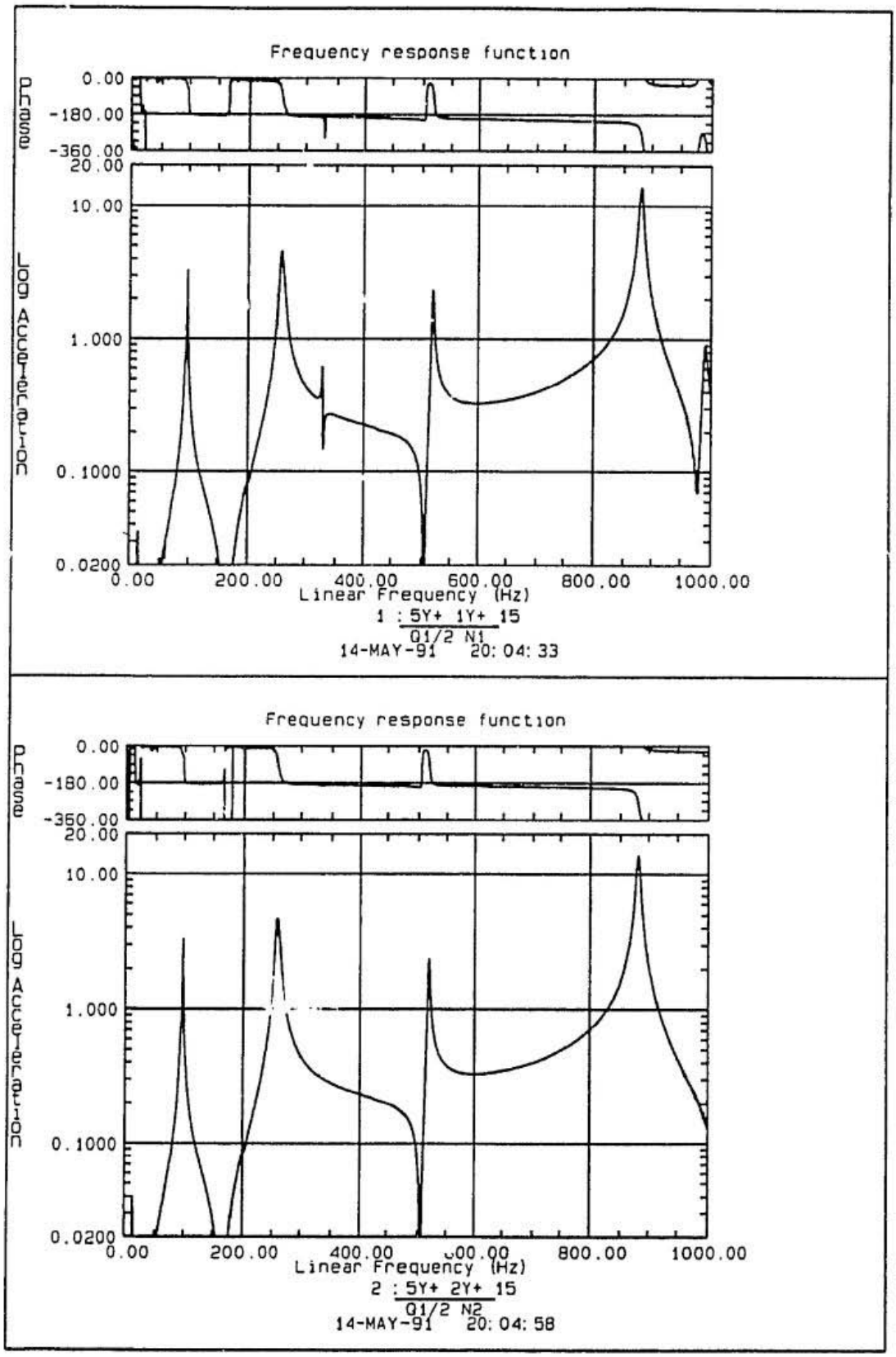
Frequency response function
Phase
0.00
-180.00
-360.00
Log Acceleration
20.00
10.00
1.000
0.1000
0.0200
0.00
200.00
400.00
600.00
800.00
1000.00
Linear Frequency (Hz)
1 : 5Y+ 1Y+ 15
Q1/2 N1
14-MAY-91 20:04:33
Frequency response function
Phase
0.00
-180.00
-360.00
Log Acceleration
20.00
10.00
1.000
0.1000
0.0200
0.00
200.00
400.00
800.00
1000.00
Linear Frequency (Hz)
2 : 5Y+ 2Y+ 15
Q1/2 N2
14-MAY-91 20:04:58

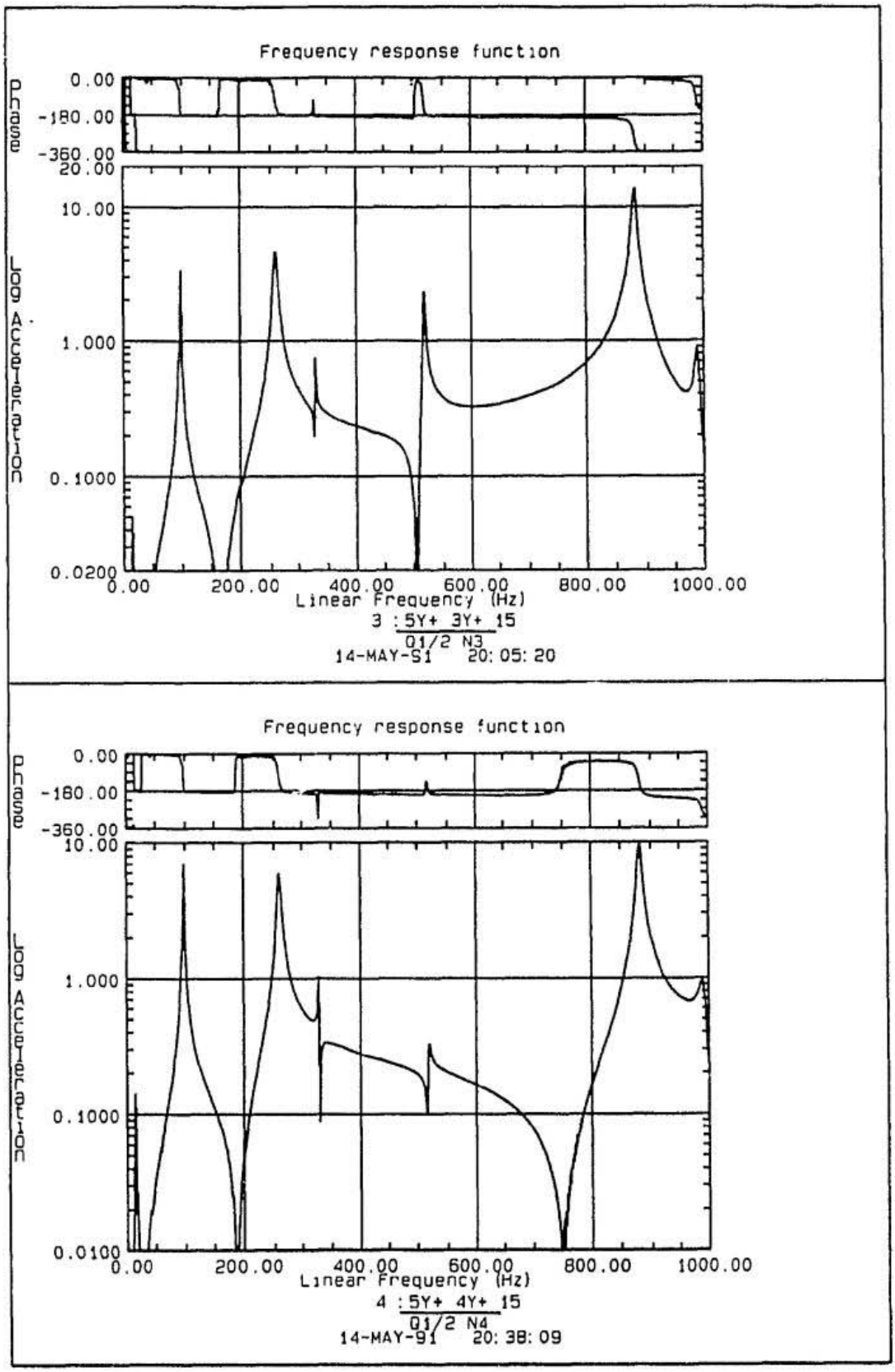
Frequency response function
Phase
0.00
-180.00
-360.00
Log Acceleration
20.00
10.00
1.000
0.1000
0.0200
0.00
200.00
400.00
600.00
800.00
1000.00
Linear Frequency (Hz)
3 : 5Y+ 3Y+ 15
01/2 N3
14-MAY-91 20:05:20
Frequency response function
Phase
0.00
-180.00
-360.00
Log Acceleration
10.00
1.000
0.1000
0.0100
0.00
200.00
400.00
600.00
800.00
1000.00
Linear Frequency (Hz)
4 : 5Y+ 4Y+ 15
01/2 N4
14-MAY-91 20:38:09

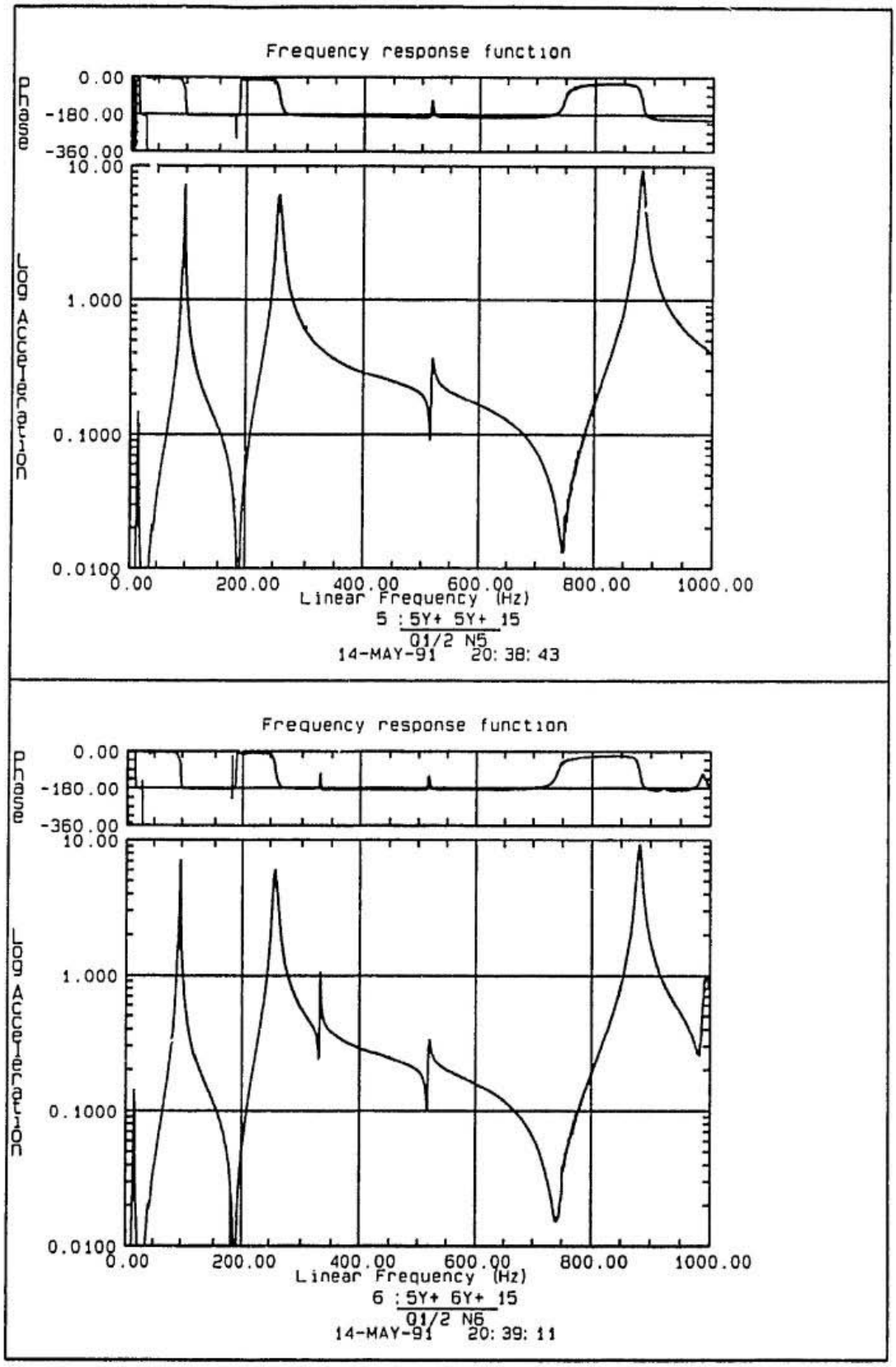
Frequency response function
Phase
0.00
-180.00
-360.00
Log Acceleration
10.00
1.000
0.1000
0.0100
0.00
200.00
400.00
600.00
800.00
1000.00
Linear Frequency (Hz)
5 : 5Y+ 5Y+ 15
01/2 N5
14-MAY-91 20:38:43
Frequency response function
Phase
0.00
-180.00
-360.00
Log Acceleration
10.00
1.000
0.1000
0.0100
0.00
200.00
400.00
600.00
800.00
1000.00
Linear Frequency (Hz)
6 : 5Y+ 6Y+ 15
01/2 N6
14-MAY-91 20:39:11

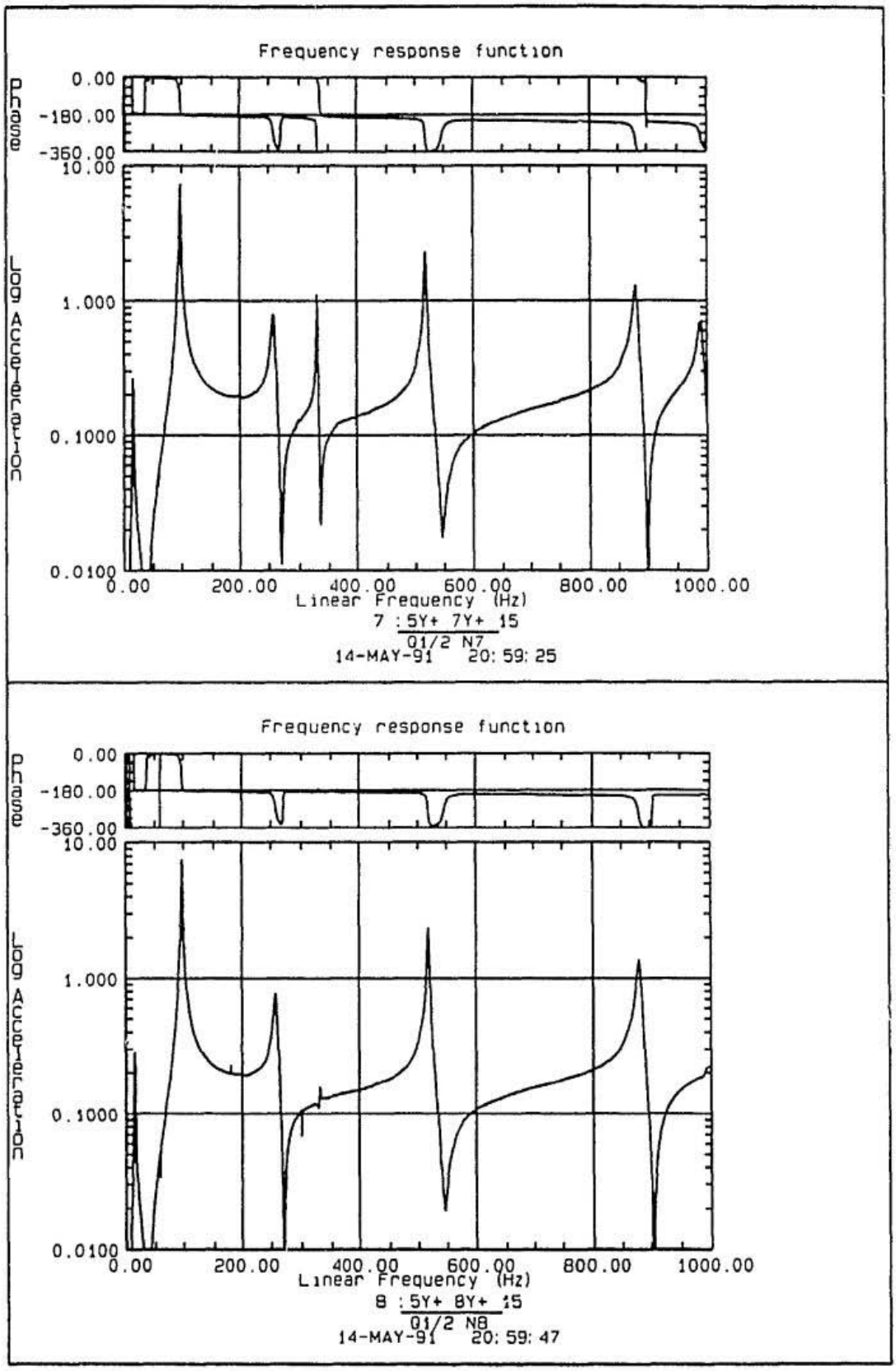
Frequency response function
Phase
0.00
-180.00
-360.00
Log Acceleration
10.00
1.000
0.1000
0.0100
0.00
200.00
400.00
600.00
800.00
1000.00
Linear Frequency (Hz)
7 : 5Y+ 7Y+ 15
01/2 N7
14-MAY-91 20:59:25
Frequency response function
Phase
0.00
-180.00
-360.00
Log Acceleration
10.00
1.000
0.1000
0.0100
0.00
200.00
400.00
600.00
800.00
1000.00
Linear Frequency (Hz)
8 : 5Y+ 8Y+ 15
01/2 N8
14-MAY-91 20:59:47

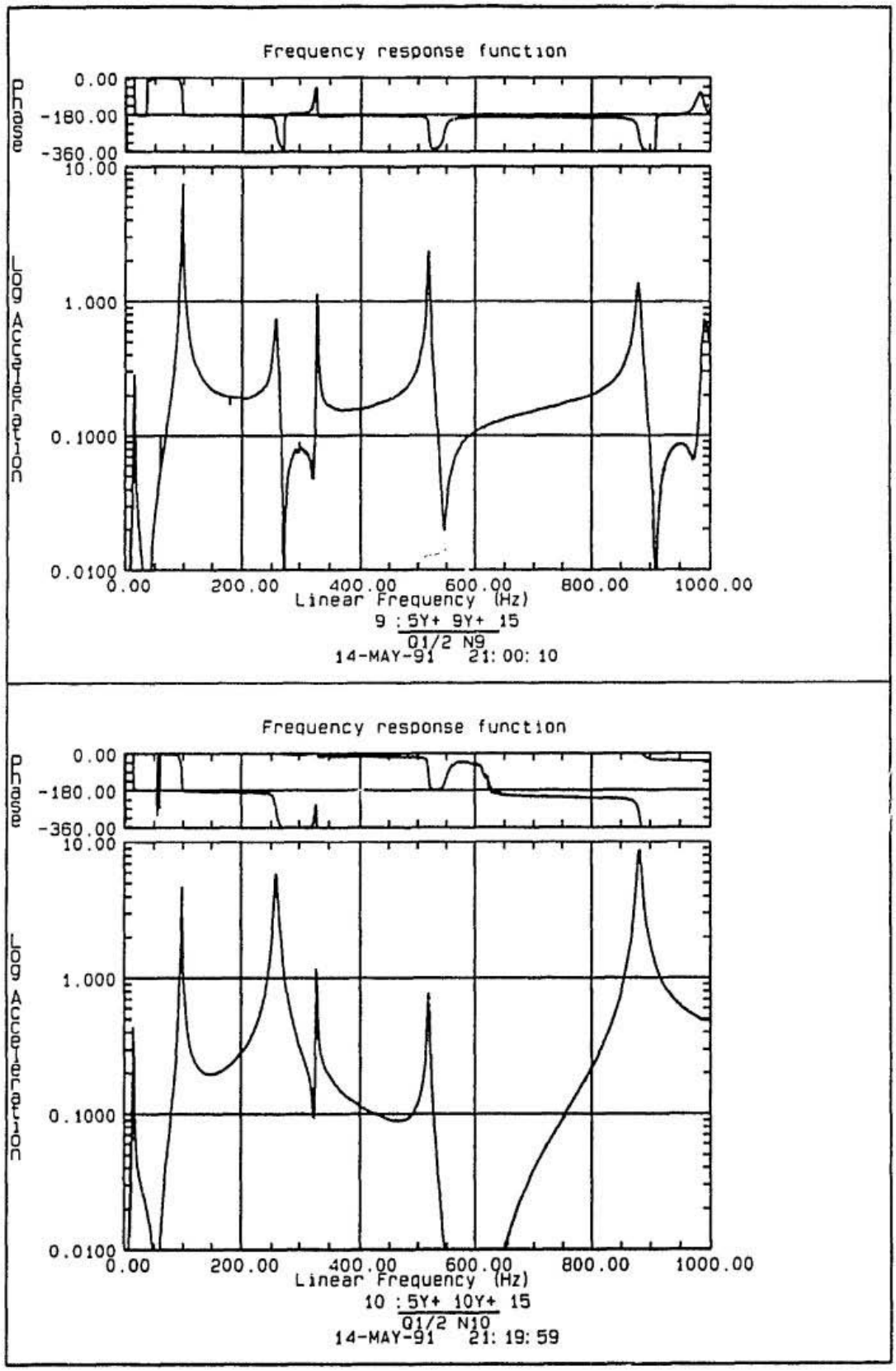
Frequency response function
Phase
0.00
-180.00
-360.00
Log Acceleration
10.00
1.000
0.1000
0.0100
0.00
200.00
400.00
600.00
800.00
1000.00
Linear Frequency (Hz)
9 : 5Y+ 9Y+ 15
Q1/2 N9
14-MAY-91 21:00:10
Frequency response function
Phase
0.00
-180.00
-360.00
Log Acceleration
10.00
1.000
0.1000
0.0100
0.00
200.00
400.00
600.00
800.00
1000.00
Linear Frequency (Hz)
10 : 5Y+ 10Y+ 15
Q1/2 N10
14-MAY-91 21:19:59

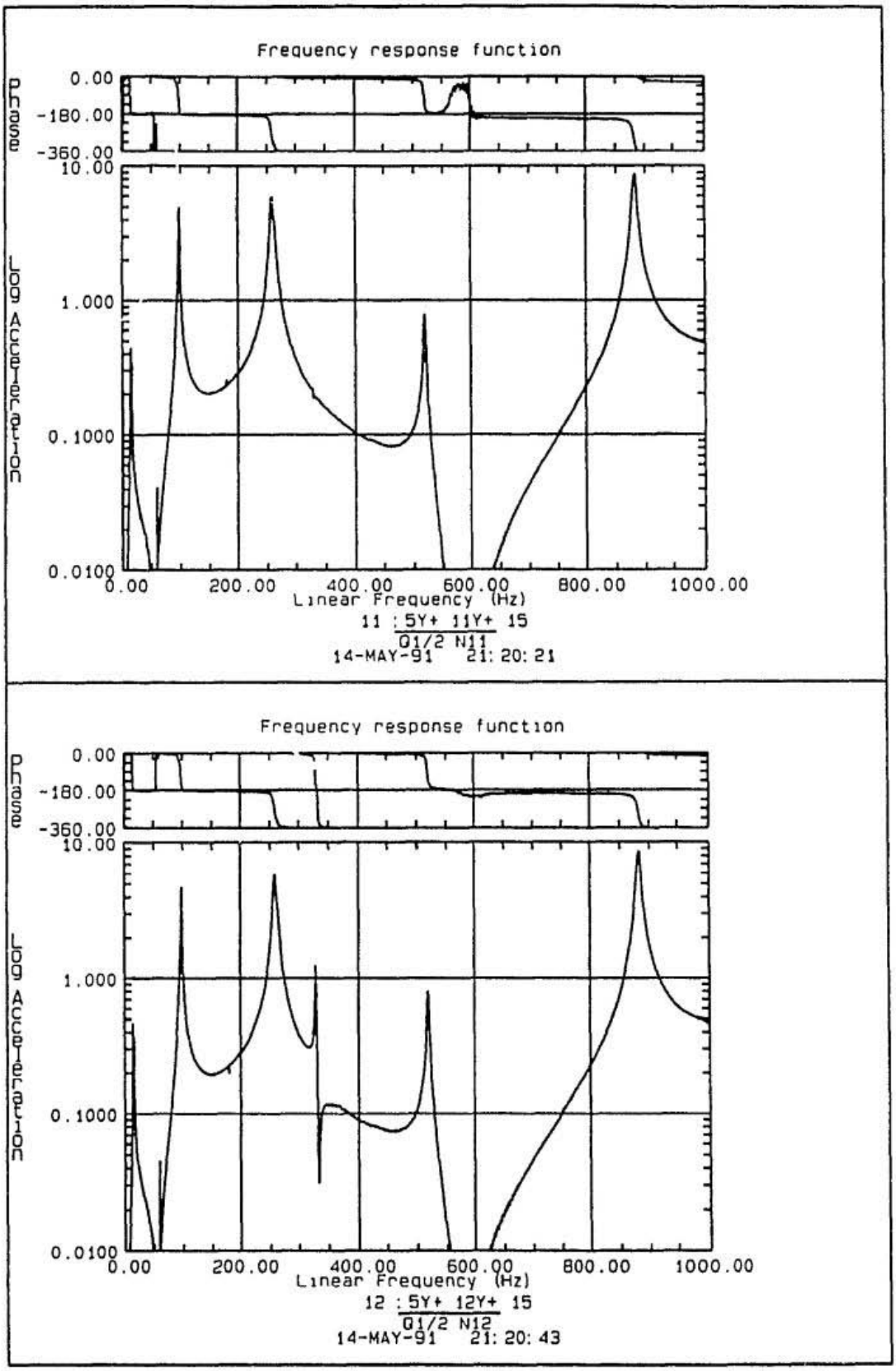
Frequency response function
Phase
0.00
-180.00
-360.00
Log Acceleration
10.00
1.000
0.1000
0.0100
0.00
200.00
400.00
600.00
800.00
1000.00
Linear Frequency (Hz)
11 : 5Y+ 11Y+ 15
Q1/2 N11
14-MAY-91 21:20:21
Frequency response function
Phase
0.00
-180.00
-360.00
Log Acceleration
10.00
1.000
0.1000
0.0100
0.00
200.00
400.00
600.00
800.00
1000.00
Linear Frequency (Hz)
12 : 5Y+ 12Y+ 15
Q1/2 N12
14-MAY-91 21:20:43

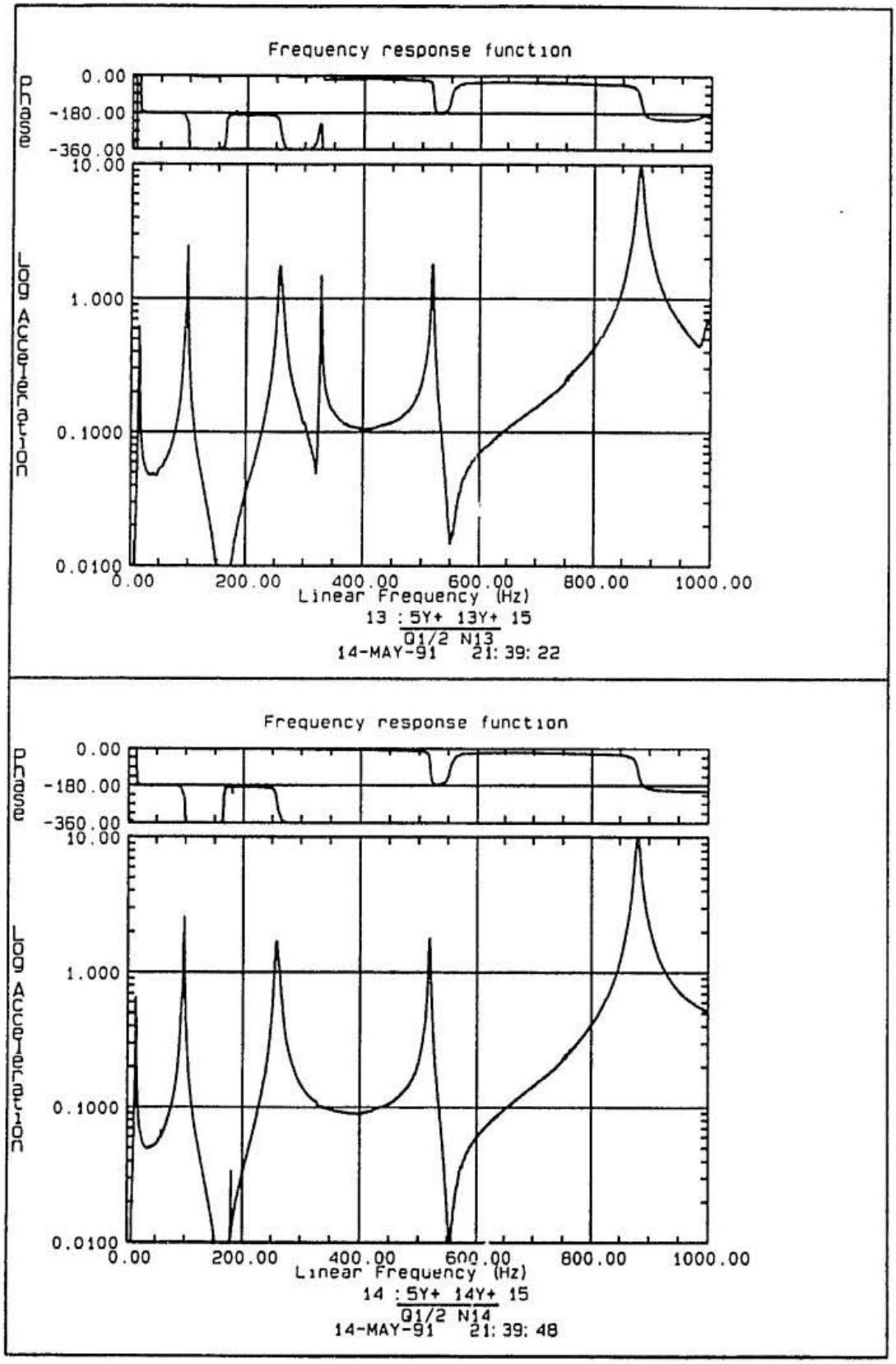
Frequency response function
Phase
0.00
-180.00
-360.00
Log Acceleration
10.00
1.000
0.1000
0.0100
0.00
200.00
400.00
600.00
800.00
1000.00
Linear Frequency (Hz)
13 : 5Y+ 13Y+ 15
Q1/2 N13
14-MAY-91 21:39:22
Frequency response function
Phase
0.00
-180.00
-360.00
Log Acceleration
10.00
1.000
0.1000
0.0100
0.00
200.00
400.00
600.00
800.00
1000.00
Linear Frequency (Hz)
14 : 5Y+ 14Y+ 15
Q1/2 N14
14-MAY-91 21:39:48

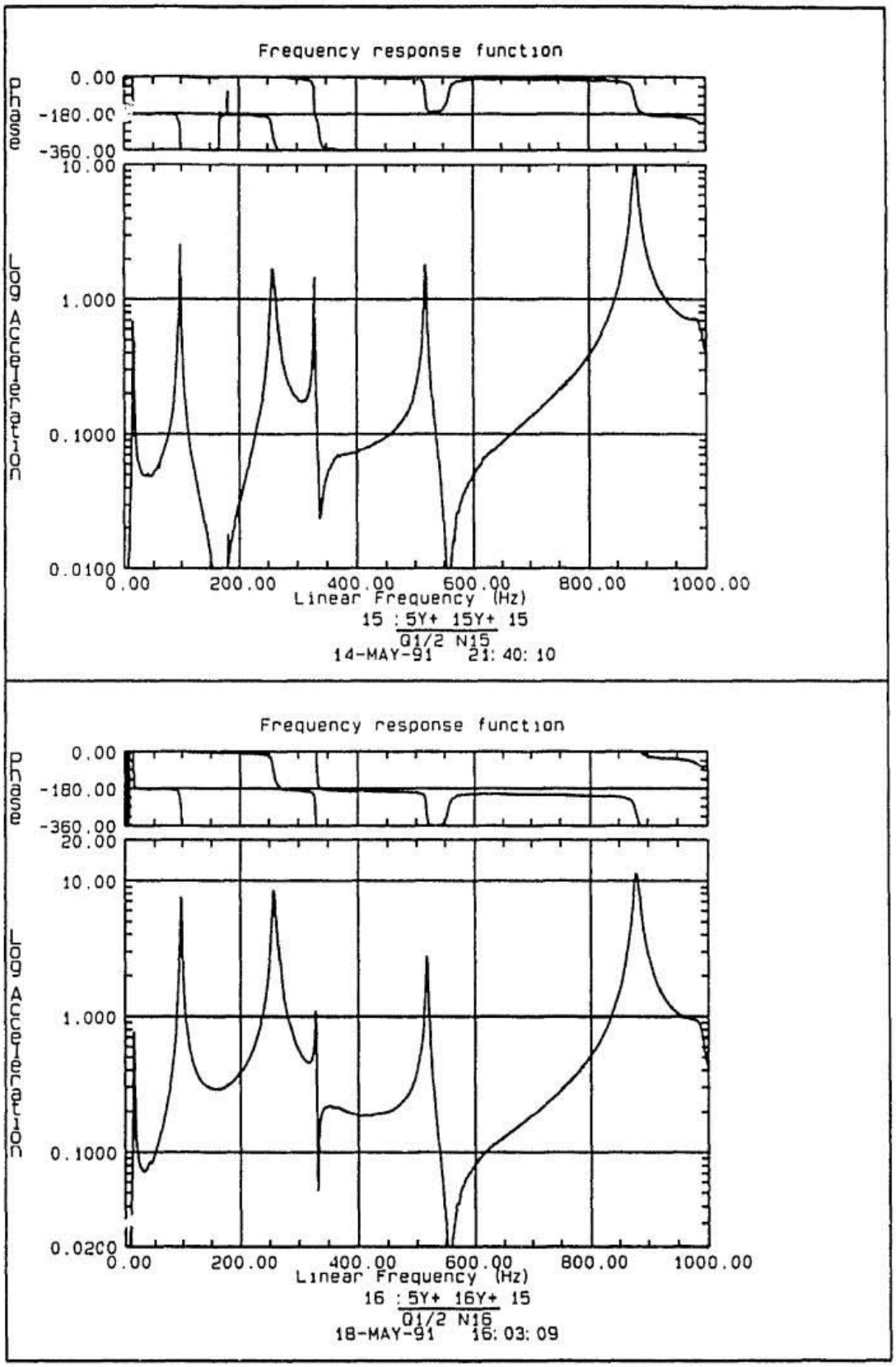
Frequency response function
Phase
0.00
-180.00
-360.00
Log Acceleration
10.00
1.000
0.1000
0.0100
0.00
200.00
400.00
600.00
800.00
1000.00
Linear Frequency (Hz)
15 : 5Y+ 15Y+ 15
Q1/2 N15
14-MAY-91 21:40:10
Frequency response function
Phase
0.00
-180.00
-360.00
Log Acceleration
20.00
10.00
1.000
0.1000
0.0200
0.00
200.00
400.00
600.00
800.00
1000.00
Linear Frequency (Hz)
16 : 5Y+ 16Y+ 15
Q1/2 N16
18-MAY-91 16:03:09

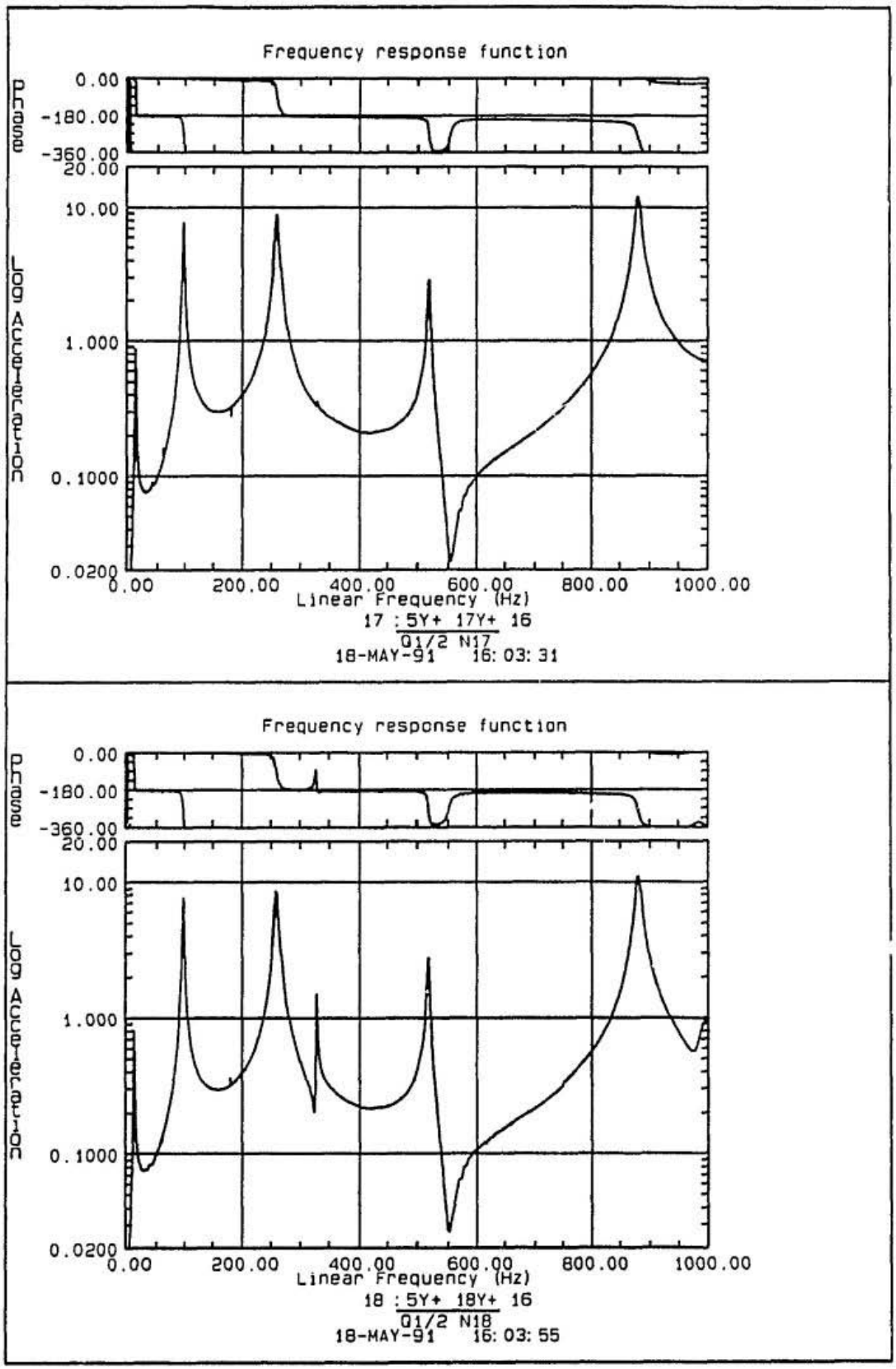
Frequency response function
Phase
0.00
-180.00
-360.00
Log Acceleration
20.00
10.00
1.000
0.1000
0.0200
0.00
200.00
400.00
600.00
800.00
1000.00
Linear Frequency (Hz)
17 : 5Y+ 17Y+ 16
01/2 N17
18-MAY-91 16:03:31
Frequency response function
Phase
0.00
-180.00
-360.00
Log Acceleration
20.00
10.00
1.000
0.1000
0.0200
0.00
200.00
400.00
600.00
800.00
1000.00
Linear Frequency (Hz)
18 : 5Y+ 18Y+ 16
01/2 N18
18-MAY-91 16:03:55

Appendix D

Zoomed View of FRF Peaks for Centerline Nodes on All Plates

Note: For these FRF's, as with those in Appendix C, the magnitude of the FRF is a ratio of acceleration output to force input and hence, has the unit [(m/s^2)/N].

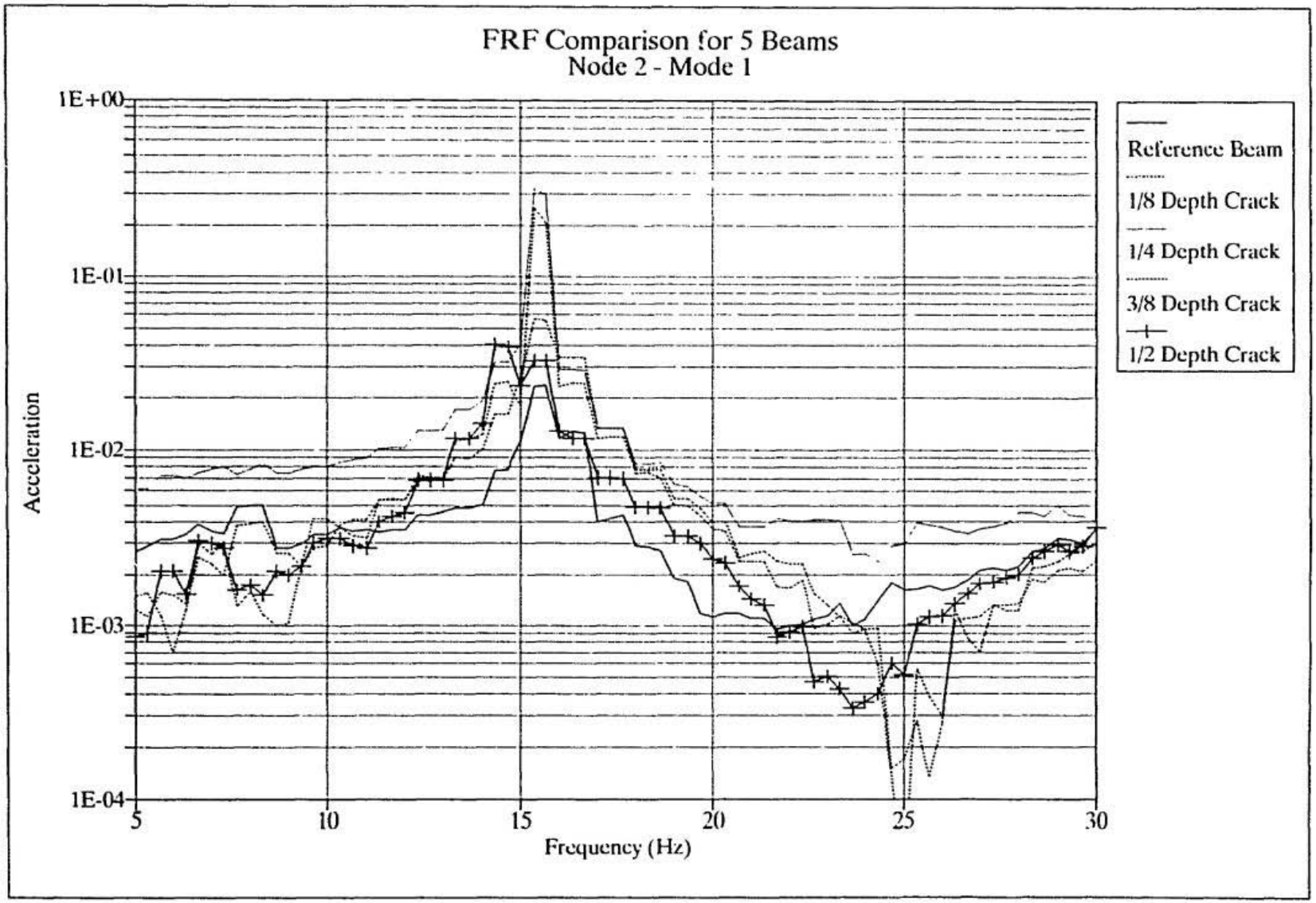
FRF Comparison for 5 Beams
Node 2 - Mode 1
1E+00
1E-01
1E-02
1E-03
1E-04
Acceleration
5
10
15
20
25
30
Frequency (Hz)
Reference Beam
1/8 Depth Crack
1/4 Depth Crack
3/8 Depth Crack
1/2 Depth Crack

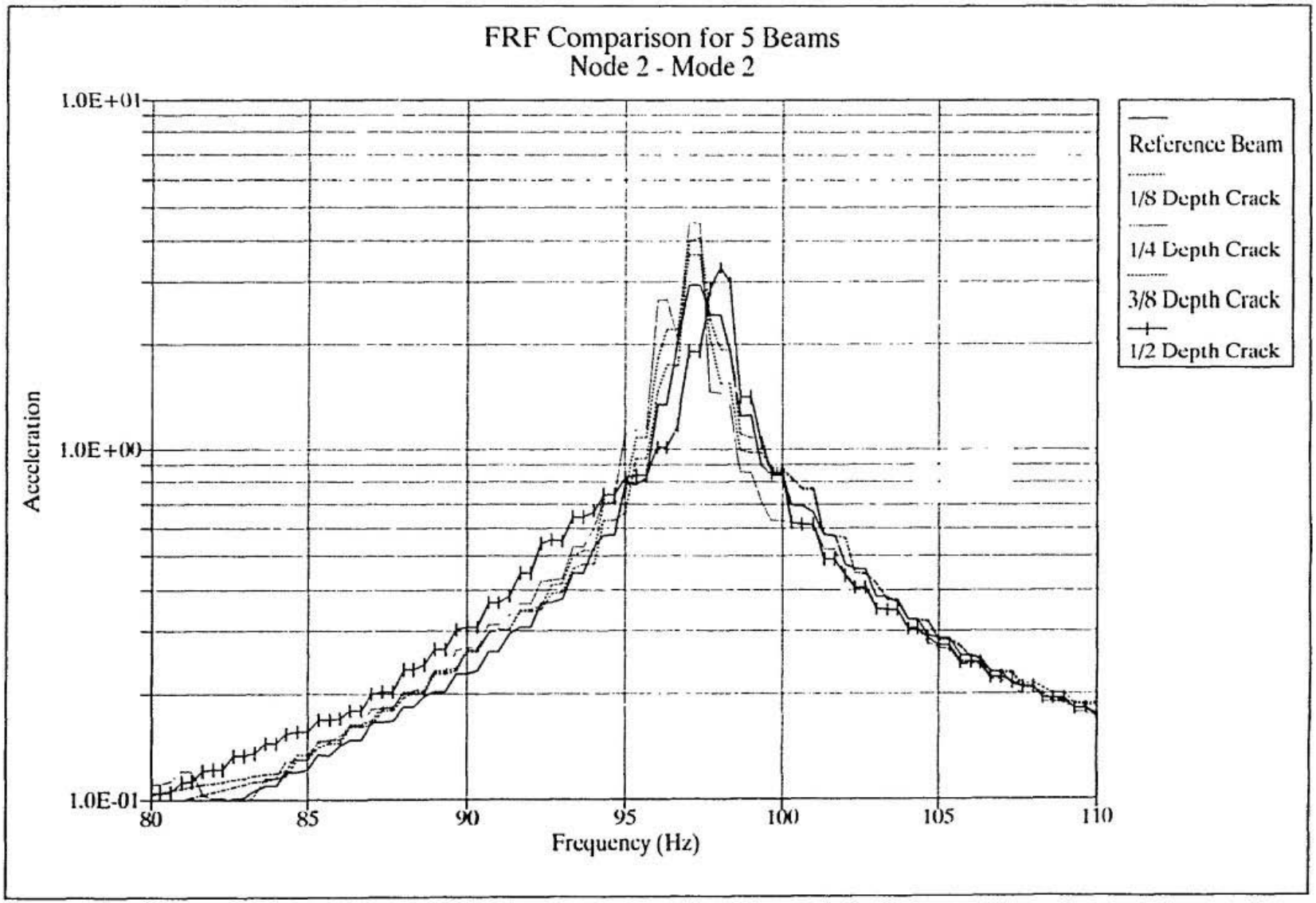
FRF Comparison for 5 Beams
Node 2 - Mode 2
1.0E+01
1.0E+00
1.0E-01
Acceleration
80
85
90
95
100
105
110
Frequency (Hz)
Reference Beam
1/8 Depth Crack
1/4 Depth Crack
3/8 Depth Crack
1/2 Depth Crack

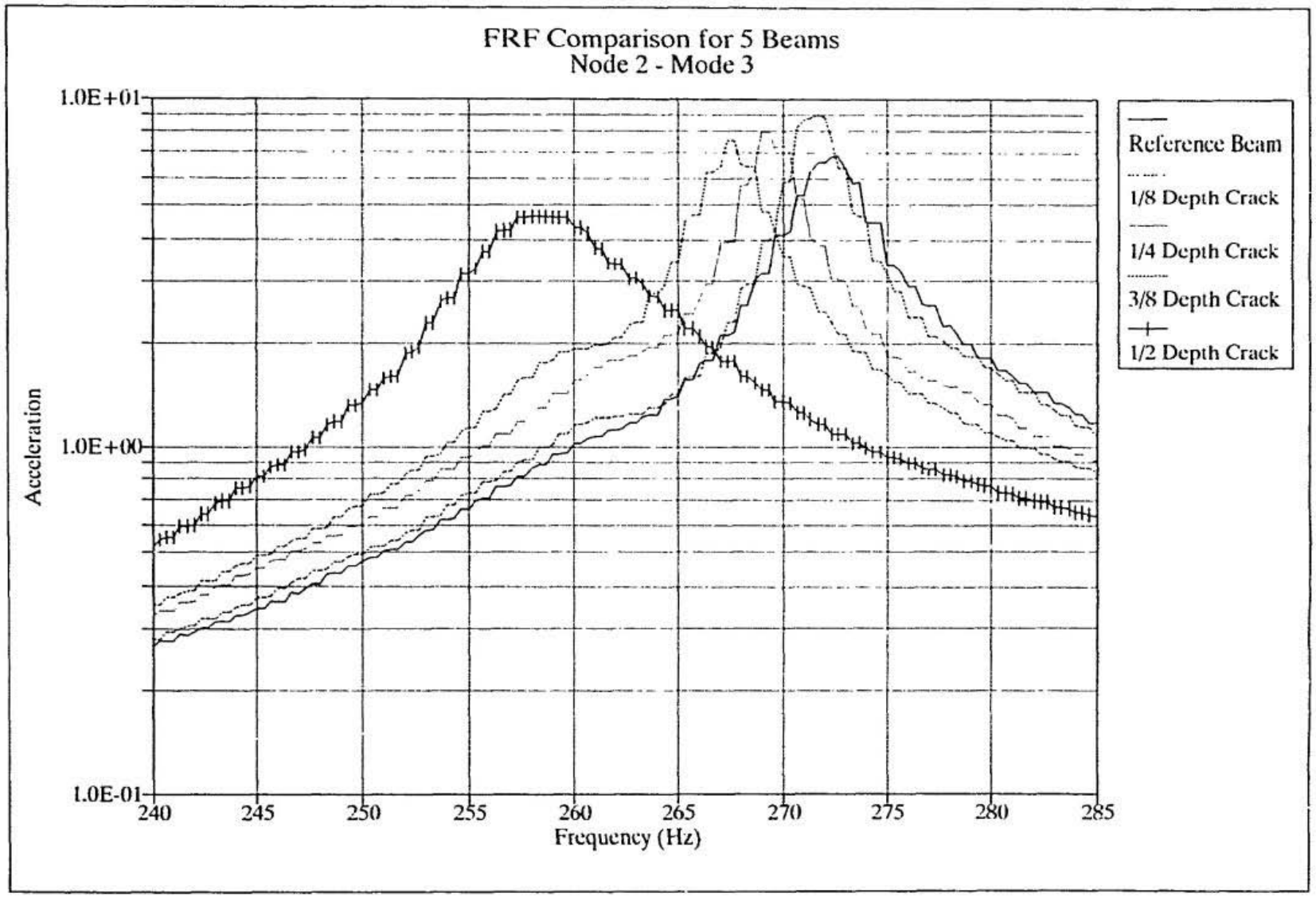
FRF Comparison for 5 Beams
Node 2 - Mode 3
1.0E+01
1.0E+00
1.0E-01
Acceleration
240
245
250
255
260
265
270
275
280
285
Frequency (Hz)
Reference Beam
1/8 Depth Crack
1/4 Depth Crack
3/8 Depth Crack
1/2 Depth Crack

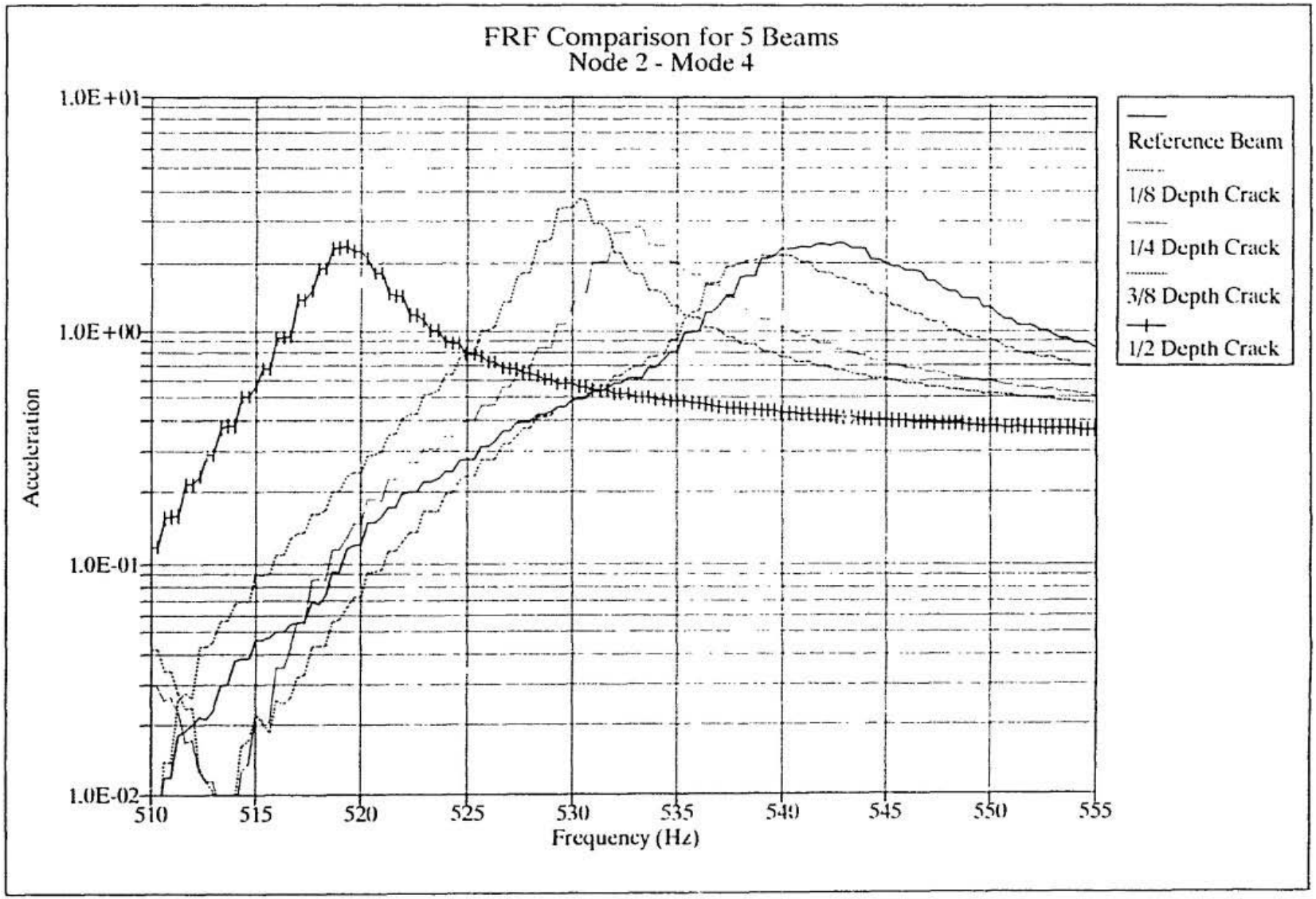
FRF Comparison for 5 Beams
Node 2 - Mode 4
1.0E+01
1.0E+00
1.0E-01
1.0E-02
Acceleration
510
515
520
525
530
535
540
545
550
555
Frequency (Hz)
Reference Beam
1/8 Depth Crack
1/4 Depth Crack
3/8 Depth Crack
1/2 Depth Crack

FRF Comparison for 5 Beams
Node 2 - Mode 5
Reference Beam
1/8 Depth Crack
1/4 Depth Crack
3/8 Depth Crack
1/2 Depth Crack
Acceleration
1.0E+02
1.0E+01
1.0E+00
870
875
880
885
890
895
900
Frequency (Hz)

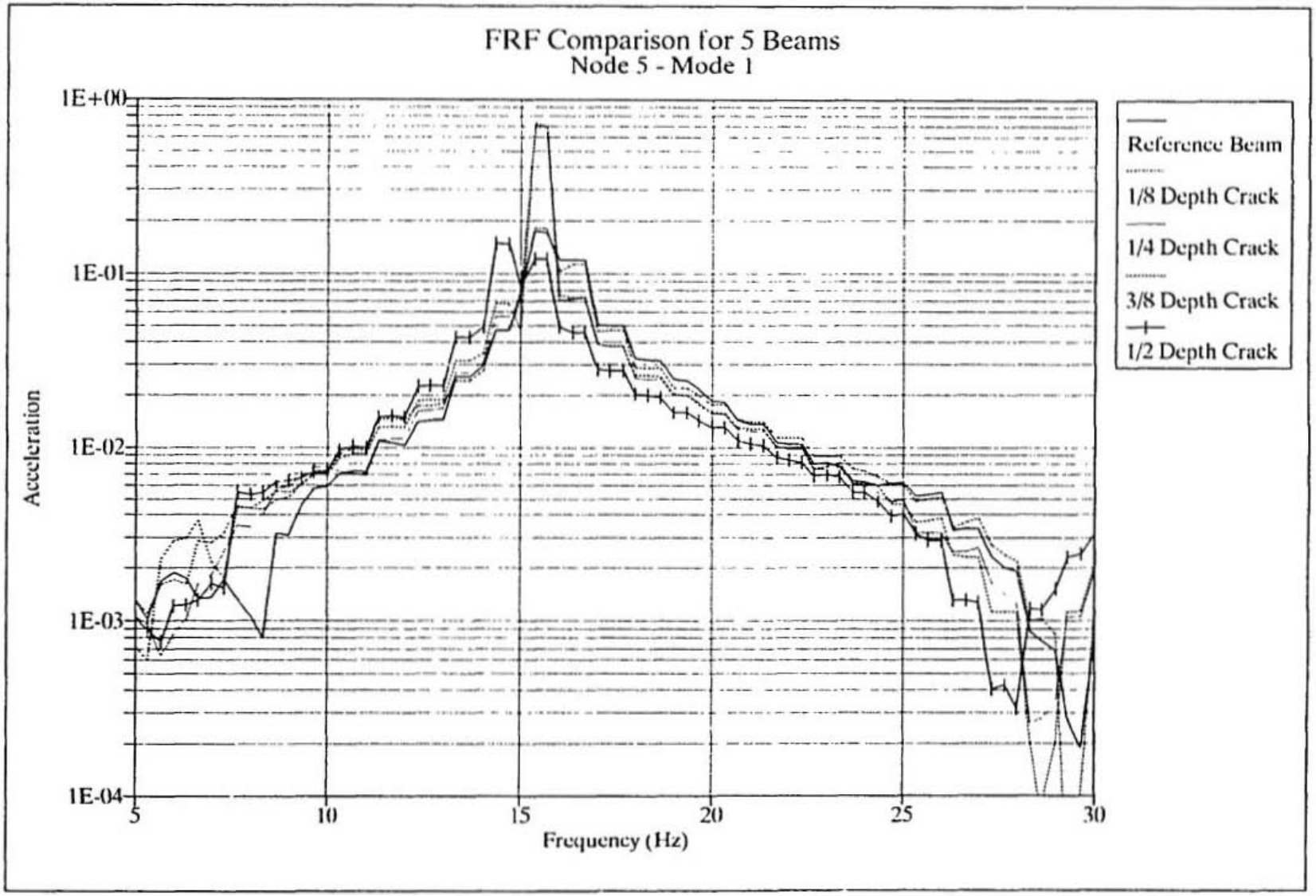
FRF Comparison for 5 Beams
Node 5 - Mode 1
1E+00
1E-01
1E-02
1E-03
1E-04
Acceleration
5
10
15
20
25
30
Frequency (Hz)
Reference Beam
1/8 Depth Crack
1/4 Depth Crack
3/8 Depth Crack
1/2 Depth Crack

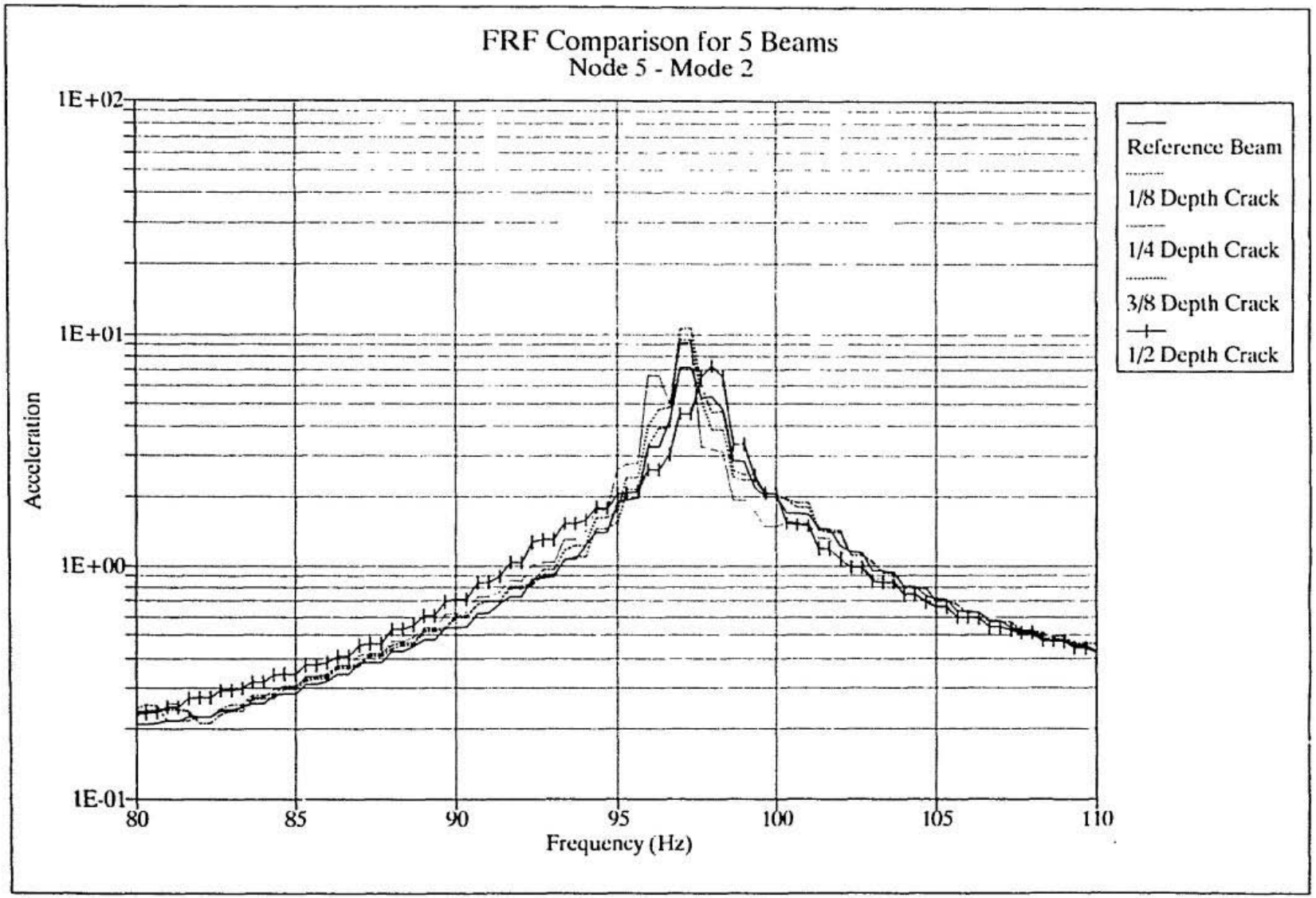
FRF Comparison for 5 Beams
Node 5 - Mode 2
1E+02
1E+01
1E+00
1E-01
Acceleration
80
85
90
95
100
105
110
Frequency (Hz)
Reference Beam
1/8 Depth Crack
1/4 Depth Crack
3/8 Depth Crack
1/2 Depth Crack

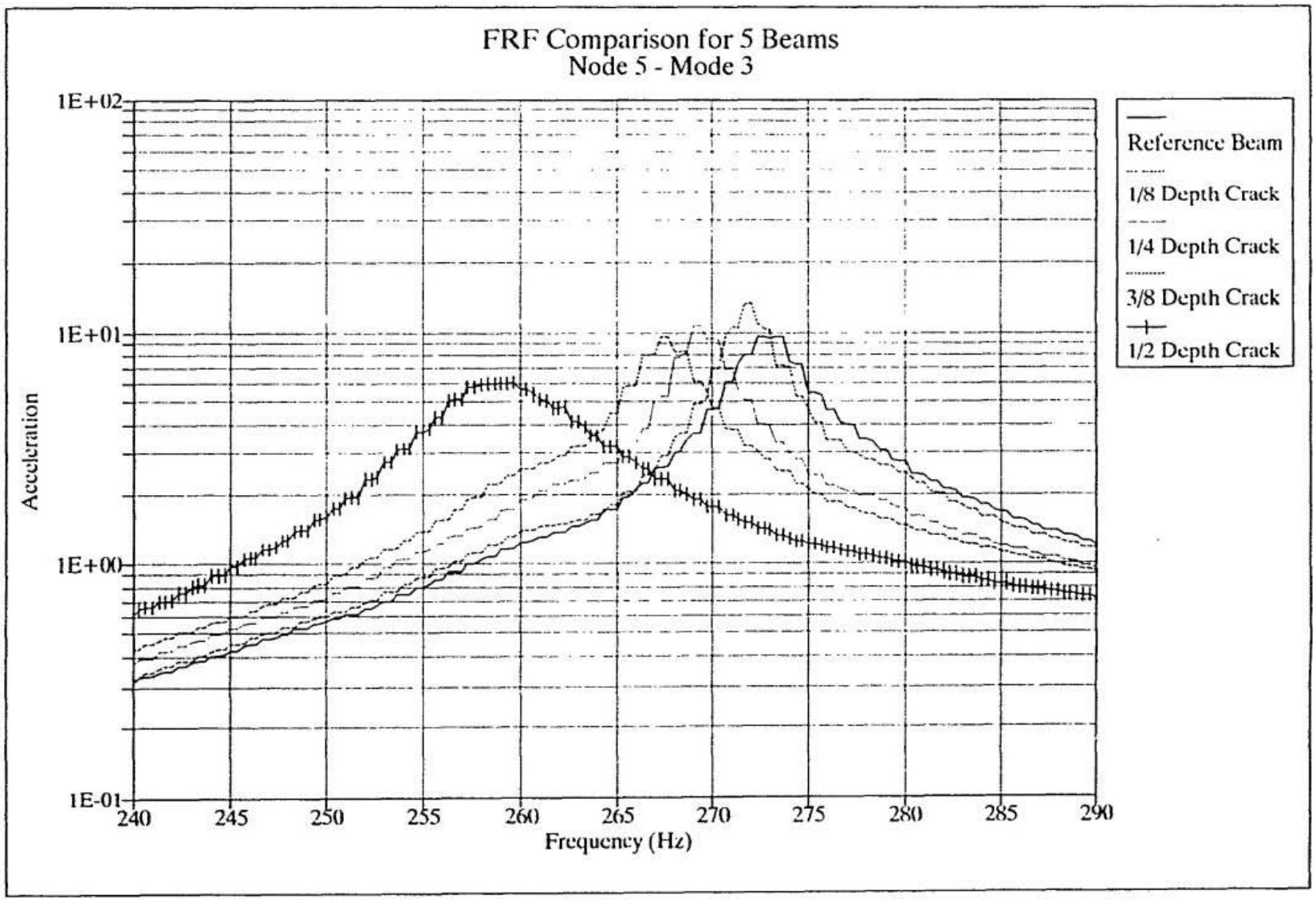
FRF Comparison for 5 Beams
Node 5 - Mode 3
1E+02
1E+01
1E+00
1E-01
Acceleration
240
245
250
255
260
265
270
275
280
285
290
Frequency (Hz)
Reference Beam
1/8 Depth Crack
1/4 Depth Crack
3/8 Depth Crack
1/2 Depth Crack

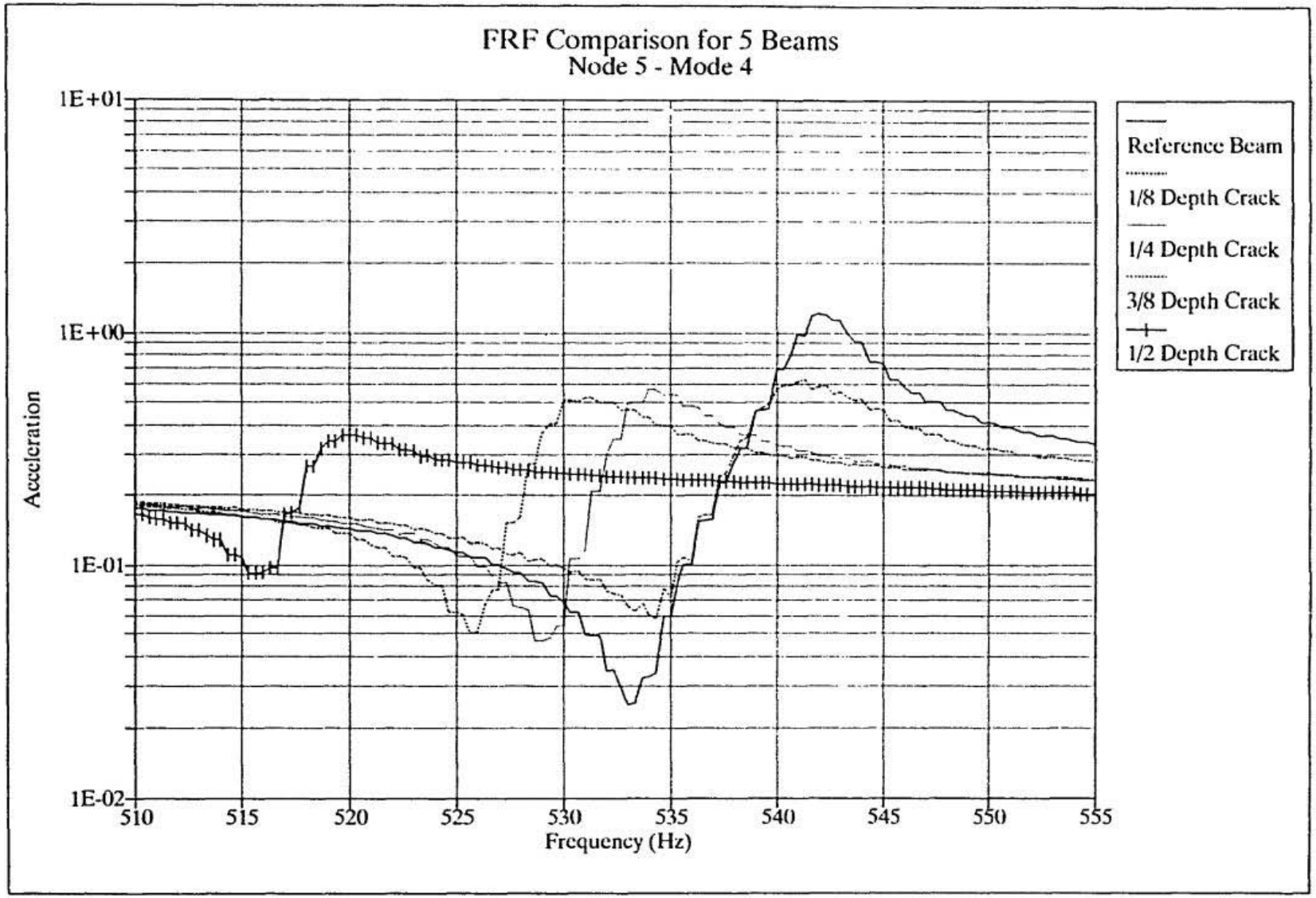
FRF Comparison for 5 Beams
Node 5 - Mode 4
1E+01
1E+00
1E-01
1E-02
Acceleration
510
515
520
525
530
535
540
545
550
555
Frequency (Hz)
Reference Beam
1/8 Depth Crack
1/4 Depth Crack
3/8 Depth Crack
1/2 Depth Crack

FRF Comparison for 5 Beams
Node 5 - Mode 5
Reference Beam
1/8 Depth Crack
1/4 Depth Crack
3/8 Depth Crack
1/2 Depth Crack
Acceleration
1E+01
1E+00
870
875
880
885
890
895
900
Frequency (Hz)

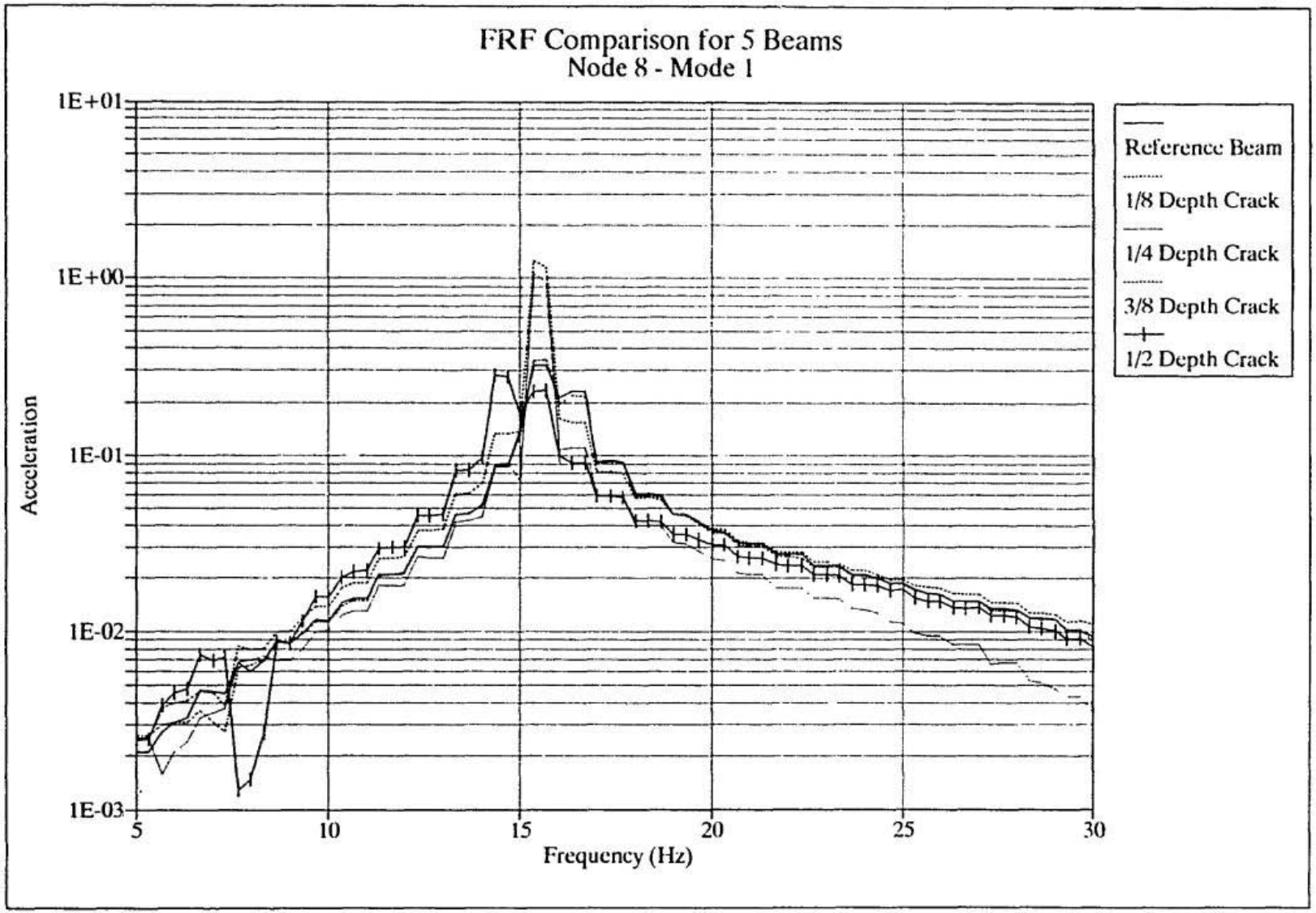
FRF Comparison for 5 Beams
Node 8 - Mode 1
1E+01
1E+00
1E-01
1E-02
1E-03
Acceleration
5
10
15
20
25
30
Frequency (Hz)
Reference Beam
1/8 Depth Crack
1/4 Depth Crack
3/8 Depth Crack
1/2 Depth Crack

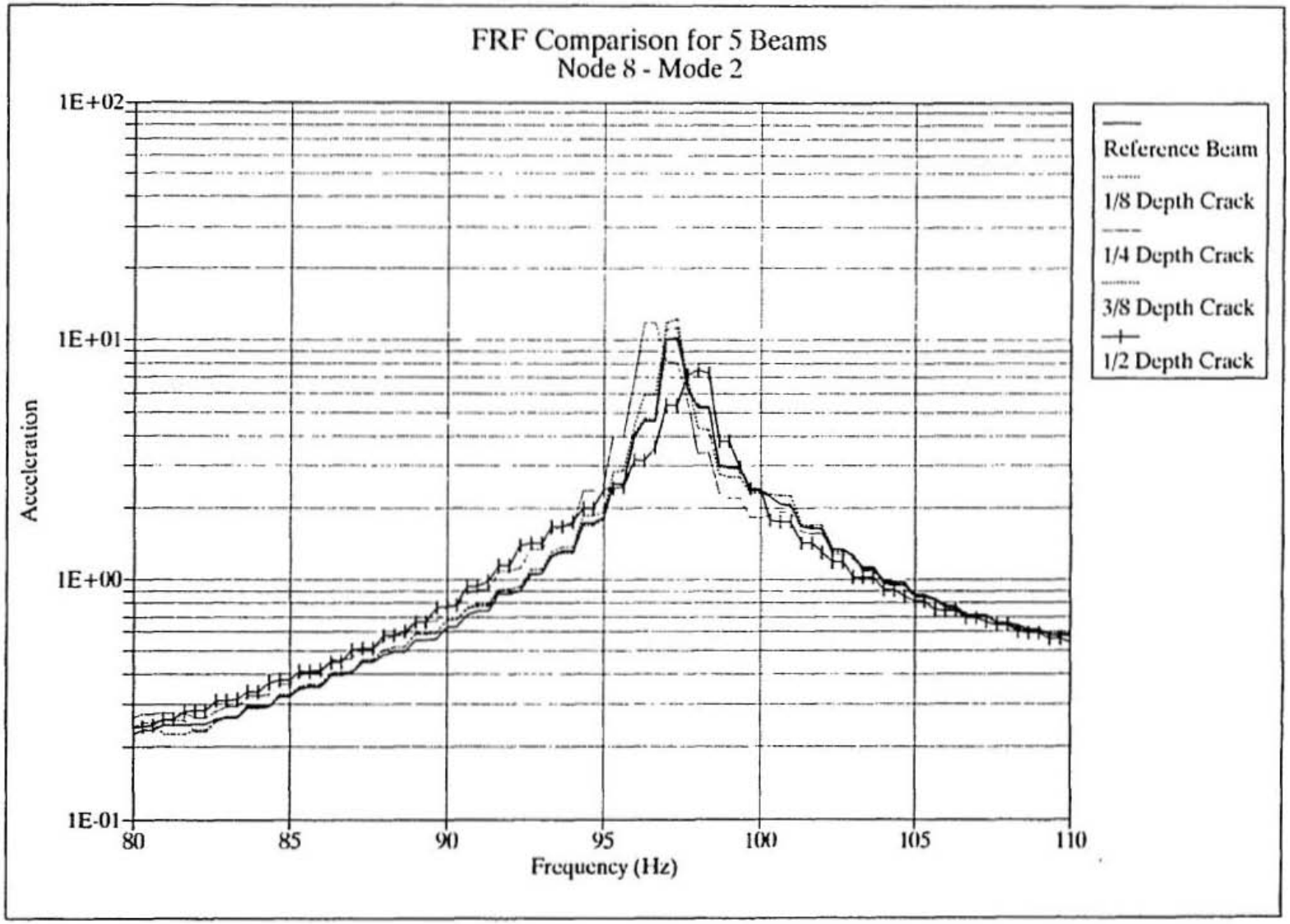
FRF Comparison for 5 Beams
Node 8 - Mode 2
1E+02
1E+01
1E+00
1E-01
Acceleration
80
85
90
95
100
105
110
Frequency (Hz)
Reference Beam
1/8 Depth Crack
1/4 Depth Crack
3/8 Depth Crack
1/2 Depth Crack

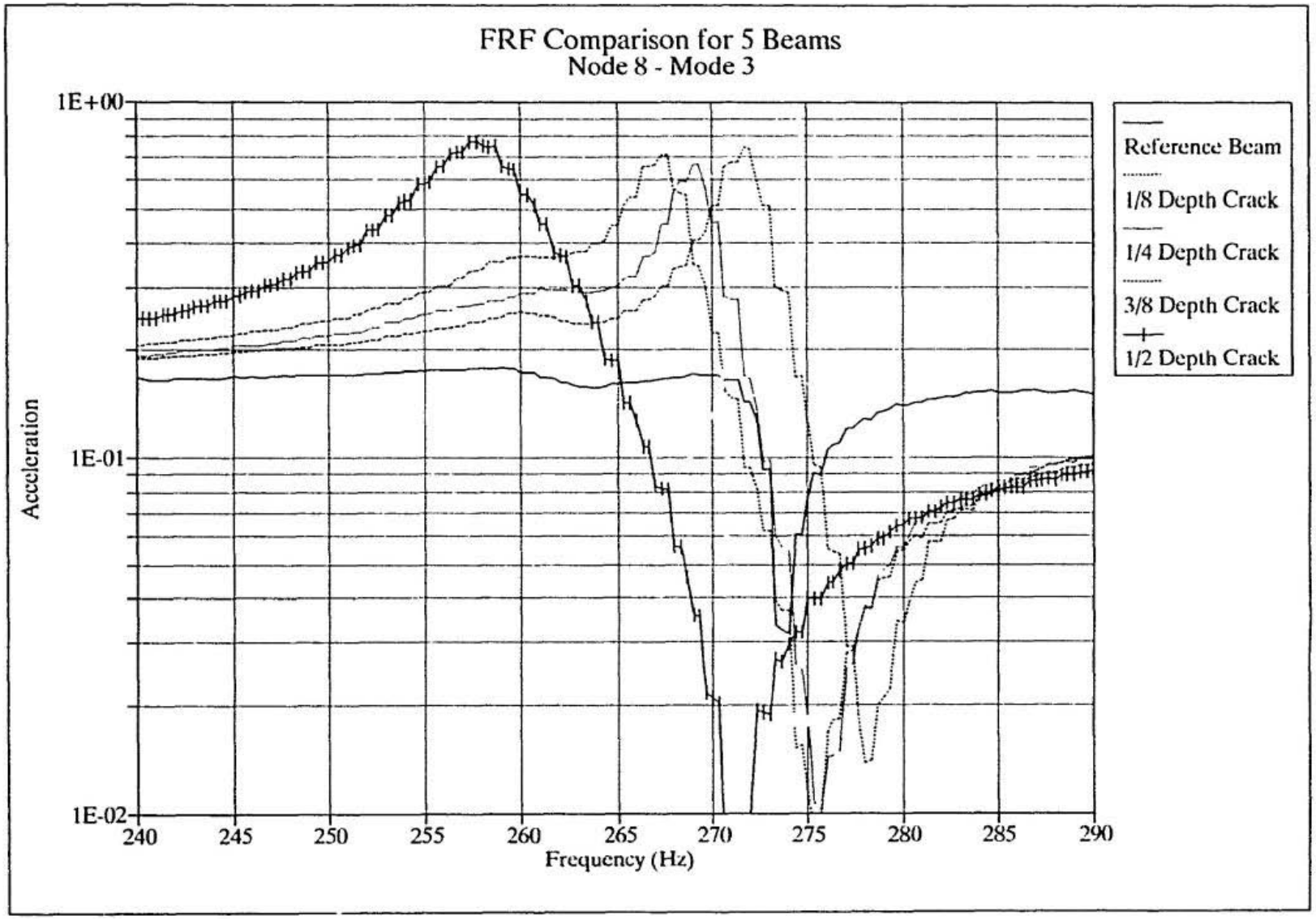
FRF Comparison for 5 Beams
Node 8 - Mode 3
1E+00
1E-01
1E-02
Acceleration
240
245
250
255
260
265
270
275
280
285
290
Frequency (Hz)
Reference Beam
1/8 Depth Crack
1/4 Depth Crack
3/8 Depth Crack
1/2 Depth Crack

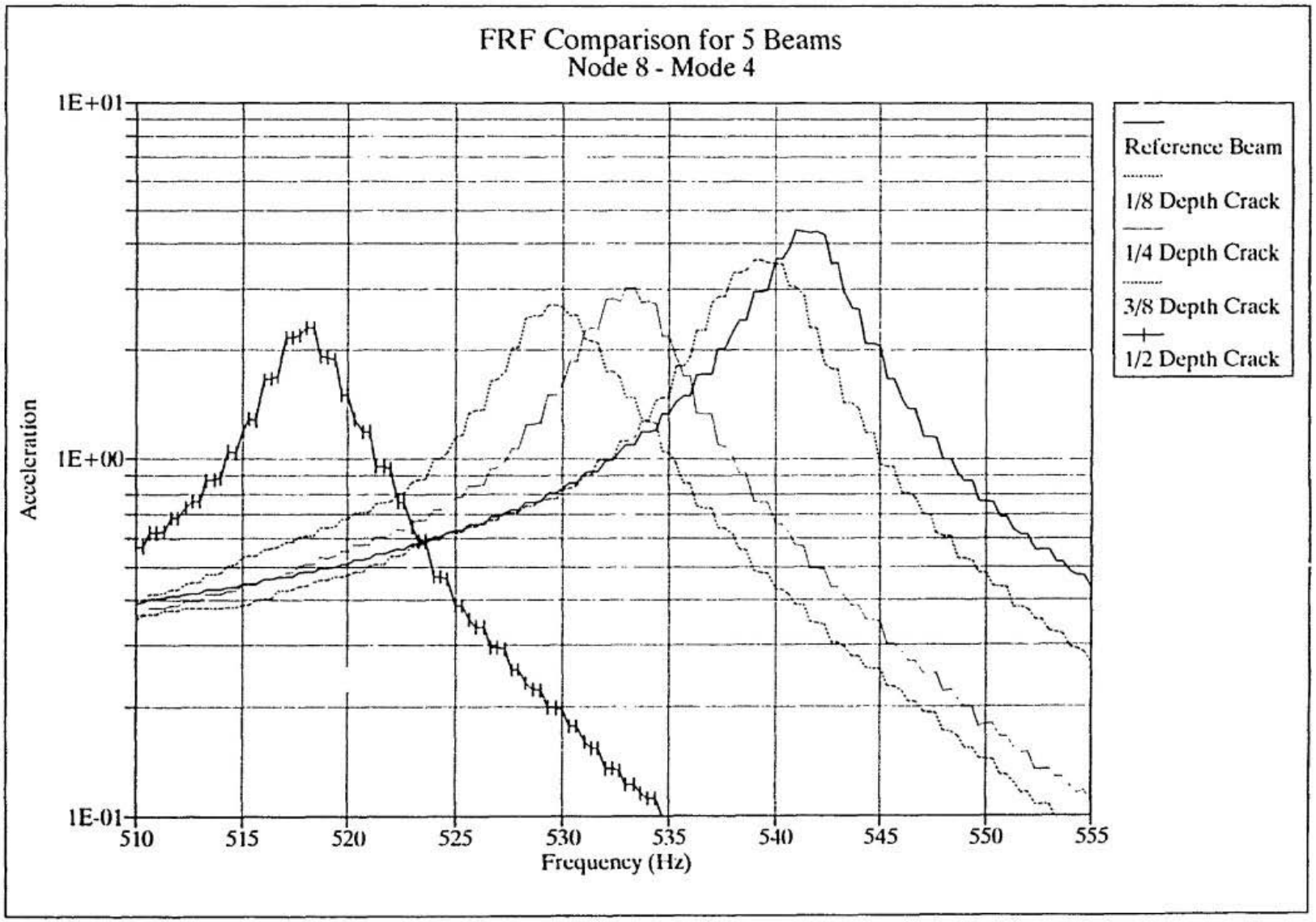
FRF Comparison for 5 Beams
Node 8 - Mode 4
1E+01
1E+00
1E-01
Acceleration
510
515
520
525
530
535
540
545
550
555
Frequency (Hz)
Reference Beam
1/8 Depth Crack
1/4 Depth Crack
3/8 Depth Crack
1/2 Depth Crack

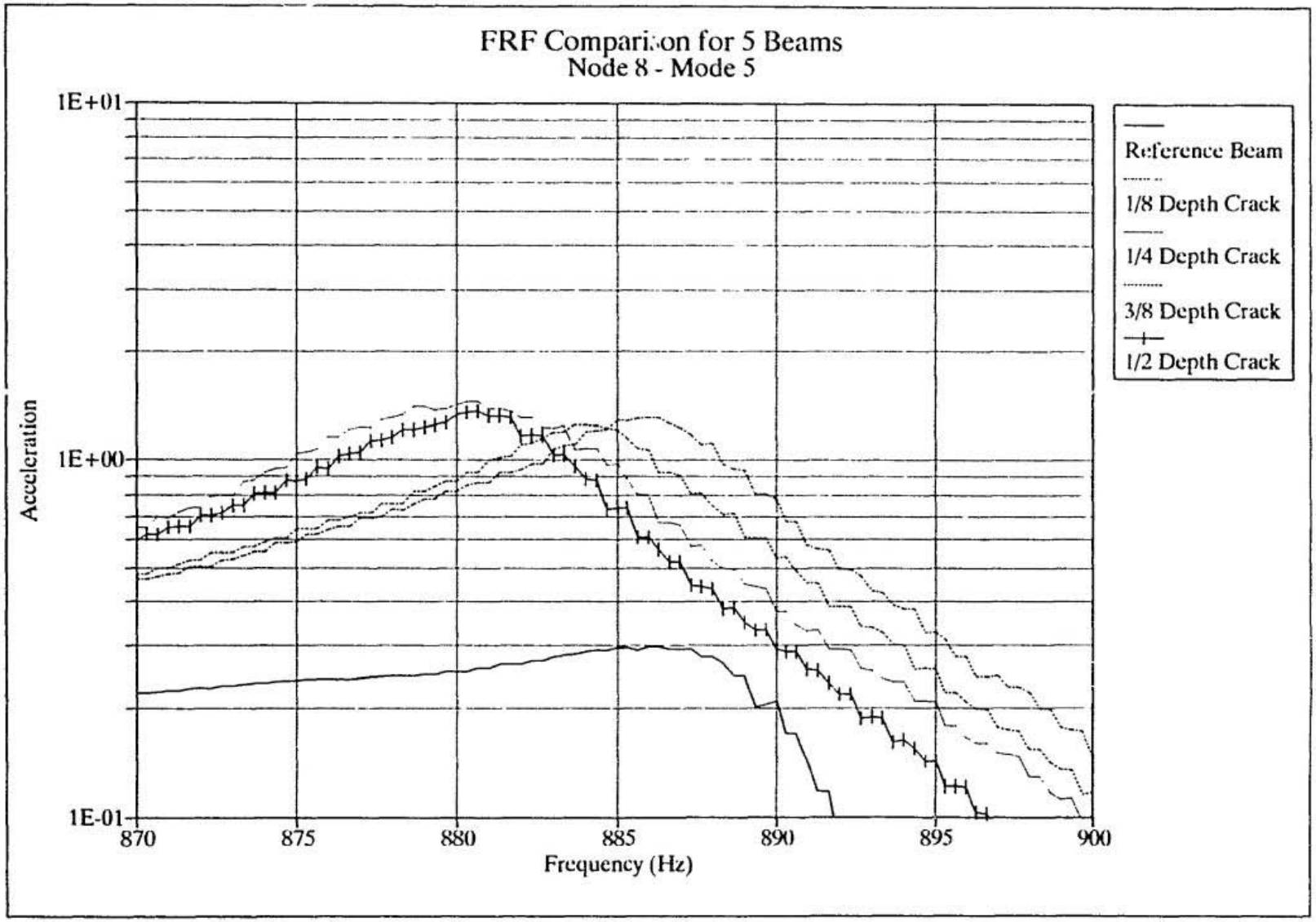
FRF Comparison for 5 Beams
Node 8 - Mode 5
1E+01
1E+00
1E-01
Acceleration
870
875
880
885
890
895
900
Frequency (Hz)
Reference Beam
1/8 Depth Crack
1/4 Depth Crack
3/8 Depth Crack
1/2 Depth Crack

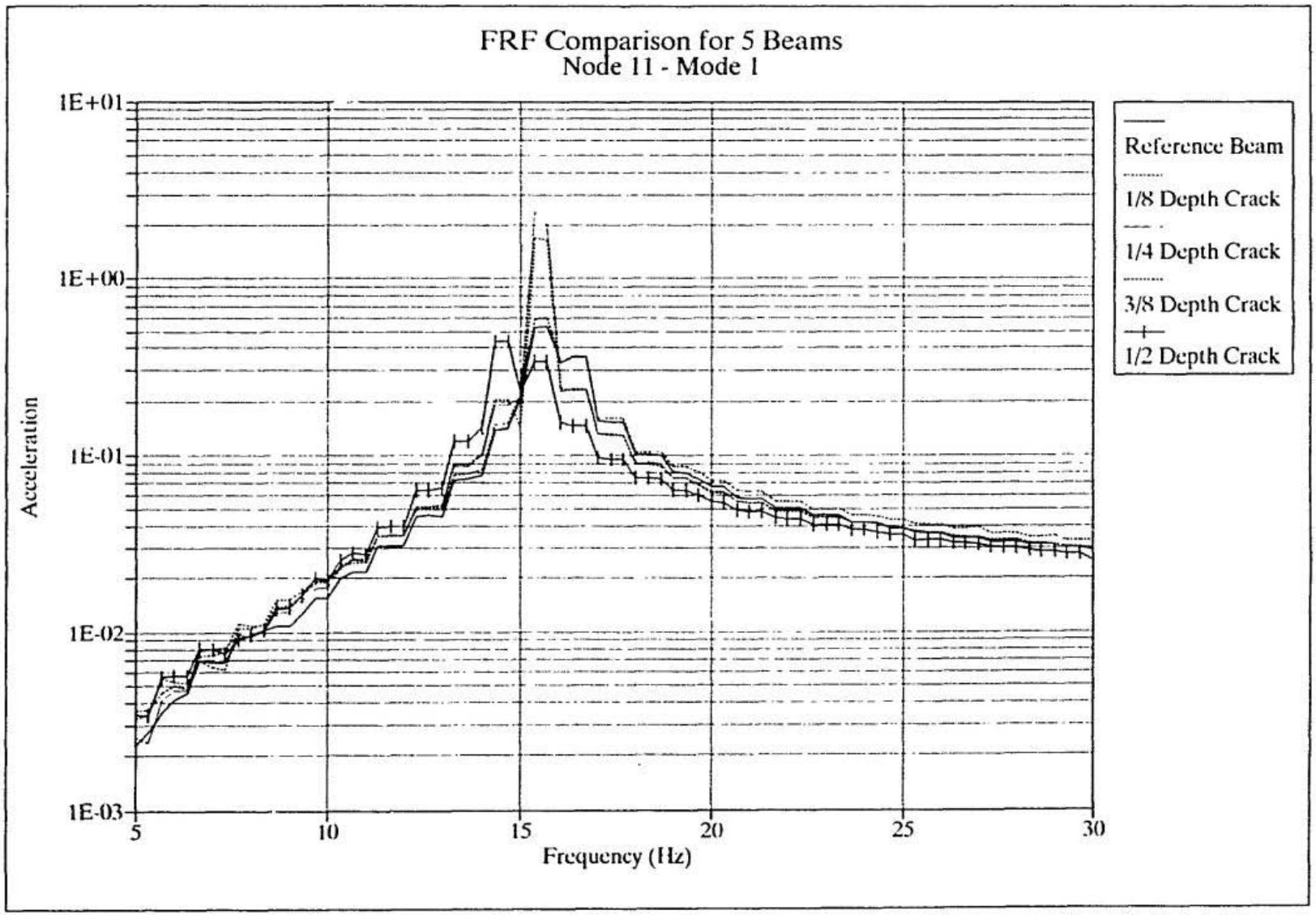
FRF Comparison for 5 Beams
Node 11 - Mode 1
Acceleration
1E+01
1E+00
1E-01
1E-02
1E-03
5
10
15
20
25
30
Frequency (Hz)
Reference Beam
1/8 Depth Crack
1/4 Depth Crack
3/8 Depth Crack
1/2 Depth Crack

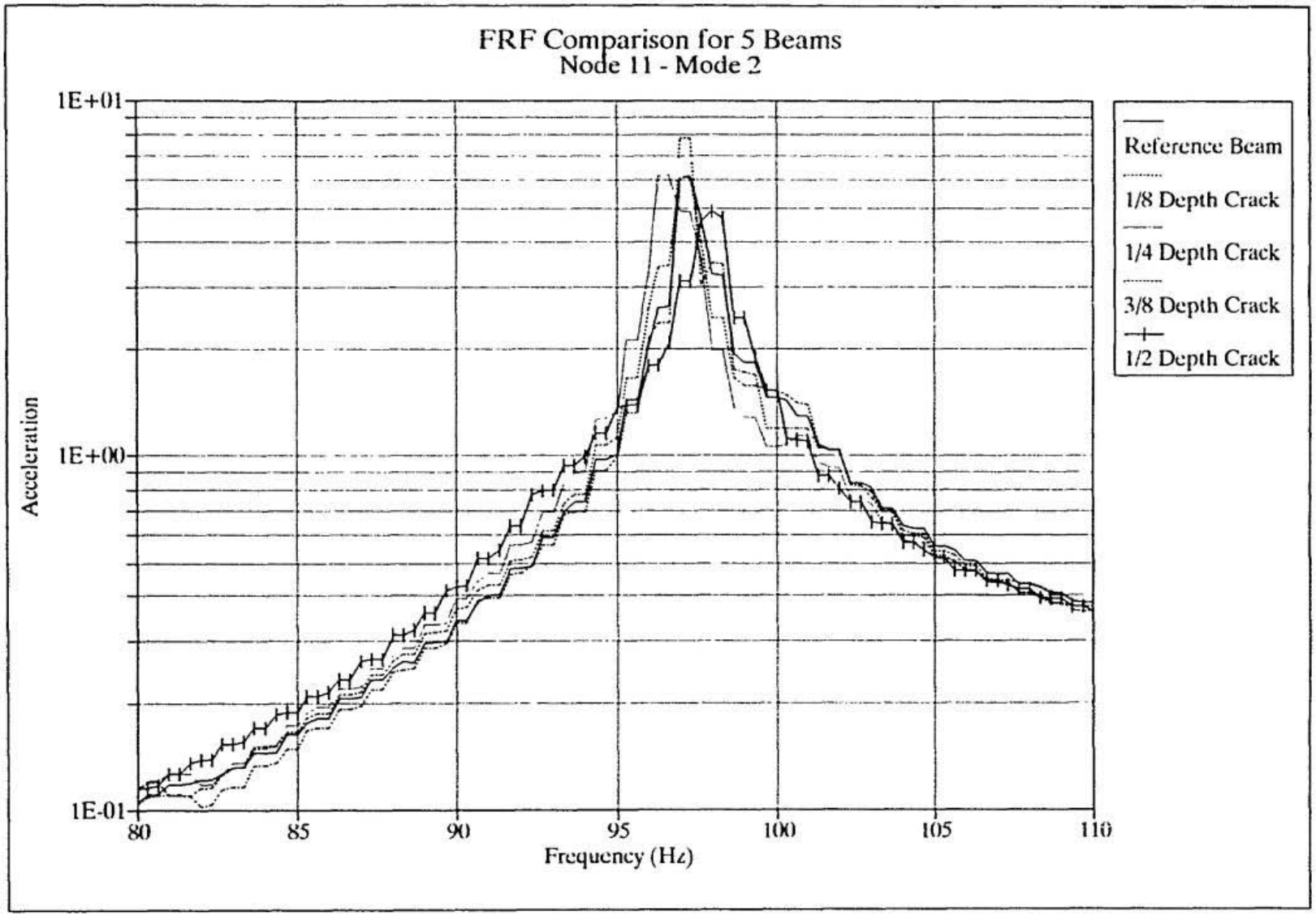
FRF Comparison for 5 Beams
Node 11 - Mode 2
1E+01
1E+00
1E-01
Acceleration
80
85
90
95
100
105
110
Frequency (Hz)
Reference Beam
1/8 Depth Crack
1/4 Depth Crack
3/8 Depth Crack
1/2 Depth Crack

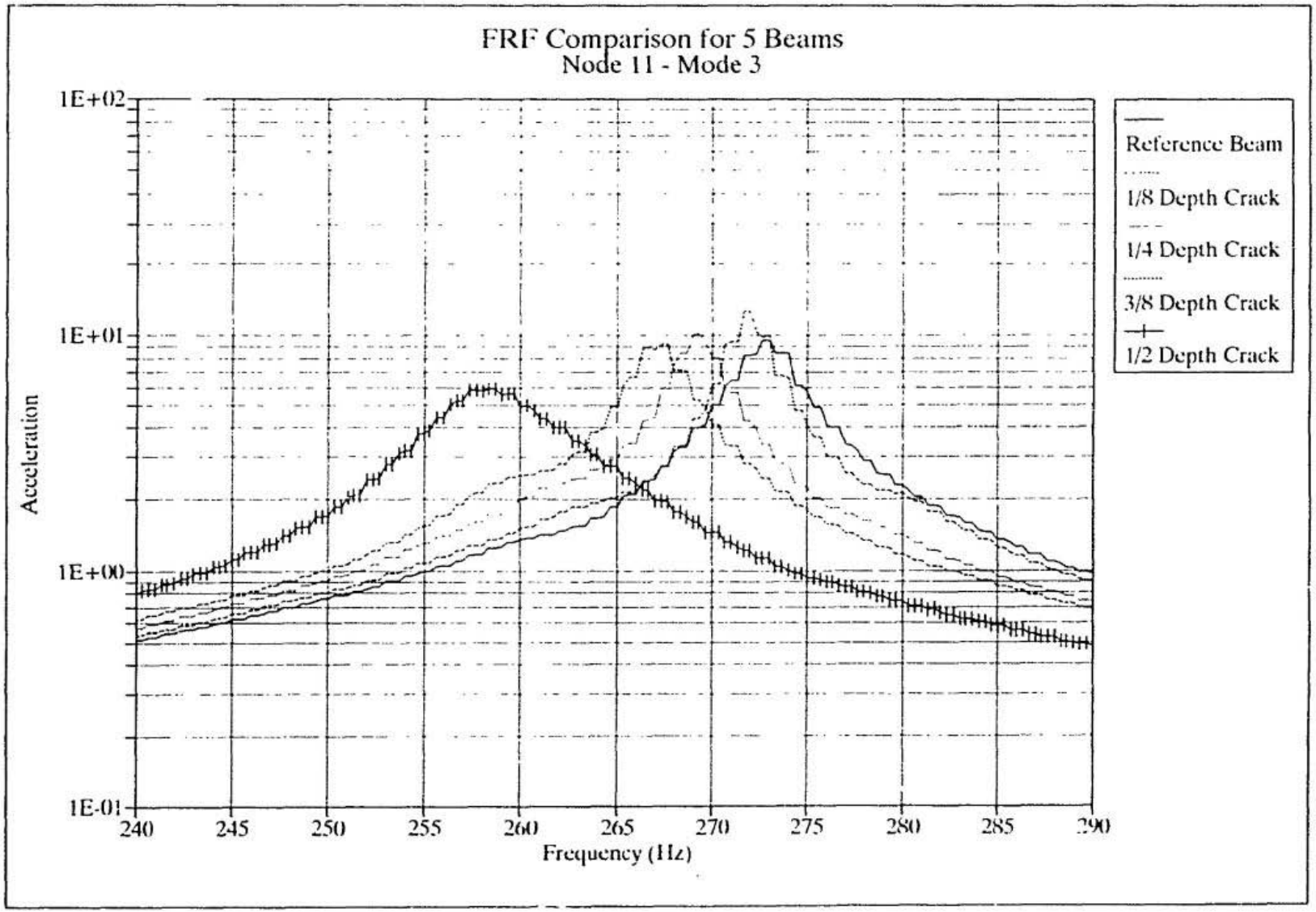
FRF Comparison for 5 Beams
Node 11 - Mode 3
1E+02
1E+01
1E+00
1E-01
Acceleration
240
245
250
255
260
265
270
275
280
285
290
Frequency (Hz)
Reference Beam
1/8 Depth Crack
1/4 Depth Crack
3/8 Depth Crack
1/2 Depth Crack

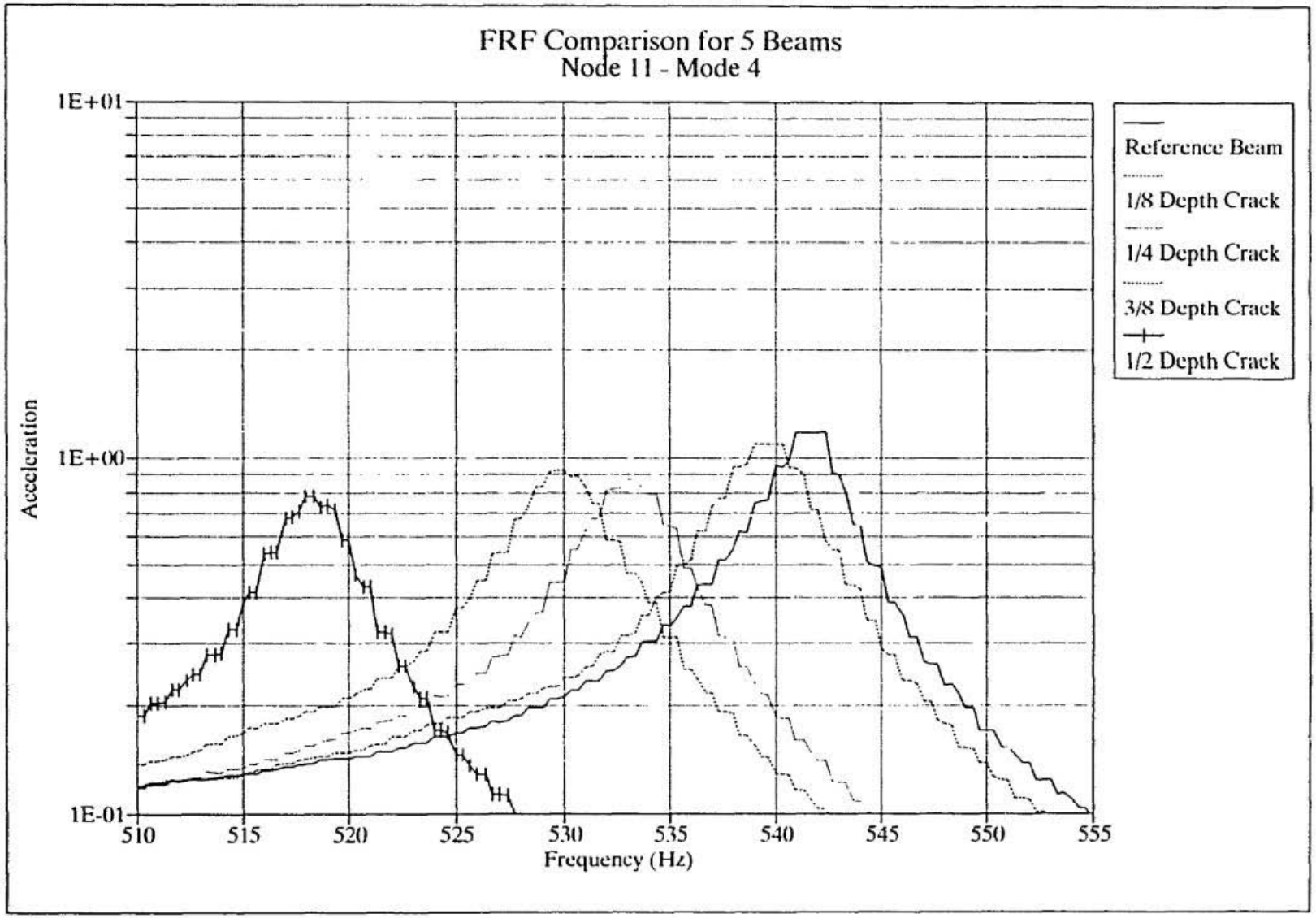
FRF Comparison for 5 Beams
Node 11 - Mode 4
Acceleration
1E+01
1E+00
1E-01
510
515
520
525
530
535
540
545
550
555
Frequency (Hz)
Reference Beam
1/8 Depth Crack
1/4 Depth Crack
3/8 Depth Crack
1/2 Depth Crack

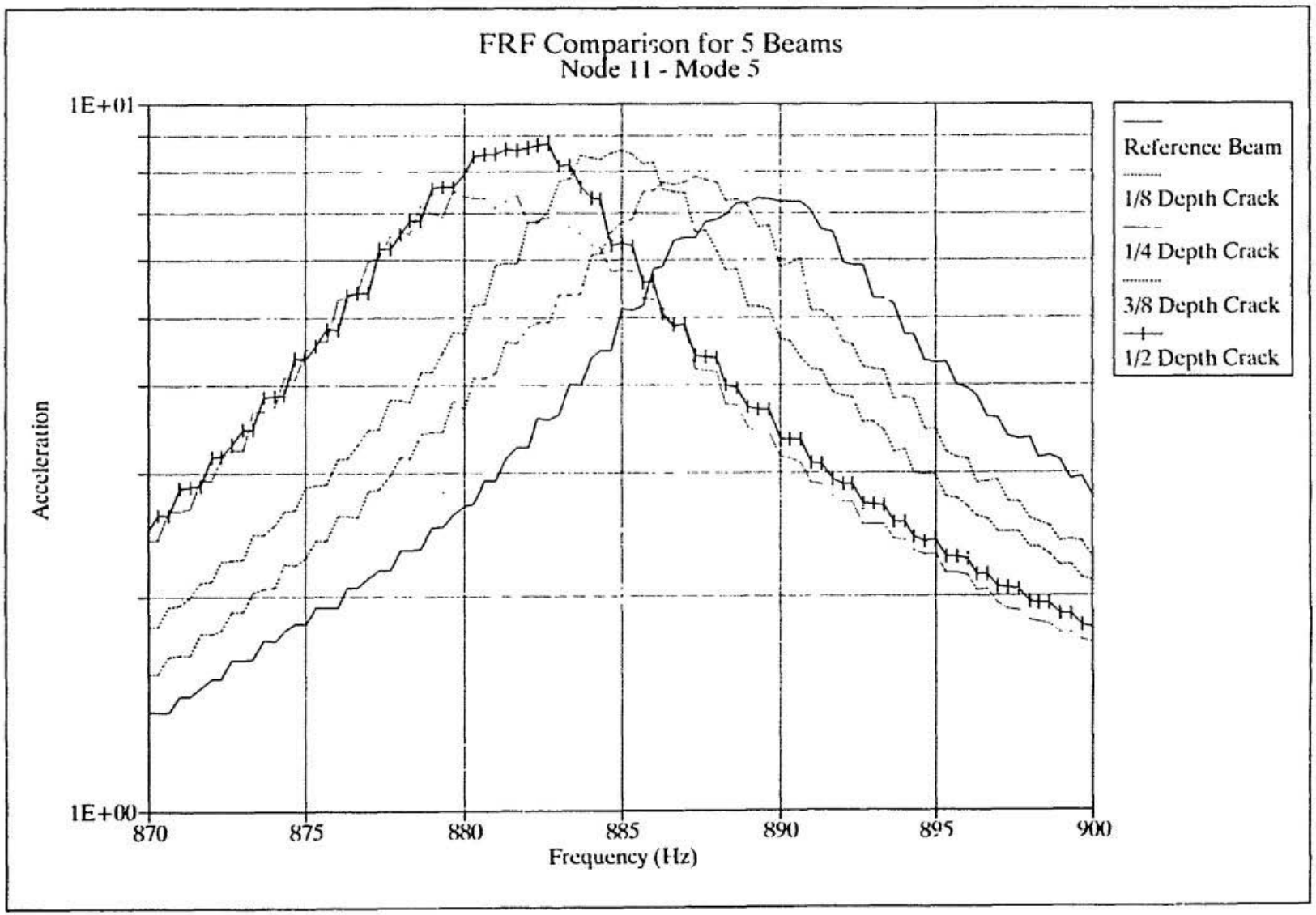
FRF Comparison for 5 Beams
Node 11 - Mode 5
1E+01
1E+00
Acceleration
870
875
880
885
890
895
900
Frequency (Hz)
Reference Beam
1/8 Depth Crack
1/4 Depth Crack
3/8 Depth Crack
1/2 Depth Crack

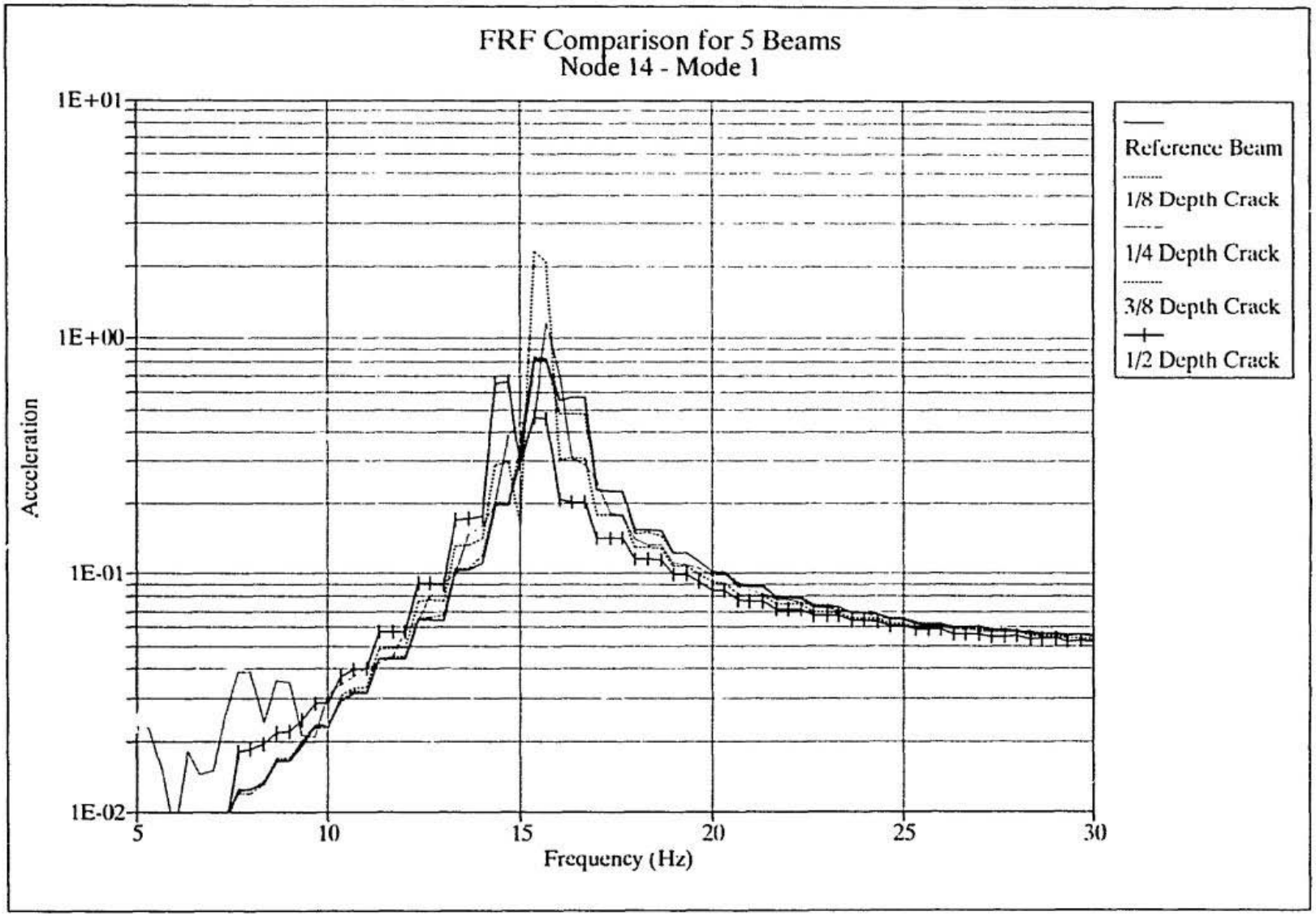
FRF Comparison for 5 Beams
Node 14 - Mode 1
1E+01
1E+00
1E-01
1E-02
Acccleration
5
10
15
20
25
30
Frequency (Hz)
Reference Beam
1/8 Depth Crack
1/4 Depth Crack
3/8 Depth Crack
1/2 Depth Crack

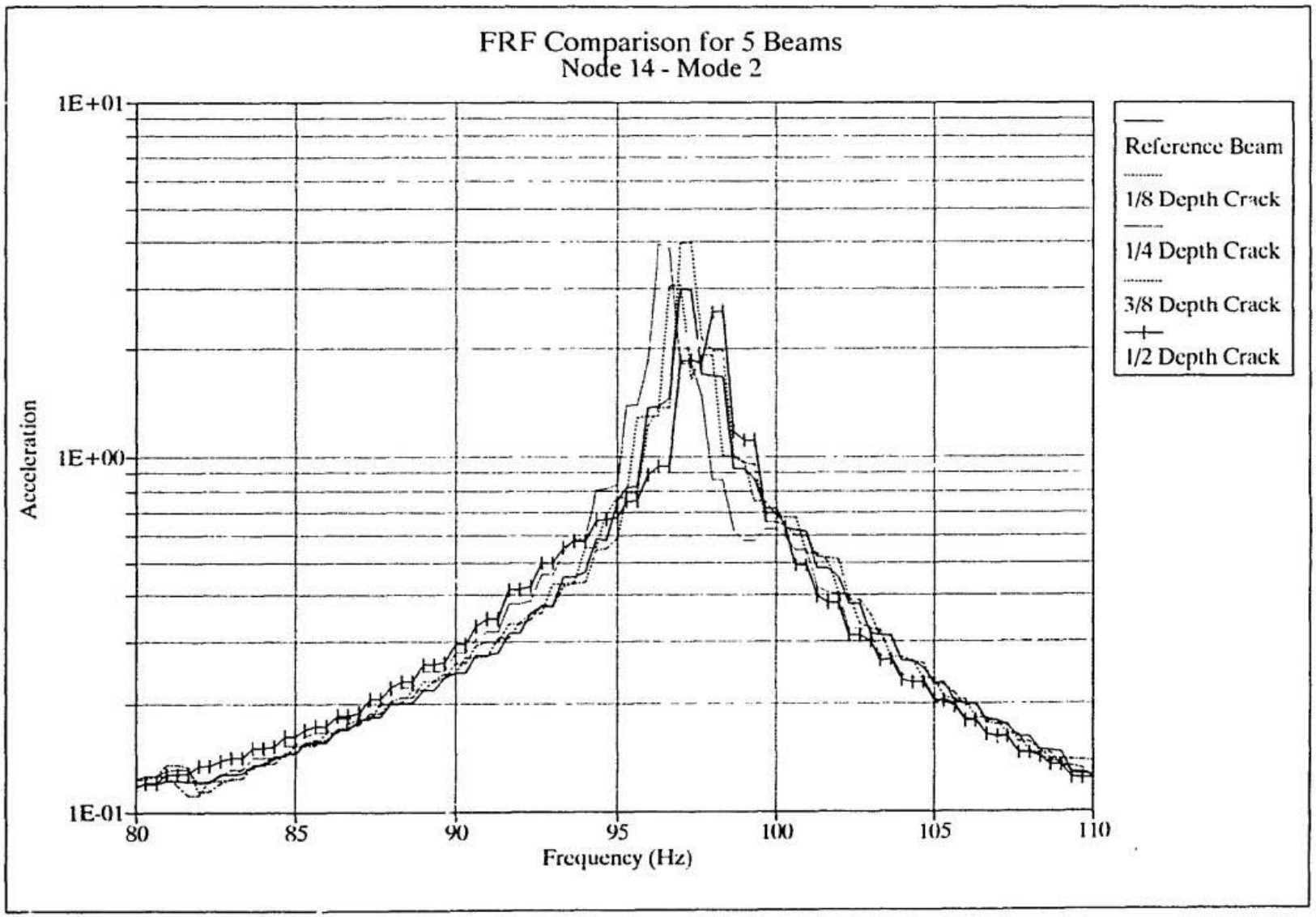
FRF Comparison for 5 Beams
Node 14 - Mode 2
1E+01
1E+00
1E-01
Acceleration
80
85
90
95
100
105
110
Frequency (Hz)
Reference Beam
1/8 Depth Crack
1/4 Depth Crack
3/8 Depth Crack
1/2 Depth Crack

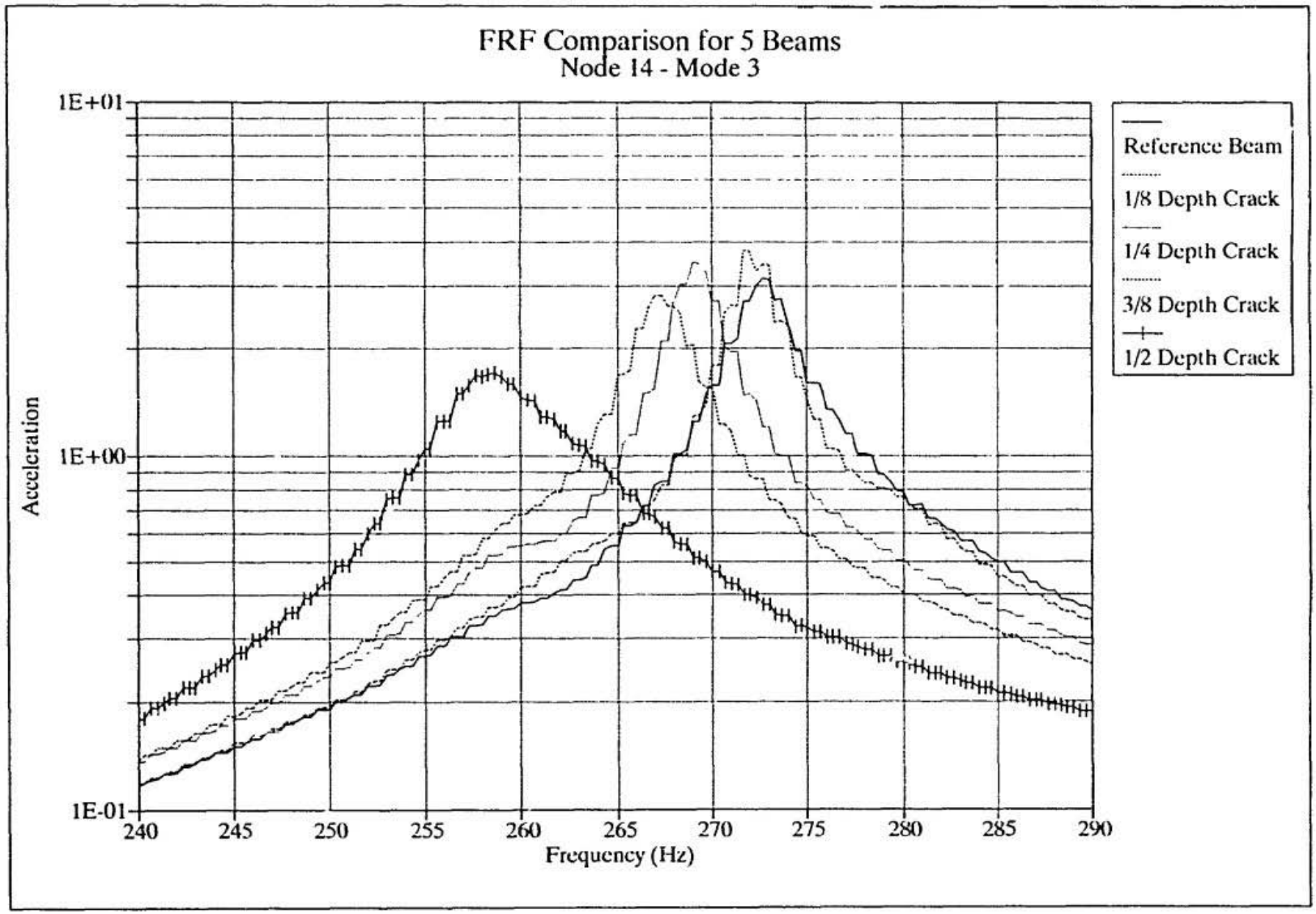
FRF Comparison for 5 Beams
Node 14 - Mode 3
1E+01
1E+00
1E-01
Acceleration
240
245
250
255
260
265
270
275
280
285
290
Frequency (Hz)
Reference Beam
1/8 Depth Crack
1/4 Depth Crack
3/8 Depth Crack
1/2 Depth Crack

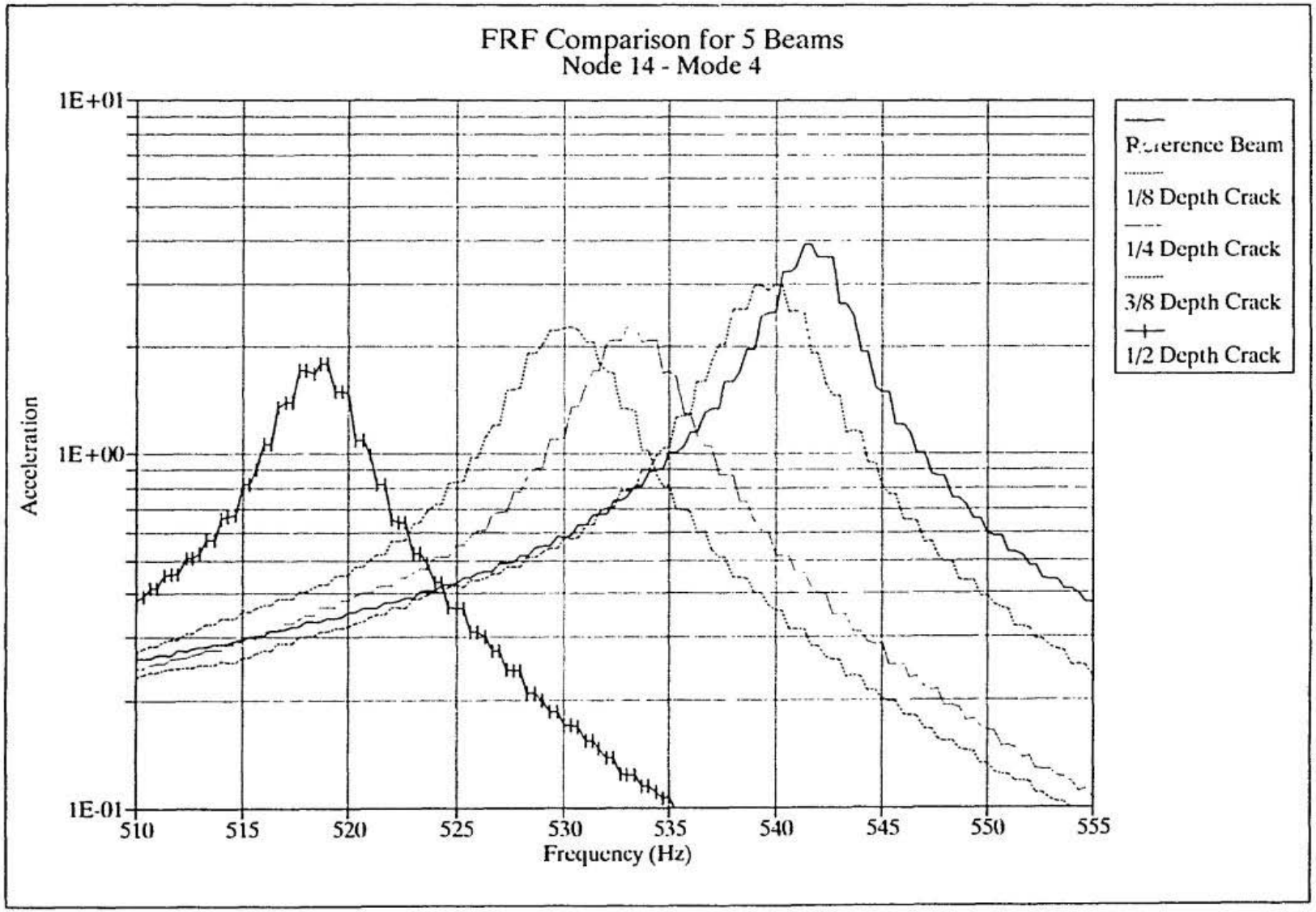
FRF Comparison for 5 Beams
Node 14 - Mode 4
1E+01
1E+00
1E-01
Acceleration
510
515
520
525
530
535
540
545
550
555
Frequency (Hz)
Reference Beam
1/8 Depth Crack
1/4 Depth Crack
3/8 Depth Crack
1/2 Depth Crack

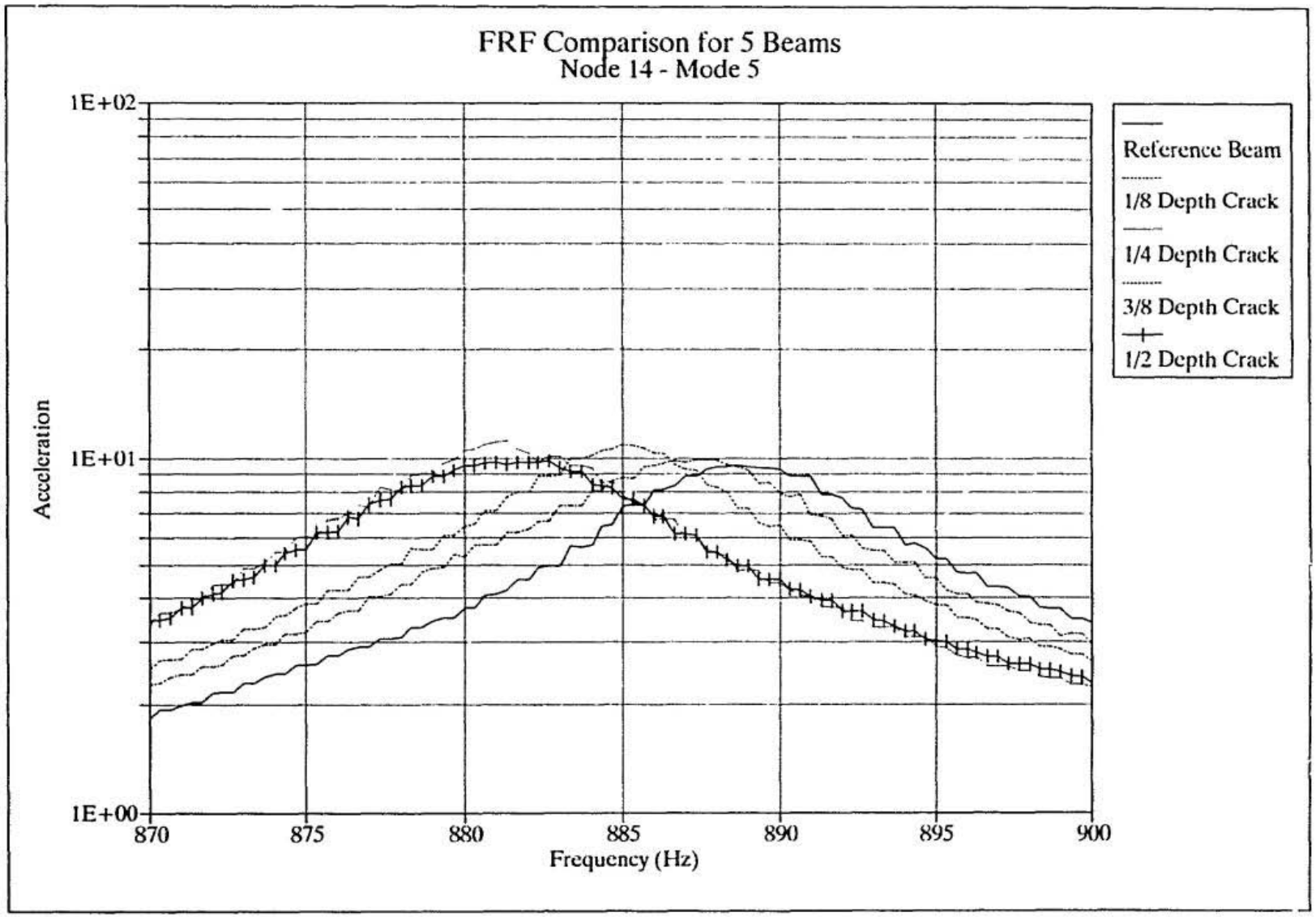
FRF Comparison for 5 Beams
Node 14 - Mode 5
1E+02
1E+01
1E+00
Acceleration
870
875
880
885
890
895
900
Frequency (Hz)
Reference Beam
1/8 Depth Crack
1/4 Depth Crack
3/8 Depth Crack
1/2 Depth Crack

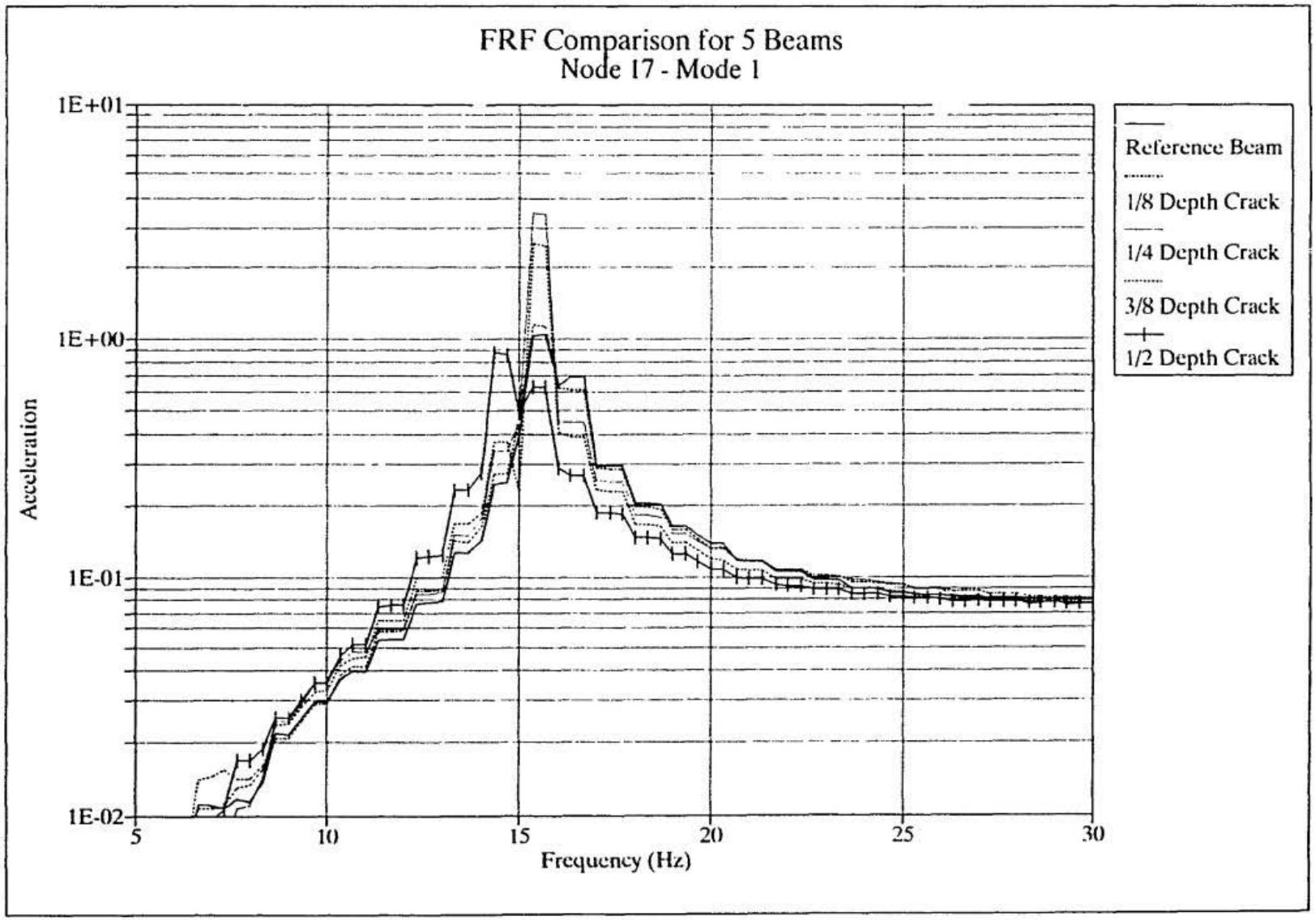
FRF Comparison for 5 Beams
Node 17 - Mode 1
1E+01
1E+00
1E-01
1E-02
Acceleration
5
10
15
20
25
30
Frequency (Hz)
Reference Beam
1/8 Depth Crack
1/4 Depth Crack
3/8 Depth Crack
1/2 Depth Crack

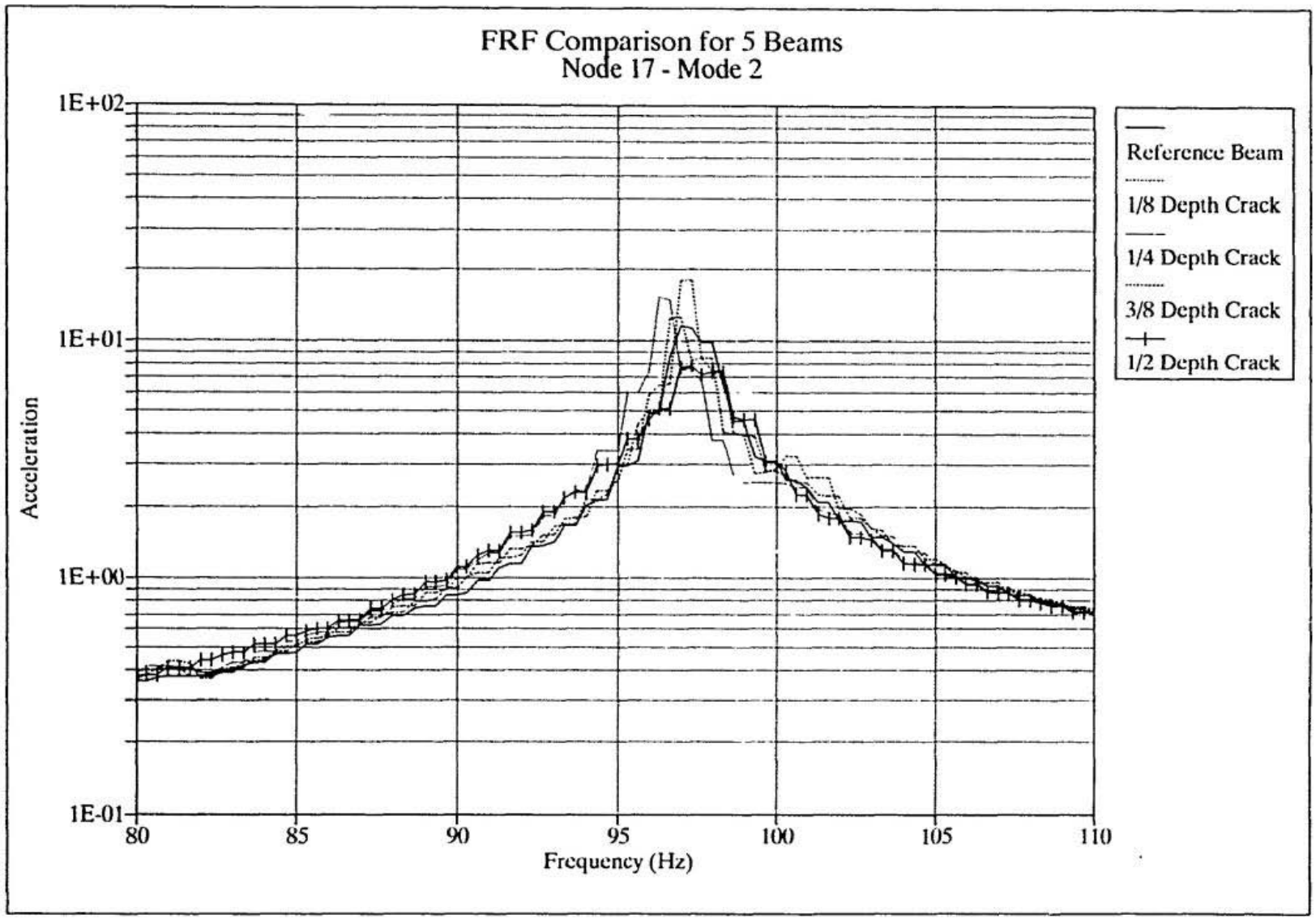
FRF Comparison for 5 Beams
Node 17 - Mode 2
1E+02
1E+01
1E+00
1E-01
Acceleration
80
85
90
95
100
105
110
Frequency (Hz)
Reference Beam
1/8 Depth Crack
1/4 Depth Crack
3/8 Depth Crack
1/2 Depth Crack

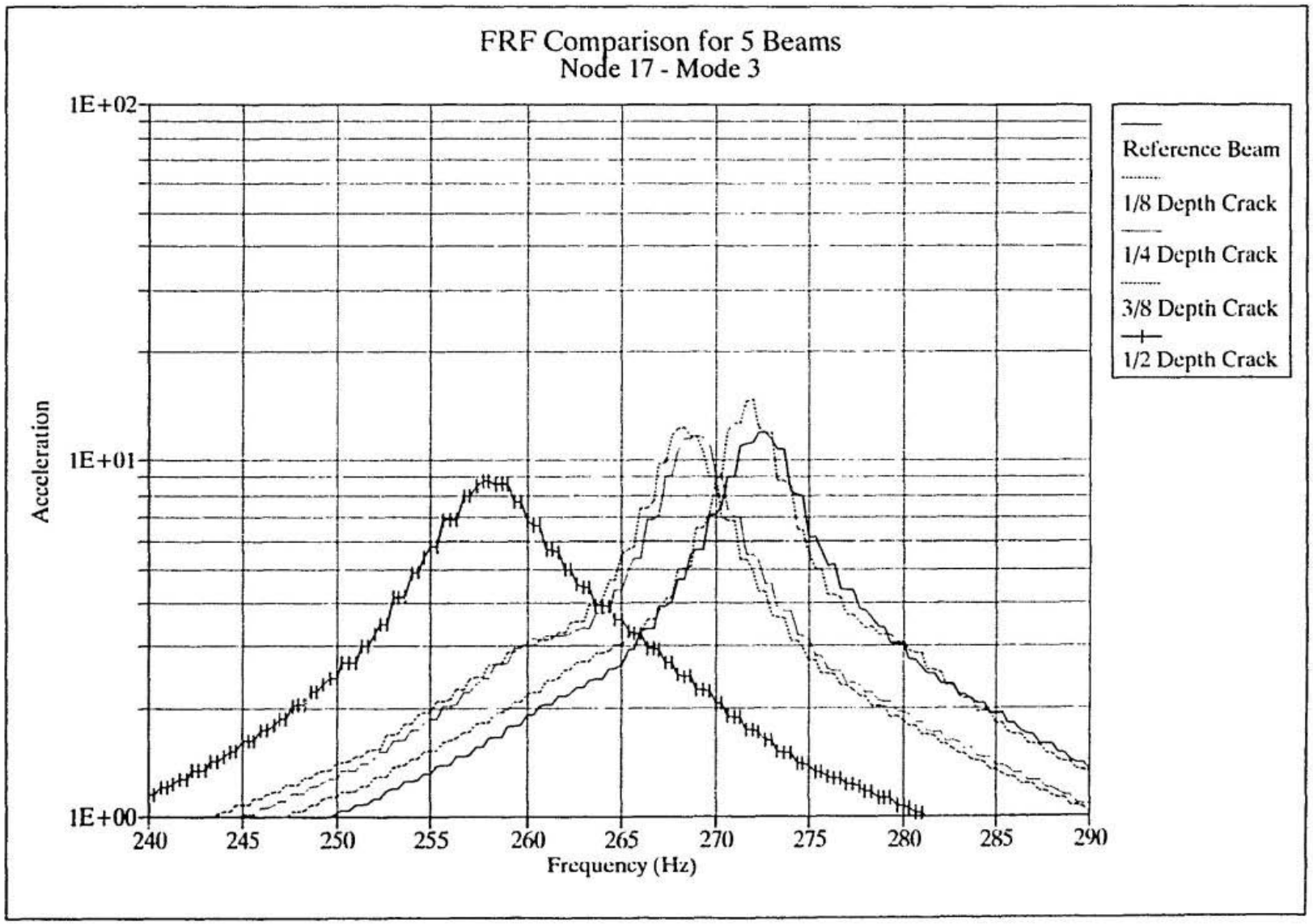
FRF Comparison for 5 Beams
Node 17 - Mode 3
1E+02
1E+01
1E+00
Acceleration
240
245
250
255
260
265
270
275
280
285
290
Frequency (Hz)
Reference Beam
1/8 Depth Crack
1/4 Depth Crack
3/8 Depth Crack
1/2 Depth Crack

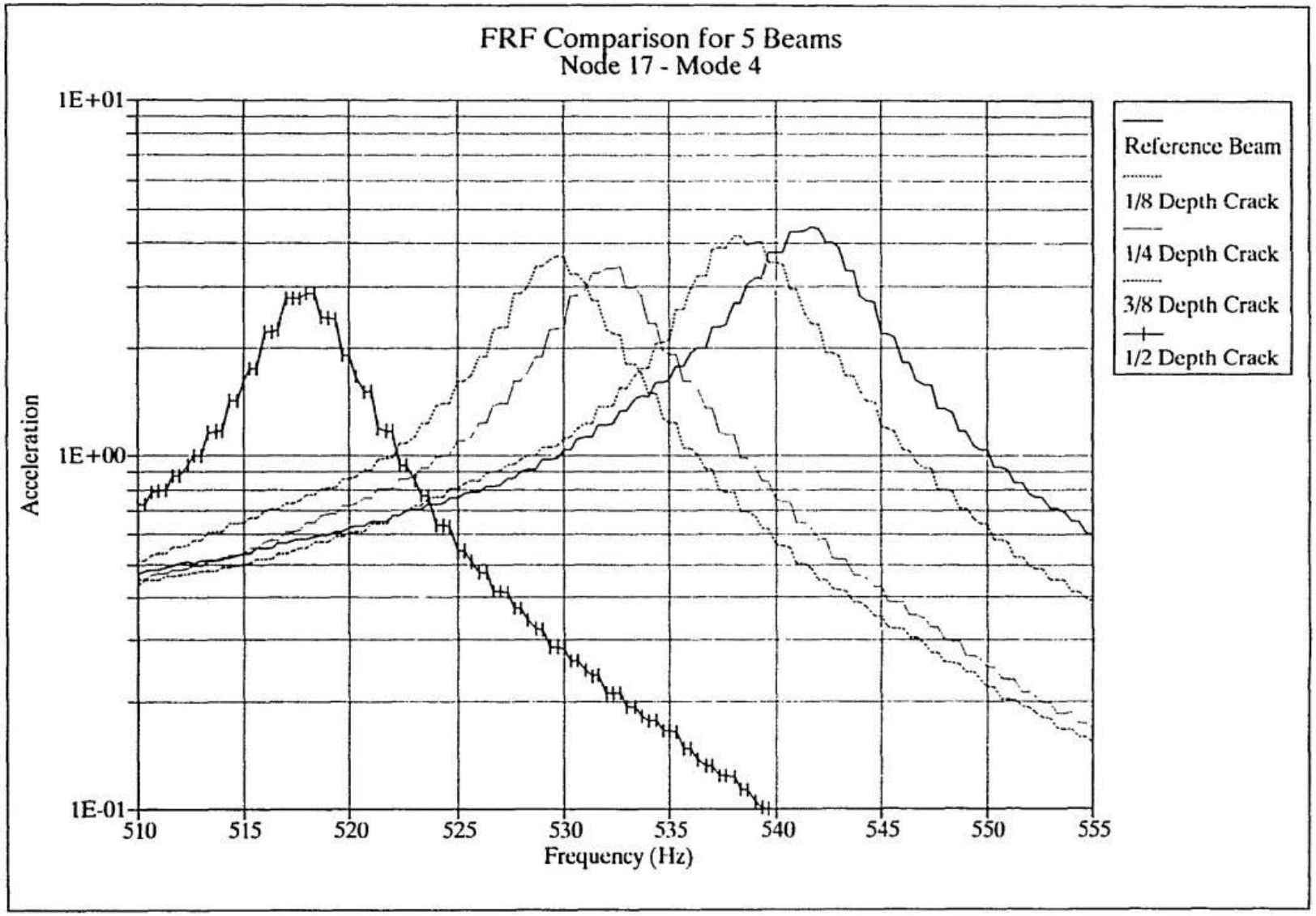
FRF Comparison for 5 Beams
Node 17 - Mode 4
1E+01
1E+00
1E-01
Acceleration
510
515
520
525
530
535
540
545
550
555
Frequency (Hz)
Reference Beam
1/8 Depth Crack
1/4 Depth Crack
3/8 Depth Crack
1/2 Depth Crack

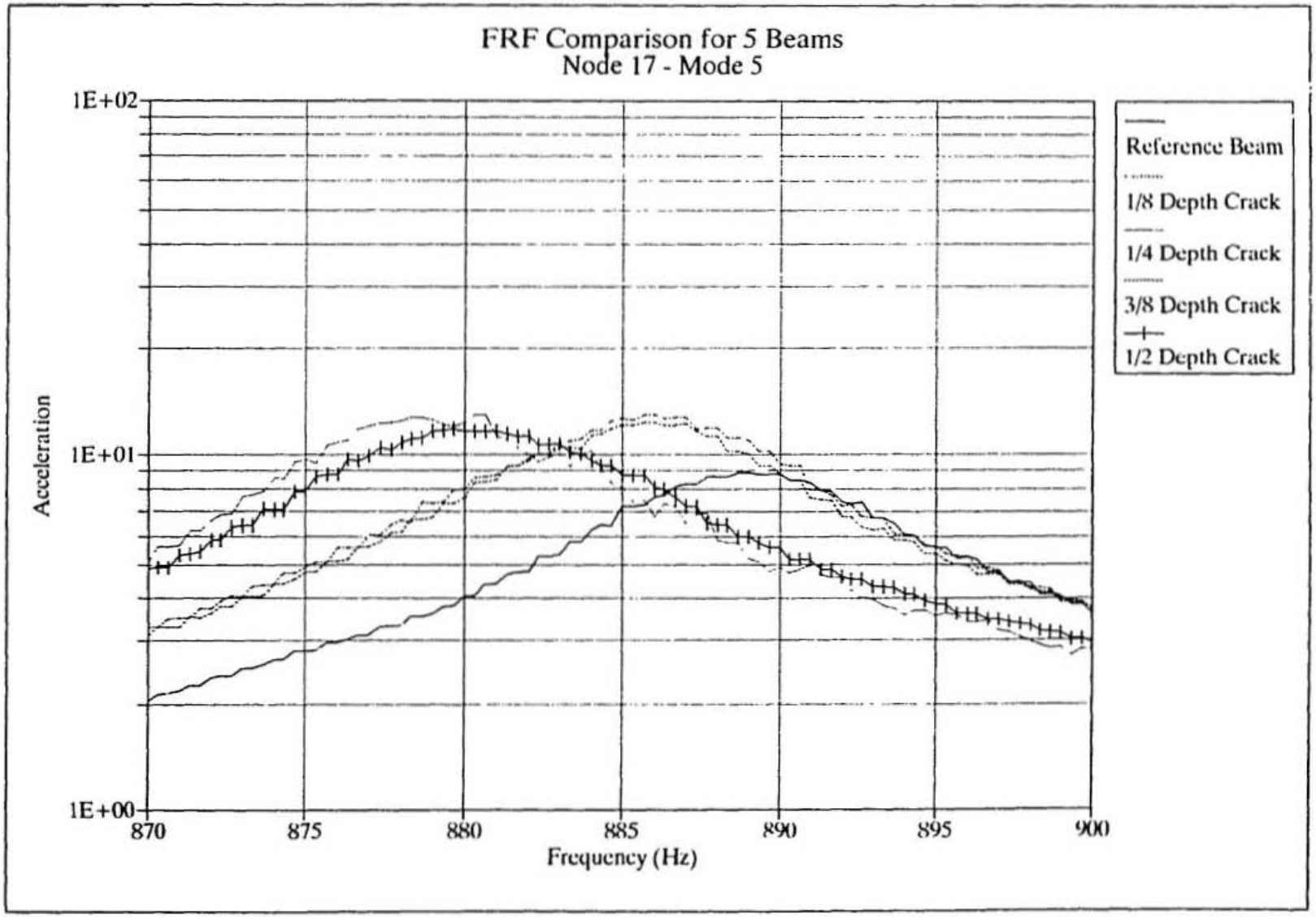
FRF Comparison for 5 Beams
Node 17 - Mode 5
1E+02
1E+01
1E+00
Acceleration
870
875
880
885
890
895
900
Frequency (Hz)
Reference Beam
1/8 Depth Crack
1/4 Depth Crack
3/8 Depth Crack
1/2 Depth Crack

Appendix E

Photos of Experimental Set-up

TEST PLATE WITH ELECTROMAGNETIC EXCITER

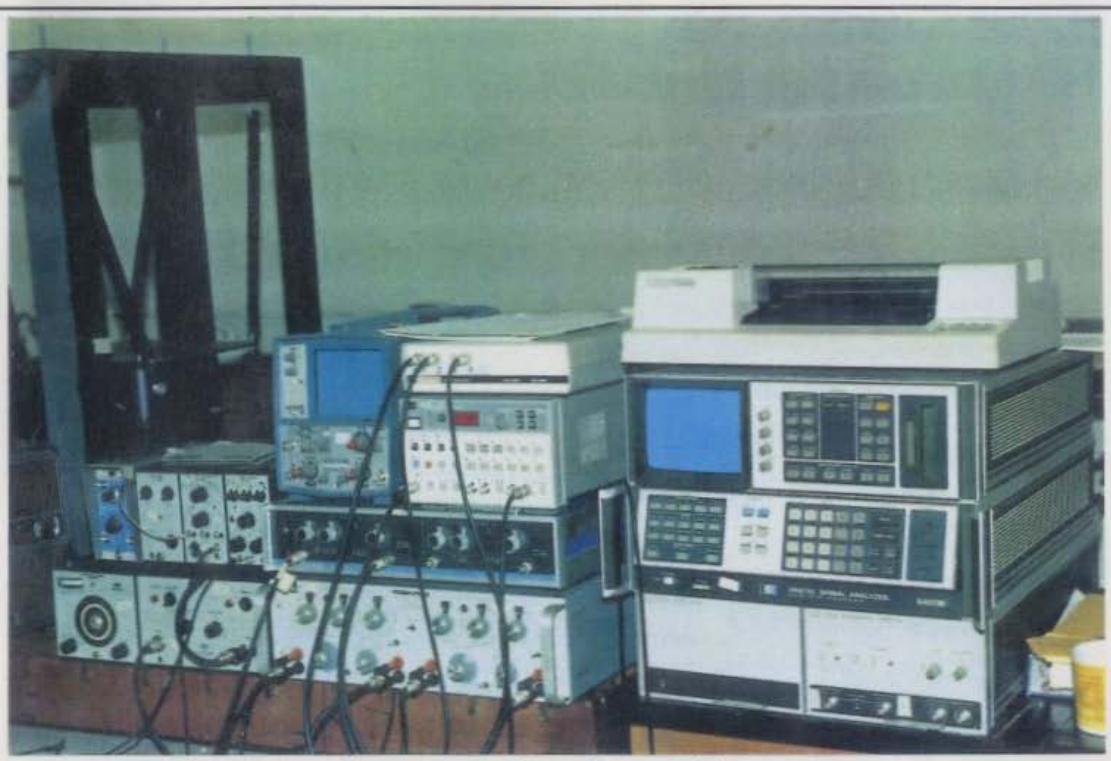

ELECTRONIC EQUIPMENT USED DURING EXPERIMENTATION